NASA SP-224 (03)

THE NASTRAN DEMONSTRATION PROBLEM MANUAL

(Level 16.0)

Date of general release March 9, 1978.

March 1976

Scientific and Technical Information Division
NATIONAL AERONAUTICS AND SPACE ADMINISTRATION
Washington, D C

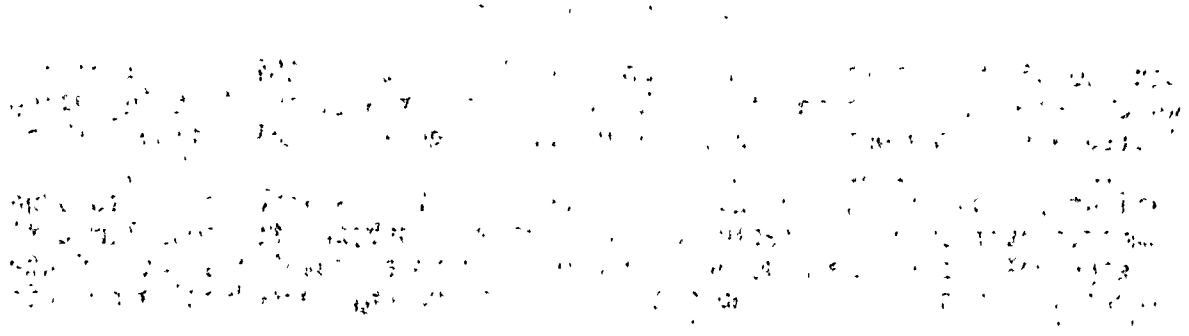

For sale from Computer Software Management and Information Center (COSMIC)
Barrows Hall, University of Georgia, Athens, Georgia 30601 - Price $8.50

INTRODUCTION

The Demonstration Problem Manual is one of four manuals that constitute the documentation for NASTRAN. The other three are the Theoretical Manual, the User's Manual and the Programmer's Manual.

The Theoretical Manual contains discussions of the underlying theory relative to the engineering equations utilized and mathematical operations. There is some discussion relative to data processing techniques and software organization.

The User's Manual is an instructional and encyclopedic reference that describes finite element modeling techniques and shows the requirements for data preparation to obtain solutions in several engineering disciplines.

The Programmer's Manual contains descriptions of the Functional Modules, subroutines and operating systems from a software point of view. It also contains detailed derivations of the mathematical equations employed by the program.

The Demonstration Problem Manual illustrates the types of problems that can be solved with NASTRAN and shows that the results obtained are valid. Generally, this manual discusses the nature of the problem, the underlying theory, the specific geometric and physical input quantities, and the comparison of theoretical and NASTRAN results. At least one problem for each of the rigid formats and nearly all of the elements is provided. The features of NASTRAN demonstrated by specific problems are listed in tables which follow.

The data decks necessary to execute these problems are contained on a tape compatible with each of the NASTRAN computers (See the Programmer's Manual, Section 5.4 for system descriptions.) The driver decks include the Executive, Case and Substructure Control decks plus changes to the Bulk Data (where restarts are involved). The Bulk Data decks are contained on a NASTRAN generated UMF (User Master File). To obtain the decks, it is necessary to print the contents of the tape By using the provided driver decks, NASTRAN may be executed as a UMF job to obtain the results for a particular demonstration problem (or the user's desired variation thereof).

Each demonstration problem is assigned a problem number to key it to the Rigid Format. In turn, the UMF problem identification (pid) is an adaptation of the problem number The UMF tape identification (tid) is the year in which the set of demonstration problems was generated so this would tend to change from level to level of NASTRAN caused by the inclusion of new capabilities. Furthermore, it may not always be possible to execute the new UMF on a previous level due to changes in data handling techniques.

A UMF problem identification number is made up of four elements: The Rigid Format number, the problem number, the version number, and a trailing dummy zero. Thus the general UMF number is xxyyz0. The Rigid Format number is one or two digits; the problem number is always two digits; the version number is always one digit; and the 0 always trails to allow the insertion of additional problems. A UMF pid of 10210 means the problem runs on Rigid Format 1, it is the second demonstration problem on that Rigid Format, and it is version 1 of that problem. Another example, 110110, is a problem for Rigid Format 11, problem 1, version 1, and the trailing zero is a dummy.

A table of pid numbers for each demonstration problem is included in this manual. Restart problem driver decks do not contain a UMF card because the data is already stored on a checkpoint tape which must have been created by the user.

TABLE OF CONTENTS

TABLE OF CONTENTS (Continued)

UMF pid (tid 1976)	NASTRAN DEMONSTRATION PROBLEMS ON UMF TAPE
10110	Delta Wing with Biconvex Cross Section, Load on Trailing Edge
RESTART	Delta Wing with Biconvex Cross Section, Load on Leading Edge
RESTART	Delta Wing with Biconvex Cross Section, Switch to Rigid Format 3
10120	Delta Wing with Biconvex Cross Section Using QDMEM1 and QDMEM2 Elements
10130	Delta Wing with Biconvex Cross Section Using QDMEM1 Elements
10140	Delta Wing with Biconvex Cross Section Using QDMEM2 Elements
10210	Spherical Shell with Pressure Loading, No Moments on Boundary
RESTART	Spherical Shell with Pressure Loading, Clamped Boundary
10310	Free Rectangular QDMEM Plate with Thermal Loading
10320	Free Rectangular QDMEM1 Plate with Thermal Loading
10330	Free Rectangular QDMEM2 Plate with Thermal Loading
10410	Long, Narrow, 5x50 Orthotropic Plate
RESTART	Long, Narrow, 5x50 Orthotropic Plate, Modified Output
10420	Long, Narrow, 5x60 Orthotropic Plate
10430	Long, Narrow, 5x50 Orthotropic Plate (via INPUT Module)
10440	Long, Narrow, 5x60 Orthotropic Plate (via INPUT Module)
10510	Nonsymmetric Bending of a Cylinder of Revolution
10610	Solid Disc with Radially Varying Thermal Load
10710	Shallow Spherical Shell Subjected to External Pressure Loading
10810	Bending of a Beam Fabricated with HEXA1 Solid Elements
10910	Thermal and Applied Loads on HEXA2 Solid Elements
11010	Thermal Bending of a Bar
11110	Simply-Supported Rectangular Plate with a Thermal Gradient
11120	Simply-Supported Rectangular Plate with a Thermal Gradient (via INPUT Module)
11210	Linear Steady State Heat Conduction Through a Washer Using Solid Elements
11220	Linear Steady State Heat Conduction Through a Washer Using Ring Elements
11310	Thermal and Pressure Loads on a Long Pipe Using Linear Isoparametric Elements
11320	Thermal and Pressure Loads on a Long Pipe Using Quadratic Isoparametric Elements
11330	Thermal and Pressure Loads on a Long Pipe Using Cubic Isoparametric Elements
11410	Static Analysis of a Beam Using General Elements

11510	Asymmetric Pressure Loading of an Axisymmetric Cylindrical Shell
11610	Fully Stressed Design of a Plate with a Reinforced Hole
20110	Inertia Relief Analysis of a Circular Ring Under Concentrated and Centrifugal Loads
20210	Windmill Panel Sections for Multi-stage Substructuring (Run 1, Phase 1)
20220	Windmill Panel Sections for Multi-stage Substructuring (Run 2, Phase 1)
20230	Windmill Panel Sections for Multi-stage Substructuring (Run 3, Phase 1)
20240	Windmill Panel Sections for Multi-stage Substructuring (Run 4, Phase 2)
20250	Windmill Panel Sections for Multi-stage Substructuring (Run 5, Phase 3)
20260	Windmill Panel Sections for Multi-stage Substructuring (Run 6, Phase 3)
20270	Windmill Panel Sections for Multi-stage Substructuring (Run 7, Phase 2)
30110	Vibration of a 10x20 Plate
30120	Vibration of a 20x40 Plate
30130	Vibration of a 10x20 Plate (via INPUT Module)
30140	Vibration of a 20x40 Plate (via INPUT Module)
30210	Vibration of a Compressible Gas in a Rigid Spherical Tank
30310	Vibration of a Liquid in a Half Filled Rigid Sphere
30410	Acoustic Cavity Analysis
30510	Nonlinear Heat Transfer in an Infinite Slab
30610	Nonlinear Radiation and Conduction of a Cylinder
40110	Differential Stiffness Analysis of a Hanging Cable
50110	Symmetric Buckling of a Cylinder
60110	Piecewise Linear Analysis of a Cracked Plate
70110	Complex Eigenvalue Analysis of a 500-Cell String
70120	Complex Eigenvalue Analysis of a 500-Cell String (via INPUT Module)
70210	Third Harmonic Complex Eigenvalue Analysis of a Gas-Filled Thin Elastic Cylinder
70220	Fifth Harmonic Complex Eigenvalue Analysis of a Gas-Filled Thin Elastic Cylinder
80110	Frequency Response of a 10x10 Plate
80120	Frequency Response of a 20x20 Plate
80130	Frequency Response of a 10x10 Plate (via INPUT Module)
80140	Frequency Response of a 20x20 Plate (via INPUT Module)
90110	Transient Analysis with Direct Matrix Input

UMF pid (tid 1976)	NASTRAN DEMONSTRATION PROBLEMS ON UMF TAPE
90210	Transient Analysis of a 1000-Cell String, Traveling Wave Problem
90220	Transient Analysis of a 1000-Cell String, Traveling Wave Problem (via INPUT Module)
90310	Transient Analysis of a Fluid-Filled Elastic Cylinder
90410	Linear Transient Heat Transfer in a Plate
100110	Complex Eigenvalue Analysis of a Rocket Control System
100210	Aeroelastic Flutter Analysis of a 15° Swept Wing
110110	Frequency Response and Random Analysis of a Ten Cell Beam
RESTART	Frequency Response and Random Analysis of a Ten Cell Beam, Enforced Deformation and Gravity Load
110210	Frequency Response of a 500-Cell String
110220	Frequency Response of a 500-Cell String (via INPUT Module)
120110	Transient Analysis of a Free One Hundred Cell Beam
130110	Normal Modes Analysis of a One Hundred Cell Beam with Differential Stiffness
140110	Static Analysis of a Circular Plate Using Dihedral Cyclic Symmetry
150110	Normal Modes Analysis of a Circular Plate Using Rotational Cyclic Symmetry

DEMONSTRATED FEATURES OF NASTRAN

A. PHYSICAL PROBLEMS

Structures

1. Line
2. Plate or Shell
3. Solids
4. Rotational Symmetry

Fluid Dynamics

5. Flexible Boundary
6. Rigid Boundary
7. Sloshing
8. Acoustic
9. Aeroelastic

Heat Transfer

10. Conduction
11. Convection
12. Radiation

B. SOLUTION METHODS

Steady State

1. Linear Statics
2. Inertia Relief
3. Nonlinear Geometry
4. Material Plasticity
5. Fully Stressed Design
6. Linear Heat Transfer
7. Nonlinear Heat Transfer

Eigenvalue Analysis

8. Real Modes
9. Complex Modes
10 Inverse Power
11. Determinant
12. Givens
13. Upper Hessenberg

Dynamic Response

14. Direct Formulation
15. Modal Formulation
16. Transient Response
17. Frequency Response
18. Random Analysis
19. Flutter Analysis

C. ELEMENT TYPES

1. Bar, Rod, Tube or Conrod
2. Shear or Twist Panel
3. Plate or Membrane
4. Scalar Springs, Mass and Dampers
5. Concentrated Mass
6. Viscous Dampers
7. Plot (PLØTEL)
8. General (GENEL)
9. Conical Shell
10. Toroidal Shell
11. Axisymmetric Solids
12. Linear Solids
13. Isoparametric Solids
14. Solid Heat Conductors
15. Heat Transfer Boundary Elements

16. Fluid Elements
17. Acoustic Elements
18. Aerodynamic

D. CONSTRAINTS

1. Single-Point Constraints
2. Multipoint Constraints
3. Omitted Coordinates
4. Free-Body Supports
5. Fluid Free Surface
6. Symmetry Used on Boundary
7. "Grounded" Stiffness Terms

E. GEOMETRY AND PROPERTY DEFINITIONS

1. Property ID Default
2. Local Coordinate System
3. Resequenced Grid Points
4. Thermal Dependent Materials
5. Nonlinear Materials
6. Anisotropic Materials
7. Offset BAR Connections
8. Structural Mass
9. Nonstructural Mass
10. Structural Element Damping
11. Compressibility of Fluid
12. Fluid Gravity Effects
13. Multiple Fluid Harmonics

F. SPECIAL MATRIX OPTIONS

1. General Element (GENEL)
2 Direct Input Matrices
3. Transfer Functions
4. Extra Points
5. Direct Damping Matrix Input
6. Modal Damping
7. Substructuring
8 Cyclic Symmetry
9. Uniform Structure Damping

G. LOADING OPTIONS

Static

1. Concentrated Loads
2. Pressure Loads
3. Gravity Loads
4. Thermal Loads
5. Harmonic Loads
6. Centrifugal Field Loads
7. Enforced Element Deformation
8. Enforced Displacement

Dynamic Excitation

9. Tabular Loads vs. Frequency or Time
10. Direct Time Function Loads
11. Loading Phase Angles
12. Loading Time Lags
13. Load Combinations (DLØAD)
14. Transient Initial Conditions
15. Random Analysis Power Spectral Density Functions

Heat Transfer

16. Volume Heating
17. Area Heating
18. Radiation Heating
19. Enforced Boundary Temperature

H. EXECUTION OPTIONS

Multiple Solution Techniques

1. Loads
2. Boundary Constraints
3. Cyclic Cymmetry
4. Direct Input Matrices
5. Aerodynamic Coefficients

Operational Techniques

6. Checkpoint
7 Restart with Modified Case Control
8. Restart with Rigid Format Change
9. Restart with Modified Bulk Data
10. Altered Rigid Format Using DMAP Statements
11. Multi-stage Substructuring

I. OUTPUT OPTIONS

Print and/or Punched

1. Point Output Selections
2. Element Output Selections
3. Subcase Level Request Changes
4. Sorted by Frequency or Time (SØRT2)
5. Magnitude and Phase of Complex Numbers
6. Mode Acceleration Data Recovery

7. Solution Set Output Requests
8. Frequency Set Selections
9. Punched Output Selections
10. Weight and Balance
11. Grid Point Force Balance
12. Element Strain Energy

Plot

13. Structures Plot of Undeformed Structure
14. Structures Plot of Deformed Structure
15. Curve Plotting vs. Frequency
16. Curve Plotting vs. Time
17. Curve Plotting vs. Subcase

Item	Feature	Problem Numbers																								
		1-1	1-2	1-3	1-4	1-5	1-6	1-7	1-8	1-9	1-10	1-11	1-12-1	1-12-2	1-13	1-14	1-15	1-16	2-1	2-2	3-1	3-2	3-3	3-4	3-5	3-6
A	PHYSICAL PROBLEMS																									
	Structures																									
1	line	X							X	X	X					X			X	X					X	X
2	plate or shell	X	X	X	X	X		X				X						X			X					
3	solids						X		X	X			X	X	X		X									
4	rotational symmetry		X			X	X	X					X	X	X		X		X							
	Fluid Dynamics																									
5	flexible boundary																									
6	rigid boundary																					X	X			
7	sloshing																						X			
8	acoustic																					X		X		
9	aeroelastic																									
	Heat Transfer																									
10	conduction												X	X											X	X
11	convection													X												
12	radiation																									X

Note: Two-digit problem numbers refer to all problems in the series; three-digit numbers refer to a specific version.

Item	Feature	Problem Numbers																
		4-1	5-1	6-1	7-1	7-2	8-1	9-2	9-3	9-4	10-1	10-2	11-1	11-2	12-1	13-1	14-1	15-1
A	PHYSICAL PROBLEMS																	
	Structures																	
1	line	X			X			X		X	X	X	X	X	X	X		
2	plate or shell		X	X		X	X		X								X	X
3	solids																	
4	rotational symmetry		X			X			X								X	X
	Fluid Dynamics																	
5	flexible boundary					X			X									
6	rigid boundary																	
7	sloshing																	
8	acoustic					X												
9	aeroelastic											X						
	Heat Transfer																	
10	conduction									X								
11	convection																	
12	radiation																	

Note: Two-digit problem numbers refer to all problems in the series: three-digit numbers refer to a specific version.

Item	Feature	Problem Numbers																								
		1-1	1-2	1-3	1-4	1-5	1-6	1-7	1-8	1-9	1-10	1-11	1-12	1-13	1-14	1-15	1-16	2-1	3-5	3-6	4-1	5-1	6-1	9-4	11-1-1A	13-1	14-1
B	SOLUTION METHODS																										
	Steady State																										
1	linear statics	X	X	X	X	X	X	X	X	X	X	X	X	X	X	X	X								X		X
2	inertia relief																	X									
3	nonlinear geometry																				X	X				X	
4	material plasticity																						X				
5	fully stressed																X										
6	linear heat transfer												X											X			
7	non-linear heat transfer																		X	X							

Item	Feature	Problem Numbers															
		1-1-1B	3-1	3-2	3-3	3-4	5-1	7-1	7-2	10-1	10-2	11-1	11-2	12-1	13-1	15-1
B	SOLUTION METHODS															
	Eigenvalue Analysis															
8	real modes	X	X	X	X	X	X			X	X	X	X	X	X	X
9	complex modes							X	X	X	X					
10	inverse power	X	X	X	X	X				X		X	X	X	X	X
11	determinant						X	X	X	X						
12	Givens										X					
13	upper Hessenberg										X					

Note: Two-digit problem numbers refer to all problems in the series; three-digit numbers refer to a specific version.

Item	Feature	Problem Numbers											
		7-1	7-2	8-1	9-1	9-2	9-3	9-4	10-1	10-2	11-1	11-2	12-1
B	SOLUTION METHODS												
	Dynamic Response												
14	direct formulation	X	X	X	X	X	X	X					
15	modal formulation								X	X	X	X	X
16	transient response				X	X	X	X					X
17	frequency response			X							X	X	
18	random analysis										X		
19	flutter analysis									X			

Note: Two-digit problem numbers refer to all problems in the series; three-digit numbers refer to a specific version.

Item	Feature	Problem Numbers																		
		1-1	1-2	1-3	1-4	1-5	1-6	1-7	1-8	1-9	1-10	1-11	1-12-1	1-12-2	1-13	1-14	1-15	1-16	2-1	2-2
C	ELEMENT TYPES																			
1	bar, rod, tube or conrod	X									X					X		X	X	
2	shear or twist panels	X																		
3	plate or membrane	X	X	X	X							X						X		X
4	scalar																			
5	concentrated mass																			
6	viscous damping																			
7	plot (PLØTEL)		X																	
8	general (GENEL)															X				
9	conical shell					X														
10	toroidal shell							X												
11	axisymmetric solids						X							X			X			
12	linear solids								X	X			X							
13	isoparametric solids														X					
14	solid heat conductors												X	X						
15	heat transfer boundary elements												X	X						
16	fluid elements																			
17	acoustic elements																			
18	aerodynamic																			

Note: Two-digit problem numbers refer to all problems in the series; three-digit numbers refer to a specific version.

Item	Feature	Problem Numbers																					
		3-1	3-2	3-3	3-4	3-5	3-6	4-1	5-1	6-1	7-1	7-2	8-1	9-2	9-3	9-4	10-1	10-2	11-1	11-2	12-1	13-1	14-1	15-1
C	ELEMENT TYPES																							
1	bar, rod, tube or conrod					X		X								X	X	X	X		X	X	X	X
2	shear or twist panels																							
3	plate or membrane	X							X	X		X	X		X								X	X
4	scalar										X			X		X	X	X		X				
5	concentrated mass										X			X			X	X	X	X	X			
6	viscous damping										X													
7	plot (PLØTEL)	X																						
8	general (GENEL)																		X					
9	conical shell																							
10	toroidal shell																							
11	axisymmetric solids																							
12	linear solids																							
13	isoparametric solids																							
14	solid heat conductors															X								
15	heat transfer boundary elements					X	X									X								
16	fluid elements		X	X								X			X									
17	acoustic elements				X																			
18	aerodynamic																	X						

Note: Two-digit problem numbers refer to all problems in the series; three-digit numbers refer to a specific version.

Item	Feature	Problem Numbers																
		1-1	1-2	1-3	1-4	1-5	1-6	1-7	1-8	1-9	1-10	1-11	1-12	1-13	1-14	1-15	1-16	2-1
D	CONSTRAINTS																	
1	single-point	X	X	X	X	X	X	X	X	X	X	X	X	X	X	X	X	X
2	multi-point																	
3	omitted																	
4	free body supports																	X
5	fluid free surface																	
6	boundary symmetry	X	X	X	X				X	X		X	X	X			X	
7	grounded stiffness														X			

Item	Feature	Problem Numbers																							
		3-1	3-3	3-4	3-5	3-6	4-1	5-1	6-1	7-1	7-2	8-1	9-1	9-2	9-3	9-4	10-1	10-2	11-1	11-2	12-1	13-1	14-1	15-1
D	CONSTRAINTS																							
1	single-point	X			X	X	X	X	X		X	X			X	X	X	X	X		X	X	X	X
2	multi-point																X							
3	omitted						X														X			
4	free body supports			X													X				X			
5	fluid free surface		X								X				X									
6	boundary symmetry	X						X	X			X												
7	grounded stiffness									X			X	X		X				X				

Note: Two-digit problem numbers refer to all problems in the series; three-digit numbers refer to a specific version.

Item	Feature	Problem Numbers																																
		1-1-1B	1-2	1-3	1-4	1-12-1	1-12-2	1-13	1-16	2-1	2-2	3-1	3-2	3-3	3-4	3-5	3-6	4-1	5-1	6-1	7-1	7-2	8-1	9-3	9-4	10-1	10-2	11-1	12-1	13-1	14-1	15-1
D	GEOMETRY & PROPERTY																																	
1	property id. default								X																									
2	local coord. system		X			X		X		X	X		X	X			X	X	X			X		X			X				X	X
3	resequenced grid point				X	X	X												X			X		X			X				X	X
4	thermal dep. material			X					X							X																	
5	nonlinear materials															X				X													
6	anisotropic materials				X																													
7	offset bar connection									X																								
8	structural mass	X								X		X						X				X		X			X	X	X	X		X
9	nonstructural mass											X											X										
10	structural elem. damping																				X												
11	fluid compressibility												X		X							X											
12	fluid gravity													X																			
13	multiple fluid harmonic												X																				

Note: Two-digit problem numbers refer to all problems in the series; three-digit numbers refer to a specific version.

Item	Feature	Problem Numbers								
		1-14	2-2	7-1	9-1	10-1	11-1	12-1	14-1	15-1
F	MATRIX OPTIONS									
1	general element	X					X			
2	direct input matrices				X					
3	transfer functions					X				
4	extra points				X	X				
5	direct damping matrix input				X	X				
6	modal damping						X	X		
7	substructuring		X							
8	cyclic symmetry								X	X
9	uniform damping			X						

Note: Two-digit problem numbers refer to all problems in the series; three-digit numbers refer to a specific version.

Item	Feature	Problem Numbers																								
		1-1	1-1-1A	1-2	1-3	1-4	1-5	1-6	1-7	1-8	1-9	1-10	1-11	1-13-1	1-13-2	1-13-3	1-14	1-15	1-16	2-1	4-1	5-1	6-1	11-1-1A	13-1	14-1
G	LOADING																									
	Static																									
1	concentrated	X	X			X	X		X	X	X						X		X	X		X	X		X	
2	pressure			X										X	X	X		X								X
3	gravity																				X			X		
4	thermal				X			X			X	X	X	X	X	X										
5	harmonic						X											X								
6	centrifugal field																			X						
7	enf. elem. deform.																							X		
8	enf. displacement																									

Note: Two-digit problem numbers refer to all problems in the series; three-digit numbers refer to a specific version.

Item	Feature	Problem Numbers							
		8-1	9-1	9-2	9-3	9-4	11-1-1	11-2	12-1
G	LOADING								
	Dynamic								
9	tabular	X	X				X	X	
10	direct time func.				X	X	X		X
11	phase angles						X		
12	time lags		X				X		
13	combinations						X		
14	initial conditions		X	X		X			
15	random						X		

Item	Feature	Problem Numbers			
		1-12	3-5	3-6	9-4
G	LOADING				
	Heat Transfer				
16	volume heating		X		
17	area heating	X			X
18	radiation heating			X	
19	enf. bdy. temp.	X	X	X	X

Note: Two-digit problem numbers refer to all problems in the series; three-digit numbers refer to a specific version.

Item	Feature	Problem Numbers										
		1-1-2	1-9	1-10	1-13	1-14	1-16	9-1	10-2	11-1	14-1	15-1
H	EXECUTION OPTIONS											
	Multiple Solutions											
1	loads	X	X		X	X	X			X		
2	boundary constraints			X								
3	cyclic symmetry										X	X
4	direct input matrices							X				
5	aerodynamic coefficients								X			

Item	Feature	Problem Numbers											
		1-1-1	1-1-1A	1-1-1B	1-2-1	1-2-1A	1-4-1	1-4-1A	2-2	10-1-1	10-2-1	11-1-1	11-1-1A
H	EXECUTION OPTIONS												
	Operational												
6	checkpoint	X			X		X					X	
7	restart-C.C. change		X	X		X		X					X
8	restart-R.F. change			X									X
9	restart-B.D. change			X									X
10	DMAP alters									X	X	X	
11	substructuring								X				

Note: Two-digit problem numbers refer to all problems in the series; three-digit numbers refer to a specific version.

Item	Feature	Problem Numbers																					
		1-1-1	1-1-2	1-1-3	1-1-4	1-2	1-2-1A	1-3	1-4	1-4-1A	1-5	1-6	1-7	1-8	1-9	1-10	1-11	1-12	1-13	1-14	1-15	1-16	2-1
I	OUTPUT																						
	Print/Punch																						
1	point	X	X	X	X	X	X	X	X	X	X	X	X	X	X	X	X	X	X	X	X	X	X
2	element	X	X	X	X	X	X	X		X	X	X	X	X	X	X	X	X	X	X		X	X
3	subcase level change														X							X	
4	SØRT2		X																				
5	magnitude/phase																						
6	mode acceleration																						
7	solution set																						
8	frequency set																						
9	punched output	X				X			X									X				X	
10	weight and balance																					X	X
11	grid point force balance			X																			
12	element strain energy				X																		

Note: Two-digit problem numbers refer to all problems in the series; three-digit numbers refer to a specific version.

Item	Feature	Problem Numbers																							
		3-1	3-2	3-3	3-4	3-5	4-1	5-1	6-1	7-1	7-2	8-1	9-1	9-2	9-3	9-4	10-1	11-1	11-1-1A	11-2	12-1	13-1	14-1	15-1
I	OUTPUT																							
	Print/Punch																							
1	point	X	X	X	X	X	X	X	X	X	X	X	X	X	X	X	X	X	X	X	X	X	X	X
2	element				X	X	X	X	X									X	X		X	X		
3	subcase level change						X	X														X		
4	SØRT2												X	X	X	X		X		X	X			
5	magnitude/phase											X					X	X		X				
6	mode acceleration																			X				
7	solution set												X				X			X	X			
8	frequency set											X												
9	punched output					X												X						
10	weight and balance	X					X										X	X			X			
11	grid point force balance																							
12	element strain energy																							

Note: Two-digit problem numbers refer to all problems in the series; three-digit numbers refer to a specific version.

Item	Feature	Problem Numbers											
		1-2-1	1-15	1-16	3-1	3-4	5-1	9-1	9-3	10-2	11-1	11-2	12-1
I	OUTPUT												
	Plot												
13	structure-undeformed	X	X	X	X	X	X						
14	structure-deformed	X		X	X	X	X						X
15	curve vs. frequency										X	X	
16	curve vs. time							X	X				X
17	curve vs. subcase												
18	curve-aerodynamic									X			

Note: Two-digit problem numbers refer to all problems in the series; three-digit numbers refer to a specific version.

REFERENCES FOR DEMONSTRATION PROBLEMS SOLUTIONS

1. Richard H. MacNeal and Stanley U. Benscoter, "Analysis of Multicell Delta Wings on Cal-Tech Analog Computer", NACA TN 3114, 1953.

2. George W. Zender, "Comparison of Theoretical Stresses and Deflections of Multicell Wings with Experimental Results Obtained from Plastic Models", NACA TN 3913.

3. Richard H. MacNeal, ELECTRIC CIRCUIT ANALOGIES FOR ELASTIC STRUCTURES. John Wiley & Sons, 1962.

4. S. Timoshenko, THEORY OF PLATES AND SHELLS. McGraw-Hill, 1940.

5. Richard R. Heldenfels and William M. Roberts, "Experimental and Theoretical Determination of Thermal Stresses in a Flat Plate", NACA TN 2769, 1952.

6. B. Budiansky and P. P. Radkowski, "Numerical Analysis of Unsymmetric Bending of Shells of Revolution", AIAA Journal, August, 1963.

7. C. O. Harris, INTRODUCTION TO STRESS ANALYSIS. MacMillan Co., 1959.

8. W. F. Stokey, "Vibration of Systems Having Distributed Mass and Elasticity", Chap. 7, SHOCK AND VIBRATION HANDBOOK, C. M. Harris and C. E. Crede, Editors, McGraw-Hill, 1961.

9. S. Timoshenko, THEORY OF ELASTIC STABILITY. McGraw-Hill, 1936.

10. J. L. Swedlow, "The Thickness Effect and Plastic Flow in Cracked Plates", Office of Aerospace Research, USAF, ARL 65-216.

11. I. S. Sokolnikoff and R. M. Redheffer, MATHEMATICS OF PHYSICS AND MODERN ENGINEERING. McGraw-Hill, 1958.

12. H. Yeh and J. I. Abrams, MECHANICS OF SOLIDS AND FLUIDS. Vol. I, Particle and Rigid Body Mechanics. McGraw-Hill, 1960.

13. C. J. Savant, BASIC FEEDBACK CONTROL SYSTEM DESIGN. McGraw-Hill, 1958.

14. C. T. Wang, "APPLIED ELASTICITY", McGraw-Hill, 1953.

15. S. H. Crandall and W. D. Mark, RANDOM VIBRATION IN MECHANICAL SYSTEMS. Academic Press, 1963.

16. J. G. Berry and E. Reissner, "The Effect of an Internal Compressible Fluid Column on the Breathing Vibrations of a Thin Pressurized Cylindrical Shell", Journal of the Aeronautical Sciences, Vol. 25, No. 5, pp 288-294, May 1958.

17. B. Budiansky, "Sloshing of Liquids in Circular Canals and Spherical Tanks", Journal of the Aerospace Sciences, Vol. 27, No. 3, pp 161-173, March 1960.

18. B. Rayleigh, THE THEORY OF SOUND. Section 330, 331, MacMillan Co., 1945.

19. Herting, David N.; Joseph, Jerrard A.; Kuusinen, Loren R.; and MacNeal, Richard H.: Acoustic Analysis of Solid Rocket Motor Cavities by a Finite Element Method. NASA TM X-2378, September, 1971, pp. 285-324.

20. Biljaard, P. P., ASME "Pressure Vessel and Piping Design", Welding Journal Research Supplement, 1954, pp 567-575.

21. Pope, G. G., "Optimum Design of Stresses Skin Structures", AIAA Journal, Vol. 11, No. 11, pp 1545-1552, November 1973.

22. Yates, E. C. and R. M. Bennett, "Use of Aerodynamic Parameters From Nonlinear Theory in Modified-Strip-Analysis Flutter Calculations for Finite-Span Wings at Supersonic Speeds; NASA TN D-1824, July 1963.

23. Timoshenko, S. P., Theory of Elastic Stability, McGraw-Hill, 1961, p 159.

24. Timoshenko, S. P. and J. N. Goodier, Theory of Elasticity, McGraw-Hill, Inc., 1961.

25. Spiegel, Murray R.: Applied Differential Equations. Prentice-Hall, Inc., 1958, pp. 105-108.

RIGID FORMAT No. 1, Static Analysis

Delta Wing with Biconvex Cross Section (1-1-1)
Delta Wing with Biconvex Cross Section Using QDMEM1 and QDMEM2 Elements (1-1-2)
Delta Wing with Biconvex Cross Section Using QDMEM1 Elements (1-1-3)
Delta Wing with Biconvex Cross Section Using QDMEM2 Elements (1-1-4)

This problem illustrates the use of various NASTRAN elements in the solution of an actual structural problem. Figure 1 shows the delta wing to be modeled and Figures 2 and 3 shows the finite element model. The delta wing model is composed of membrane, shear panel and rod elements. Due to the existence of symmetry or antisymmetry in the structure and loading conditions, only one-quarter of the wing needs to be modeled. The midplane of the wing (the plane dividing the wing into upper and lower halves) is a plane of symmetry as is the center plane (the plane that divides the wing into left and right halves). The loading conditions are antisymmetrical with respect to the midplane of the wing and symmetric with respect to the center plane.

The surface skin of the wing is modeled with membrane elements while the ribs and spars are modeled with a combination of shear panels and rods. The shear load carrying capability of ribs and spars is represented by shear panels. The bending stiffness of the ribs and spars is modeled with rod elements placed in the plane of the skin surface.

Since a quarter model is used, the loading conditions require that an antisymmetric boundary be provided on the midplane and a symmetric boundary must be provided on the center plane. These boundary conditions are provided by constraining all grid points on the midplane in the x and y directions and all grid points on the center plane in the x direction. Supports for the structure are provided by constraining grid points 13, 33, 53, 73 and 93 in the z direction. Since no rotational rigidity is provided by the elements used in the model, all rotational degrees of freedom have been removed by the use of the GRDSET card.

Figure 4 shows the two loading conditions analyzed. The modified restart capability is used to perform the analysis associated with the second loading condition. The ability of NASTRAN to change rigid formats on a restart is demonstrated by the third case. The natural modes of the structure are extracted using the inverse power method. Since the symmetric boundary conditions are used, only the modes with symmetric motion about the center line will be extracted. If the unsymmetric modes were required, a separate run with the appropriate boundary conditions could be submitted.

A comparison of the displacements due to the loads calculated by NASTRAN and the experimentally measured displacements from Reference 2 is shown in Tables 1 and 2. Also included in these tables are the displacements calculated on a passive analog computer (Reference 1). A comparison of the natural frequencies and modal displacements is shown in Tables 3 and 4.

Another variation of this problem can be obtained by replacing the quadrilateral membrane elements (CQDMEM) with the newer CQDMEM1 and CQDMEM2 elements. This modification demonstrates the ability to reproduce previously derived theoretical results. Table 5 shows the difference in displacements obtained when elements 1 through 9 are CQDMEM1 elements and the other quadrilaterals are CQDMEM2 elements.

Table 1 Comparison of NASTRAN and Experimental Deflections - Concentrated Load on Outboard Trailing Edge

GRID NUMBER	Z DISPLACEMENT		
	NASTRAN	EXPERIMENTAL	ANALOG
14	-.082	-.08	-.080
15	- 221	-.22	-.210
16	-.424	-.39	-.400
34	-.063	-.07	-.061
35	-.162	-.16	- 157
36	-.293	-.28	-.286
54	-.043	-.05	-.044
55	-.104	-.12	-.144
74	-.025	-.03	-.030

Table 2 Comparison of NASTRAN and Experimental Deflections - Concentrated Load on Outboard Leading Edge

GRID NUMBER	Z DISPLACEMENT		
	NASTRAN	EXPERIMENTAL	ANALOG
14	-.063	- 06	- 060
15	-.163	-.15	- 157
16	- 293	-.28	- 286
34	- 057	-.06	- 057
35	-.148	-.15	-.150
36	-.280	- 30	-.290
54	-.046	-.05	- 048
55	- 118	- 13	-.127
74	- 030	-.04	- 035

TABLE 3 Comparison of NASTRAN and analog computer analysis eigenvalues.

Mode No.	NASTRAN (cps.)	ANALOG (cps.)
1	40.9	41.3
2	115.3	131.0
3	156.2	167.0

TABLE 4 Comparison of mode displacements for first mode.

GRID NUMBER	Z DISPLACEMENT	
	NASTRAN	ANALOG
14	.250	.273
15	.601	.630
16	1.000	1.000
34	.210	.239
35	.504	.558
36	.854	.902
54	.162	.192
55	.391	.462
74	.112	.148

TABLE 5. Comparison of Z Displacements

Grid Point	Trailing Edge Load		Leading Edge Load	
	CQDMEM Elements	CQDMEM1 and CQDMEM2 Elements	CQDMEM Elements	CQDMEM1 and CQDMEM2 Elements
14	-.082	- 082	- 063	-.064
15	-.221	- 224	-.163	-.167
16	-.424	-.433	- 293	-.300
34	-.063	-.064	- 057	-.059
35	-.162	- 166	- 148	-.154
36	-.293	- 300	-.280	-.294
54	-.043	- 044	- 046	- 047
55	-.104	-.108	-.118	- 123
74	-.025	-.026	- 030	-.031

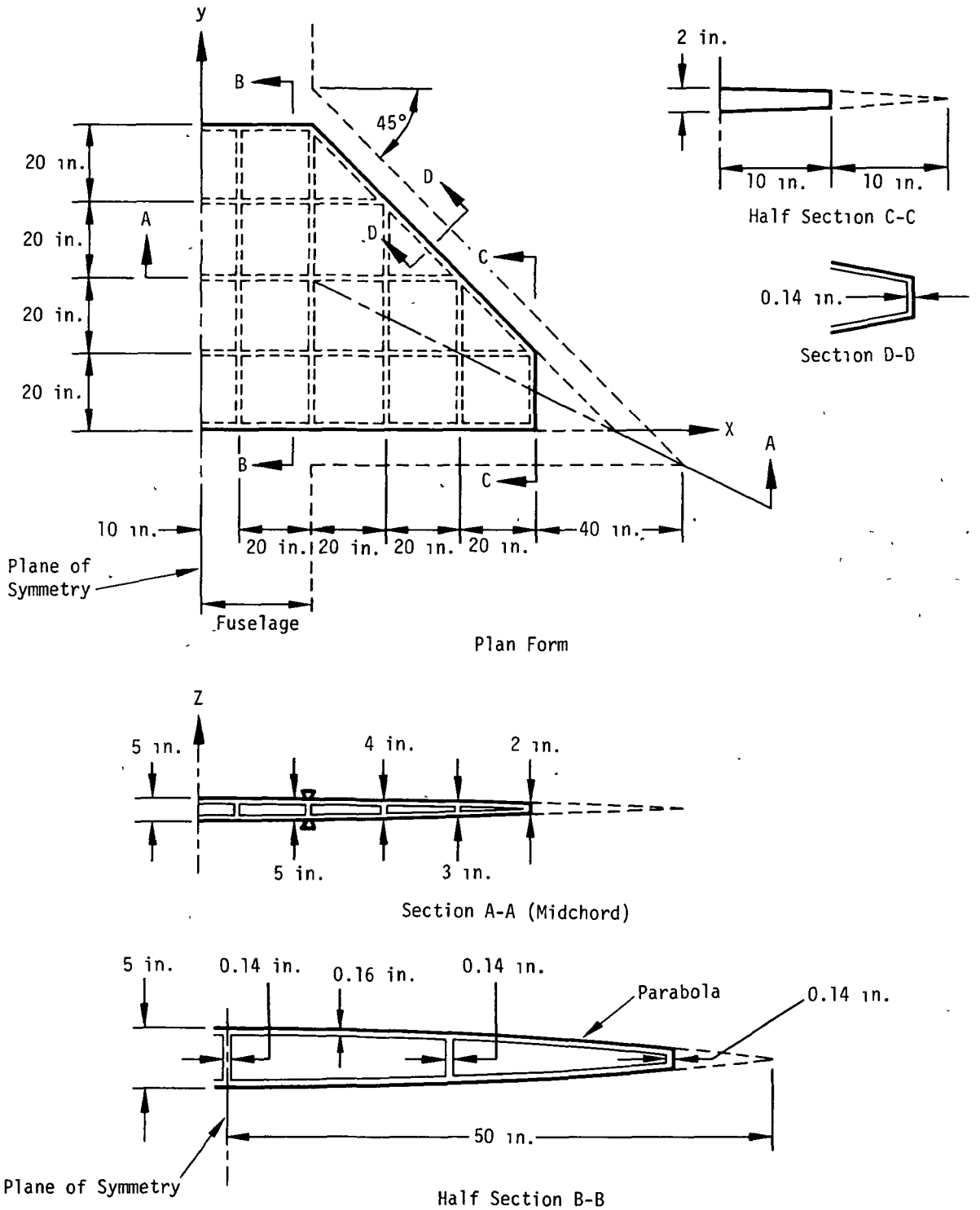

Figure 1. Delta wing with biconvex section.

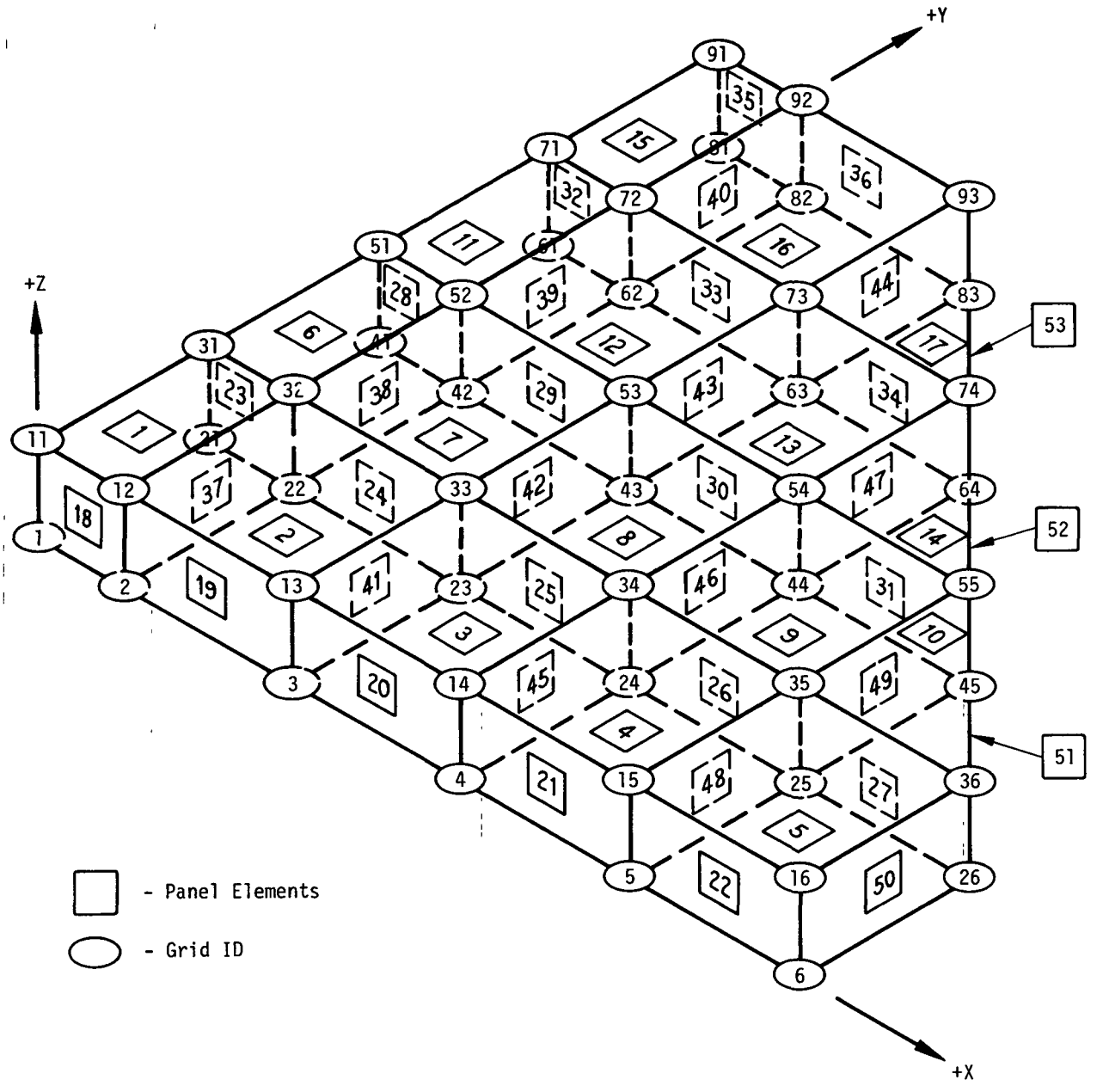

Figure 2. Delta wing with biconvex section model.

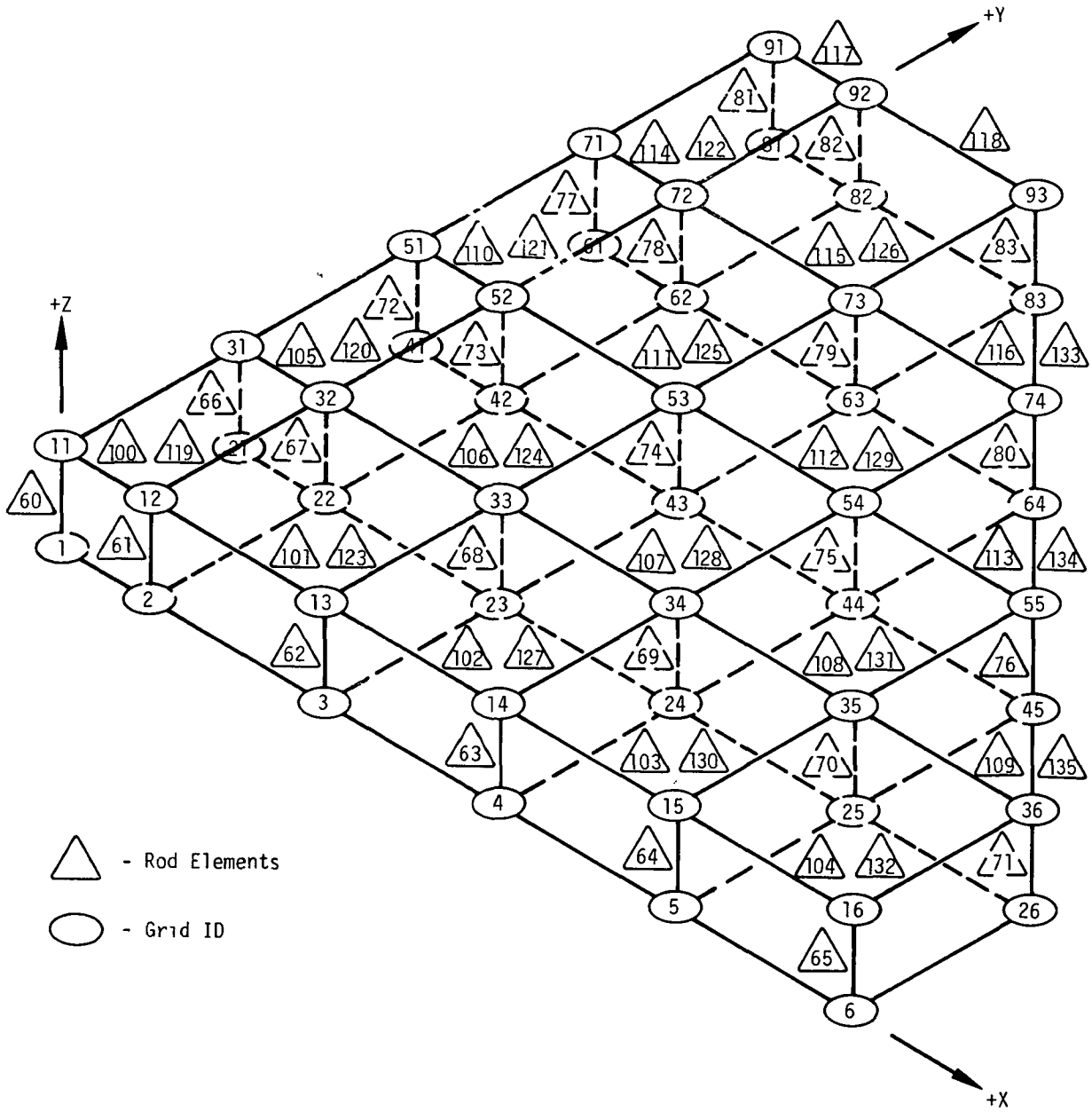

Figure 3. Delta wing with biconvex section model.

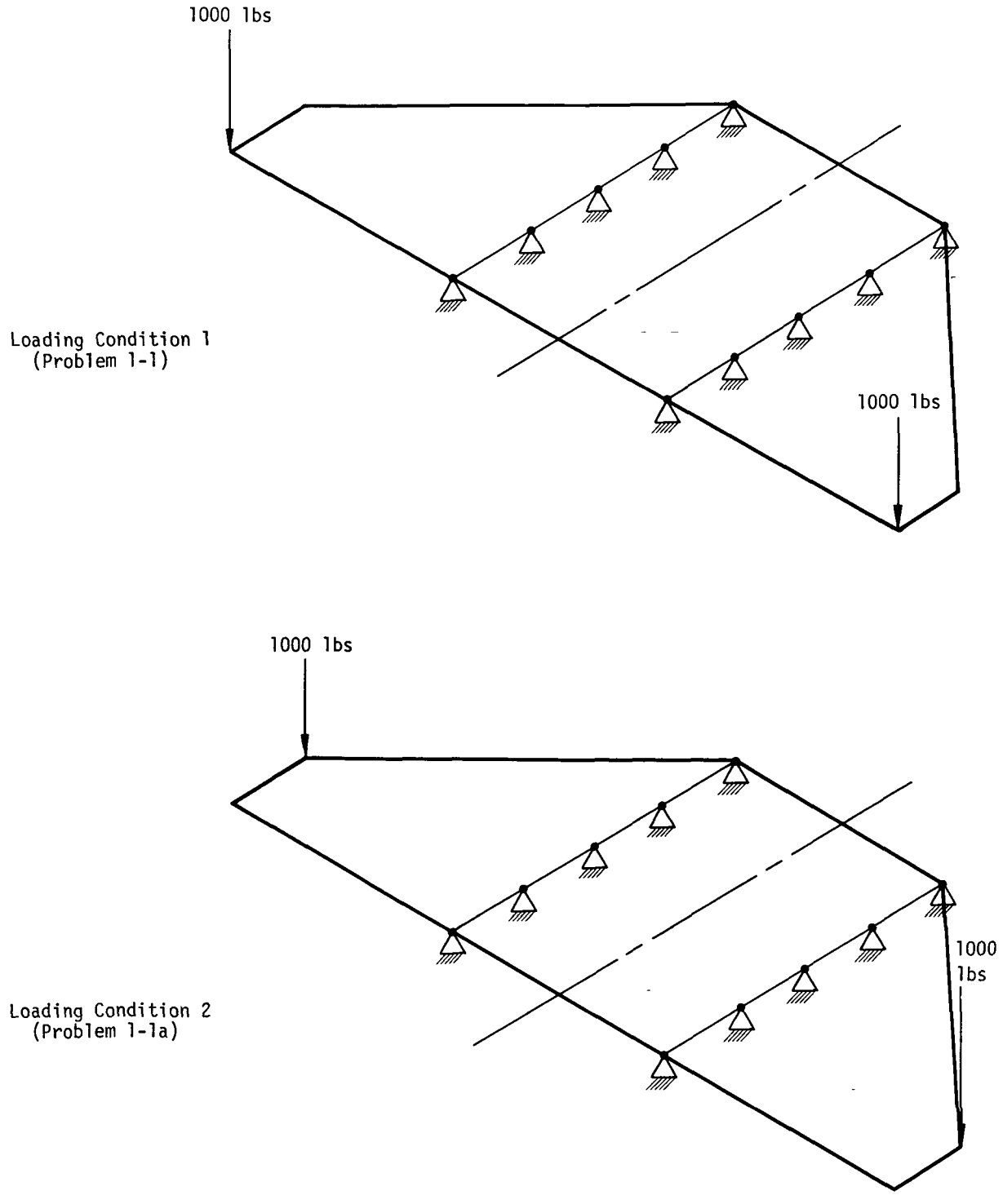

Figure 4. Loading conditions for Delta wing.

RIGID FORMAT No. 1, Static Analysis

Spherical Shell with Pressure Loading (1-2-1)

This problem demonstrates the finite element approach to the modeling of a uniform spherical shell. A spherical coordinate system is chosen to describe the location and displacement degrees of freedom at the grid points. Triangular plate elements are chosen to provide a nearly uniform pattern. Two symmetric boundaries are used to analyze the structure with a symmetric pressure load. Figure 1 describes the model.

Two boundary conditions are used on the outside edge to demonstrate the ability of NASTRAN to restart with different constraint sets by simply changing the case control request. The effective boundary constraints are shown in Figure 2. The membrane support, under a uniform pressure load, should result in uniform in-plane compression in two directions. The clamped support produces bending moments in addition to in-plane stresses.

The grid point numbering sequence used minimizes the computer time required to perform the triangular decomposition of the constrained stiffness matrix. This numbering sequence results in a partially banded matrix with all terms outside the band located in a single column. The grid points are arranged to form five rings; the center point is sequenced last.

Analytic solutions for the continuum shell were obtained from Reference 4 using the first 20 terms of the series shown in Equation (j) of Section 94. Comparisons of the answers obtained using NASTRAN and the analytical solution for the membrane boundary condition are shown in Figures 3 and 4. Also included on these figures are the NASTRAN answers obtained using a 10-ring model Figures 5 thru 7 show a comparison of the NASTRAN answers and the analytical solution for the shell with a clamped boundary.

The slight differences between theoretical and computed answers are due to: 1) The finite element model assumes a constant in-plane stress and a linearly varying bending moment for each element. In the clamped edge case these quantities have large changes, and 2) the irregularities of the finite element model cause some extra coupling between the bending and membrane action. Since the elements are planar the curvature is modeled, in effect, by the dihedral angles between elements. Since the elements are different sizes and shapes these dihedral angles vary, which results in slight differences in curvature that cause small errors.

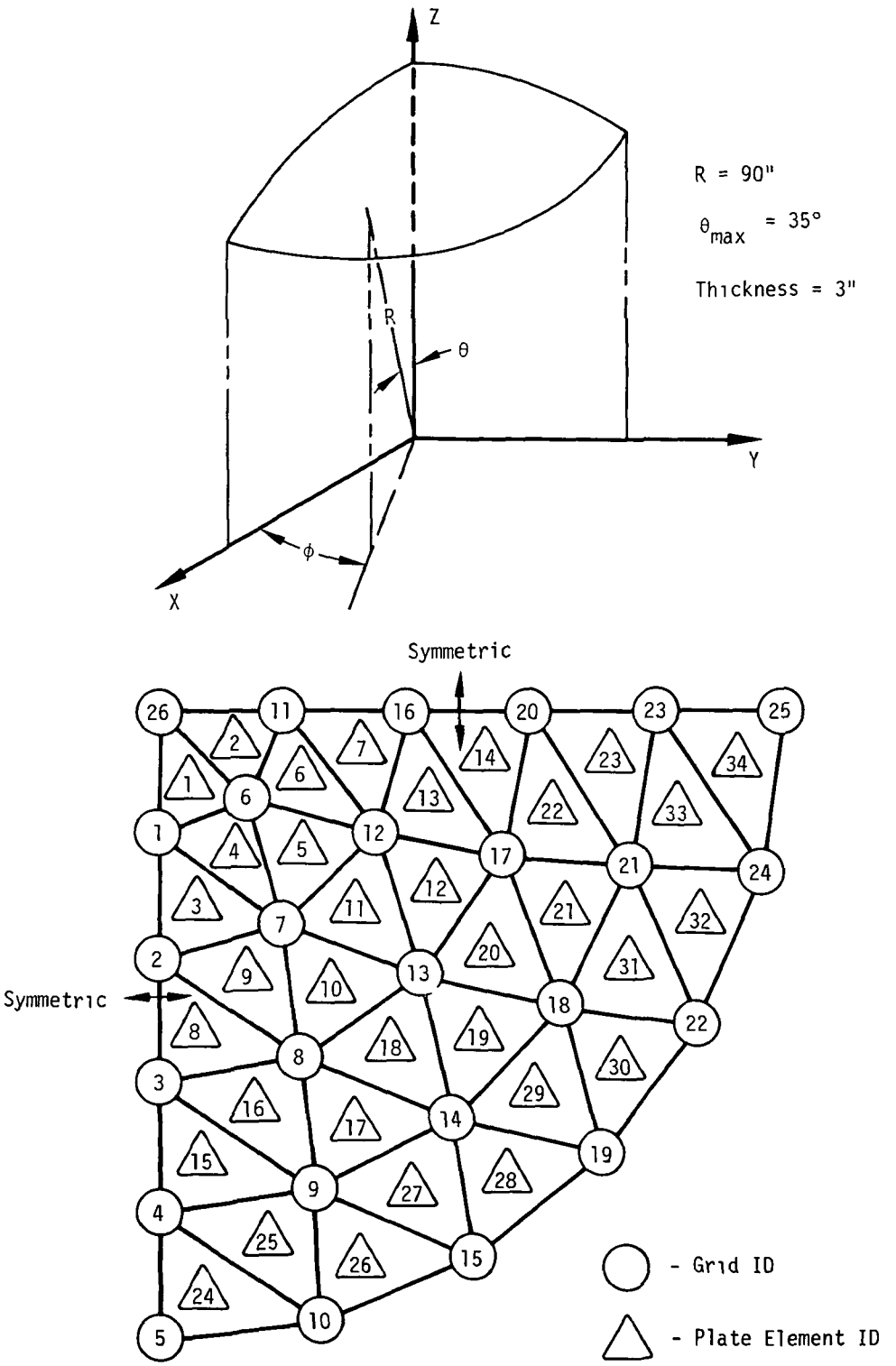

Figure 1. 5 ring spherical shell model.

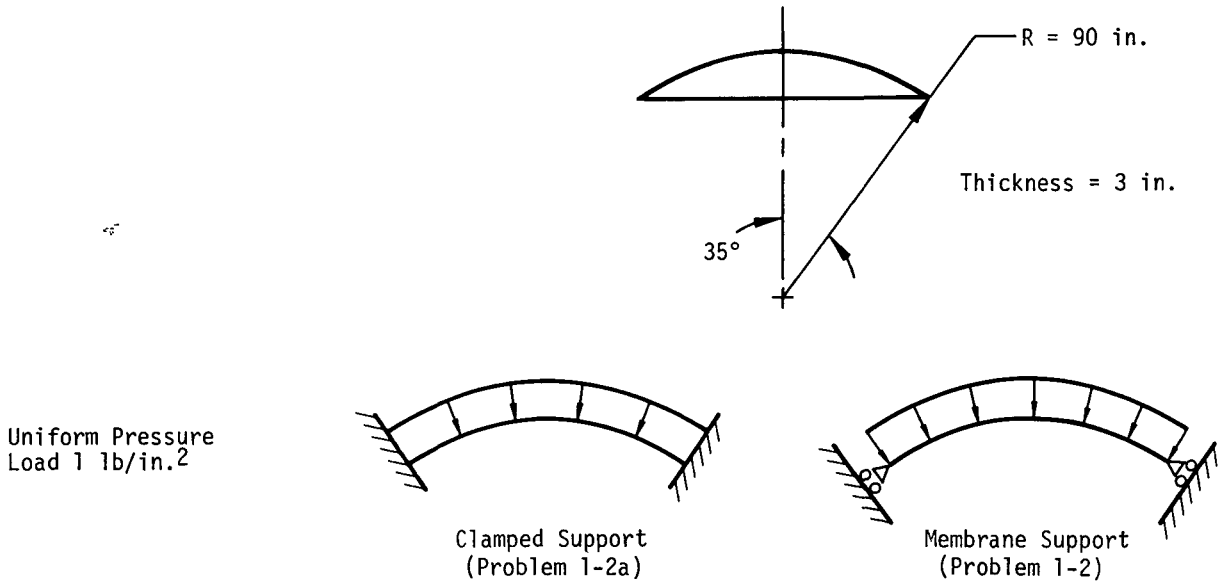

Figure 2. Spherical shell loading and edge support conditions.

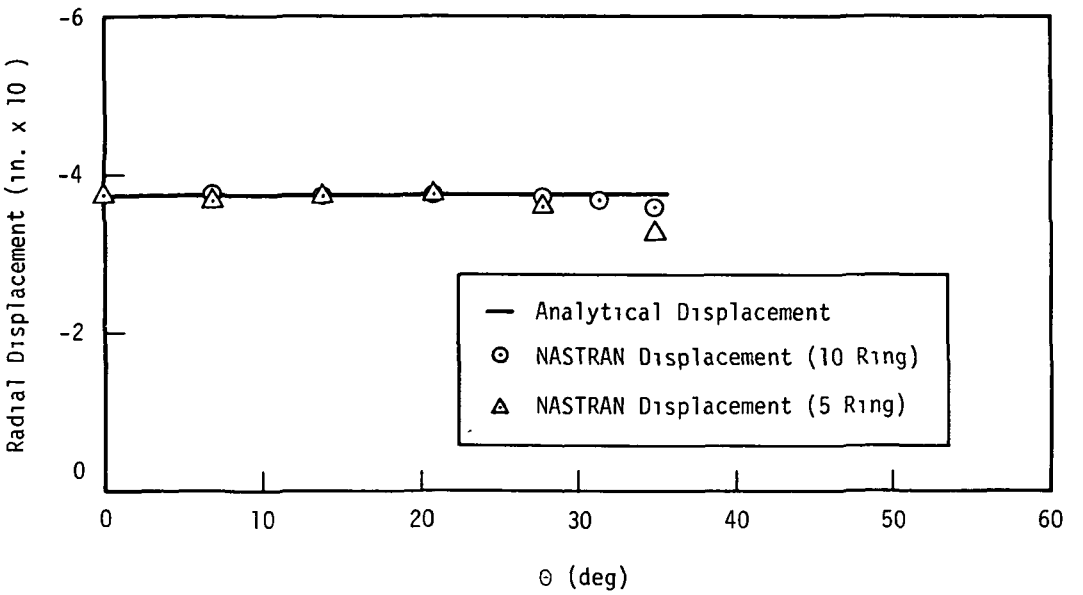

Figure 3. Comparison of NASTRAN and analytical displacements for spherical shell - membrane boundary

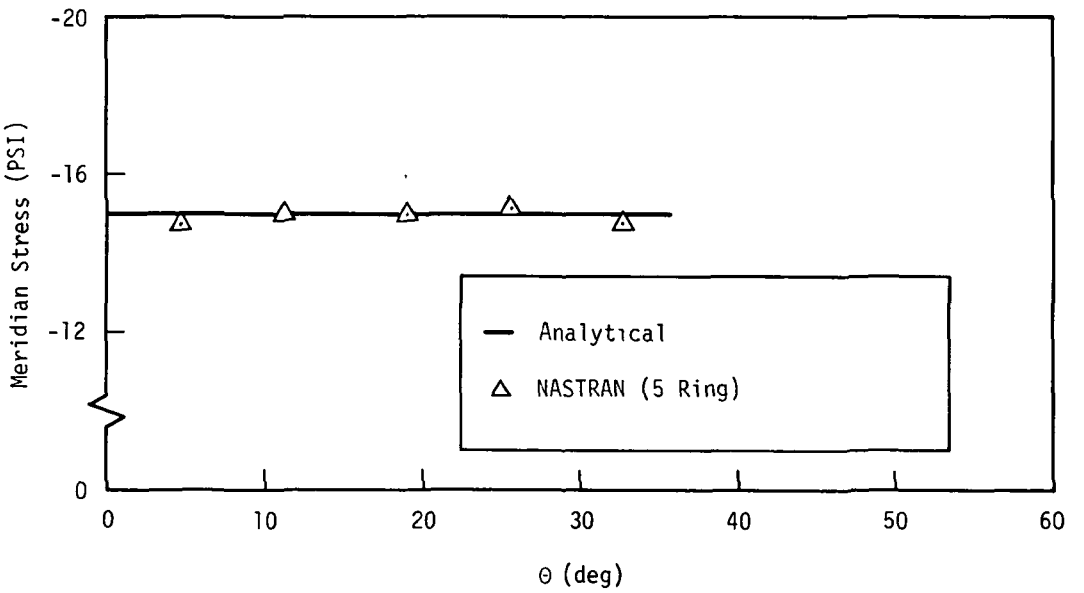

Figure 4. Comparison of NASTRAN and analytical stresses for spherical shell - membrane boundary

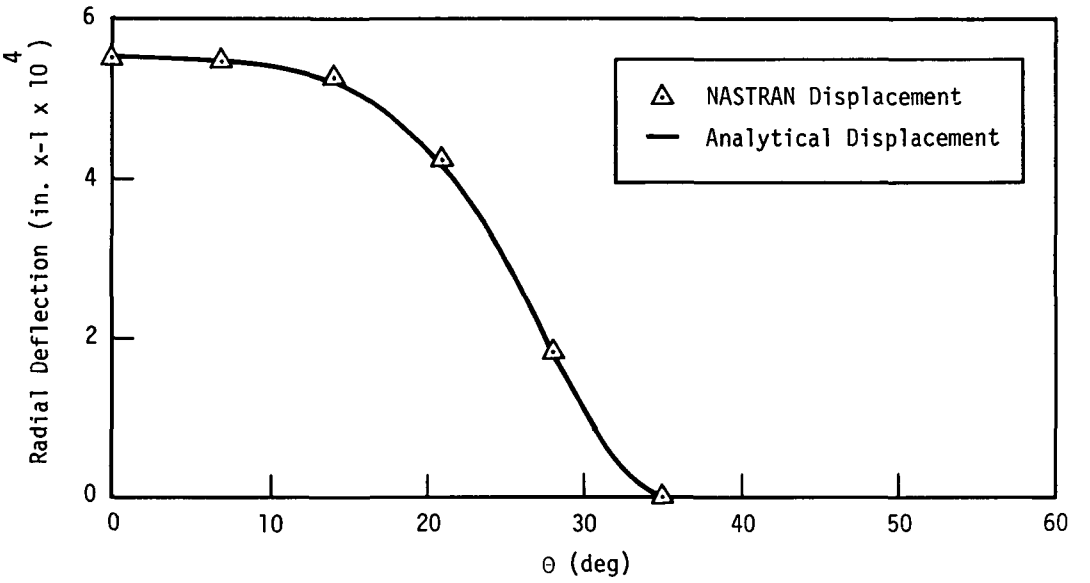

Figure 5. Comparison of NASTRAN and analytical displacements for 5 ring spherical shell - clamped boundary.

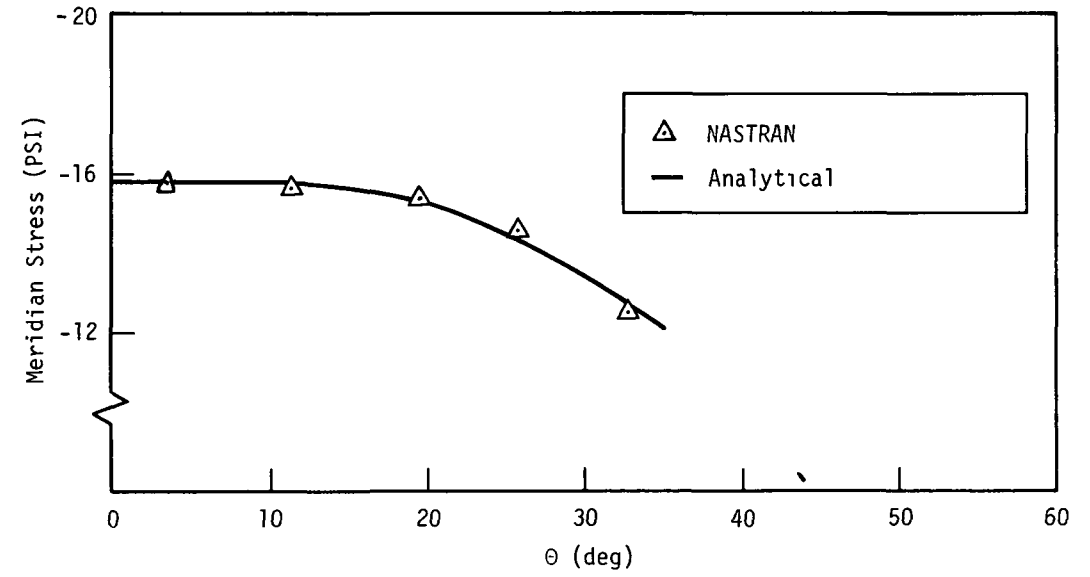

Figure 6. Comparison of NASTRAN and analytical meridian stress for 5 ring spherical shell - clamped boundary.

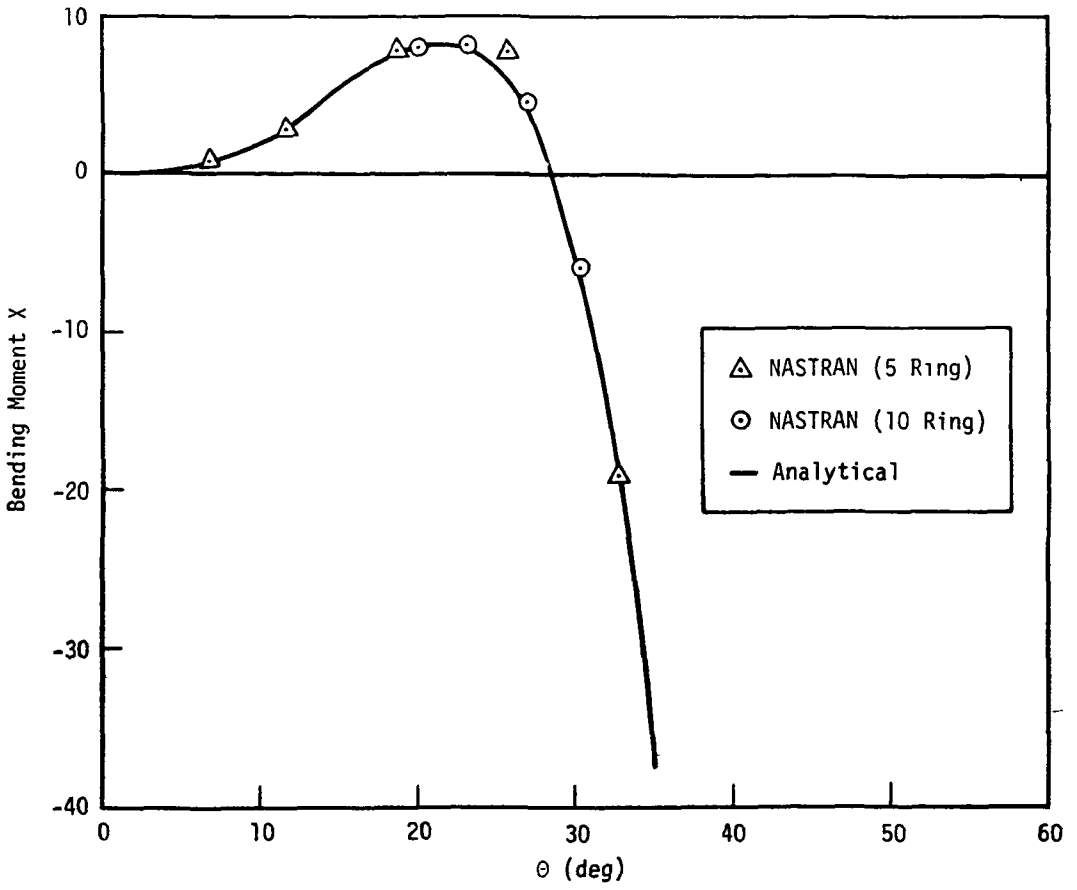

Figure 7. Comparison of NASTRAN and analytical bending moment for 5 ring spherical shell - clamped boundary.

RIGID FORMAT No. 1, Static Analysis

Free Rectangular (QDMEM) Plate with Thermal Loading (1-3-1)
Free Rectangular (QDMEM1) Plate with Thermal Loading (1-3-2)
Free Rectangular (QDMEM2) Plate with Thermal Loading (1-3-3)

This problem demonstrates the use of thermal loading conditions and temperature dependent materials. The model, a rectangular plate shown in Figure 1, is given a temperature gradient which causes internal loads and elastic deflections. Since there are two planes of symmetry, only one-quarter of the structure needs to be modeled (the shaded portion shown in Figure 1).

The finite element model for the quarter section is shown in Figure 2. Figure 3 shows the thermal loading condition. The temperature load is constant in the y direction and symmetric about the y-axis. Since membrane elements are used to model the structure, it is necessary to remove all rotational degrees of freedom and translational degrees of freedom normal to the plate. The symmetric boundary conditions were modeled by constraining the displacements normal to the planes of symmetry. The material used has temperature dependent elasticity (as defined in Reference 5) therefore the INPUT module cannot be used for this application. The CNGRNT bulk data card can be used if the congruency is defined in one direction.

Figures 4 and 5 show a comparison of NASTRAN stresses and the experimentally measured stresses reported in Reference 5.

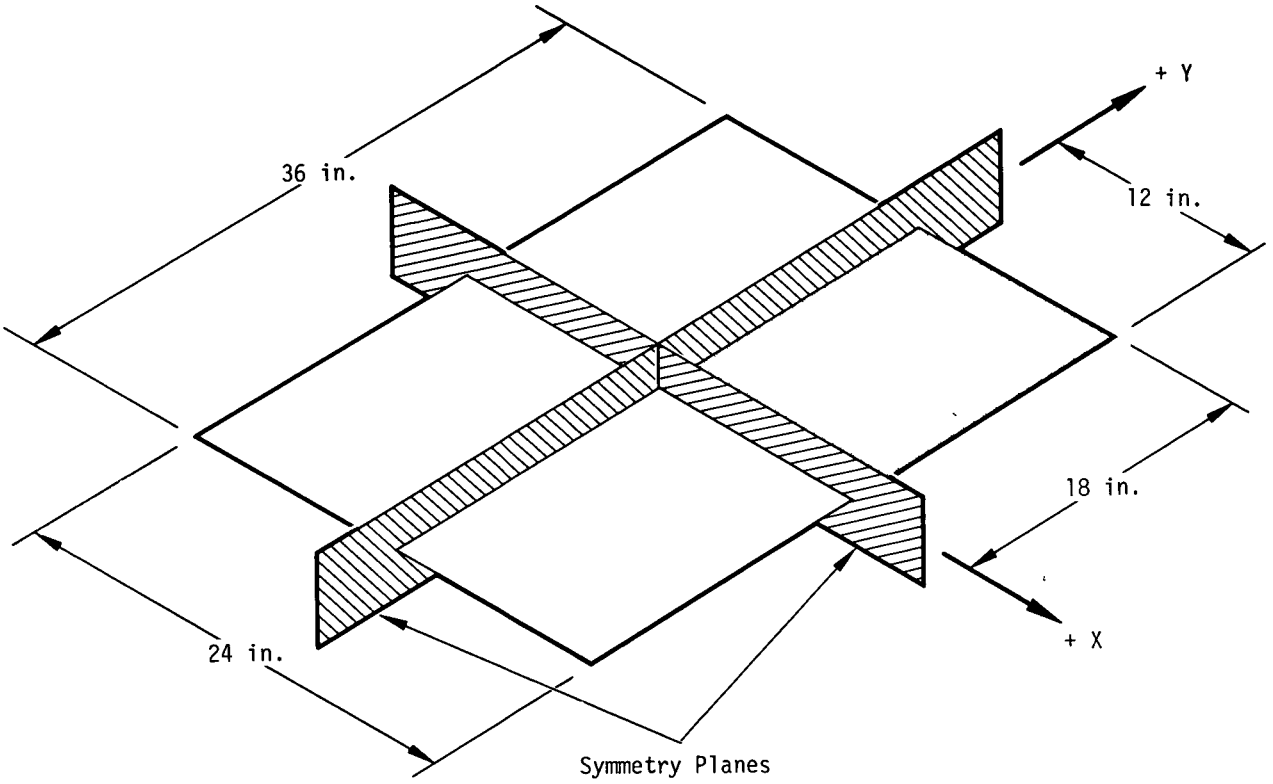

Note: Shaded area is quarter of plate modeled.

Figure 1. Free plate structure.

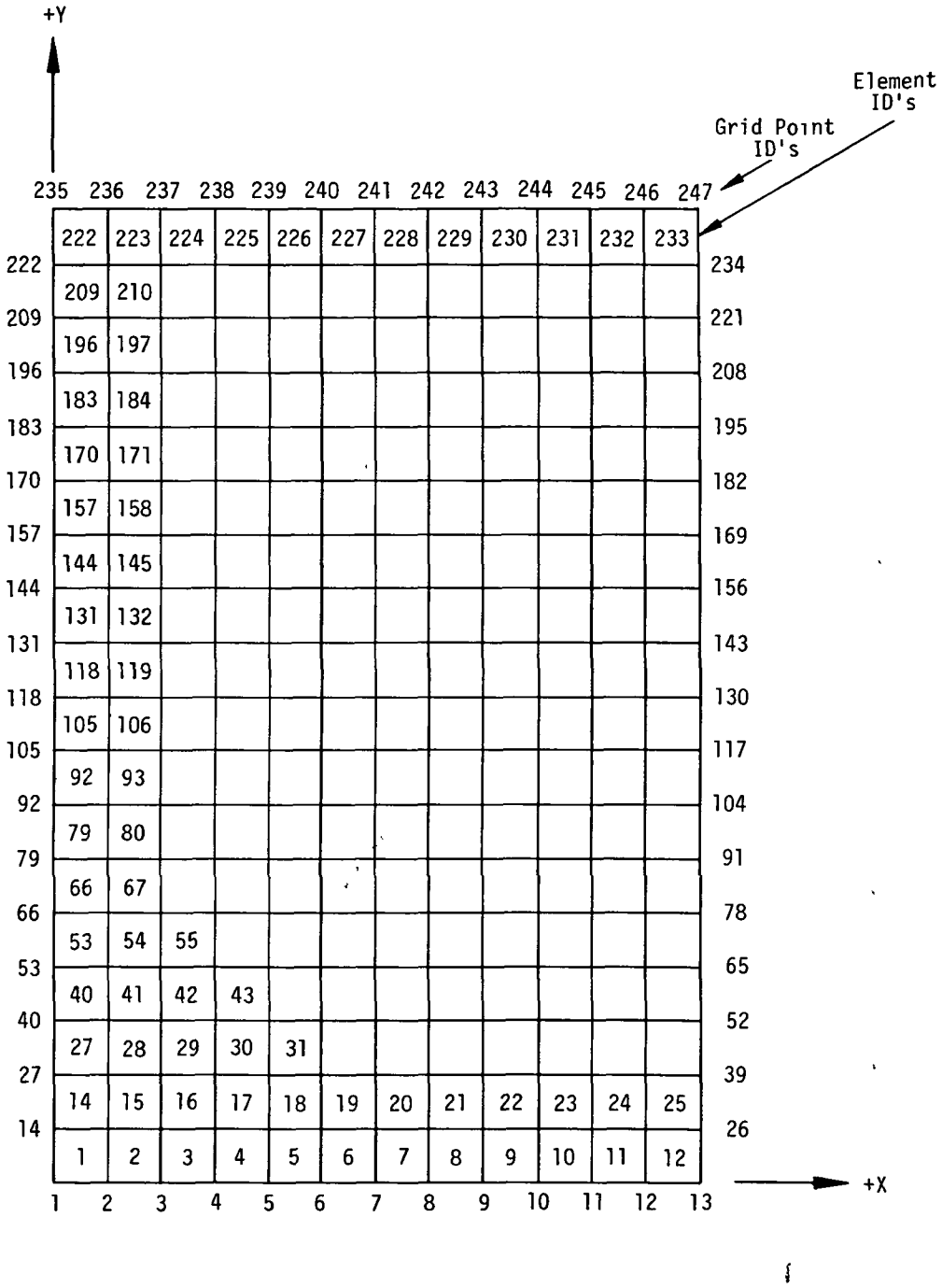

Figure 2. Free rectangular plate model.

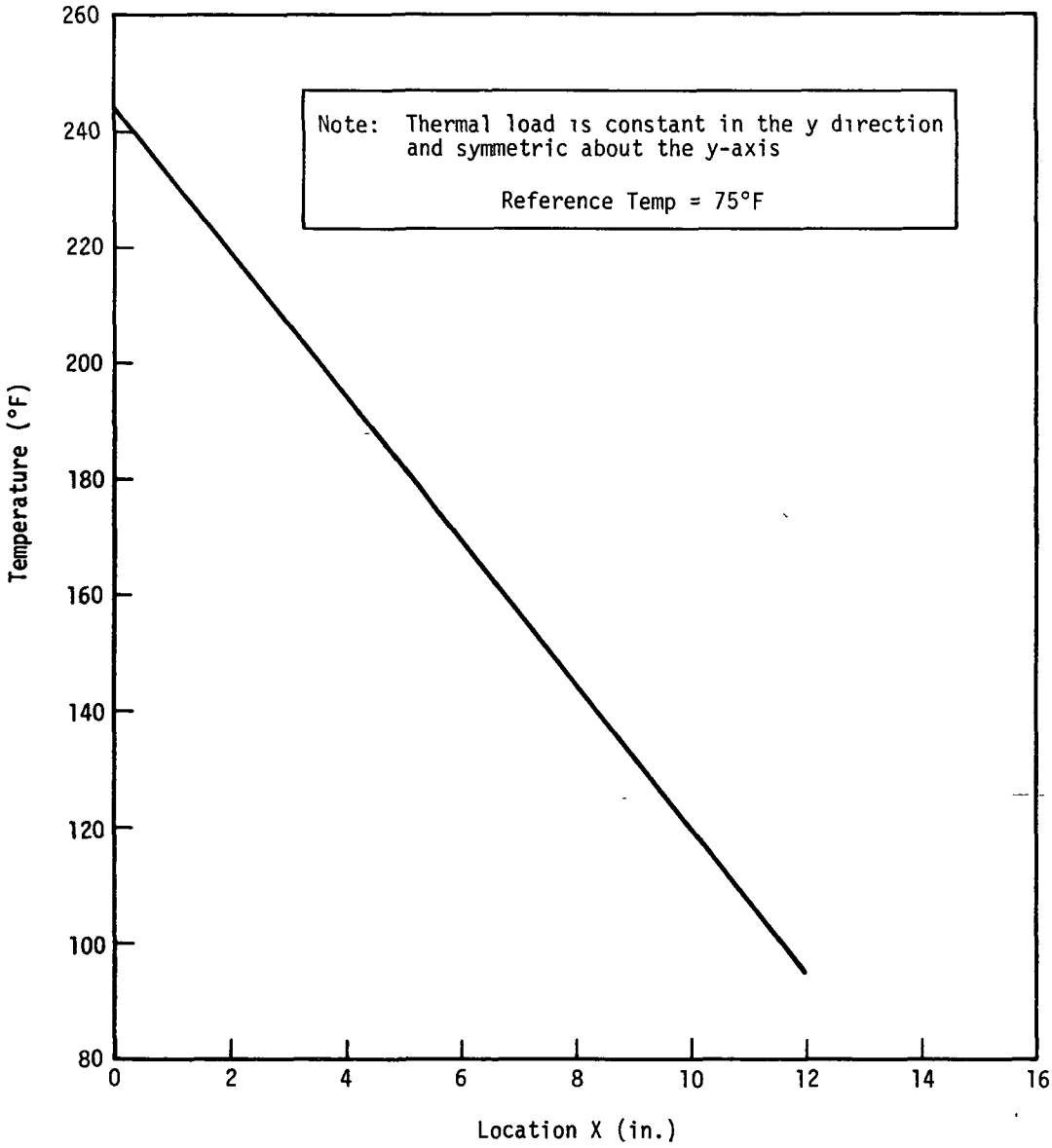

Figure 3. Thermal load applied to free rectangular plate.

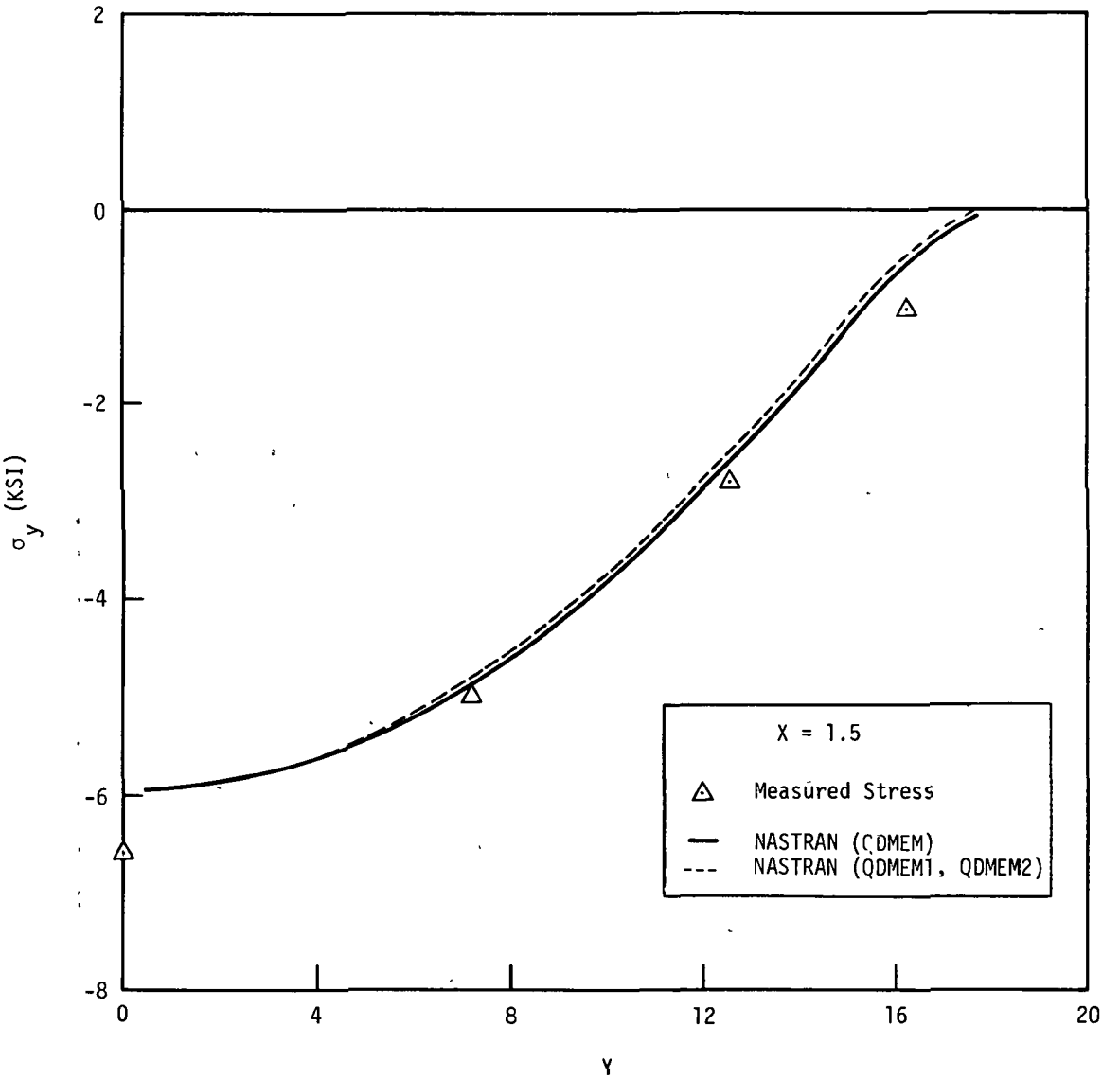

Figure 4. Comparison of NASTRAN and experimental stresses for free rectangular plate with thermal loading - temperature dependent properties.

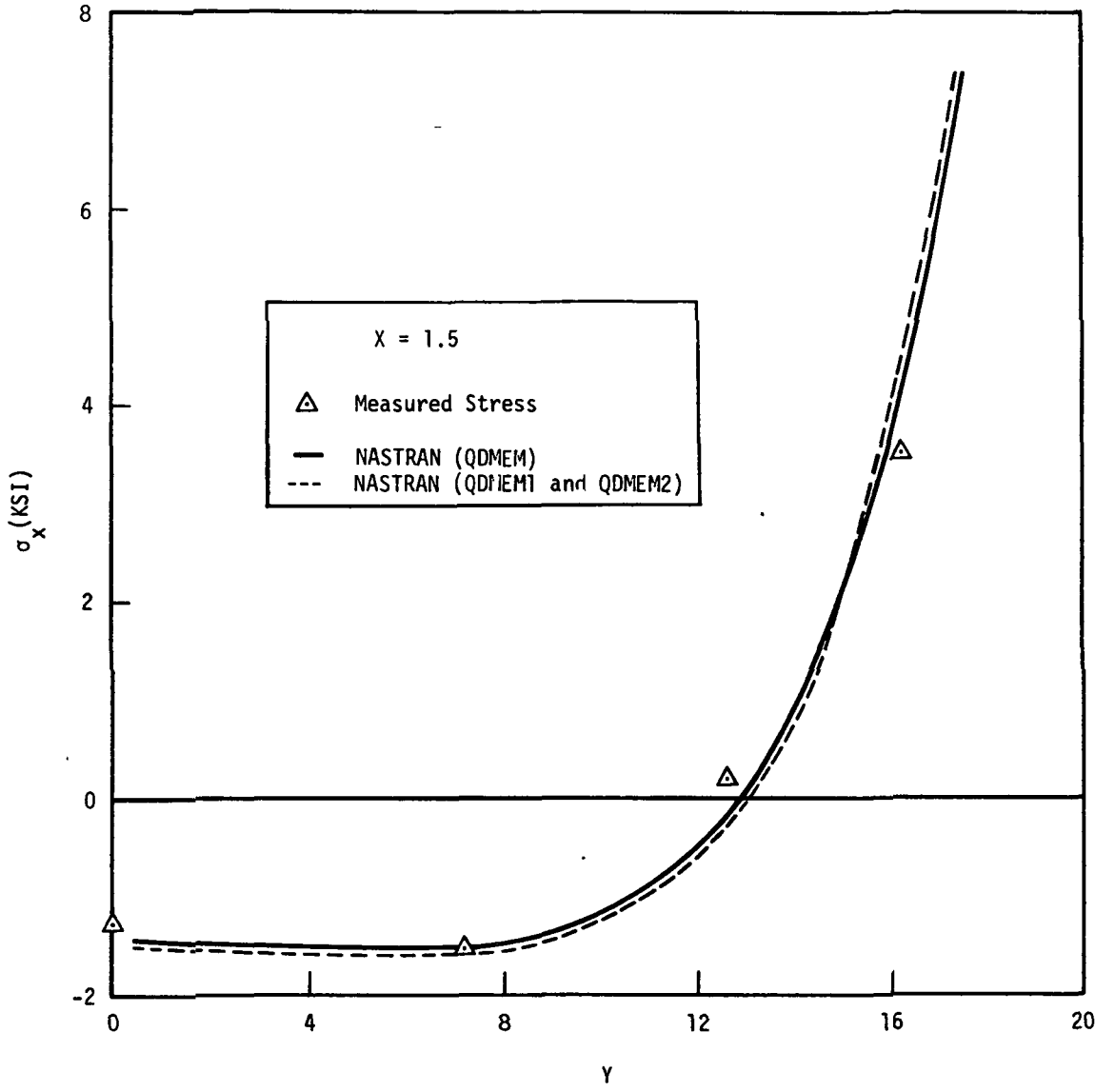

Figure 5. Comparison of NASTRAN and experimental stresses for free rectangular plate with thermal loading - temperature dependent properties

RIGID FORMAT No. 1, Static Analysis

Long, Narrow, 5 x 50 Orthotropic Plate (1-4-1)
Long, Narrow, 5 x 60 Orthotropic Plate (1-4-2)
Long, Narrow, 5 x 50 Orthotropic Plate (INPUT, 1-4-3)
Long, Narrow, 5 x 60 Orthotropic Plate (INPUT, 1-4-4)

This problem demonstrates triangular decomposition spill logic, orthotropic materials, and the use of a modified restart to obtain additional output. A sketch of the rectangular plate and the applied loading is shown in Figure 1.

The 5 x 50 finite element quarter-section model shown in Figure 2 is constructed with quadrilateral bending elements. In order to demonstrate the triangular decomposition spill logic (i.e. the necessary computation space is larger than available core storage), the model is internally resequenced for a wide band as shown in Figure 3. Although the 5 x 50 model is sufficient to create spill on the IBM 7094 DCS, the number of elements in the longitudinal direction must be increased to create spill on machines having larger random-access memories.

The analytical solution for the infinitely long continuum plate is given in Section 37 of Reference 4. A comparison with the NASTRAN solutions are given in Tables 1 and 2.

A modified restart was used to obtain additional output.

Table 1. Comparison of NASTRAN and Analytical Displacements for Long, Narrow, Orthotropic Plate.

GRID	Z DISPLACEMENT x 10^4	
	THEORY	NASTRAN
1	3.048	3.037
2	2.899	2.889
3	2.466	2.457
4	1.792	1.785
5	0.942	0.939
7	2.949	2.940
13	2.723	2.714
19	2.446	2.435
25	2.157	2.145
31	1.880	1.866
37	1.625	1.611
43	1.397	1.383

Table 2. Comparison of NASTRAN and Analytical Displacements for Long, Narrow, Orthotropic Plate.

EL. ID.	STRESS X		STRESS Y		SHEAR STRESS	
	THEORY	NASTRAN	THEORY	NASTRAN	THEORY	NASTRAN
1	19.05	18.90	20.35	20.40	-0.39	-0.39
2	17.19	17.05	18.36	18.40	-1.12	-1.13
3	13.64	13.53	14.57	14.60	-1.74	-1.76
4	8.76	8.69	9.35	9.38	-2.19	-2.22
5	3.02	2.99	3.22	3.23	-2.43	-2.46
7	15.86	15.76	12.91	12.90	-0.84	-0.88
13	13.27	13.20	8.28	8.23	-1.03	-1.06
19	11.14	11.08	5.38	5.33	-1.07	-1.09
25	9.37	9.33	3.55	3.51	-1.02	-1.04
31	7.90	7.86	2.38	2.36	-0.94	-0.95
37	6.67	6.63	1.64	1.63	-0.84	-0.85

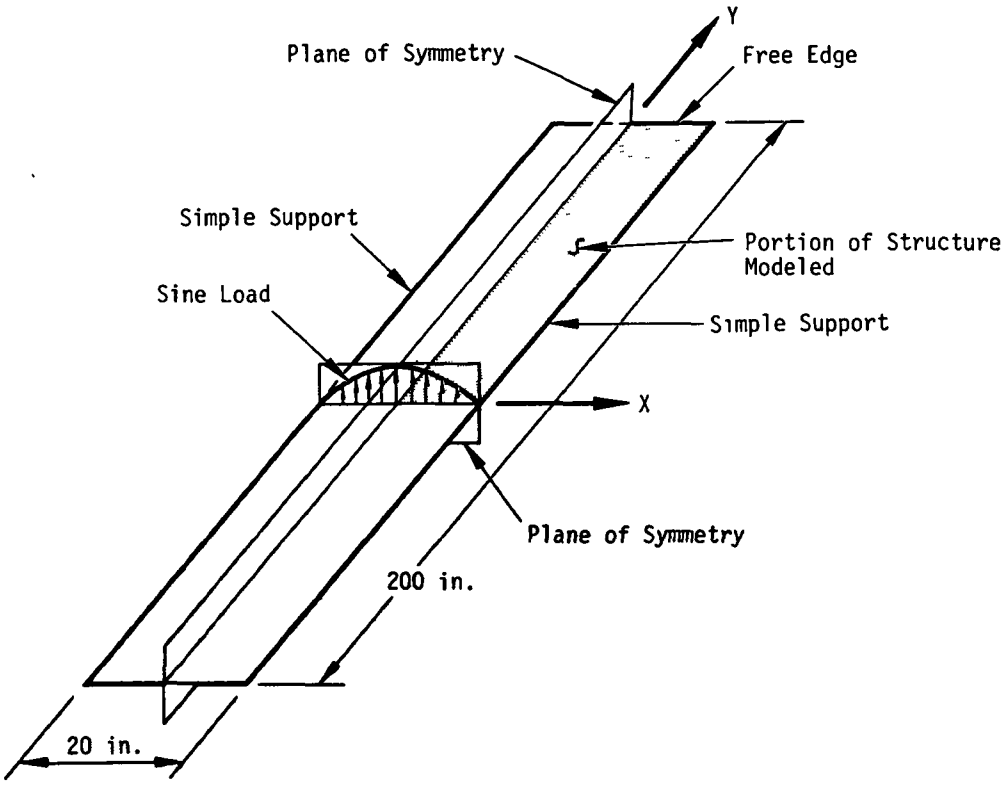

Figure 1. Simply-supported long narrow orthotropic plate

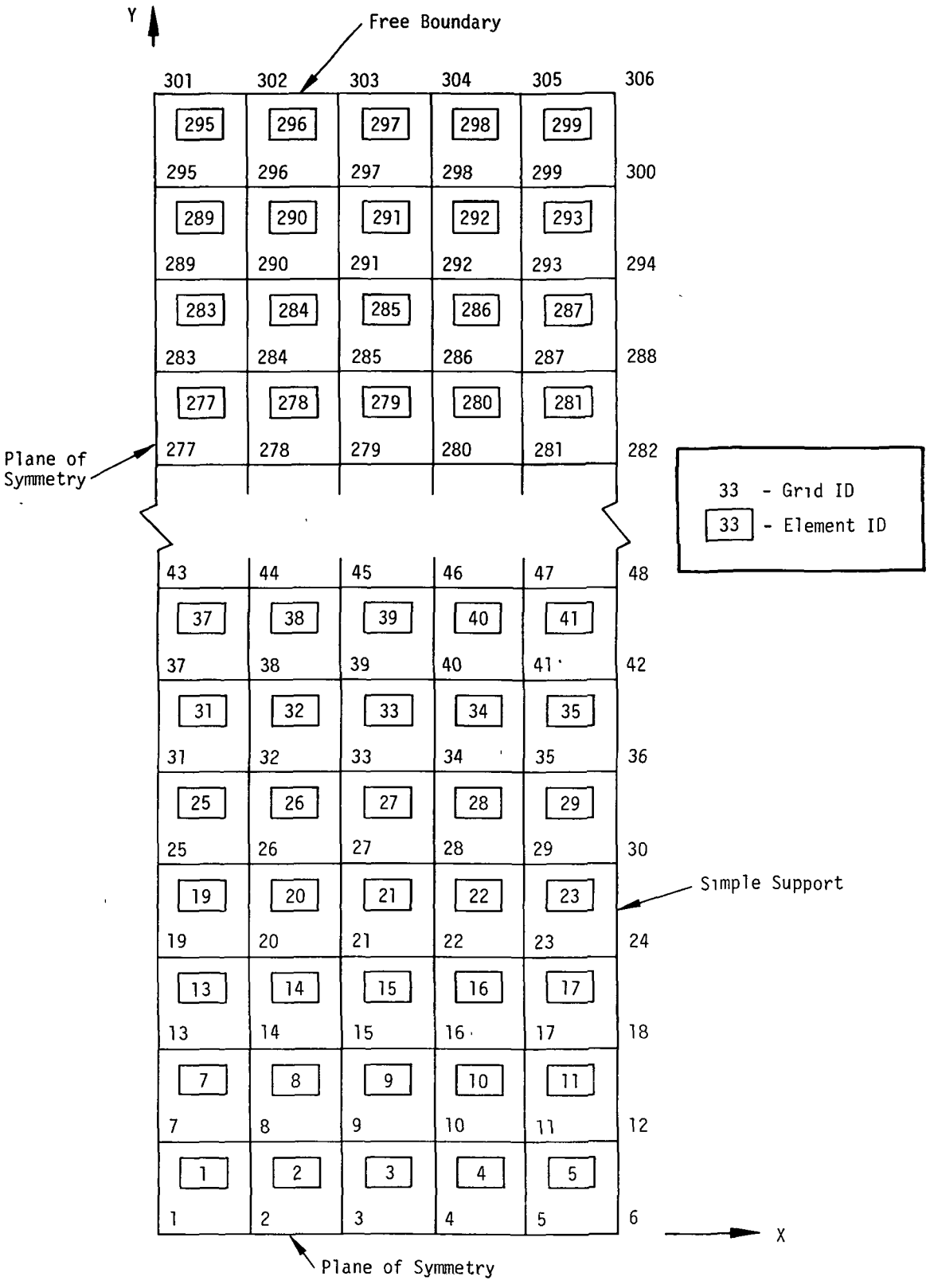

Figure 2. 5 x 50 Long, narrow, orthotropic plate model.

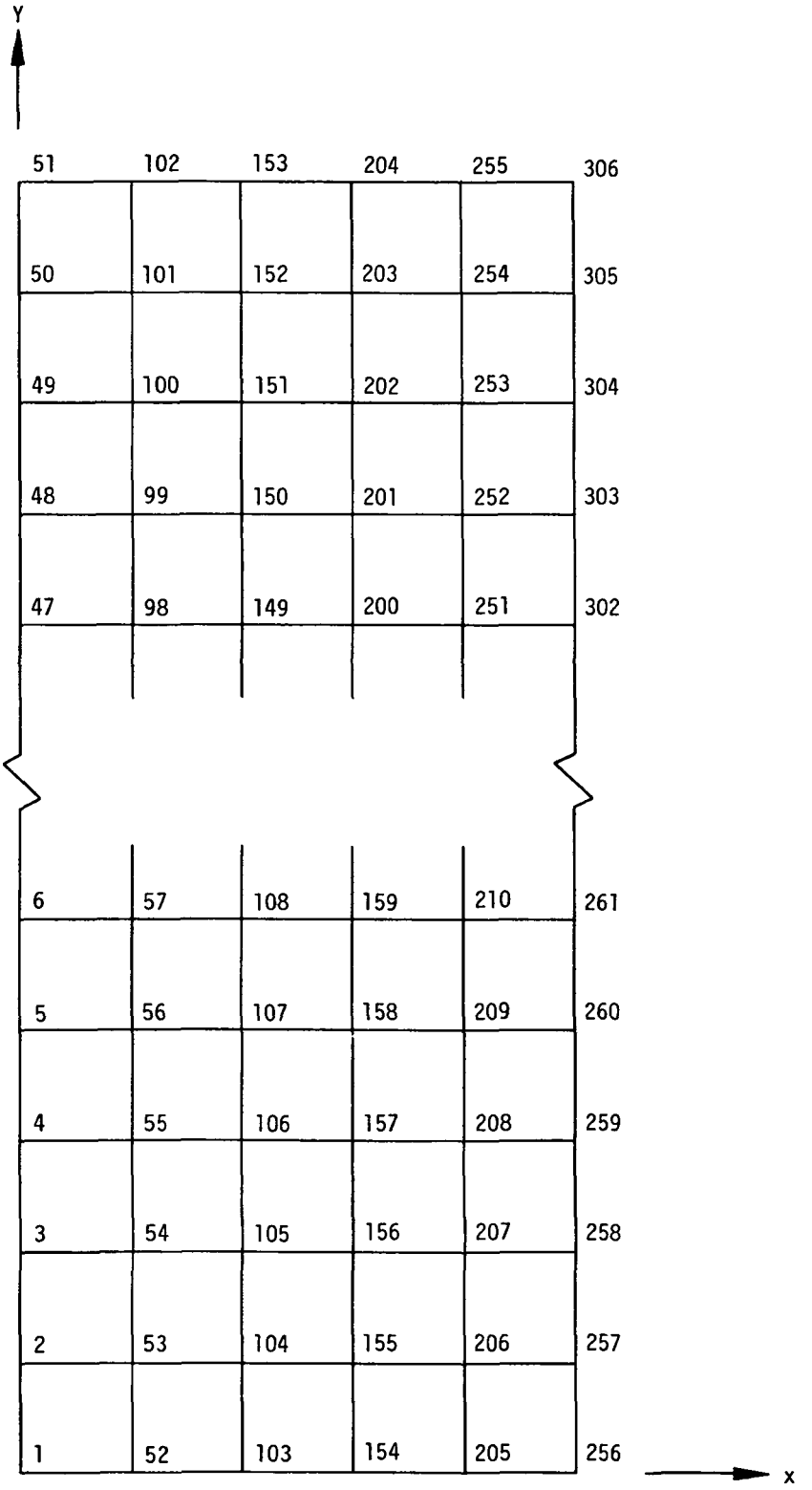

Figure 3. Long, narrow, orthotropic plate model resequenced for wide band.

RIGID FORMAT No. 1, Static Analysis

Nonsymmetric Bending of a Cylinder of Revolution (1-5-1)

A. Description

This problem illustrates the application of the conical shell element and its related special data. This element uses the Fourier components of displacement around an axisymmetric structure as the solution coordinates. The geometry of the structure is defined by rings instead of grid points. Its constraints must be defined by the particular Fourier harmonics, and the loads must be defined either with special data or in a harmonic form. This element may not be used in conjunction with any of the other structural elements.

The structure to be solved is described in Reference 6 and illustrated in Figure 1. It consists of a short, wide cylinder with a moderate thickness ratio. The applied loads and the output stresses are pure uncoupled harmonics. The basic purpose of this problem is to check the harmonic deflections, element stresses, and forces. Figures 2 and 3 compare the NASTRAN results with the results given in Reference 6.

B. Input

The Fourier coefficients of the applied moment per length are:

$$m_n = \cos(n\theta)$$

The applied input loads are defined as:

$$M_n = \int_0^{2\pi} m_n \cos(n\theta)\, R\, d\theta$$

The values of applied moment on the MØMAX cards are:

$$M_{n\phi} = \pi R \quad , \quad n > 0$$

$$M_{o\phi} = 2\pi R \quad , \quad n = 0$$

The applied moments for each harmonic are shown in Figure 1. The bending moments in the elements are defined as:

M_v = Moment about u_ϕ

M_u = Moment about u_z

Positive bending moments indicate compression on the outer side.

1. Parameters:

   R = 50 Radius

   s = 50 Height

   t = 1.0 Thickness

   E = 91.0 Modulus of Elasticity

   ν = 0.3 Poisson's Ratio

2. Loads:

   $M_{n(100)}$ = 157.0796 Force·Length

   $M_{n(50)}$ = -157.0796 Force·Length

3. Single Point Constraints:

Ring ID	Harmonic	Coordinates	
50	all	u_r, u_ϕ, u_z	Radial, tangential and axial translations
100	all	u_r, u_ϕ, u_z	Radial, tangential and axial translations
all	all	θ_r	Rotation normal to surface

The AXISYM = CØSINE statement in case control defines the motions to be symmetric with respect to the x-z plane.

C. Answers

Theoretical and NASTRAN results for element bending moments and radial deflections for 4 of the 20 harmonics used are given in Figure 2 and 3. Notice that for higher harmonics the effect of the load is limited to the edges. A smaller element size at the edges and a relatively large size in the center would have given the same accuracy with fewer degrees of freedom.

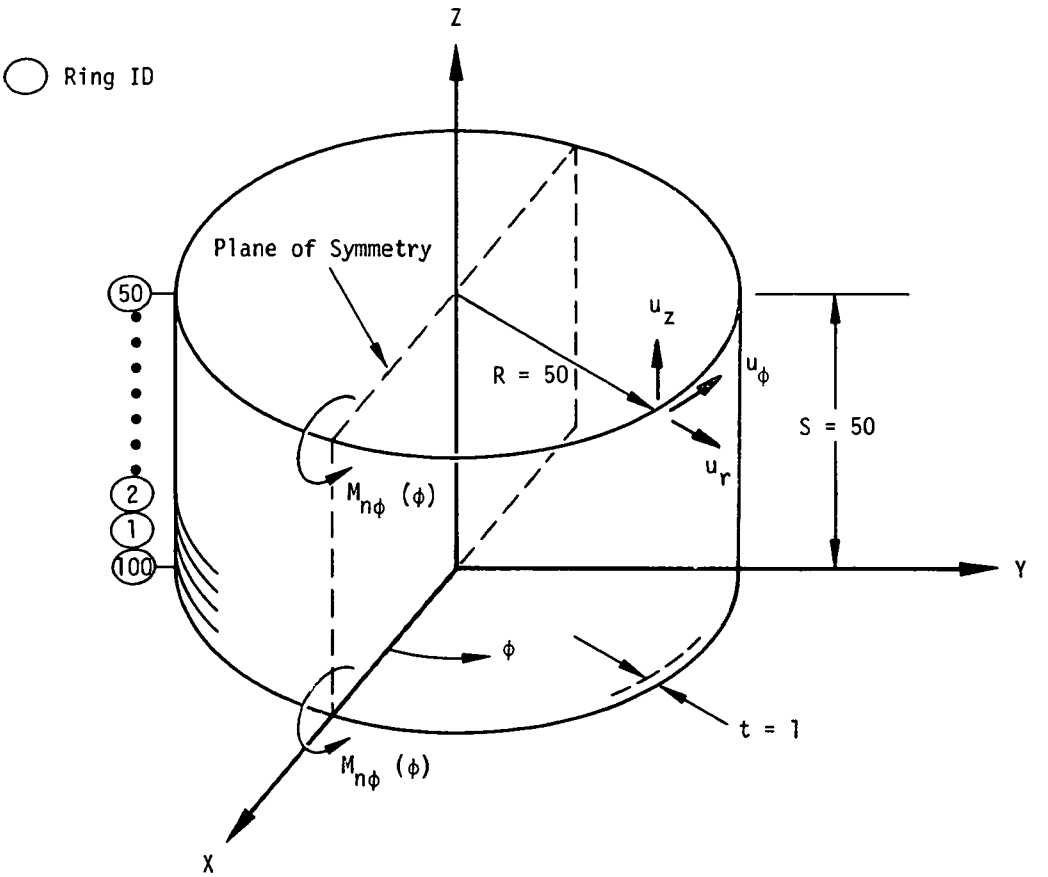

Figure 1. Cylinder under harmonic loads.

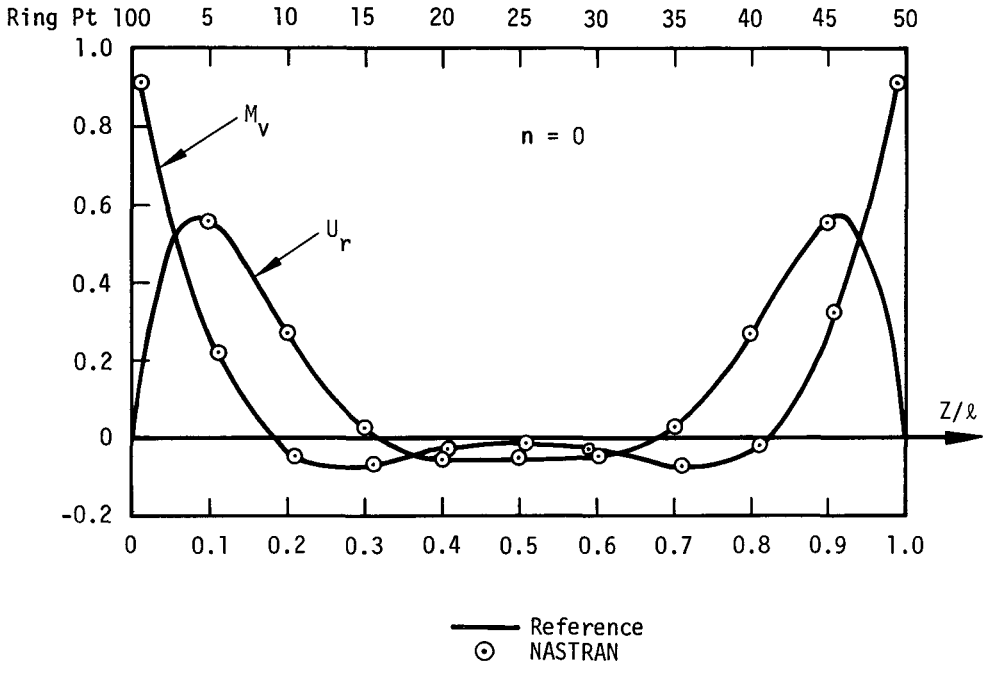

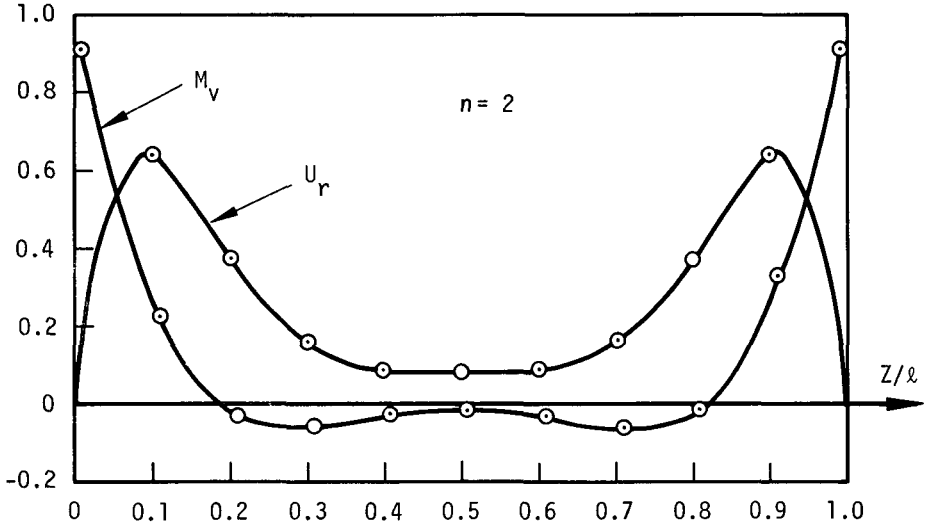

Figure 2. Element bending moments and radial deflections along length of cylinder.

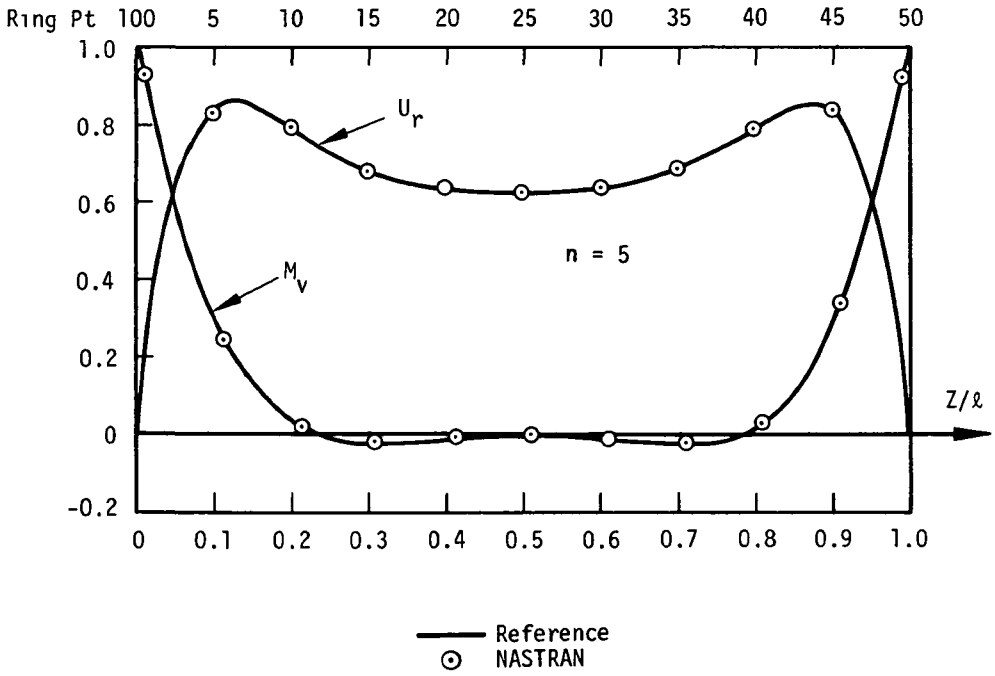

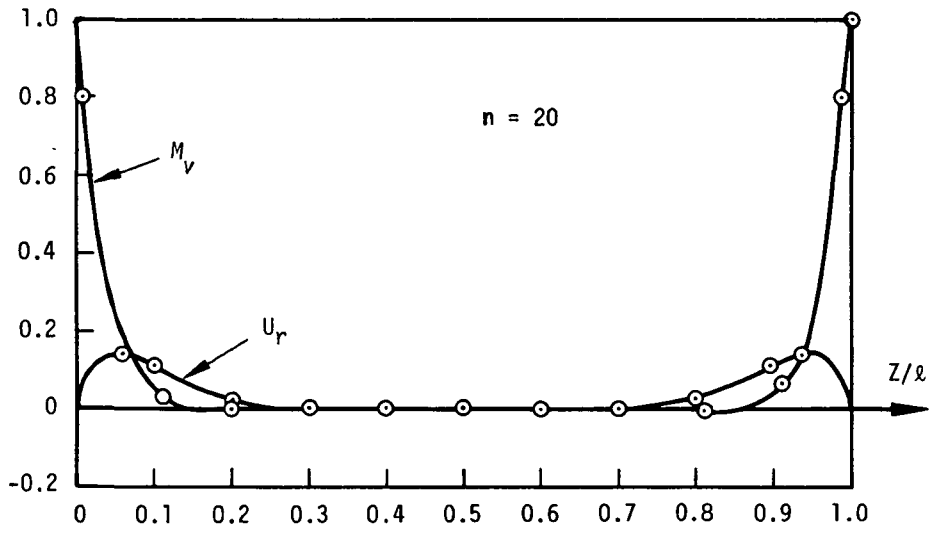

Figure 3. Element bending moments and radial deflections along length of cylinder.

RIGID FORMAT No. 1, Static Analysis

Solid Disk with Radially Varying Thermal Load (1-6-1)

A solid free circular disk in a plane is subjected to a radially varying thermal load of the form

$$T = 100\left(1 - \frac{r^2}{b^2}\right)$$

where

r = the radius at any point in the disk

b = the outside radius = 0 10 inches

The structure is shown in Figure 1 along with its associated material properties and pertinent dimensions The finite element idealization employed for this structure is shown in Figure 2. The thermal loading on the solid disk is established via an internally generated thermal load vector derived from data specified grid point temperature values.

Figure 3 displays the radial displacement utilizing the idealization shown in Figure 2. Figure 4 presents radial and circumferential stress values which result from the thermal loading. Reference 14 provides an analytical solution to this problem which is based on the theory of elasticity. Note that the solid lines represent the analytical solution while the circles and squares represent the solution obtained utilizing the finite element solution

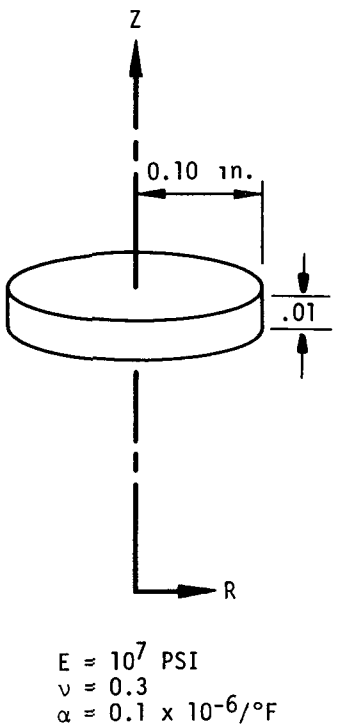

Figure 1. Solid circular disk

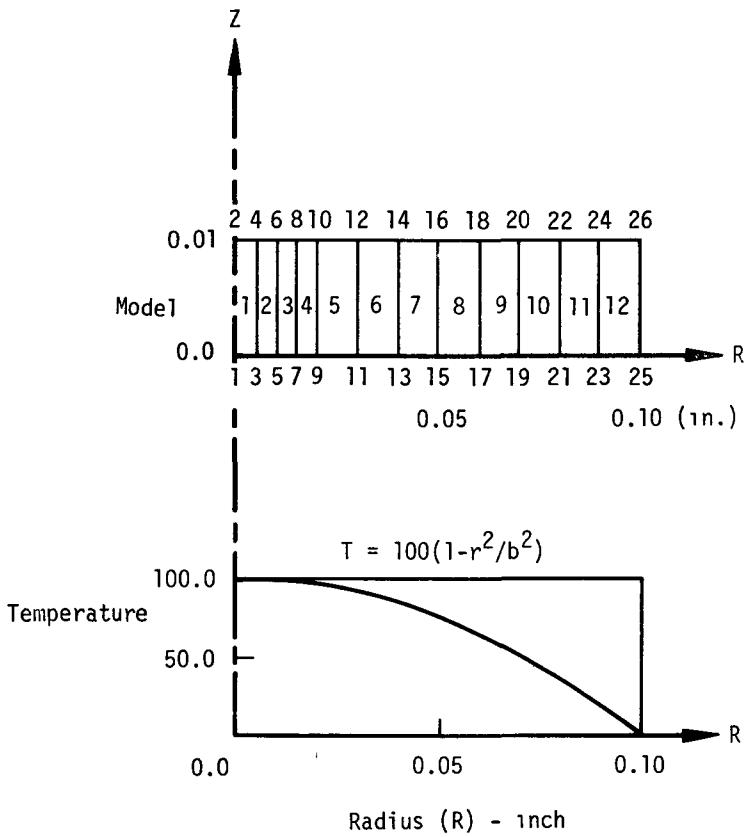

Figure 2. Finite element idealization and temperature distribution.

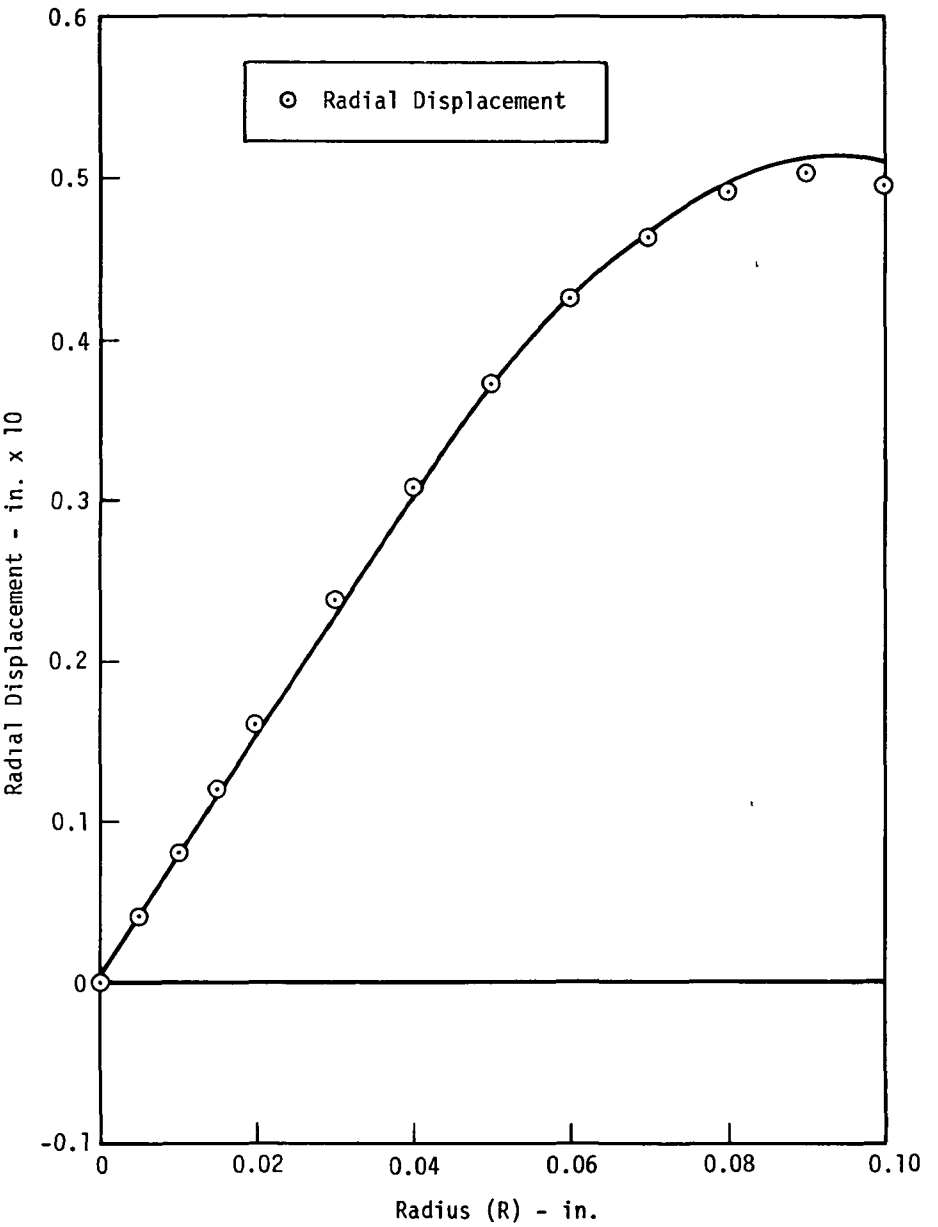

Figure 3. Radial displacement, solid disk with radially varying thermal load.

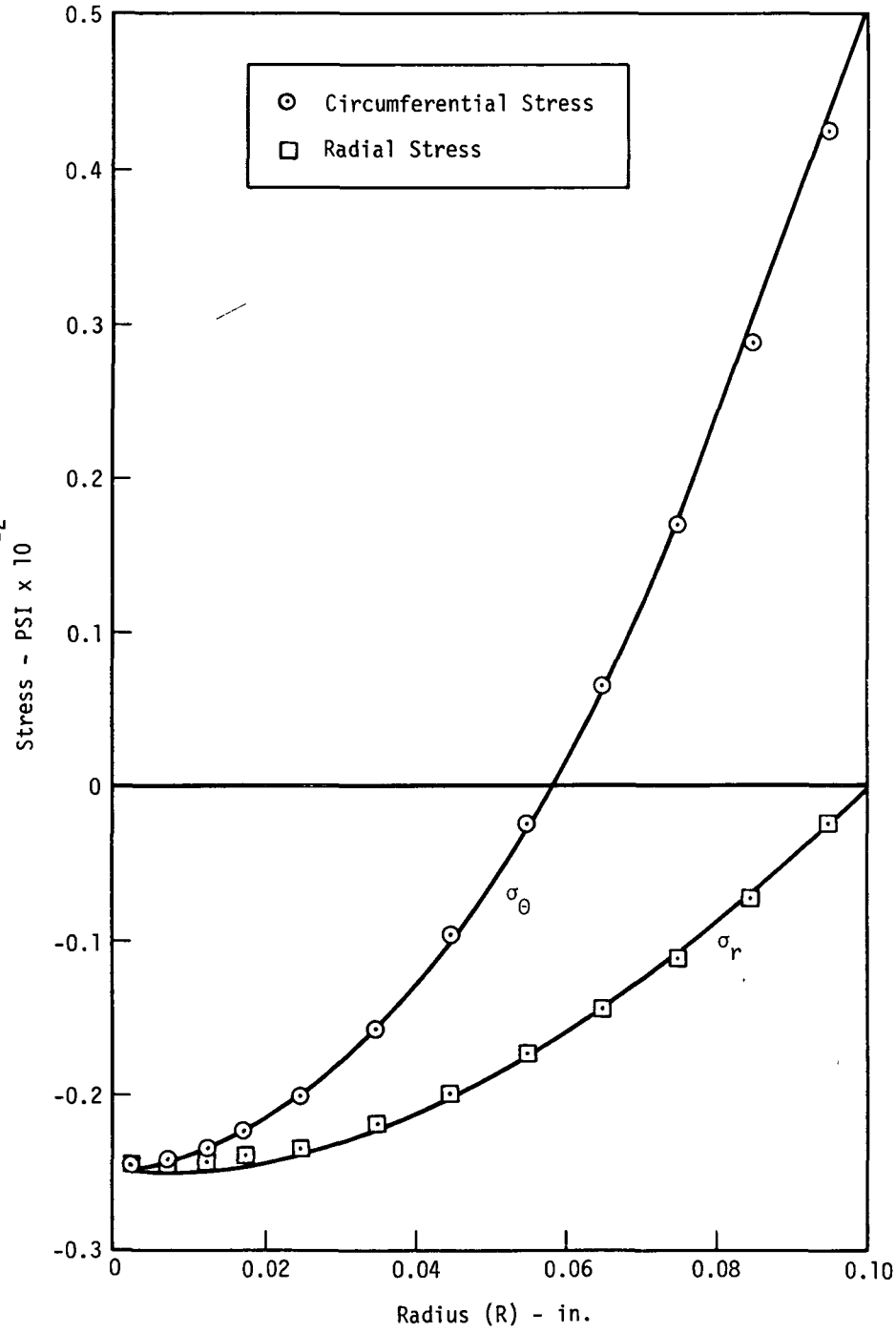

Figure 4. Radial and circumferential stress in solid disk at the centroid of the elements with radially varying thermal load.

RIGID FORMAT No. 1, Static Analysis

Shallow Spherical Shell Subjected to External Pressure Loading (1-7-1)

A shallow spherical shell with a built-in edge is subjected to an external pressure loading of 1 psi. The shell is shown in Figure 1 along with its pertinent dimensions and associated material properties. The finite element idealization for the shell is displayed in Figure 2.

Due to symmetry only one half of the shell was analyzed. The primary purpose of this analysis was to demonstrate the applicability of the shell cap generalization of the toroidal ring to this class of problem.

The meridional bending moment is taken to characterize the behavior predicted for this structure. The exact solution from Reference 4 is compared to the 13 element finite element solution in Figure 3. The reference solution is designated by the solid line while the finite element solution is designated by the circles. Figure 4 displays the radial displacement obtained utilizing this idealization and compares it to that obtained in the Reference Solution.

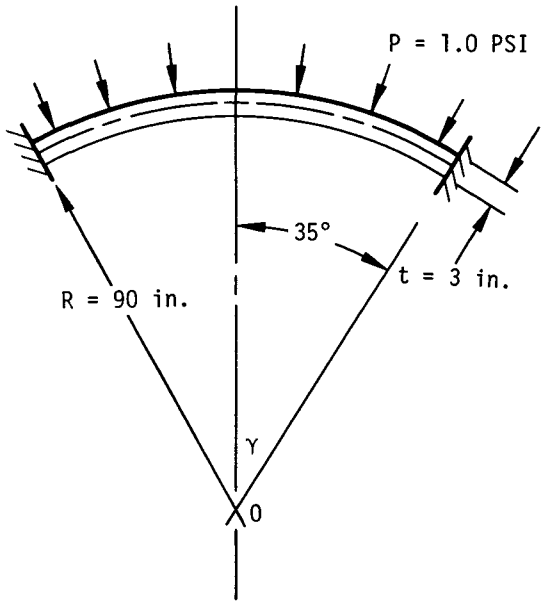

$E = 3.0 \times 10^6$ PSI
$\nu = 0.167$

Figure 1. Shallow spherical shell

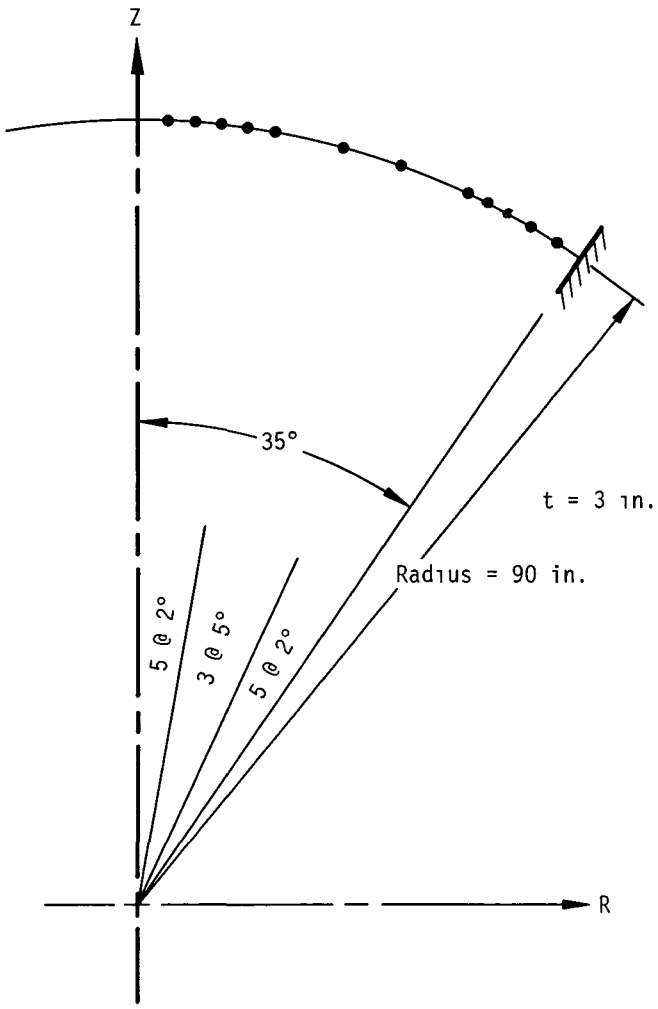

Figure 2. Finite element idealization

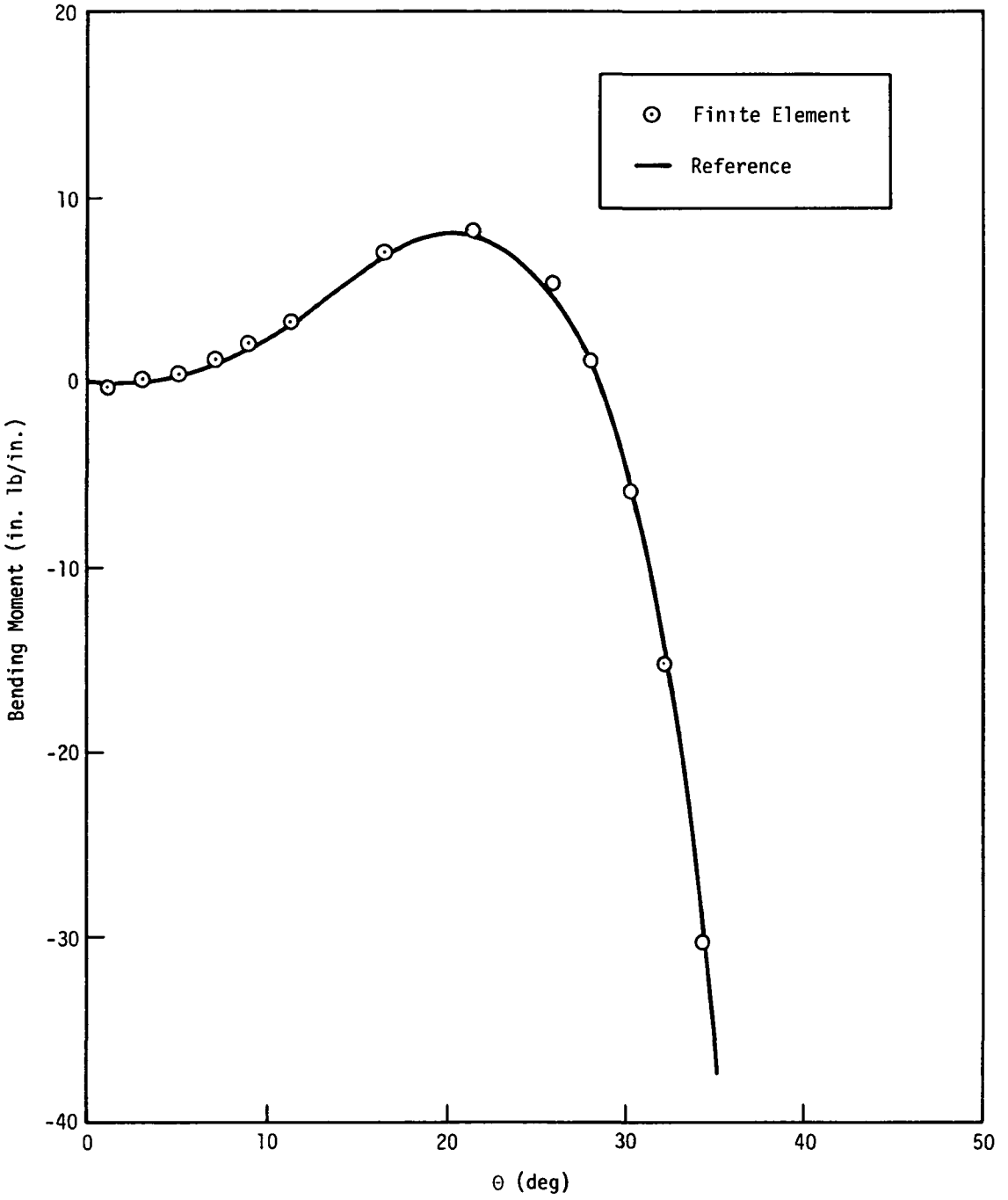

Figure 3. Meridional moment, shallow spherical shell.

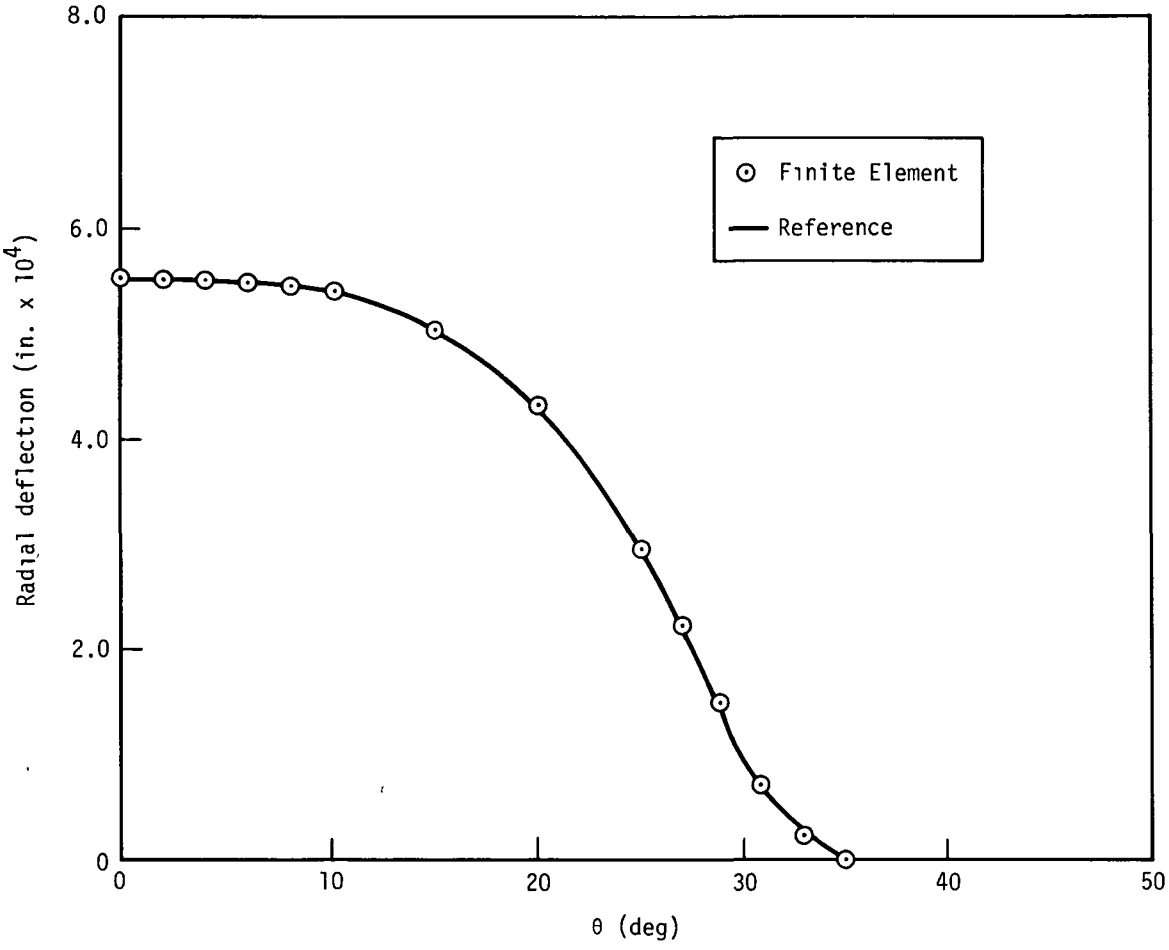

Figure 4. Radial displacement, shallow spherical shell.

RIGID FORMAT No. 1, Static Analysis

Bending of a Beam Fabricated from HEXA1 Solid Elements (1-8-1)

A. Description

The properties of solid bodies may be modeled with the NASTRAN tetrahedra, wedge, or hexahedron finite elements. This problem demonstrates the analysis of a solid fabricated from the six-sided HEXA1 solid elements. The problem consists of a rectangular parallelepiped subdivided into forty cubic subelements as shown in Figure 1.

The loads were chosen to approximate the stress distribution due to a moment on one end of a beam; the other end is constrained to resist the moment. Two planes of symmetry were used to simulate an actual problem having twice the width and twice the height.

B. Input

1. Parameters:

   ℓ = 20.0 (length)

   w = 4.0 (width of full section)

   h = 16.0 (height of full section)

   E = 3.0×10^6 (modulus of elasticity)

   ν = 0.2 (Poisson's ratio)

2. Boundary Constraints:

   on y = 0 plane, $u_x = u_z = 0$ (antisymmetry)

   on z = 0 plane, $u_z = 0$ (symmetry)

   on x = 0 plane, $u_x = 0$ (symmetry)

3. Loads:

   Total Moment: $M_y = 2.048 \times 10^3$

   This moment will produce bending about the z axis. It is modeled by a set of axial loads at x = ℓ which, in turn, represent an axial stress distribution:

$$\sigma_{xx} = 1.5y$$

C. Analysis and Results

A prismatic beam with an axial stress which varies linearly over the cross section has an exact solution. In the demonstration problem, the theoretical stress distribution is:

$$\sigma_{xx} = -\frac{M}{I} y$$

$$\sigma_{yz} = \sigma_{zz} = \tau_{xy} = \tau_{xz} = \tau_{yz} = 0 \ ,$$

where $I = \frac{1}{12} wh^3$.

The displacements are:

$$u_x = -\frac{M}{EI} xy$$

$$u_y = \frac{M}{2EI} (x^2 - \nu y^2 - \nu z^2)$$

$$u_z = \nu \frac{M}{EI} yz.$$

Tables 1 and 2 are comparisons of displacements and stresses for the theoretical case and the NASTRAN model.

	DISPLACEMENT x 10^{-4}	
POINT/DIRECTION	THEORY	NASTRAN
21/y	.0400	.0417
41/y	.1600	.1607
61/y	.360	.366
81/y	.640	.651
101/y	1.000	1.016
109/x	0.800	0.844
110/z	.016	0.007

Table 1. Comparisons of Displacement

ELEMENT	THEORY			NASTRAN		
	σ_{xx}	σ_{yy}	τ_{xy}	σ_{xx}	σ_{yy}	τ_{xy}
1	-1.5	0	0	-1.56	.02	-.01
2	-4.5	0	0	-4.53	.036	-.05
3	-7.5	0	0	-7.39	.06	-.06
4	-10.5	0	0	-9.95	-.11	.12

NOTE: NASTRAN stresses are average; theoretical stresses are calculated at the center of the element.

Table 2. Comparisons of Stress

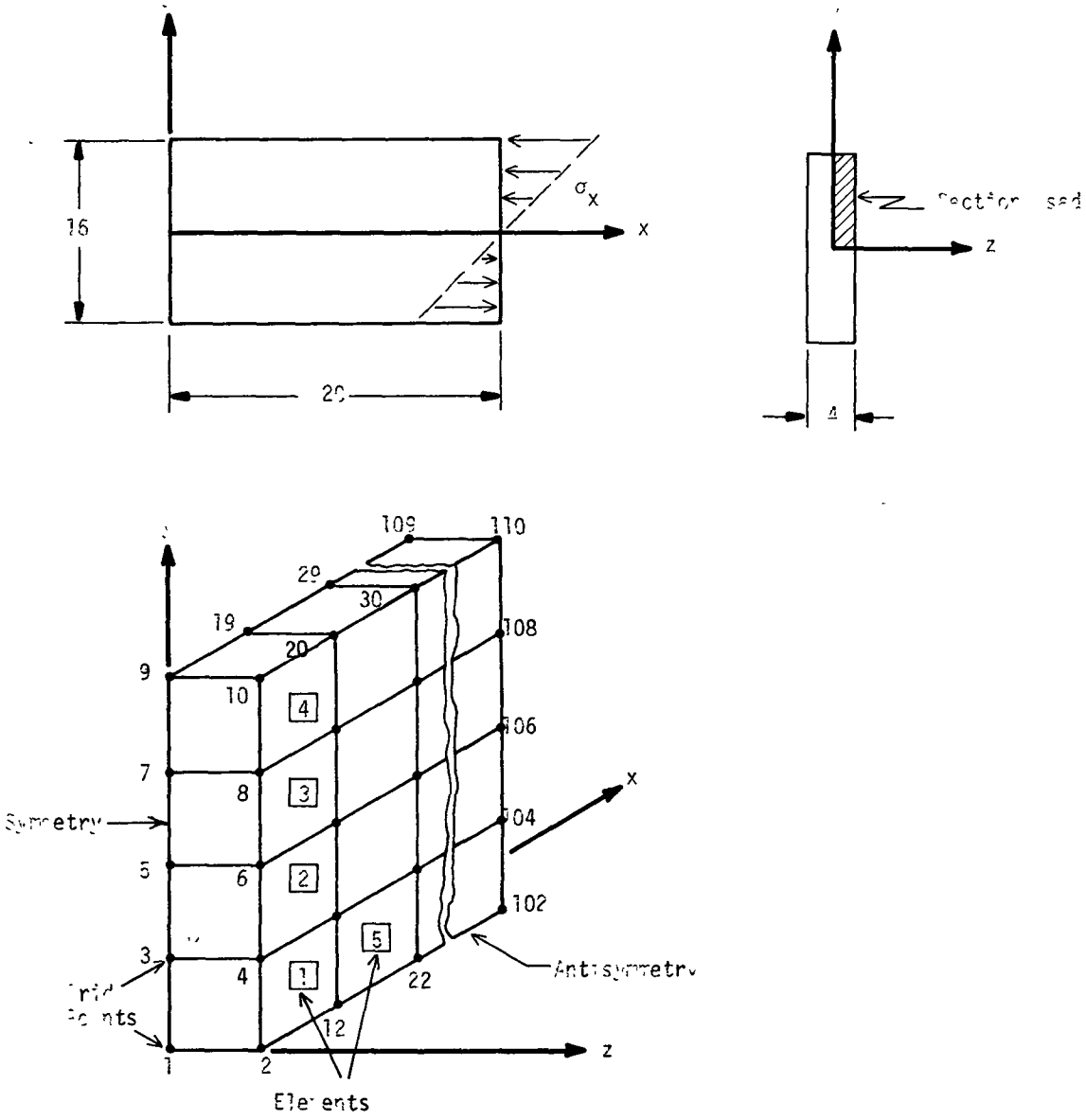

Figure 1. Model of solid using hexahedrons.

RIGID FORMAT No. 1, Static Analysis

Thermal and Applied Loads on HEXA2 Solid Elements (1-9-1)

A. Description

This problem demonstrates the use of the HEXA2 solid hexahedron elements. Forty rectangular elements are used to model a 2x2x10 beam. The dimensions and boundary conditions are shown in Figure 1. Two loading conditions are applied: axial stress and thermal expansion. Symmetry boundary conditions are used.

B. Input

1. Parameters:

ℓ = 20 (length)

w = 4.0 (width)

h = 4.0 (height)

E = 3.0×10^6 (modulus of elasticity)

ν = 0.2 (Poisson's ratio)

α = .001 (thermal expansion coefficient)

T_o = 10° (reference temperature)

2. Boundary Constraints:

u_x = 0 at x = 0

u_y = 0 at y = 0

u_z = 0 at z = 0

3. Loads:

Subcase 1,

$F_x = 24 \times 10^3$ (total axial force)

Subcase 2,

T = 60° (uniform temperature field)

T_o = 10° (reference temperature)

C. Analysis and Results

1. Subcase 1

The distributed axial load is equivalent to a stress field of:

$$\sigma_{xx} = 1.5 \times 10^{3} ,$$

$$\sigma_{yy} = \sigma_{zz} = \tau_{xy} = \tau_{xz} = \tau_{yz} = 0 .$$

The displacement field is:

$$u_x = \frac{\sigma_{xx}}{E} x = 0.5 \times 10^{-3} x$$

$$u_y = \frac{-\nu\sigma_{xx}}{E} y = -0.1 \times 10^{-3} y$$

$$u_z = \frac{-\nu\sigma_{xx}}{E} z = -0.1 \times 10^{-3} z$$

2. Subcase 2

The uniform expansion due to temperature will not cause any stress. The strains, however, are uniform and equal. The displacements are, therefore:

$$u_x = \alpha(T-T_o)x = .05x$$

$$u_y = \alpha(T-T_o)y = .05y$$

$$u_z = \alpha(T-T_o)z = .05z$$

where T is the uniform temperature and T_o is the reference temperature.

3. Results

The results of both subcases are exact to the single precision limits of the particular computer used.

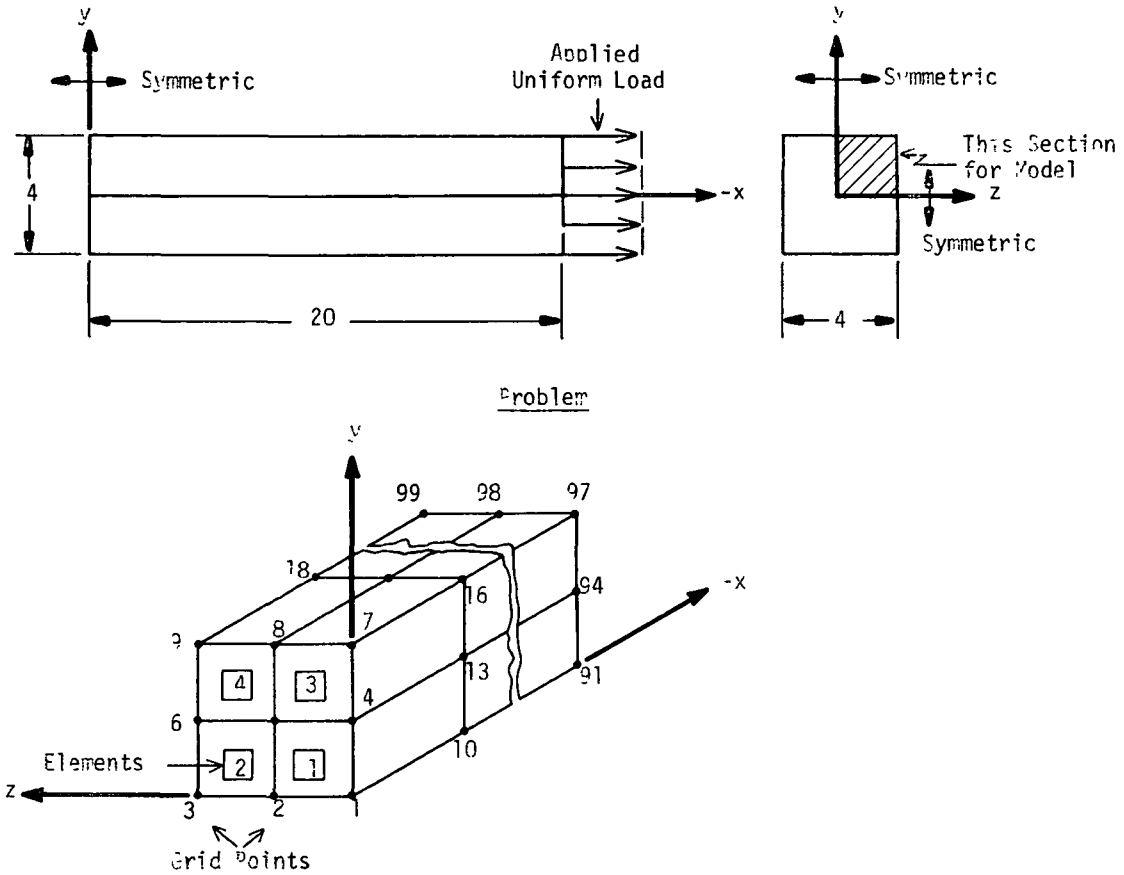

Figure 1 Model of solid using HEXA2 elements

RIGID FORMAT No. 1, Static Analysis

Thermal Bending of a Beam (1-10-1)

A. Description

This problem demonstrates the solution of a beam subjected to a thermal gradient over the cross-section. Two end conditions are solved, clamped-free and clamped-pinned end conditions.

An equivalent linear gradient in the normal direction was used for the input data. However, the actual temperatures at points on the cross-section were input on the TEMPRB card in order to produce correct stresses. The beam was subdivided into 14 variable lengths for maximum efficiency.

B. Input

Figure 1 describes the beam and the thermal field to be analyzed and Figure 2 shows the finite element model.

C. Theory

For subcase 1, the effective temperature gradient, T', (see NASTRAN Theoretical Manual) is:

$$T'(x) = \frac{1}{I} \int_z \int_y T(x,y,z) y \, dy \, dz \quad , \tag{1}$$

where

$$I = \int_z \int_y y^2 \, dy \, dz \quad . \tag{2}$$

Using the given temperature distribution the effective gradient is:

$$T' = T_c x^3 \quad , \tag{3}$$

where T_c is calculated to be $0.170054°/in^4$ by substituting the temperature distribution into Equation 1 and evaluating the expression:

$$T_c = \frac{1}{I} \int_z \int_y C y^4 \, dy \, dz \tag{4}$$

Since the bar is not redundantly constrained the curvature at the center line is:

$$\frac{d^2v}{dx^2} = -\alpha T' = -\alpha T_c x^3 \quad . \tag{5}$$

The slope is:

$$\frac{dv}{dx} = \int_0^x \frac{d^2v}{dx^2}\, dx = -\frac{\alpha}{4} T_c x^4 \quad . \tag{6}$$

The deflection is:

$$v(x) = \int_0^x \frac{dv}{dx}\, dx = -\frac{\alpha}{20} T_c x^5 \quad . \tag{7}$$

The moment, M, shear, V, and axial stress, σ_x, are:

$$\left.\begin{aligned} M &= EI\left(\frac{d^2v}{dx^2} + \alpha T'\right) = 0 \quad , \\ V &= \frac{dM}{dx} = 0 \quad , \\ \sigma_x(x,y) &= E(\varepsilon_x - \alpha T) = E(\sigma y T' - \alpha T) = E\alpha(T_c y - Cy^3)\, x^3 \quad , \end{aligned}\right\} \tag{8}$$

where C = 1 has dimensions of degrees/length^6.

For subcase 2, with a simple support at x = 10.0, we calculate the deflection due to subcase 1 and apply a constraint load P_L to remove the deflection at the end.

$$P_L = -\frac{3EI}{L^3} v(L) = 3EI\, \frac{\alpha T_c}{20} L^2 \quad . \tag{9}$$

Note: Transverse shear deflection is neglected.

The deflections and slopes are the sum of the results for the two independent loads as follows

deflection: $$v(x) = \frac{P_L}{6EI}(3Lx^2 - x^3) - \frac{\alpha T_c}{20} x^5 = \frac{\alpha T_c}{40}(3L^3 - L^2x - 2x^3)\, x^2 \quad , \tag{10}$$

slope: $$\theta_z(x) = \frac{\partial v}{\partial x} = \frac{\alpha T_c}{40}(6L^3 - 3L^2x - 10x^3)x \quad . \tag{11}$$

The net stress is the sum of the stress due to each load:

$$\sigma_x(x,y) = E\alpha(T_c y - Cy^3)x^3 - \frac{M_L y}{I} = E\alpha\left[\left(T_c y - Cy^3\right)x^3 - \frac{3}{20} T_c L^2 (L - x)\, y\right] \quad (12)$$

where M_L is the moment due to the constraint load.

D. Results

Tables 1 and 2 compare the analytical maximum value of displacement, constraint force, element force, and stress to the maximum deviation of NASTRAN in each category. All results are within 2.66%.

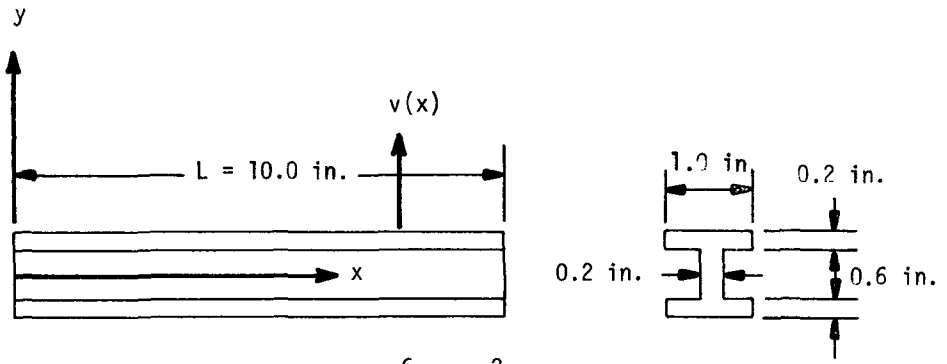

$E = 10.0 \times 10^6$ lb/in^2 (Young's modulus)

$\nu = 0.3$ (Poisson's ratio)

$\alpha = 13.0 \times 10^{-6}$ in/in/°F (Thermal expansion coefficient)

$T_R = 0.0$°F (Reference temperature)

The beam is loaded by the temperature distribution:

$$T(°F) = Cx^3y^3$$

where $C = 1.0$ °F/in^6

Figure 1. Thermal loading of a beam.

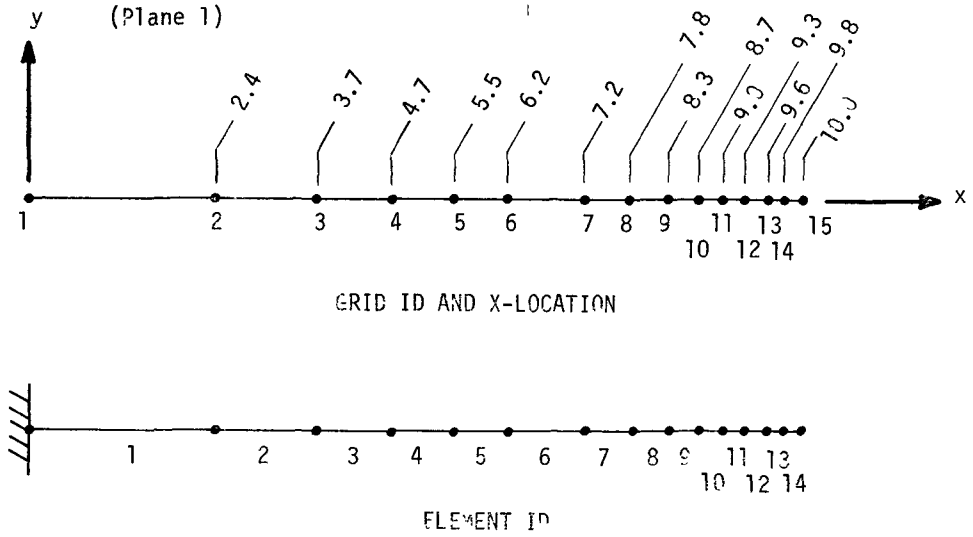

Figure 2. Finite element model.

Table 1. Comparison of NASTRAN and analytical results, clamped-free ends (subcase 1).

CATEGORY	MAXIMUM ANALYTICAL VALUE	MAXIMUM NASTRAN DIFFERENCE	PER CENT ERROR
Displacement	-1.1054×10^{-2}	2.9424×10^{-4}	2.66
Constraint Force	0	*	*
Element Force	0	*	*
Element Stress	$5.1965 \times 10^{+3}$	0.671	0.01

*These results vary with the computer. The very small numbers are essentially zero when compared to subcase 2 results.

Table 2. Comparison of NASTRAN and analytical results, clamped-pinned ends (subcase 2).

CATEGORY	MAXIMUM ANALYTICAL VALUE	MAXIMUM NASTRAN DIFFERENCE	PER CENT ERROR
Displacement	4.3936×10^{-3}	8.024×10^{-6}	0.18
Constraint Force	$-2.2859 \times 10^{+2}$	6.0841	2.66
Element Force	$2.2859 \times 10^{+2}$	6.0846	2.66
Element Stress	$5.1965 \times 10^{+3}$	4.4136×10	0.85

RIGID FORMAT No. 1, Static Analysis

Simply-Supported Rectangular Plate with a Thermal Gradient (1-11-1)
Simply-Supported Rectangular Plate with a Thermal Gradient (INPUT, 1-11-2)

A. Description

This problem illustrates the solution of a general thermal load on a plate with the use of an equivalent linear thermal gradient. The thermal field is a function of three dimensions, demonstrated by the TEMPP1 card. The plate is modeled with the general quadrilateral, QUAD1, elements as shown in Figure 1. Two planes of symmetry are used. This problem is repeated via the INPUT module to generate the QUAD1 elements.

B. Input

E	=	3.0×10^5 pounds/inch^2	(Youngs modulus)
ν	=	0.3	(Poisson's ratio)
ρ	=	1.0 pound-sec.^{2}/inch^4	(Mass density)
α	=	0.01 inch/°F/inch	(Thermal expansion coefficient)
T_R	=	0.0 °F	(Reference temperature)
T_o	=	2.5 °F	(Temperature difference)
a	=	10.0 inch	(Width)
b	=	20.0 inch	(Length)
t	=	0.5 inch	(Thickness)

The thermal field is:

$$T = T_o(\cos \frac{\pi x}{a}) (\cos \frac{\pi y}{b}) \left(\frac{2z}{t}\right)^3$$

$$= 160.0(\cos \frac{\pi x}{10}) (\cos \frac{\pi y}{20}) z^3 \text{ °F}$$

C. Theory

The plate was solved using a minimum energy solution. The net moments, $\{M_N\}$, in the plate are equal to the sum of the elastic moments, $\{M_e\}$, and the thermal moments, $\{M_t\}$.

$$\{M_N\} = \{M_t\} + \{M_e\} \quad , \tag{1}$$

where the thermal moment is

$$\{M_t\} = \alpha T_o' D(1+\nu) \begin{Bmatrix} 1 \\ 1 \\ 0 \end{Bmatrix} \cos \frac{\pi x}{a} \cos \frac{\pi y}{b} \quad , \qquad (2)$$

and

$$D = \frac{Et^3}{12(1-\nu^2)} \quad .$$

and $T_o' = 6T_o/5t$ is the effective thermal gradient.

The elastic moment is defined by the curvatures, χ, with the equation:

$$\{M_e\} = D \begin{Bmatrix} \chi_x + \nu\chi_y \\ \chi_y + \nu\chi_x \\ \frac{(1-\nu)}{2} \chi_{xy} \end{Bmatrix} \quad . \qquad (3)$$

Assuming a normal displacement function, W, of

$$W = \sum_n \sum_m W_{nm} \cos \frac{n\pi x}{a} \cos \frac{m\pi y}{b} \quad , \qquad (4)$$

then

$$\chi_x = \frac{\partial^2 W}{\partial x^2} = - \sum_n \sum_m \pi^2 W_{nm} \left(\frac{n}{a}\right)^2 \cos \frac{n\pi x}{a} \cos \frac{m\pi y}{b} \quad ,$$

$$\chi_y = \frac{\partial^2 W}{\partial y^2} = - \sum_n \sum_m \pi^2 W_{nm} \left(\frac{m}{a}\right)^2 \cos \frac{n\pi x}{a} \cos \frac{m\pi y}{b} \quad , \qquad (5)$$

$$\chi_{xy} = 2\frac{\partial^2 W}{\partial x \partial y} = 2 \sum_n \sum_m \pi^2 W_{nm} \left(\frac{nm}{ab}\right) \sin \frac{n\pi x}{a} \sin \frac{m\pi y}{b} \quad .$$

The work done by the thermal load is:

$$U = \int_A \{\chi\}^T \{M_t\} \, dA + \frac{1}{2} \int_A \{\chi\}^T \{M_e\} \, dA \quad , \qquad (6)$$

where A is the surface area. Performing the substitution and integrating results in the energy expression:

$$U = -\frac{\alpha T_o' D(1+\nu)\pi^2 (a^2+b^2)}{4ab} W_{11} + \frac{D}{2} \sum_{n=1}^{\infty} \sum_{m=1}^{\infty} \frac{\pi^4 ab}{4} \left(\frac{n^2}{a^2} + \frac{m^2}{b^2} \right)^2 W_{nm}^2 \quad . \tag{7}$$

The static solution exists at a minimum energy:

$$\frac{\partial U}{\partial W_{nm}} = 0 \quad . \tag{8}$$

This results in all but W_{11} equal to zero. The displacement function is therefore:

$$W(x,y) = \frac{\alpha T_o' (1+\nu) a^2 b^2}{\pi^2 (a^2 + b^2)} \cos \frac{\pi x}{a} \cos \frac{\pi y}{b} \quad . \tag{9}$$

Solving for moments by differentiating W and using equation (3) results in the equations for element moments:

$$M_x = \alpha T_o' D(1+\nu) \left[1 - \frac{b^2+\nu a^2}{a^2+b^2} \right] \cos \frac{\pi x}{a} \cos \frac{\pi y}{b} \quad , \tag{10}$$

$$M_y = \alpha T_o' D(1+\nu) \left[1 - \frac{a^2+\nu b^2}{a^2+b^2} \right] \cos \frac{\pi x}{a} \cos \frac{\pi y}{b} \quad , \tag{11}$$

$$M_{xy} = \frac{\alpha T_o' D(1-\nu^2) ab}{a^2 + b^2} \sin \frac{\pi x}{a} \sin \frac{\pi y}{b} \quad . \tag{12}$$

D. Results

Figure 2 compares the element forces given by the above equation and the NASTRAN results. Figure 3 compares the normal displacements. The maximum errors for displacements, constraint forces, element forces and element stresses are listed in Table 1.

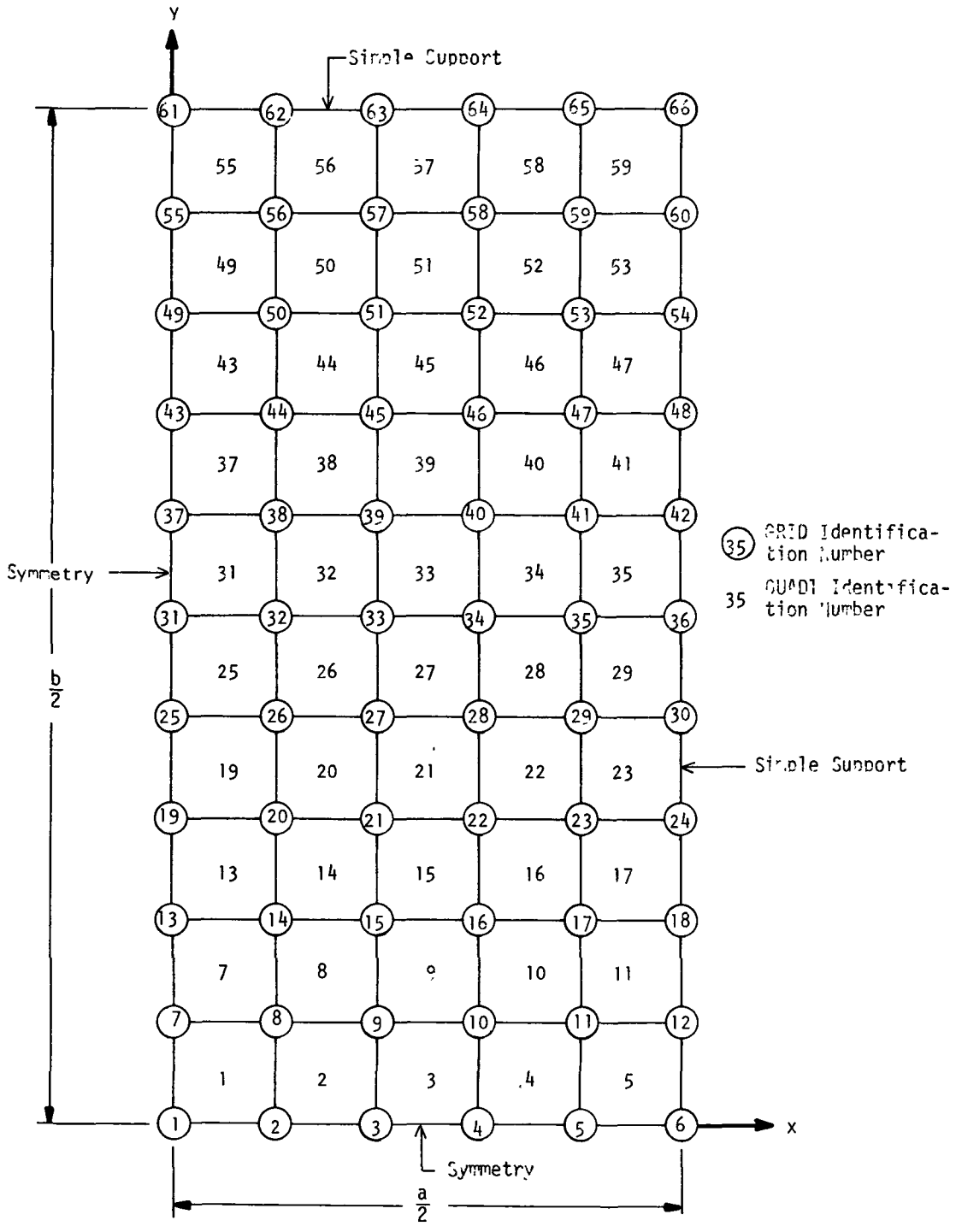

Figure 1. Simply-supported rectangular plate with a thermal gradient.

Table 1. Comparison of analytical and NASTRAN results.

CATEGORY	MAXIMUM ANALYTICAL	MAXIMUM DIFFERENCE	PER CENT ERROR
Displacement	6.2898×10^{-1}	-1.5464×10^{-3}	-0.25
Constraint Force	150.0	-.9594	-0.65
Element Mom., M_x	1.4770×10^{2}	-1.1767	-0.80
Element Stress	7.764618×10^{3}	-90.33275	-1.16

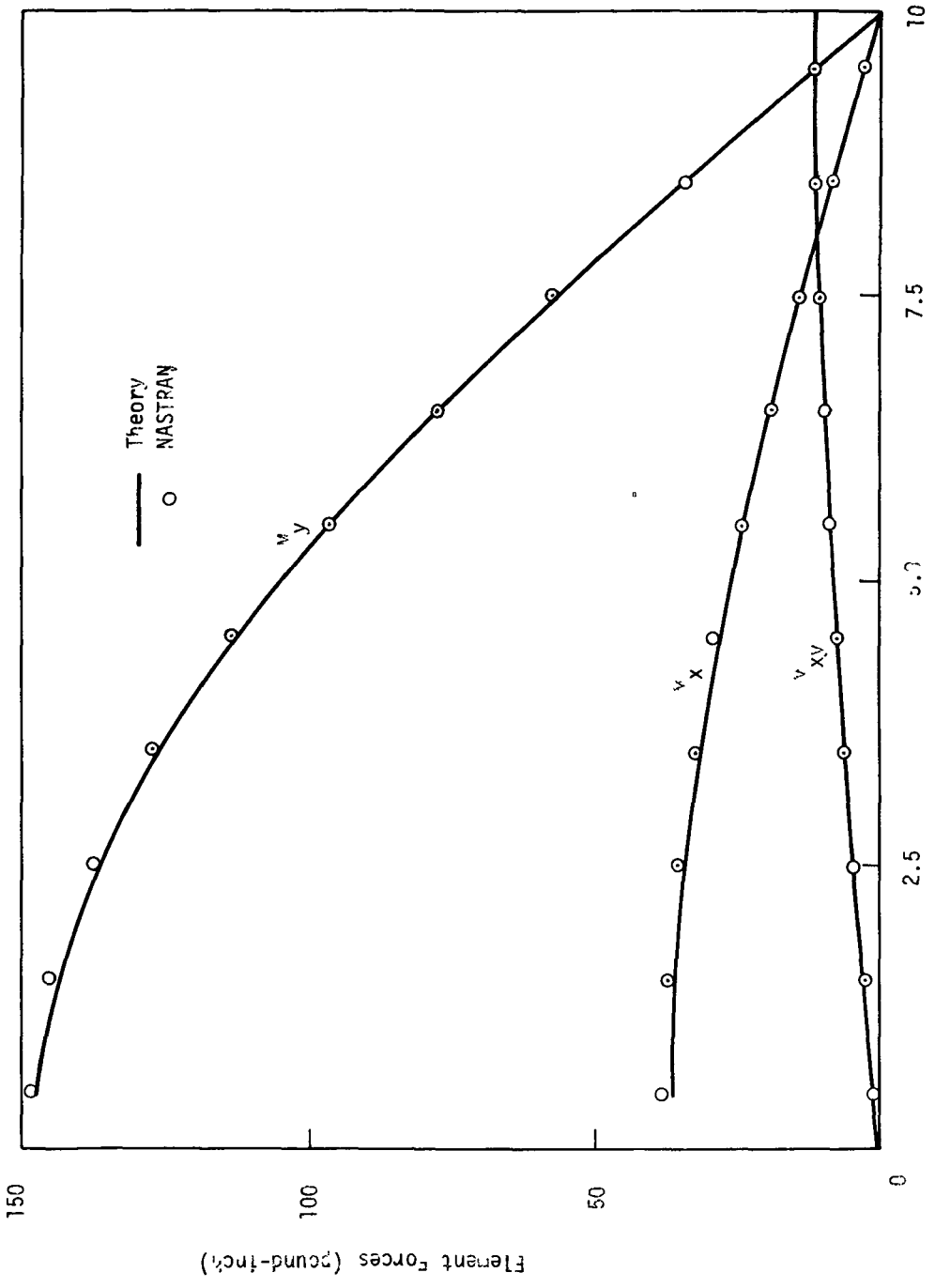

Figure 2. Element forces at x = 0.5.

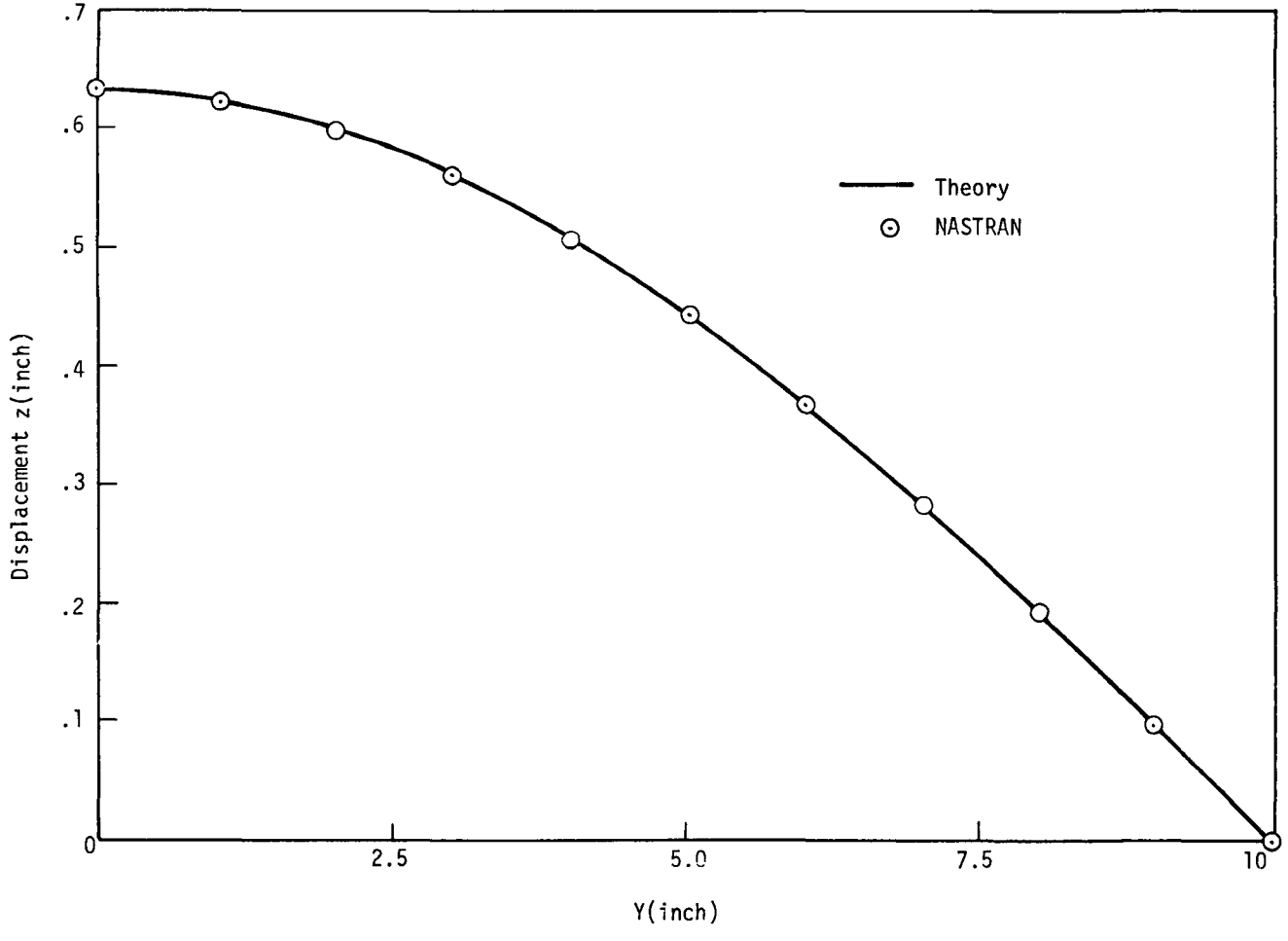

Figure 3. Displacement at x = 5.0.

RIGID FORMAT No. 1 (APP HEAT), Heat Conduction Analysis
Linear Steady State Heat Conduction Through a Washer
Using Solid Elements (1-12-1)
Linear Steady State Heat Conduction Through a Washer
Using Ring Elements (1-12-2)

A. Description

This problem illustrates the capability of NASTRAN to solve heat conduction problems. The washer, shown in Figure 1, has a radial heat conduction with the temperature specified at the outside and a film heat transfer condition at the inner edge. Due to symmetry about the axis and the assumption of negligible axial gradients, the temperature depends only upon the radius.

B. Input

The first NASTRAN model is shown in Figure 2. The solid elements (HEXA1, HEXA2, WEDGE and TETRA) and boundary condition element (HBDY, type AREA4) are used. The conductivity of the material is specified on a MAT4 card. Temperatures are specified at the outer boundary with SPC cards. Punched temperature output is placed on TEMP bulk data cards suitable for static analysis.

Another variation of the problem is shown in Figure 3. Solid of revolution elements (TRIARG and TRAPRG) and boundary condition element (HBDY, type REV) are used. The conductivity of the material and the convective film coefficient are specified on a MAT4 card The CHBDY card references a scalar point at which the ambient temperature is specified using an SPC card. An SPC1 card is used to constrain the temperature to zero degrees at gridpoints on the outer surface.

C. Theory

The mathematical theory for the continuum is simple, and can be solved in closed form. The differential equation is

$$\frac{1}{r}\ \frac{\partial}{\partial r}\left(rk\frac{\partial U}{\partial r}\right) = 0 \quad . \tag{1}$$

The boundary conditions are

$$-k\frac{\partial U}{\partial r} = H(U_a - U) \text{ at } r = r_1 \quad , \tag{2}$$

and

$$U = 0 \qquad \text{at } r = r_2 \quad . \tag{3}$$

The solution is

$$U(r) = \frac{HU_a}{(k/r_1) + H\,\ell n(r_2/r_1)}\ \ell n(r_2/r)$$

$$= 288.516\ \ell n(2/r)$$

D. Results

A comparison with the NASTRAN results is shown in Table 1.

Table 1. Comparison of Theoretical and NASTRAN Temperatures for Heat Conduction in a Washer.

r(radius)	Theoretical Temperatures	NASTRAN Temperatures (Solids)*	NASTRAN Temperatures (Rings)*
1.0	199.984	202.396	199.932
1.1	172.486	173.904	172.448
1.2	147.381	148.833	147.355
1.3	124.288	124.783	124.269
1.4	102.906	102.852	102.894
1.5	83.001	82.913	82.992
1.6	64.380	64.306	64.375
1.7	46.889	46.832	46.886
1.8	30.398	30.356	30.397
1.9	14.799	14.773	14.798
2.0	0.000	0.000	0.000

*These are the average temperatures at a radius.

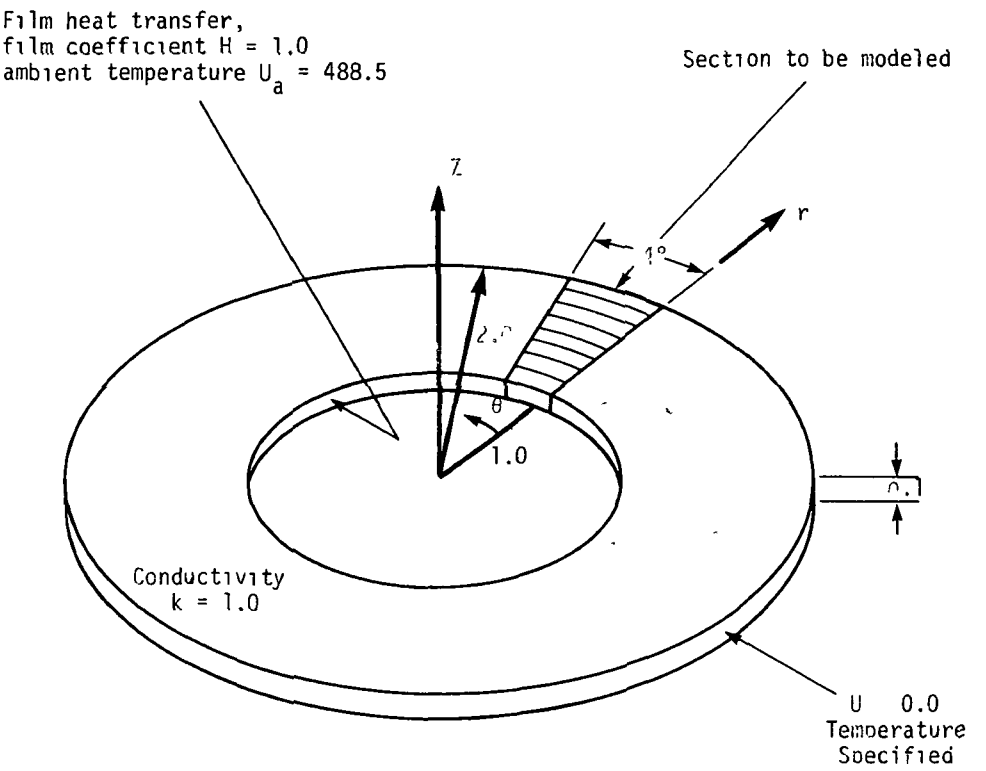

Figure 1. Washer Analyzed in Heat Conduction Demonstration Problem

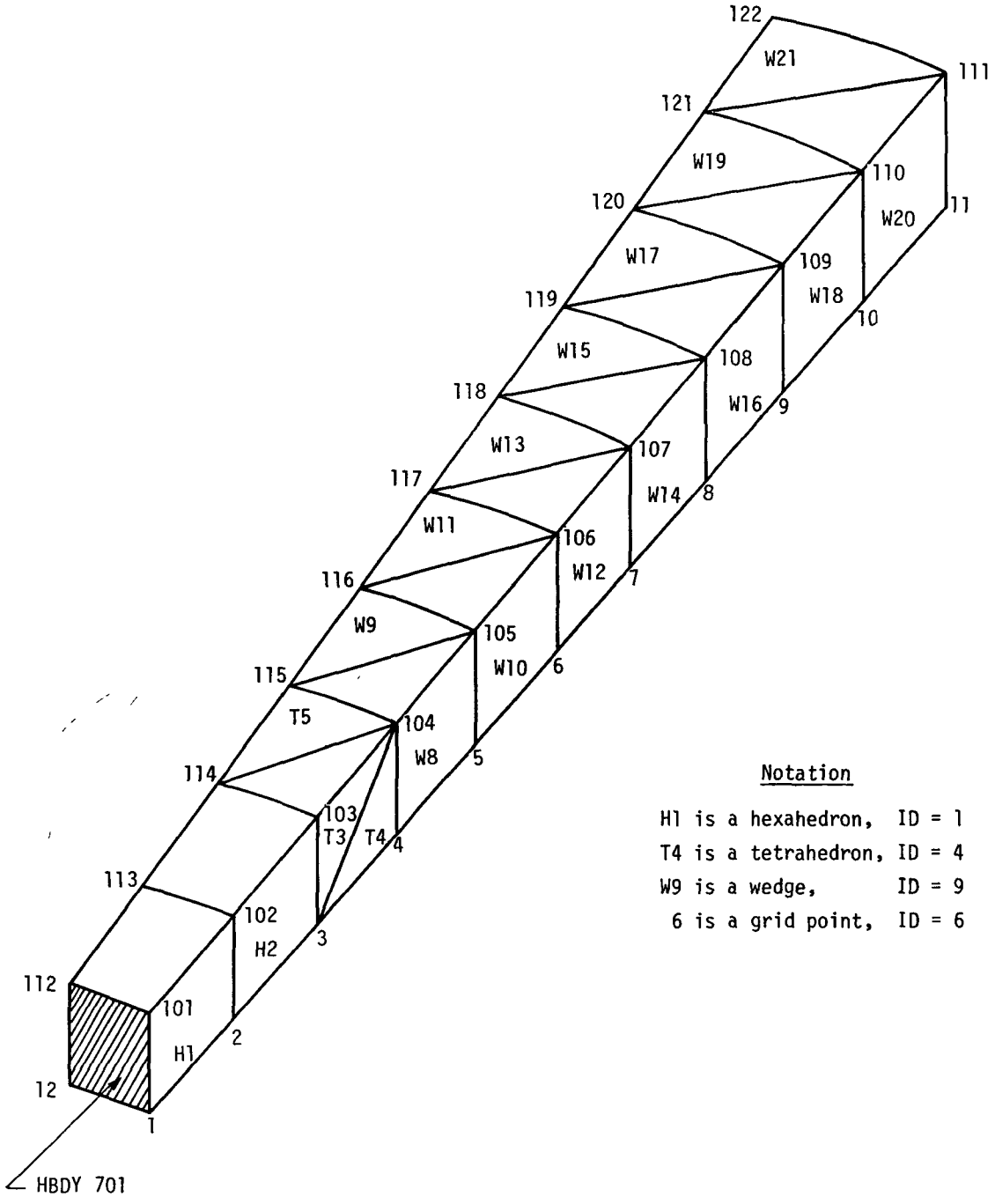

Notation

H1 is a hexahedron, ID = 1
T4 is a tetrahedron, ID = 4
W9 is a wedge, ID = 9
6 is a grid point, ID = 6

Figure 2. Elements and Grid Points

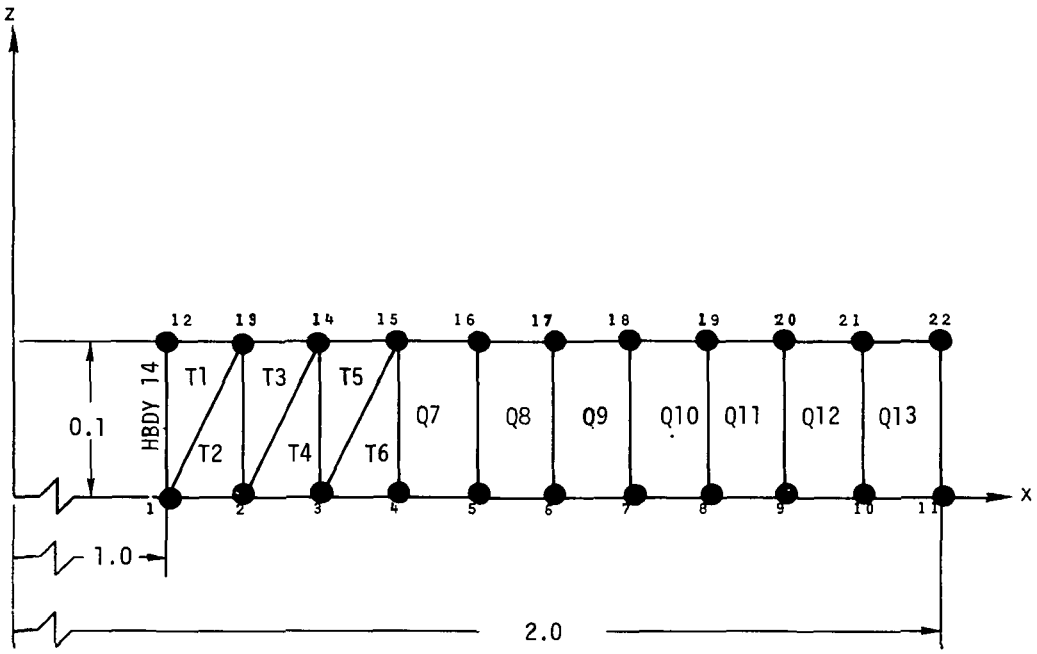

T TRIARG elements

Q TRAPRG elements

U_a = 488.5 at left end

U_a = 0.0 at right end

Figure 3. Section of a pipe, modeled with ring elements

RIGID FORMAT No. 1, Static Analysis

Thermal and Pressure Loads on a Long Pipe Using Linear Isoparametric Elements (1-13-1)
Thermal and Pressure Loads on a Long Pipe Using Quadratic Isoparametric Elements (1-13-2)
Thermal and Pressure Loads on a Long Pipe Using Cubic Isoparametric Elements (1-13-3)

A. Description

These problems demonstrate the use of the linear, quadratic and cubic isoparametric solid elements, IHEX1, IHEX2 and IHEX3, respectively. A long pipe, assumed to be in a state of plane strain, is subjected to an internal pressure and a thermal gradient in the radial direction The structure modeled is shown in Figure 1. The finite element NASTRAN models for each of the elements are shown in Figures 2, 3 and 4.

B. Input

1. Parameters:

$r_{inner} = a = 4$ in.	(radius to the inner surface)
$r_{outer} = b = 5$ in.	(radius to the outer surface)
$E = 30.x10^6$ psi	(Young's Modulus)
$\nu = 0.3$	(Poisson's Ratio)
$\alpha = 1.428 \times 10^{-5}$	(thermal expansion coefficient)
$\rho = 7.535 \times 10^{-4} \frac{lb\text{-}sec^2}{in^4}$	(mass density)
$p = 10$ psi	(inner surface pressure)
$T_1 = 100.0°F$	(inner surface temperature)
$T_o = 0.0°F$	(outer surface temperature)

2. Boundary Conditions:

$u_\theta = 0$ at all points on the right side

$u_\theta = 0$ at all points on the left side

$u_z = 0$ at all points on the bottom surface

$u_z = 0$ at all points on the top surface

3. Loads:

Subcase 1,

p = 10 psi (internal pressure)

Subcase 2,

$$T_r = \frac{(T_i - T_o)}{\ln(\frac{b}{a})} \ln(\frac{b}{r}) = \frac{100}{\ln(1.25)} \ln(\frac{5}{r}) \text{ , where r is any radius.}$$

C. Theory

1. Subcase 1

The normal stresses due to the pressure load (Reference 24) are obtained by

$$\sigma_r = -\frac{a^2b^2}{(b^2-a^2)} \frac{p}{r^2} + \frac{pa^2}{(b^2-a^2)} \quad ,$$

$$\sigma_\theta = \frac{a^2b^2}{(b^2-a^2)} \frac{p}{r^2} + \frac{pa^2}{(b^2-a^2)} \quad ,$$

and $$\sigma_z = 2\nu \frac{pa^2}{(b^2-a^2)} \quad .$$

where r is the radius and all shearing stresses are zero.

The displacement in the radial direction is

$$u_r = \frac{(1-2\nu)(1+\nu)}{E} r \frac{pa^2}{(b^2-a^2)} + \frac{(1+\nu)}{E} \frac{1}{r} \frac{pa^2b^2}{(b^2-a^2)} \quad ,$$

and all other displacements are zero.

2. Subcase 2

The stresses in the radial and tangential directions due to the thermal load (Reference 24) are given by

$$\sigma_r = \frac{\alpha E T_i}{2(1-\nu)\ln(\frac{b}{a})} \left[-\ln(\frac{b}{r}) - \frac{a^2}{(b^2-a^2)} (1 - \frac{b^2}{r^2}) \ln(\frac{b}{a}) \right] \quad ,$$

and $$\sigma_\theta = \frac{\alpha E T_i}{2(1-\nu)\ln(\frac{b}{a})} \left[1 - \ln(\frac{b}{r}) - \frac{a^2}{(b^2-a^2)} (1 + \frac{b^2}{r^2}) \ln(\frac{b}{a}) \right] \quad .$$

The stress in the axial direction is obtained via the procedure contained in the reference as

$$\sigma_z = \frac{\alpha E T_i}{2(1-\nu)\ln(\frac{b}{a})} \left[\nu - \frac{2a^2\nu}{(b^2-a^2)} \ln(\frac{b}{a}) - 2\ln(\frac{b}{r})\right] .$$

All shearing stresses are zero.

The displacement in the radial direction is

$$u_r = \frac{(1+\nu)}{(1+\nu)} \alpha \frac{T_i}{\ln(\frac{b}{a})} \left\{ -\frac{1}{r}\left[\frac{a^2b^2}{2(b^2-a^2)} \ln(\frac{b}{a})\right] \right.$$

$$\left. + \frac{r}{4}\left[2\ln(\frac{b}{r}) + 1 + (1-2\nu)\left(1 - \frac{2a^2}{(b^2-a^2)} \ln(\frac{b}{a})\right)\right]\right\} .$$

D. Results

Representative displacements and stresses for the finite element results compared to theoretical predictions are plotted in Figures 5 and 6. Note that five IHEX1 elements were used along the radial thickness whereas one element was used for each of the IHEX2 and IHEX3 cases. Two values for the stress occur at the boundary of two adjacent IHEX1 elements resulting in a sawtooth pattern.

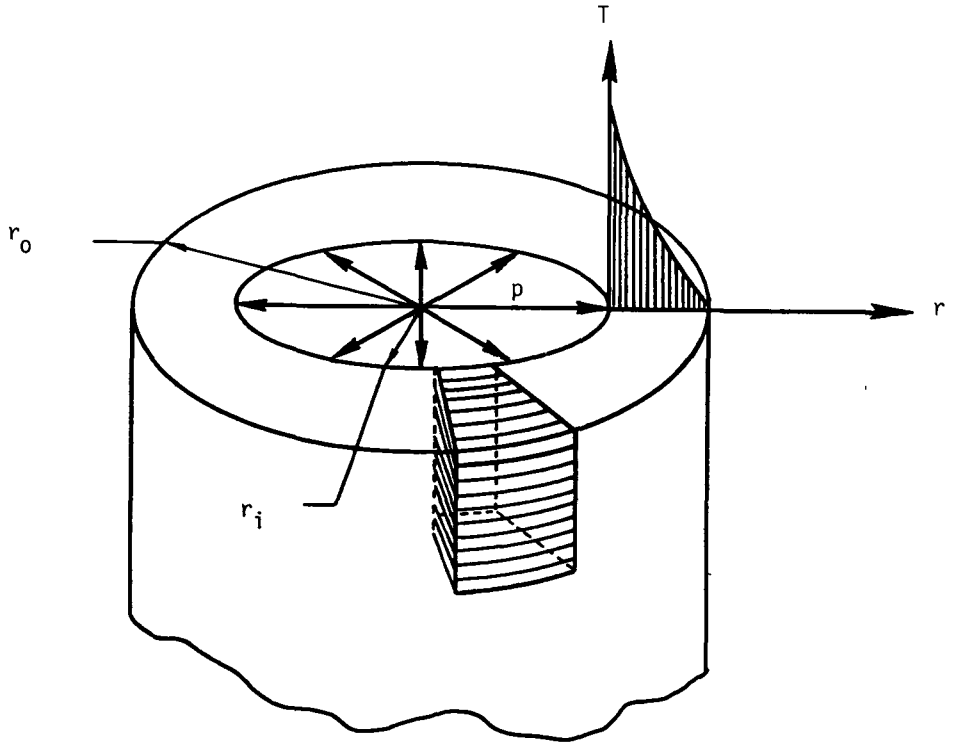

Figure 1. Long pipe with pressure and thermal loads.

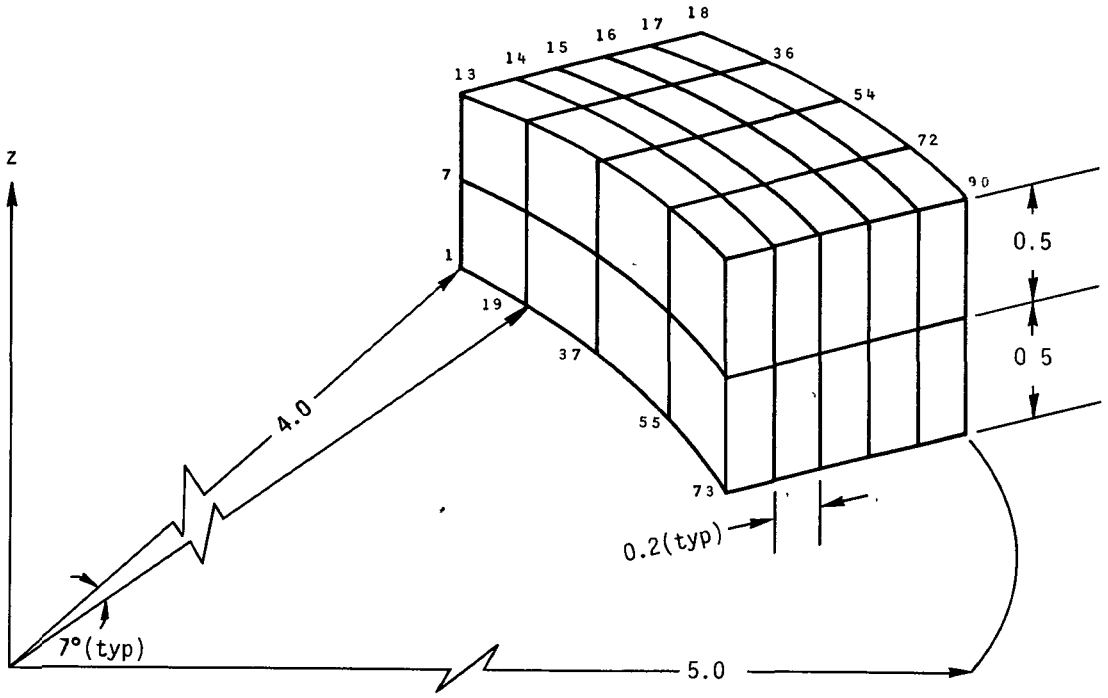

Figure 2. Model of section using forty IHEX1 elements.

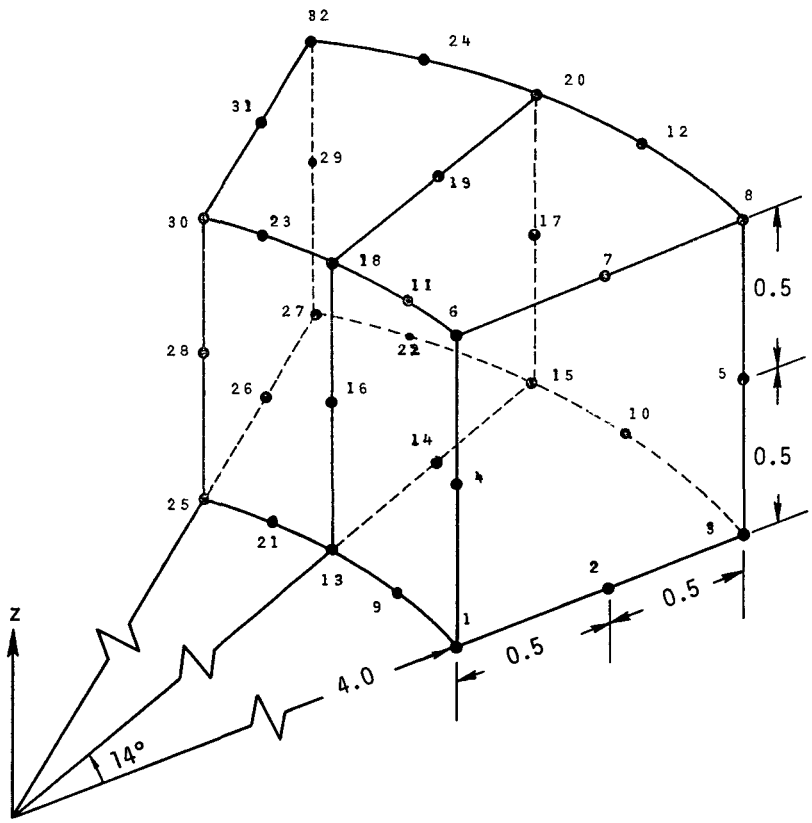

Figure 3. Model of section using two IHEX2 elements.

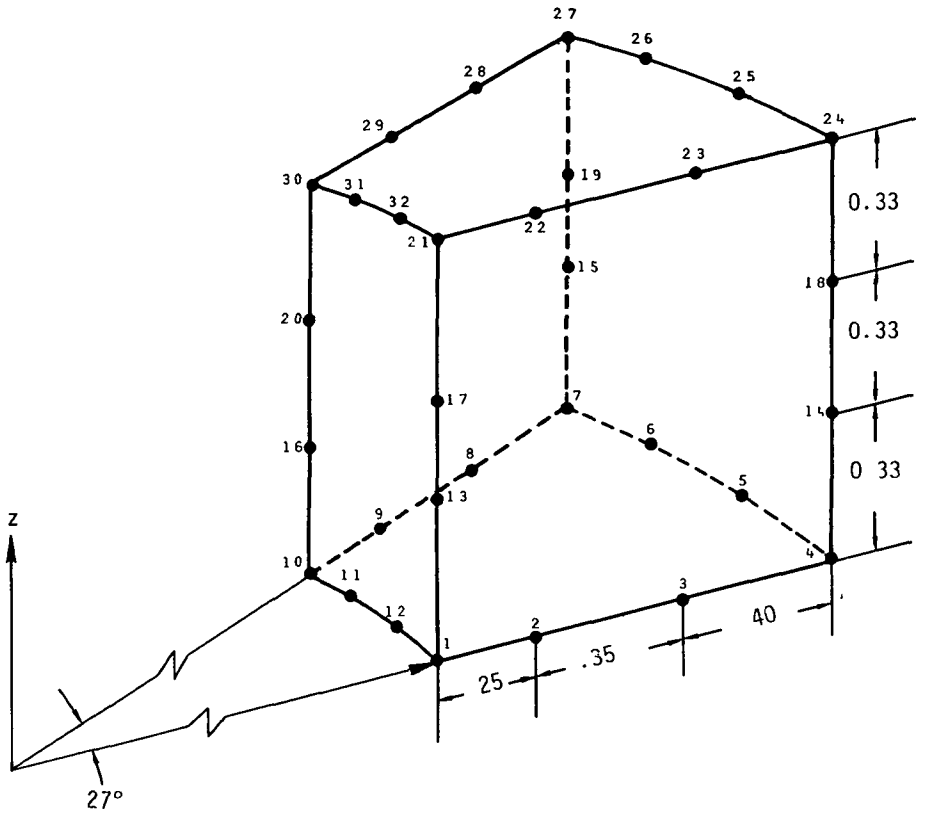

Figure 4. Model of section using one IHEX3 element.

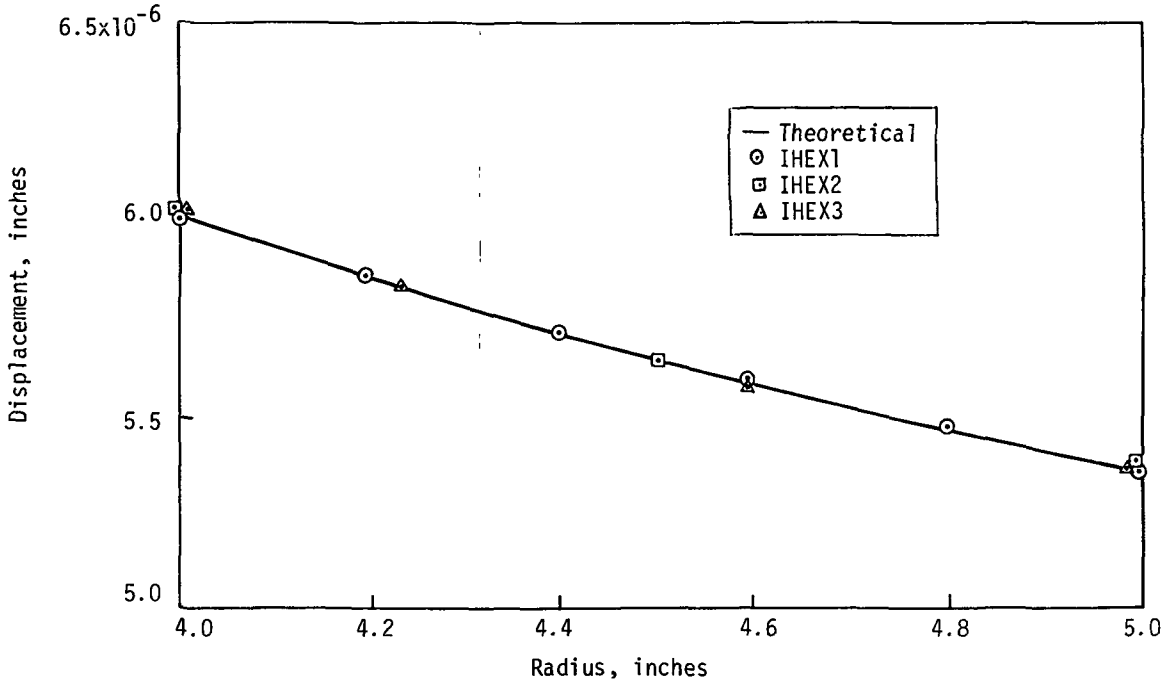

(a) Radial deflections, pressure load.

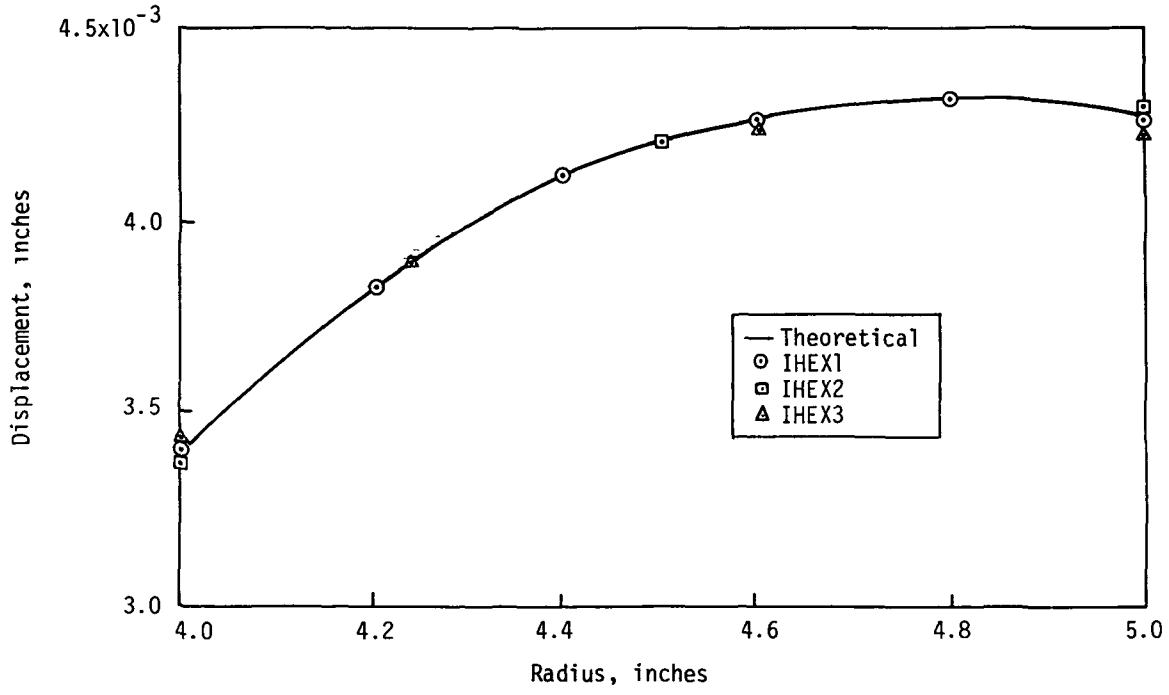

(b) Radial deflections, thermal load.

Figure 5. Deflection comparisons.

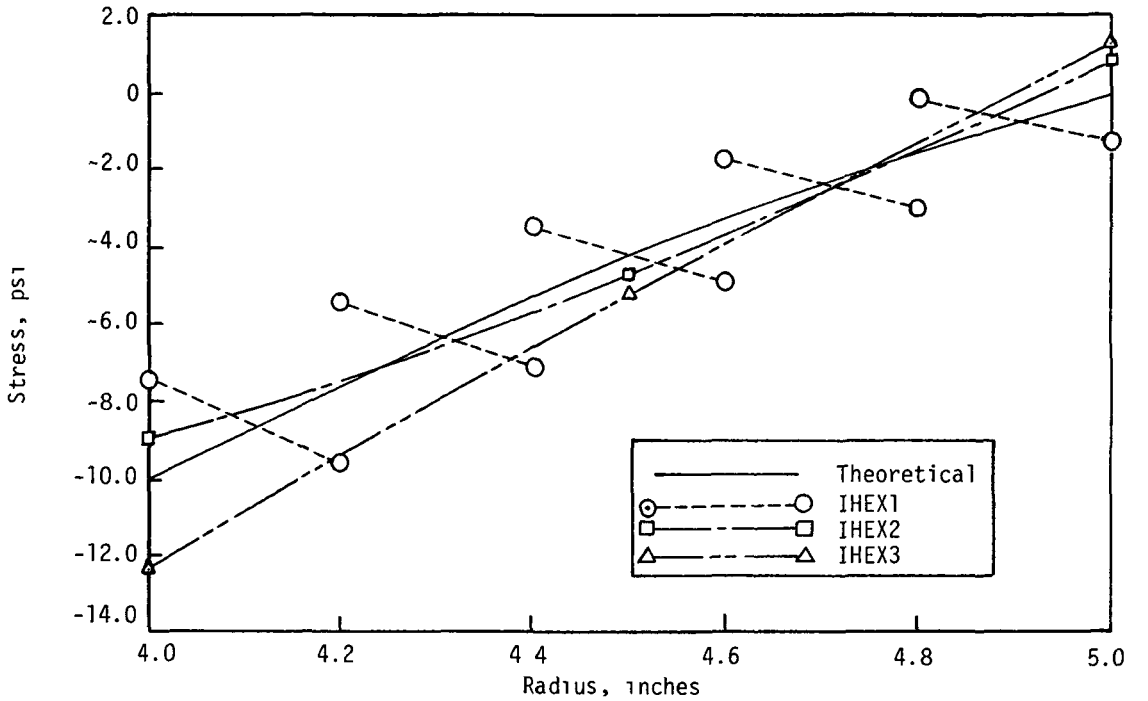

(a) Radial stress, pressure load.

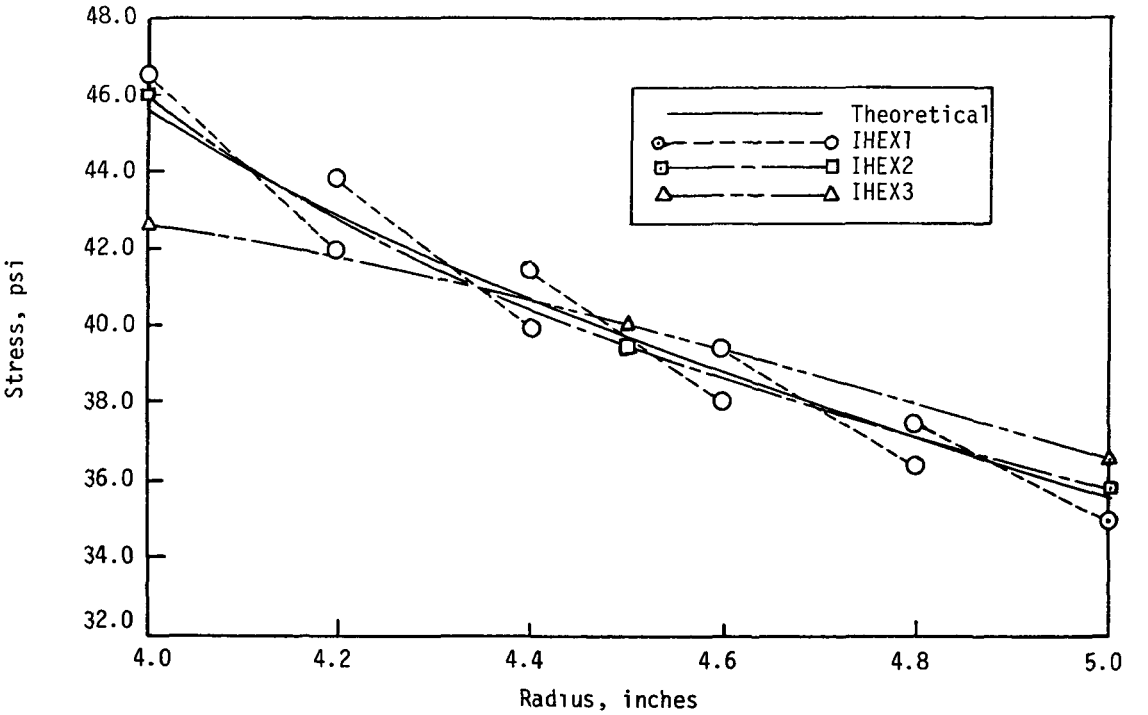

(b) Circumferential stress, pressure load.

Figure 6. Stress comparisons.

RIGID FORMAT No. 1, Static Analysis

Static Analysis of a Beam Using General Elements (1-14-1)

A. Description

This problem demonstrates the use of general GENEL elements having various types of input format in the static analysis of a cantilever beam subjected to tension and bending. The beam consists of five GENEL elements and one BAR element as shown in Figure 1

The GENEL elements are constructed as follows:

GENEL Element	Approach	Matrix Size	$\{u_d\}$	[S]
1	Flexibility	3	No	No
2	Stiffness	6	No	No
3	Stiffness	3	Yes	Yes
4	Stiffness	3	Yes	No
5	Flexibility	3	Yes	No

B. Input

1. Parameters

ℓ = 6.0 m (length)

E = 6.0 N/m^2 (modulus of elasticity)

V = 0.3 (Poisson's ratio)

A = 1.0 m^2 (cross-sectional area)

I = .083 m^4 (bending moment of inertia)

F_x = 1.0 N (axial load)

P_y = 1.0 N (transverse load)

C. Theory

The stiffness matrix for the BAR element in its general form is given in section 8 of the NASTRAN Programmer's Manual.

Define [Z] as the matrix of deflection influence coefficients (flexibility matrix) whose terms are $\{u_i\}$ when $\{u_d\}$ is rigidly constrained,

[K] as the stiffness matrix,

[S] as a rigid body matrix whose terms are $\{u_1\}$ due to unit motions of $\{u_d\}$, when all $\{f_1\}$ = 0,

$\{f_i\}$ as the vector of forces applied to the element at $\{u_i\}$,

and $\{f_d\}$ as the vector of forces applied to the element at $\{u_d\}$. They are assumed to be statically related to the $\{f_i\}$ forces, i.e., they constitute a nonredundant set of reactions for the element. If transverse shear is neglected and the beam is confined to motion in the X-Y plane, then

$$\{f_1\} = [K]\{u_i\} ,$$

where

$$\{f_i\} = \begin{Bmatrix} F \\ V_2 \\ M_1 \end{Bmatrix} \qquad \{u_1\} = \begin{Bmatrix} \delta x \\ \delta y \\ \theta z \end{Bmatrix} ,$$

$$[K] = \begin{bmatrix} \frac{AE}{\ell} & 0 & 0 \\ 0 & \frac{12EI}{\ell^3} & \frac{6EI}{\ell^2} \\ 0 & \frac{6EI}{\ell^2} & \frac{4EI}{\ell} \end{bmatrix} = \begin{bmatrix} 6 & 0 & 0 \\ 0 & 6 & 3 \\ 0 & 3 & 2 \end{bmatrix} ,$$

$$[F] = [K]^{-1} \begin{bmatrix} \frac{1}{6} & 0 & 0 \\ 0 & \frac{2}{3} & -1 \\ 0 & -1 & 2 \end{bmatrix} ,$$

and

$$[S] = \begin{bmatrix} 1 & 0 & \Delta u_y \\ 0 & 1 & \Delta u_x \\ 0 & 0 & 1 \end{bmatrix} = \begin{bmatrix} 1 & 0 & 0 \\ 0 & 1 & -1 \\ 0 & 0 & 1 \end{bmatrix} ,$$

where $\Delta u = u_d - u_i$, i.e., the difference between the dependent displacement degree of freedom $\{u_d\}$ and the independent displacement degree of freedom $\{u_1\}$.

D. Results

The theoretical maximum deflection of the cantilever beam subjected to tension and bending (for the input values) are

$$\delta x = \frac{F\ell}{AE} = 1.0 \text{ m (tension)}$$

and

$$\delta y = \frac{P\ell^3}{3EI} = 144.0 \text{ m} \quad \text{(bending)}$$

These results are obtained by NASTRAN.

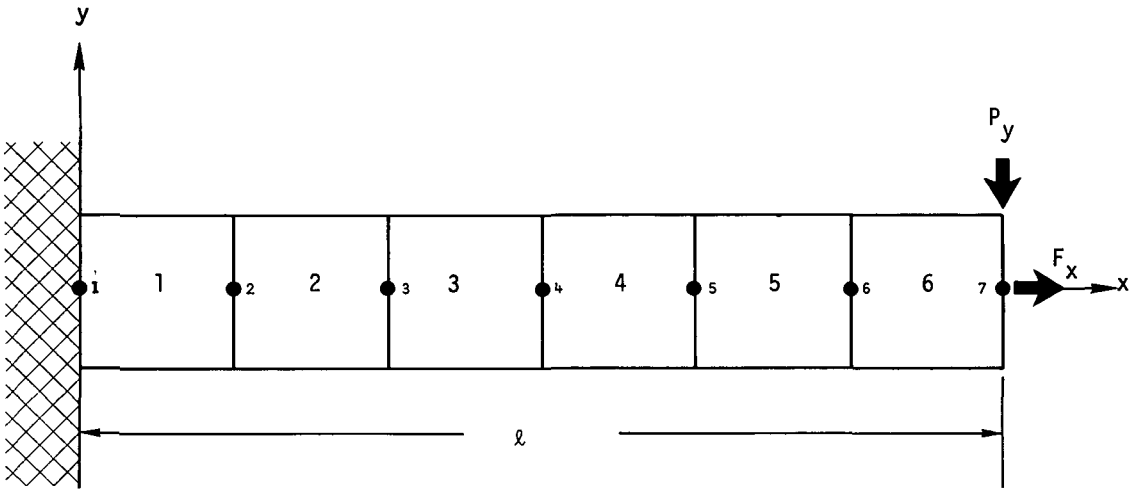

GENEL elements 1 thru 5
RØD element 6

Figure 1. NASTRAN General Element model.

RIGID FORMAT No. 1, Static Analysis

Axisymmetric Cylinderical Thick Shell Subjected to Asymmetric Pressure Loading
(1-15-1)

A. Description

This problem demonstrates the use of elements TRAPAX and TRIAAX in the analysis of asymmetrically loaded solids of revolution The structure, illustrated in Figure 1, consists of a circular cylindrical shell loaded with a uniform external pressure over a small square area.

The cylindrical shell wall is assumed to be simply supported, i.e., the radial and circumferential deflections and the bending moments are zero at the ends.

The upper half of the structure is modeled as shown in Figure 2. Trapezoidal elements having small and large dimensions, are used in the vicinity of the load and away from the load, respectively. A transition area, between the two trapezoidal configurations, is modeled with triangular elements to illustrate their use.

The loads and deflections, not required to be axisymmetric, are expanded in Fourier series with respect to the azimuthal coordinate. Due to the one plane of symmetry of this problem with respect to the $\phi = 0$ plane, the deflections are represented by a cosine series selected by the AXISYM Case Control card. The highest harmonic used, 10, is defined on the AXIC Bulk Data card. The pressure load is defined using PRESAX bulk Data cards.

B. Input

1. Parameters:

r_a	= 15 in.	(Average radius)
t	= 1 in.	(Thickness)
ℓ	= 45 in.	(Length)
$2c$	= 3.75 in.	(Load Length)
β	= 0.125 radians	(Load Arc ($\beta = c/r_a$))
E	= 66666.7 psi	(Modulus of Elasticity)
ν	= 0.3	(Poisson's Ratio)
n	= 10	(Harmonics)

2 Loads·

p	= 7.11111 psi	(Pressure)
A	= 14.063 in^2	(Area of Load ($A = 4c^2$))

3. Supports:

Simply supported at the ends: $u_r = 0, u_\phi = 0$

Symmetry at the midplane: $u_z = 0$

C. Theory

Theoretical results for this problem are taken from Reference 20, p. 568. The following theoretical values occur at the center of the load ($z = \frac{\ell}{2}, \phi = 0$):

$u_r = 272 \frac{pA}{Er_a} = 0.0272$ in. (Radial Deflection (inward))

$M_\phi = 0.1324\ pA = 13.24$ in-lb/in (Circumferential Bending Moment)

$M_z = 0.1057\ pA = 10.57$ in-lb/in (Longitudinal Bending Moment)

$F_\phi = -2.6125 \frac{pA}{r_a} = -17.42$ lb/in (Circumferential Membrane Force)

$F_z = -2.320 \frac{pA}{r_a} = -15.47$ lb/in (Longitudinal Membrane Force)

Theoretical stresses on the inside and outside walls at this point ($z = \frac{\ell}{2}, \phi = 0$) are computed as follows:

$$\sigma_z = \frac{F_z}{t} \pm \frac{6M_z}{t^2} = \begin{matrix} 47.95 \text{ psi} & \text{(Inside Wall Longitudinal Stress)} \\ -78.89 \text{ psi} & \text{(Outside Wall Longitudinal Stress)} \end{matrix}$$

$$\sigma_\phi = \frac{F_\phi}{t} \pm \frac{6M_\phi}{t^2} = \begin{matrix} 62.02 \text{ psi} & \text{(Inside Wall Circumferential Stress)} \\ -96.86 \text{ psi} & \text{(Outside Wall Circumferential Stress)} \end{matrix}$$

D. Results

Figure 3 shows the NASTRAN radial deflection at the center of the load as a function of the number of harmonics selected for the solution. As can be seen, the solution is near convergence with ten harmonics.

Figure 4 shows stresses, σ_z and σ_ϕ, through the shell wall, at the center of the load. Ten harmonics shows very good convergence to nearly the theoretical values computed above. However, seven harmonics would result in relatively poor convergence even through Figure 3 indicates the displacement was close to convergence. Thus, displacement convergence alone may be an invalid indicator of an adequate solution.

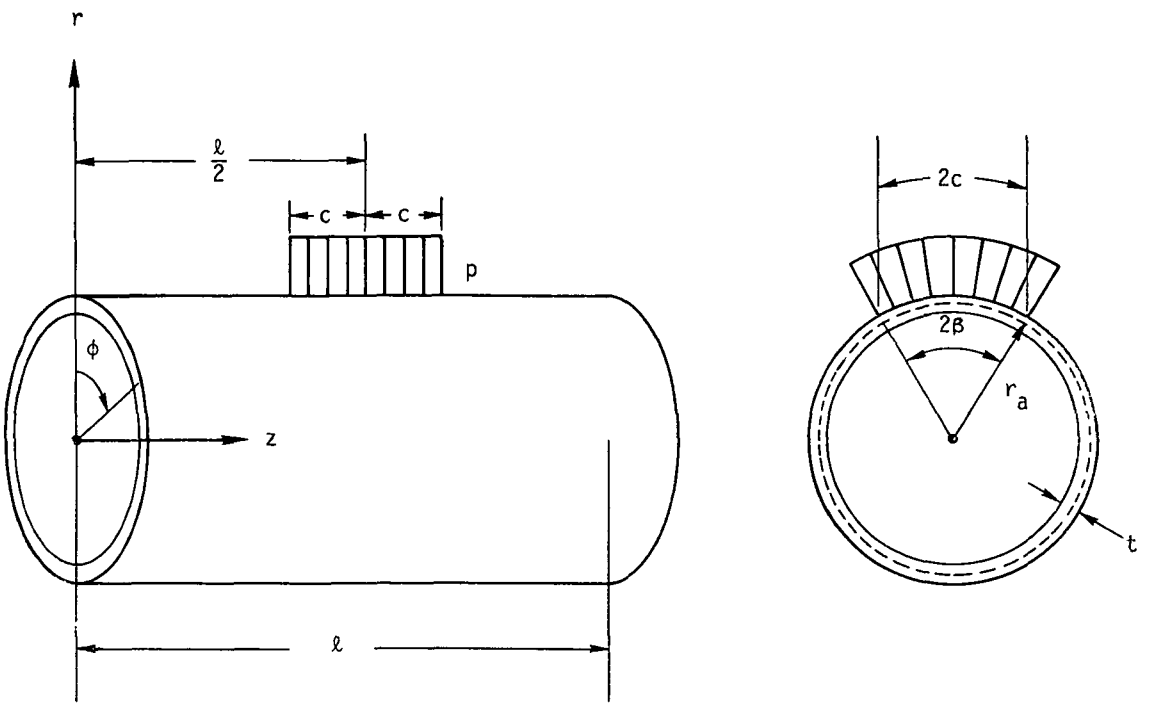

Figure 1. Cylindrical shell loaded by a uniformly distributed load

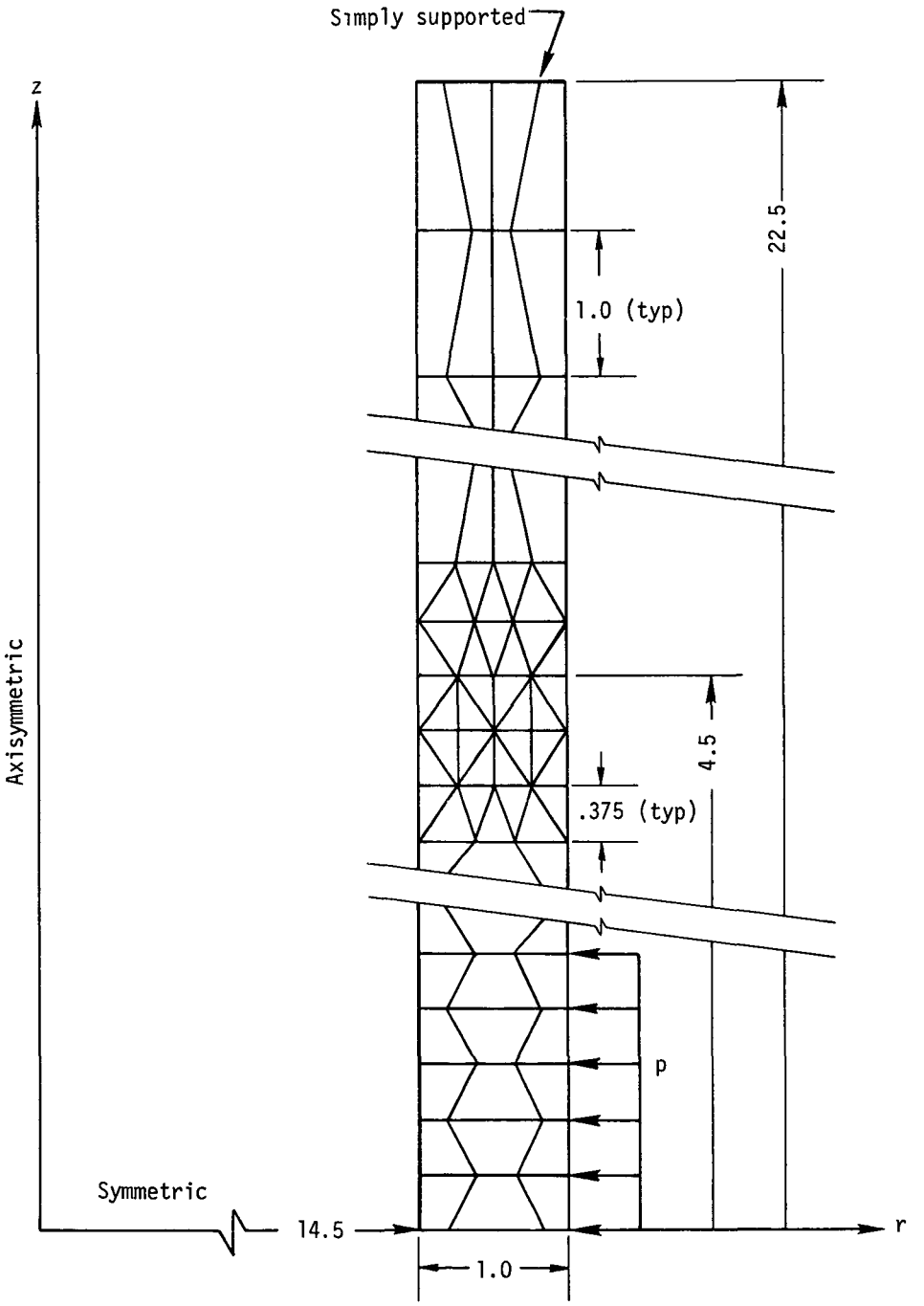

Figure 2. NASTRAN shell model.

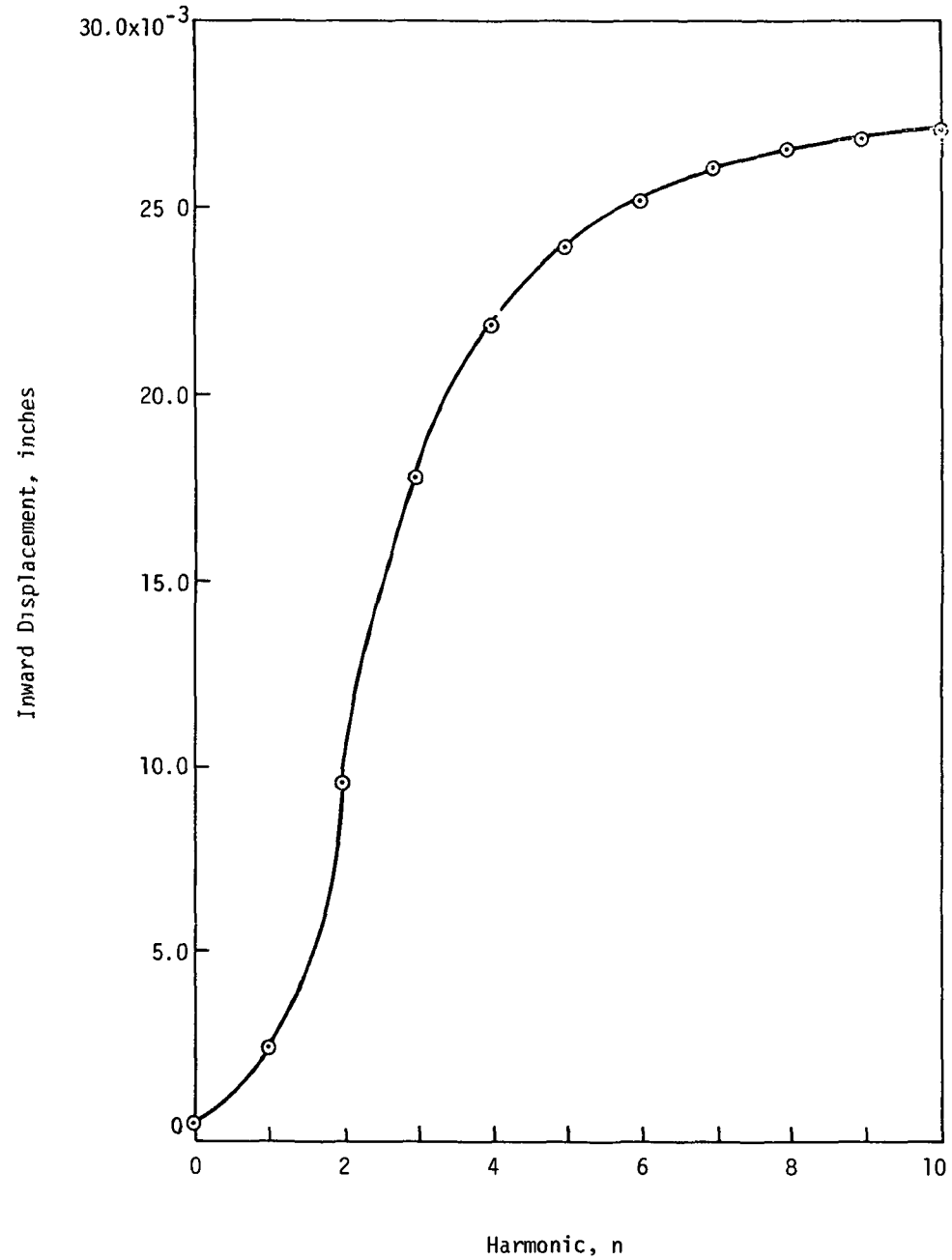

Figure 3. Radial deflection at center of load.

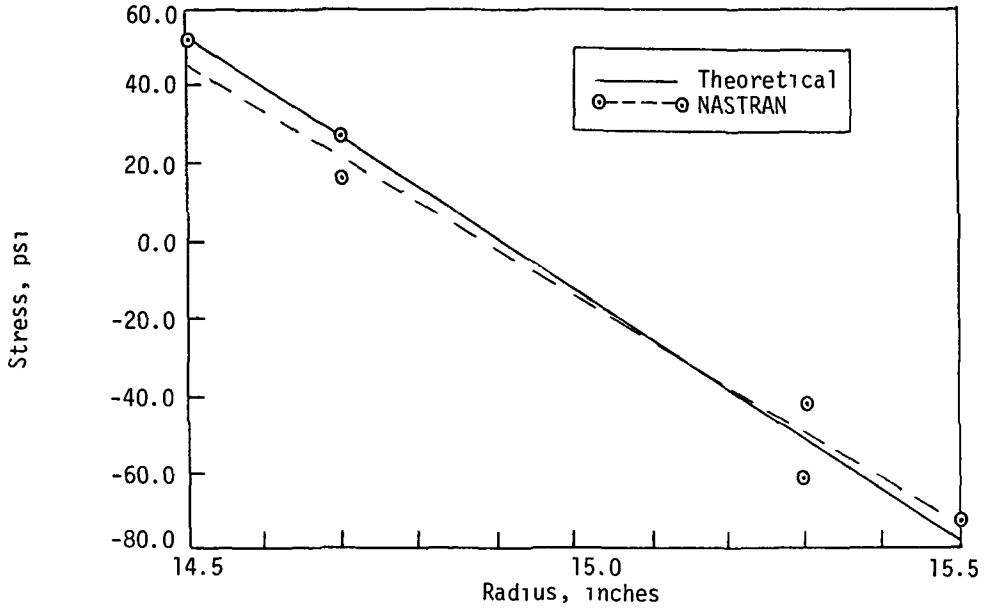

(a) Axial stress.

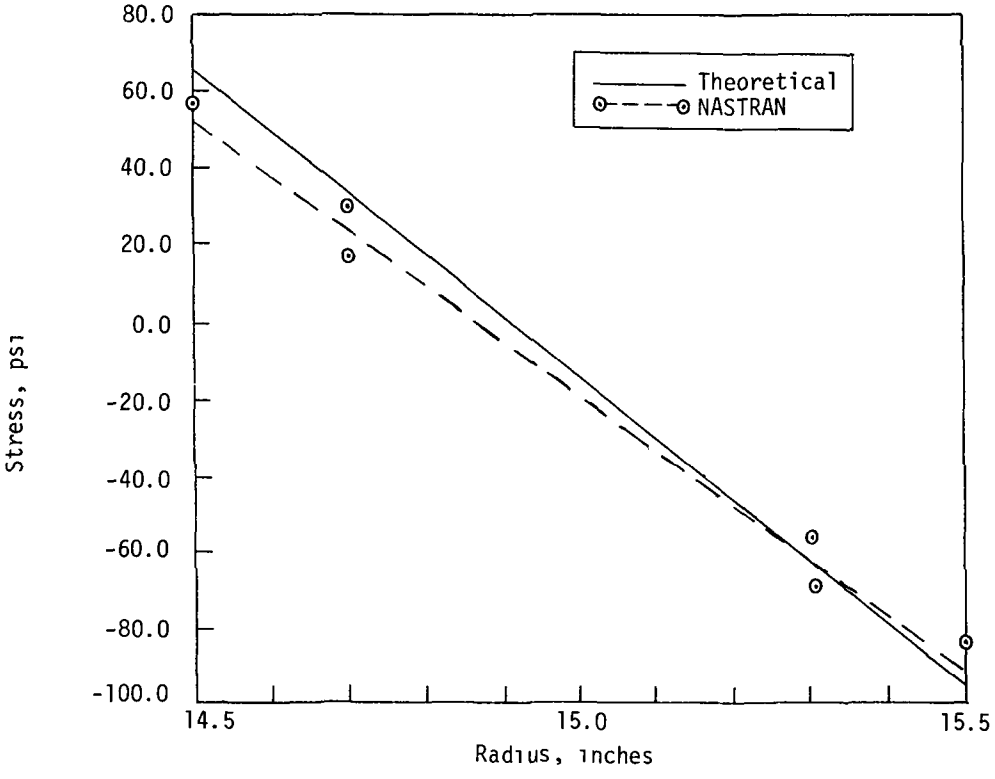

(b) Circumferential stress.

Figure 4. Stresses at center of load.

RIGID FORMAT No. 1, Static Analysis

Fully Stressed Design of a Plate with a Reinforced Hole (1-16-1)

A. Description

A flat plate with a reinforced hole in the center is optimized for stresses due to a uniform end load. Restrictions on the minimum thickness are maintained. The plate is shown in Figure 1 and the finite element idealization is illustrated in Figure 2. This problem has been investigated by G. G. Pope (Reference 21).

Due to symmetry, only one quadrant is modeled. Due to the membrane load all rotations and normal displacements are constrained. The QDMEM and TRMEM elements are used for the plate and RØD elements for the reinforcement around the hole.

The problem demonstrates several features unique to fully stressed design capability in NASTRAN. These features are:

1. Elements with no limits on the range of the property change, i.e., the RØD has no PLIMIT data.
2. Elements with a lower limit on the property optimization card. All membrane elements are required to have a resultant thickness which must not be less than a minimum thickness. This minimum is determined from the thickness obtained when the plate without a hole is subjected to an end load at a prescribed stress limit.
3. Elements whose stress is not inspected but being in an area of nearly uniform stress have their properties changed due to another element's stress. Element 7 has no stress request but does have the same property identification number as element 17. This type of optimization can save computer time at the expense of a design that may not be truely optimized.
4. A property whose value depends on the maximum stress of two elements. Elements 5 and 15 have the same property card. This option may be necessary if insufficient core is allocated.
5. Temperature dependent stress limits for material 3
6. Using one stress limit only. The membrane elements use the maximum principle shear only. This is 1/2 the major principle stress allowed. This stress limit was chosen to better model the octahedral limit in Reference 21.

   The rod elements use only the tension and compression stress appropriate to the given property, namely area.
7. An additional load case that was not included in the fully stressed design because a stress request was not made. The second subcase may be considered a displacement verification of this load case.

B. Input

1. Parameters

ℓ = 30.0 in (total length)

w = 20.0 in (total width)

d = 10.0 in (hole diameter)

t_o = 3.348 in (initial plate thickness)

A_o = 1.674 in^2 (initial rod cross sectional area)

E = 30.x10^6 psi (modulus of elasticity)

ν = 0.3 (Poisson's ratio)

t_e = 1.0 in (lower limit for plate thickness corresponding to a 25.0x10^3 maximum principle stress)

2. Boundary conditions:

on y = 0 plane, u_y = 0 (symmetry)

on x = 0 plane, u_x = 0 (symmetry)

all points $u_z = \theta_x = \theta_y = \theta_z = 0$ (permanent constraints)

3. Loads·

First subcase: uniform load, F_{10} = 25.0x10^3 lb/in

Second subcase: at grid points 69 and 79, F_{12} = -1000.0 lb

at grid point 78, F_{12} = -2000.0 lb

(contact load on rim of hole - displacement check only)

C. Theory

The theoretical approach developed for the property optimization technique in NASTRAN is contained in the NASTRAN Theoretical Manual, Section 4.4. This technique is a fully stressed design approach. A mathematical programming technique is used in reference 21 from which the example problem was taken.

The two techniques might be expected to give similar results when the same model is used. However, reference 21 employs elements which allow varying properties and stresses while NASTRAN elements allow only constant properties and constant stresses. Somewhat different geometry is used in the NASTRAN model, i.e., the use of quadrilateral elements for illustration. Additional features of the NASTRAN model are discussed in items 3, 4 and 5 of Part A.

D. Results

The optimization process in this problem is terminated at 5 iterations. The initial weight to final weight ratio is 2.70 compared to Pope's results of 2.63. Tables 1 and 2 show the optimized nondimensional properties of the elements around the arch. Note that the results from reference 21 are averaged to provide an equivalent constant property element for comparison.

Table 1. Optimized Nondimensional Thickness Comparisons.

Element	Original t/t_e	Reference 21 Average t/t_e	NASTRAN t/t_e
37	3.348	1.24	1.00
38	3.348	1.00	1.04
39	3.348	1.00	1.00
46	3.348	2.10	1.14
47	3.348	1.34	2.00
57	3.348	3.32	1.34
59	3.348	3.19	4.40
67	3.348	4.58	5.47
68	3.348	3.26	1.00
69	3.348	4.52	5.49

Table 2. Optimized Nondimensional Area Comparisons.

Element	Original A/dt_e	Reference 21 Average A/dt_e	NASTRAN A/dt_e
101	.1674	.0249	.00716
102	.1674	.0238	0.0 effective
103	.1674	.0636	.05019
104	.1674	.1880	.1839
105	.1674	.3540	.3287

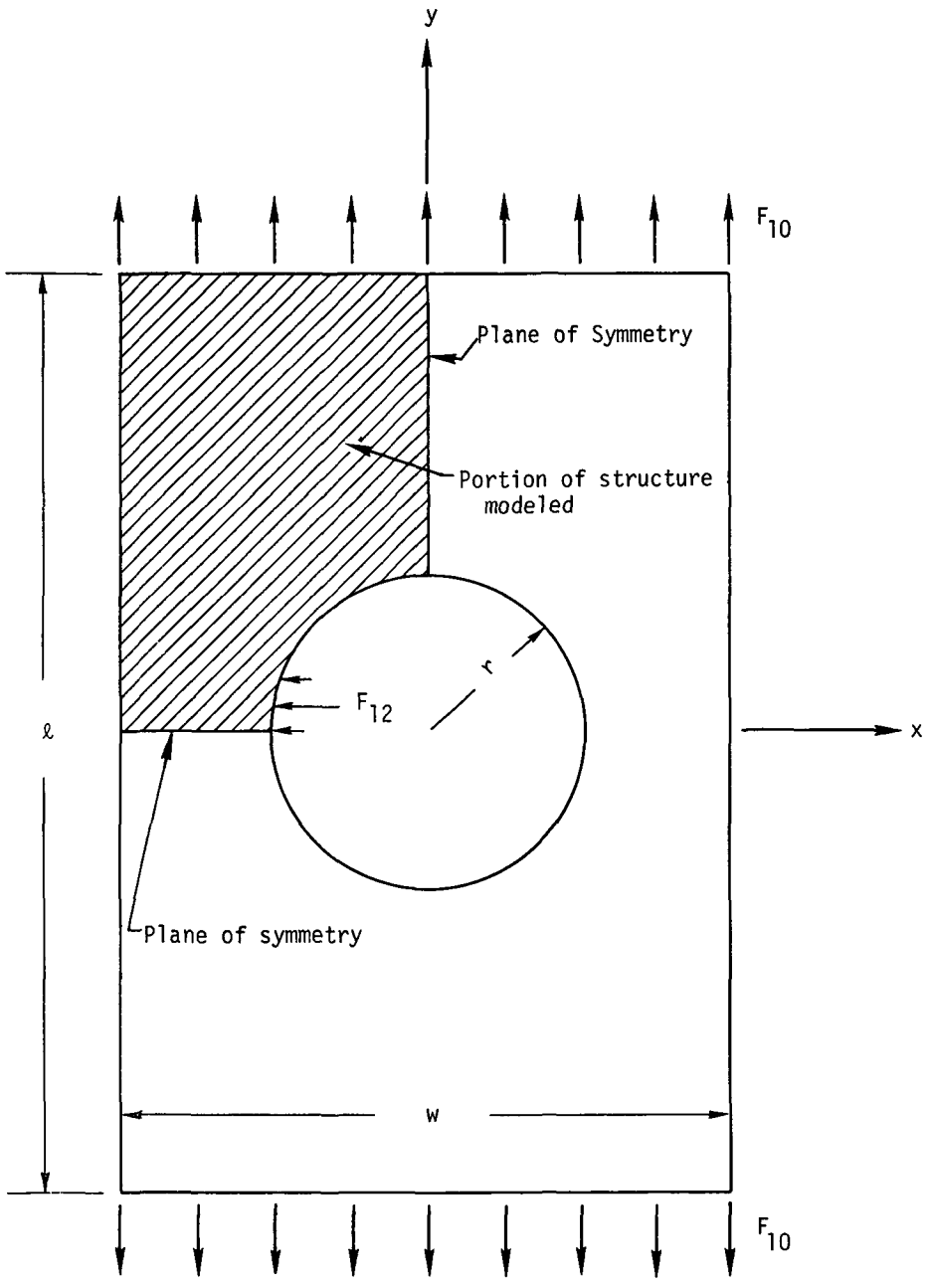

Figure 1. Plate with reinforced hole.

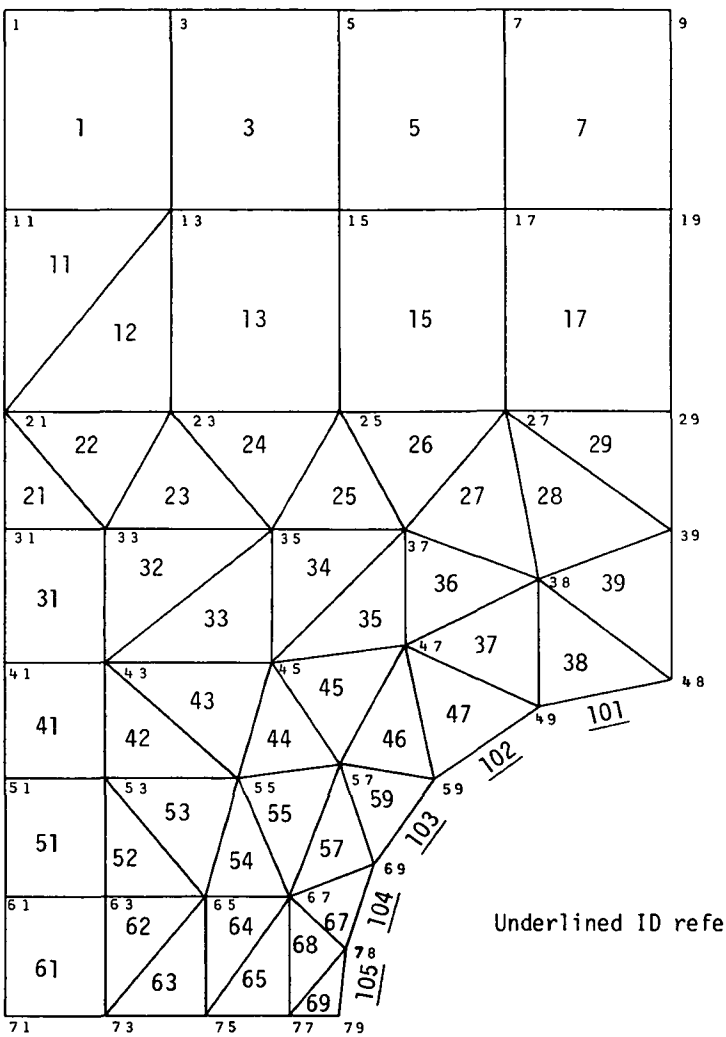

Figure 2. Finite element model.

RIGID FORMAT No. 2, Inertia Relief Analysis

Inertia Relief Analysis of a Circular Ring Under Concentrated and Centrifugal Loads (2-1-1)

A. Description

This problem illustrates the use of inertia relief analysis to solve a free-body problem. In inertia relief the structure is under constant acceleration due to the applied loads; the reactions to the applied load are due to the masses of the structure. Fictitious, nonredundant, support points must be provided to define a reference system attached to the body. The displacements of the body are measured relative to the supported coordinates.

The basic problem is illustrated in Figure 1. The structure consists of a spinning ring with a constant radial load applied to one point. The rotational velocity creates centrifugal loads and the point load causes inertia reactions. The actual dynamic motion of the whole structure is a cyclic motion of the center point coinciding with the rotation of the ring. The displacements measured by the inertia relief analysis, however, will be the static motion relative to the support point displacements.

The displacements are defined in a cylindrical coordinate system ($u_1 = u_r$, $u_2 = u_\phi$, $u_3 = u_z$). The elements used are BAR elements with a large cross-sectional area to minimize axial deformations. The BARs were offset a uniform radial distance from the grid points to demonstrate the offset option of the BAR element.

B. Input

1. Parameters:

   R = 10.0 (radius at end of BAR elements)

   R_1 = 11.0 (Radius at grid points)

   I = 10.0 (Bending inertia)

   ρ = 0.5 (Mass density)

   E = 1000. (Modulus of elasticity)

   A = 1000. (Cross-sectional area)

2. Loads:

   $P_{r,13}$ = 100

   f = 1.59 cps (Rotational velocity, ω = 1.0 radians per second)

3. Supports·

   a) The $u_{r,1}$ direction is supported to restrict vertical translation.

   b) The $u_{\phi,1}$ and $u_{\phi,13}$ directions are supported to restrict rotation and horizontal translation.

4. Grid Point Weight Generator Input:

   Weight and moment of inertia are defined relative to point 19.

C. Answers

1. The Element Forces and Moments may be solved by the following analysis, as explained in Reference 7, Chapter 12.

   a) Using symmetry the structure may be defined by the free-body diagram in figure 2. The static equilibrium equations at any angle are:

$$A = A_o \cos\phi + \mu\phi \sin\phi \quad \text{(Axial Force)}$$

$$V = A_o \sin\phi + \mu\phi \cos\phi \quad \text{(Shear)}$$

$$M = M_o + r[\mu(1 - \cos\phi - \phi \sin\phi) + A_o(1 - \cos\phi)] \quad \text{(Bending Moment)}$$

   b) Using energy and Castigliano's Theorem:

$$U = \frac{R}{2EI} \int_0^{\pi} M^2 \, d\phi$$

$$\frac{\delta U}{\delta M_o} = 0$$

$$\frac{\delta U}{\delta A_o} = 0$$

   These are the deflections at the bottom which are fixed. The resulting two equations are used in step c.

   c) Solving the equations in (b) gives the redundant forces·

$$A_o = -\frac{1}{2}\mu = -\frac{F}{4\pi}$$

$$M_o = \frac{R\mu}{2} = \frac{FR}{4}$$

d) Adding a dummy load and solving the problem with the above boundary conditions gives the displacement due to the point load:

$$\delta_f = \frac{FR^3}{\pi EI}\left(\frac{\pi^2}{8} - 1\right)$$

e) The axial stress and radial displacement due to the centrifugal load is:

$$\sigma_\omega = \rho R^2 \omega^2 = 5.0 \times 10^2$$

$$\delta_\omega = \frac{2\rho R^3 \omega^2}{E} = 1.0$$

f) The total result of summing the two loads is:

		THEORY	NASTRAN
δ	= Displacement $u_{r,13}$	1.75	1.734
M_0	= Moment BAR #1, end A	-79.5	-80.48
M_1	= Moment BAR #12, end B	-238.5	-236.0

g) The structural mass characteristics as calculated by the grid point weight generator are:

	Theoretical	NASTRAN
X_{CG}	= 11.0 from point 19	11.0
Mass	$= \pi \times 10^4 = 3.14159 \times 10^4$	3.1326×10^4
I_{xx}	$= I_{yy} = \frac{\pi}{2} \times 10^6 = 1.5708 \times 10^6$	1.5663×10^6
I_{zz}	$= \pi \times 10^6 = 3.14159 \times 10^6$	3.1326×10^6

(Inertias are about center of gravity)

NASTRAN gives slightly different answers due to the polygonal shape of the finite element model.

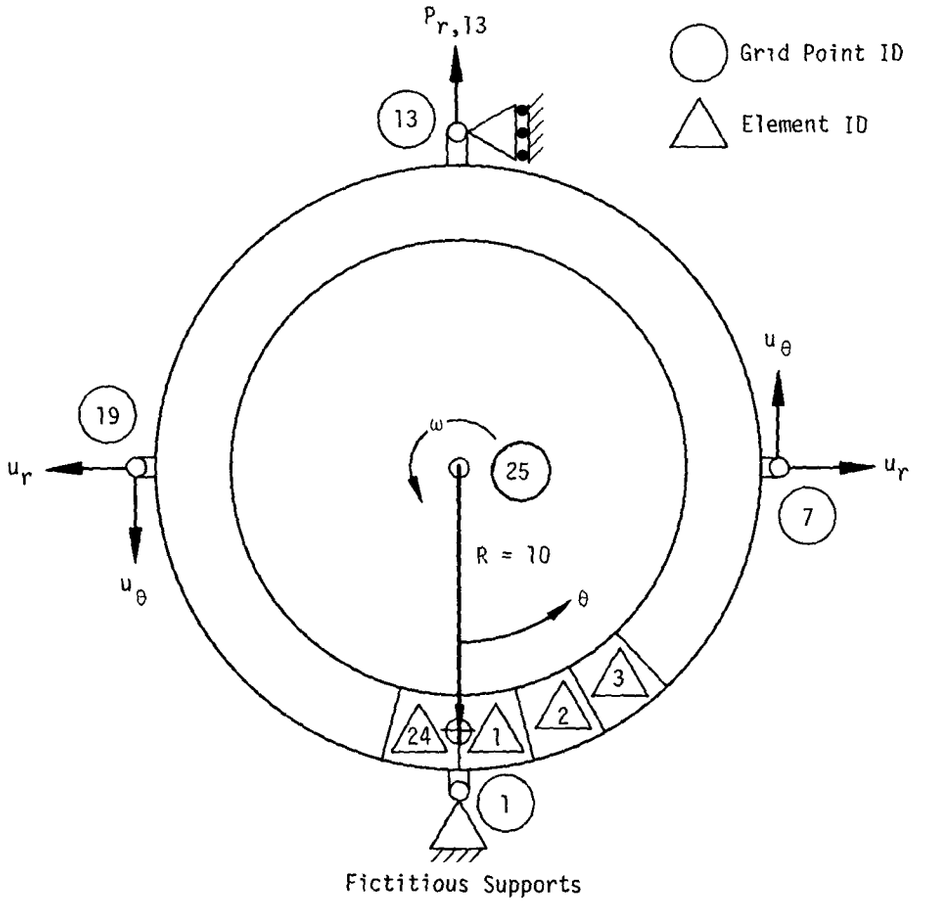

Note: Grid points are offset from center line of ring.

Figure 1. Ring under concentrated and centrifugal loads.

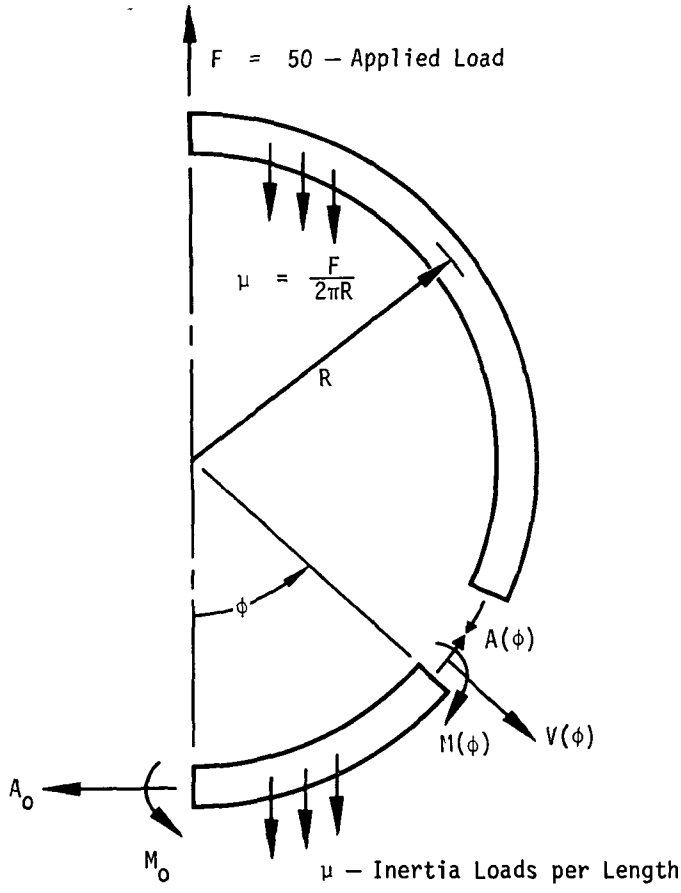

Figure 2. Free body diagram of loads in bending ring.

RIGID FORMAT NO. 2, Inertia Relief Analysis

Windmill Panel Sections for Automated Multi-stage Substructuring, Run 1, (2-2-1)
Windmill Panel Sections for Automated Multi-stage Substructuring, Run 2, (2-2-2)
Windmill Panel Sections for Automated Multi-stage Substructuring, Run 3, (2-2-3)
Windmill Panel Sections for Automated Multi-stage Substructuring, Run 4, (2-2-4)
Windmill Panel Sections for Automated Multi-stage Substructuring, Run 5, (2-2-5)
Windmill Panel Sections for Automated Multi-stage Substructuring, Run 6, (2-2-6)
Windmill Panel Sections for Automated Multi-stage Substructuring, Run 7, (2-2-7)

A. Description

This problem illustrates the fully automated multi-stage substructuring capability of NASTRAN. The single structure model for the Windmill panel problem is shown in Figure 1. Indicated in this figure are the three basic substructures used for the analysis. As can be seen, the entire structure can be composed of only these three components, thus taking advantage of symmetry. The detailed idealizations for the three basic substructures are shown in Figures 2 and 3. These figures show the three separate basic coordinate systems and the local coordinate systems for each of the three basic substructures created.

Of the total of seven runs involved, three Phase 1 runs are made, one for each basic substructure, using Rigid Format 2 in order to generate mass matrices. The combination and reduction to the final model is accomplished in seven distinct Phase 2 steps, plus eight equivalence operations. The sequence of combination steps taken is illustrated in Figures 4a and 4b. Figure 5 details the points retained in the "analysis set" following the Phase 2 Guyan reduction. A static solution, Rigid Format 1, is obtained for each of the three load cases specified. Run 4 produces actual plot output. Runs 5 and 6 demonstrate the Phase 3 data recovery for two of the basic substructures.

A seventh run is made to extract normal modes using Rigid Format 3 for the same reduced structure shown in Figure 5.

B. Input

1. Parameters.

r_o = 50.0 in (outer radius)
r_i = 10.0 in (inner radius)
t = 0.1 in (plate thickness)
E = 10×10^6 psi (modulus of elasticity)
ν = 0.25 (Poisson's ratio)

2. Boundary Conditions:

   All points $u_z = \theta_x = \theta_y = \theta_z = 0$ (permanent constraint)

   $u_x = 0$ at HUB grid points 13, 19, 37, 43

   $u_y = 0$ at HUB grid points 1, 7, 25, 31

3. Loads:

   First Subcase: centrifugal force due to unit angular velocity

   Second Subcase: unsymmetric load - right panel in tension, bottom panel in compression, F = 100 uniformly distributed over each loaded edge

   Third Subcase: F = 1.0 applied at HUB grid point 4 inward radially

4. Substructuring Parameters:

```
SØF(1) = SØFO,950 $ CDC
SØF(1) = FT18,950 $ IBM
SØF(1) = INPT,950 $ UNIVAC
PASSWØRD = DEMØ
ØPTIØNS = K, M, P
```

C. Theory

This problem is designed to illustrate the use of automated multi-stage substructuring. No closed form solution is available. Results are compared with non-substructured NASTRAN solutions.

D. Results

The solutions of the final reduced structure using both Rigid Format 1 and Rigid Format 3 are in excellent agreement with the non-substructured solutions. Displacements at selected points and eigenvalues are compared in Table 1. The values presented were obtained from executions on IBM equipment. Values obtained from CDC and UNIVAC are of the same order of magnitude with slight differences attributable to round-off of very small numbers.

Table 1. Comparison of Displacements at Selected Points for Windmill Panel Problem

Name/Point/Comp	Subcase 1		Subcase 2		Eigenvector #1	
	Single Step	Substructure	Single Step	Substructure	Single Step	Substructure
VANE1/1/X	-5.6×10^{-14}	-5.2×10^{-14}	-2.19155×10^{-5}	-2.19155×10^{-5}	1.000000	-.999752
VANE1/1/Y	-6.88493×10^{-7}	-6.88488×10^{-7}	8.6081×10^{-1}	8.6081×10^{-1}	-8.612×10^{-9}	3.297×10^{-7}
RVANE1/1/X	4.4×10^{-14}	2.1×10^{-13}	2.19155×10^{-5}	2.19155×10^{-5}	1.000000	-,999748
RVANE1/1/Y	-6.88493×10^{-7}	-6.88488×10^{-7}	3.85998×10^{-4}	-3.85997×10^{-4}	1.264×10^{-9}	-1.688×10^{-7}
HUB/5/X	-3.5×10^{-14}	-4.8×10^{-14}	$1.04757z10^{-5}$	1.04757×10^{-5}	-1.46899×10^{-1}	1.46636×10^{-1}
HUB/5/Y	6.70493×10^{-8}	6.70488×10^{-8}	-6.43969×10^{-7}	-6.4397×10^{-7}	-3.140×10^{-9}	$-7\ 8304\times10^{-6}$
Frequency, cps	-	-	-	-	288.3	288.3

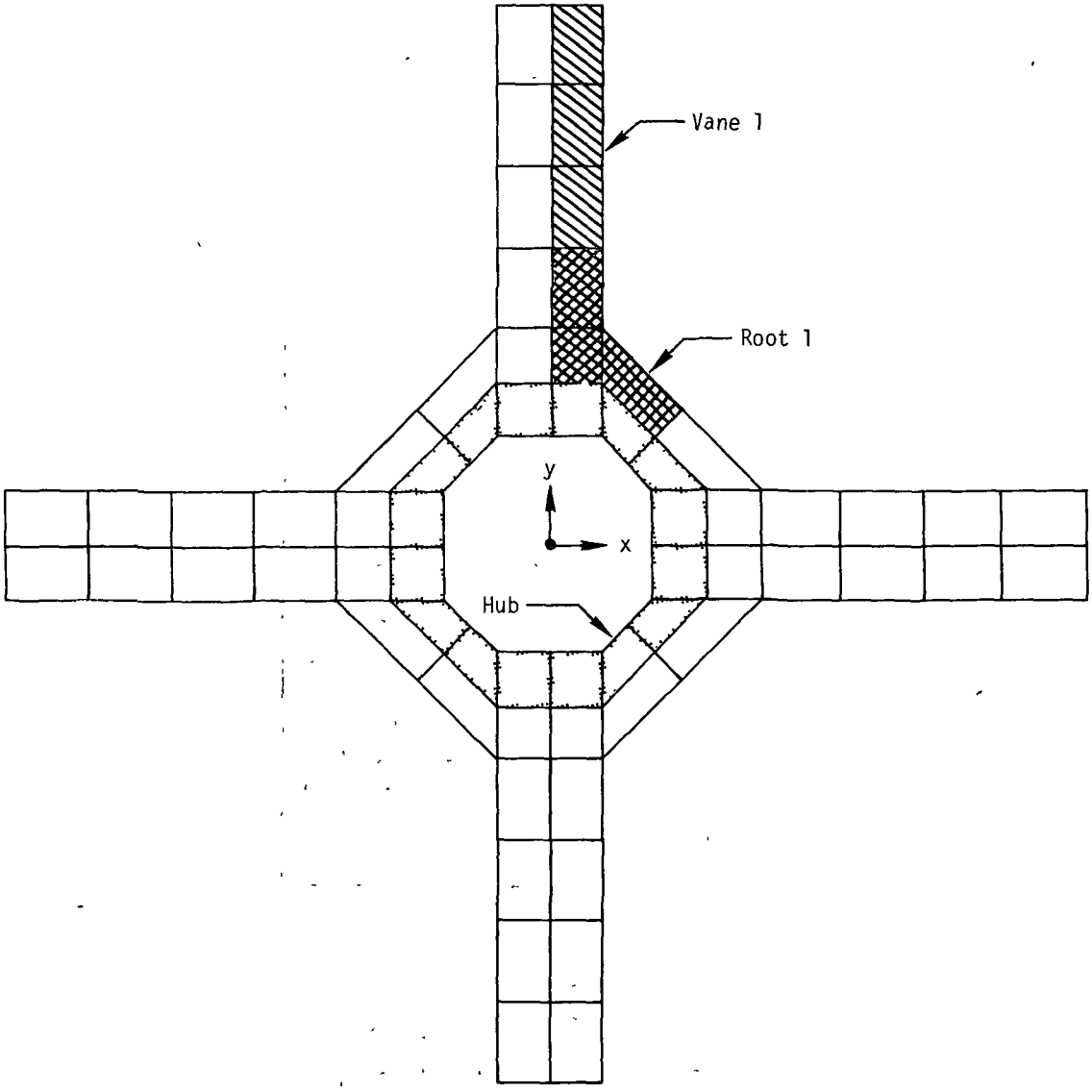

Figure 1. Windmill model, basic substructures.

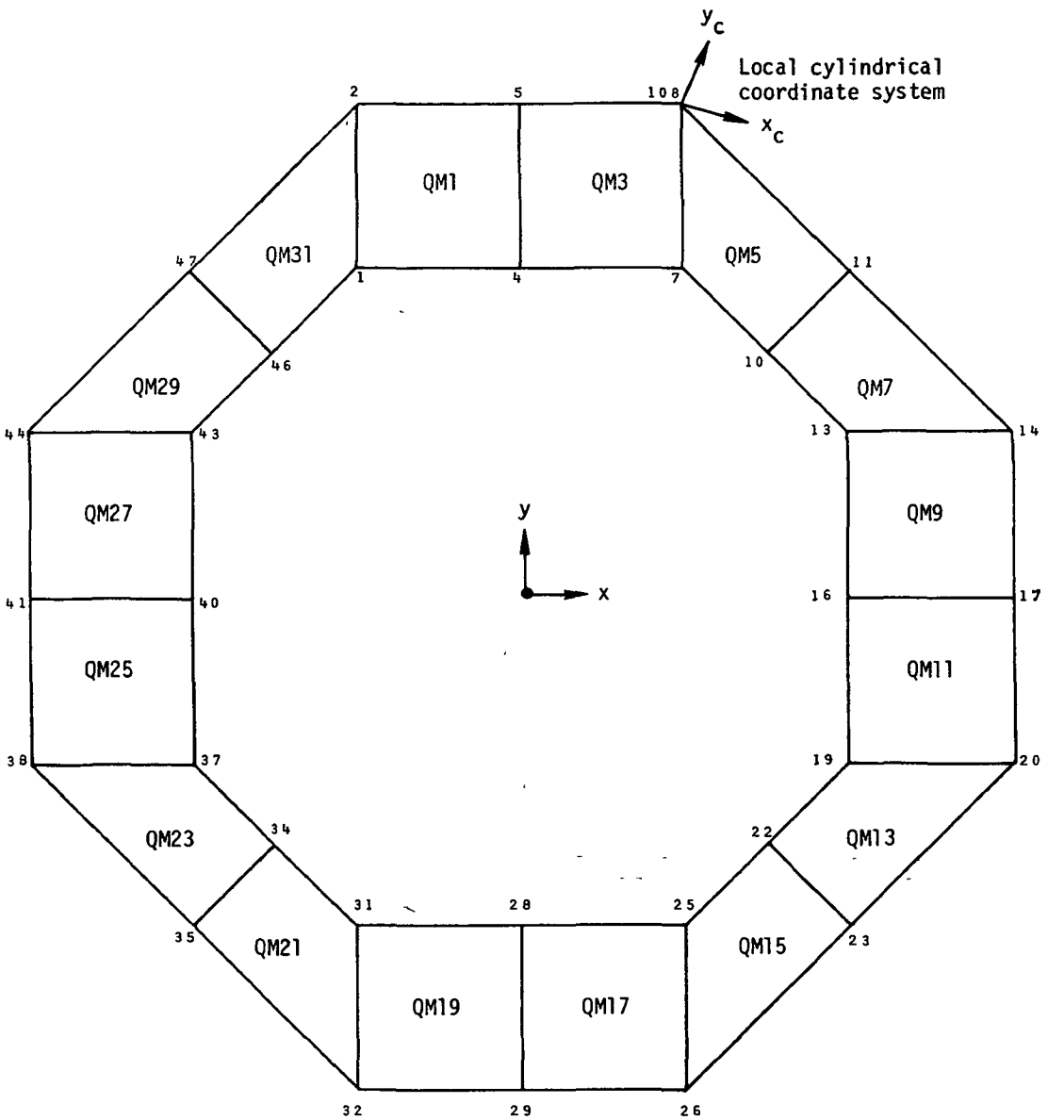

Figure 2. Hub substructure.

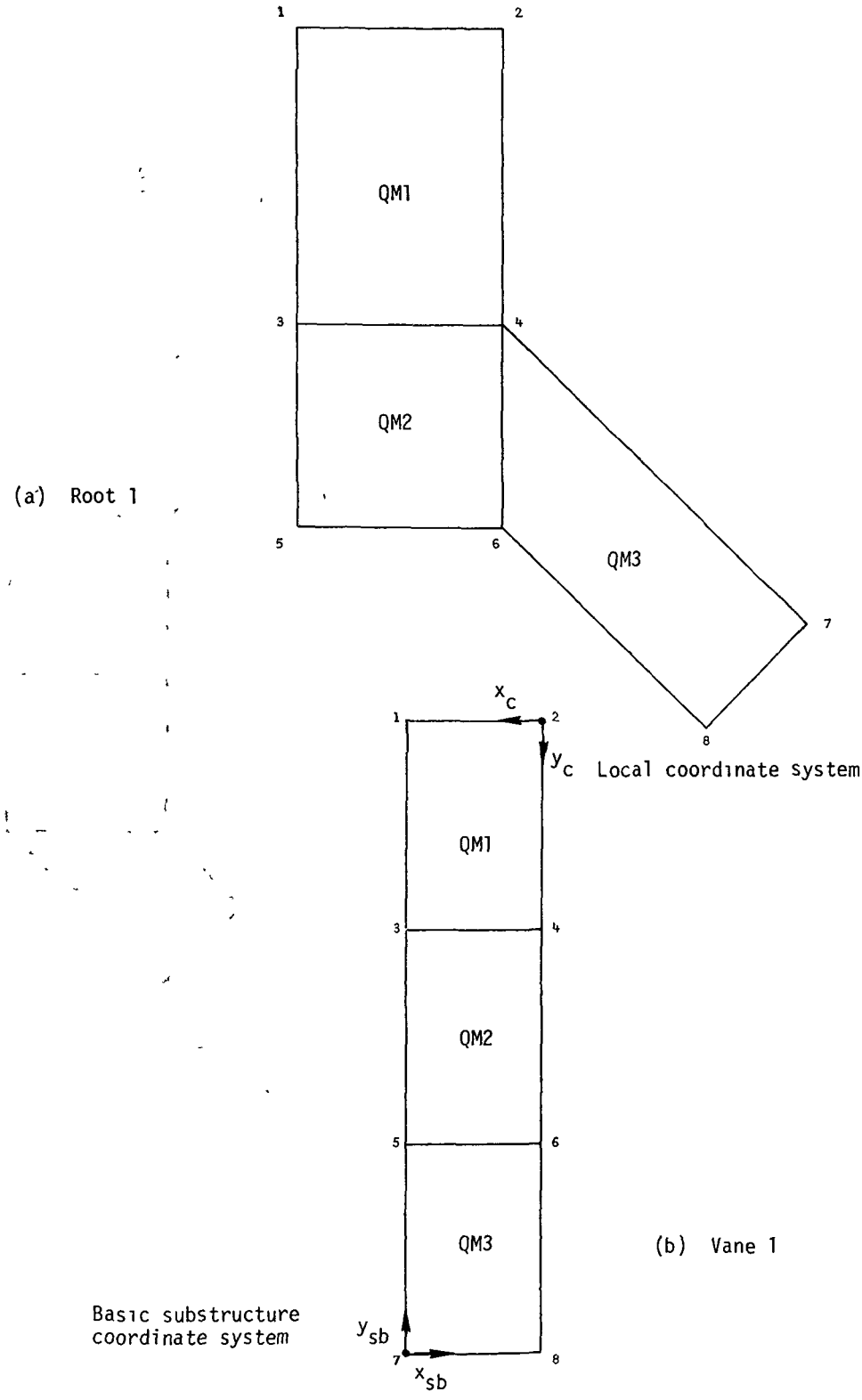

Figure 3. Windmill section substructures.

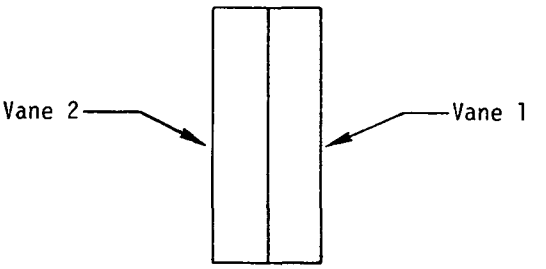

Step I - Generates VANETØP

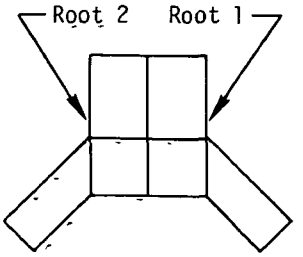

Step II - Generates RØØTTØP

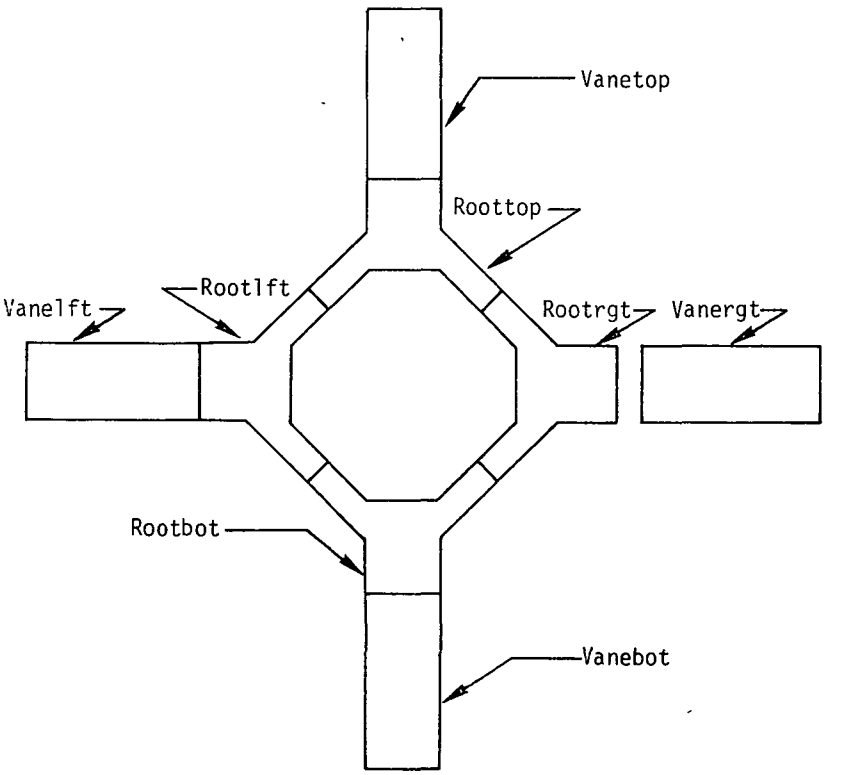

Step III - Generates RING and VANERGT

Figure 4. Sequence of combination steps.

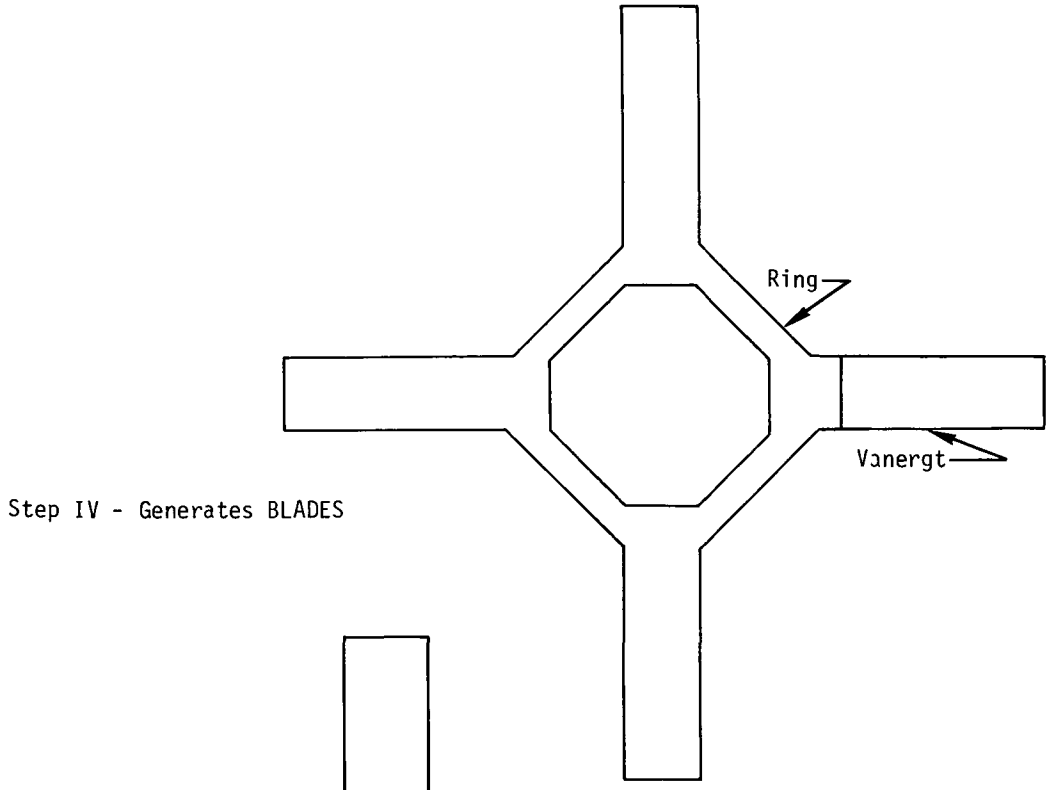

Step IV - Generates BLADES

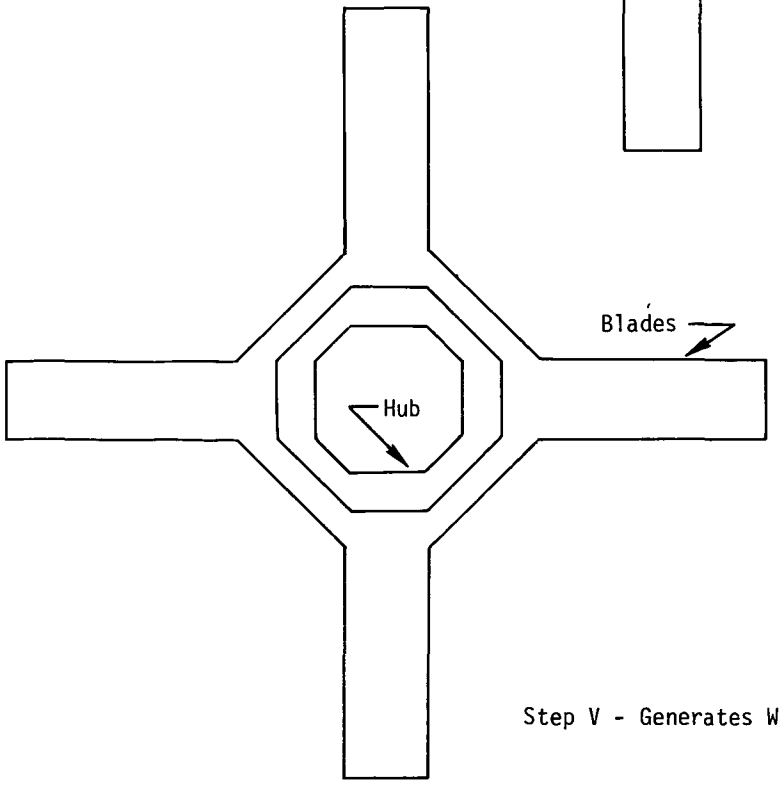

Step V - Generates WINDMILL

Figure 4. Sequence of combination steps (continued).

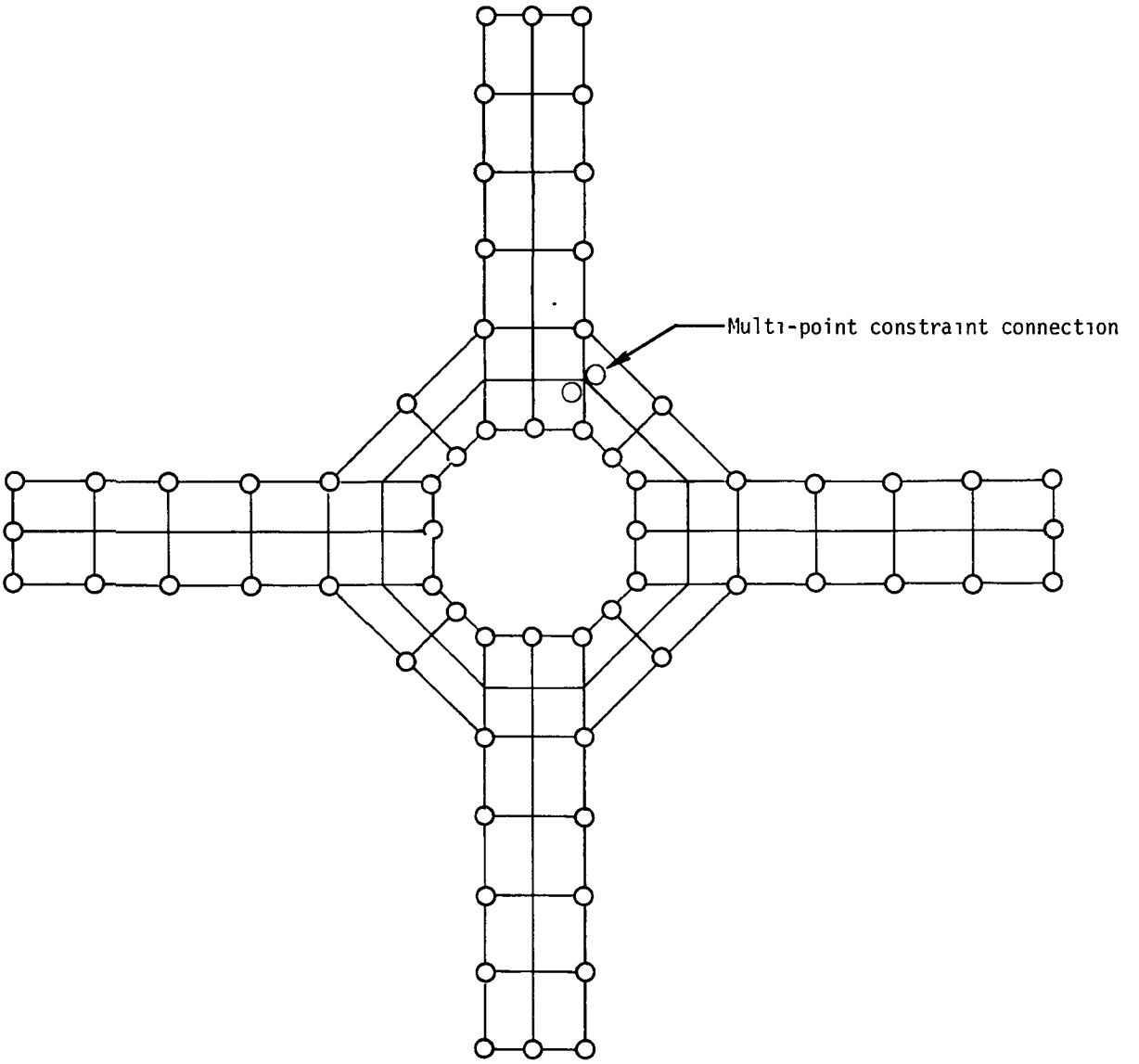

Figure 5. Solution grid points for windmill model.

RIGID FORMAT No. 3, Real Eigenvalue Analysis

Vibration of a 10x20 Plate (3-1-1)
Vibration of a 20x40 Plate (3-1-2)
Vibration of a 10x20 Plate (INPUT, 3-1-3)
Vibration of a 20x40 Plate (INPUT, 3-1-4)

A. Description

This problem demonstrates the solution for natural frequencies of a large-order problem. The structural problem consists of a square plate with hinged supports on all boundaries. The 10x20 model, as shown in Figure 1, uses one half of the structure and symmetric boundary constraints on the mid-line in order to reduce the order of the problem and the bandwidth by one-half. The 20x40 model is the same dimensions with a finer mesh. Both configurations are duplicated via the INPUT module to generate the QUAD1 elements.

Because only the bending modes are desired, the in-plane deflections and rotations normal to the plane are constrained. The inverse power method of eigenvalue extraction is selected and both structural mass density and non-structural mass-per-area are used to define the mass matrix.

Table 1 lists the NASTRAN and theoretical natural frequencies as defined in Reference 8. Figures 2 and 3 are comparisons of the first two mode shapes. The modal masses for these modes are equal to one-fourth the total mass or m_i = 10302.2 .

An undeformed structure plot is executed without plot elements. This is expensive on most plotters since all four sides of each quadrilateral are drawn. Plot elements are used to draw an edge only once and to draw selected coordinate lines (every second or fourth line depending on the model used) for the deformed plots of each eigenvector.

B. Input

1. Parameters:

$\ell = w = 20.0$ (Length and width)

$I = \frac{1}{12}$ (Moment of inertia)

$t = 1.0$ (Thickness)

$E = 3 \times 10^7$ (Modulus of elasticity)

$\nu = 0.30$ (Poisson's ratio)

$\rho = 206.0439$ (Mass density)

2. Boundary constraints:

along x = 0, θ_y = 0 — Symmetric Boundary

along y = 0, u_z = θ_y = 0
along x = 10, u_z = θ_x = 0
along y = 20, u_z = θ_y = 0
— Hinged Supports

3. Eigenvalue extraction data:

Method: Inverse power

Region of interest: $.89 \leq f \leq 1.0$

Number of desired roots: 3

Number of estimated roots: 1

Table 1. Natural Frequency Comparisons, cps.

Mode No.	Theoretical	NASTRAN 10x20	NASTRAN 20x40
1	.9069	.9056	.9066
2	2.2672	2.2634	
3	4.5345	4.5329	

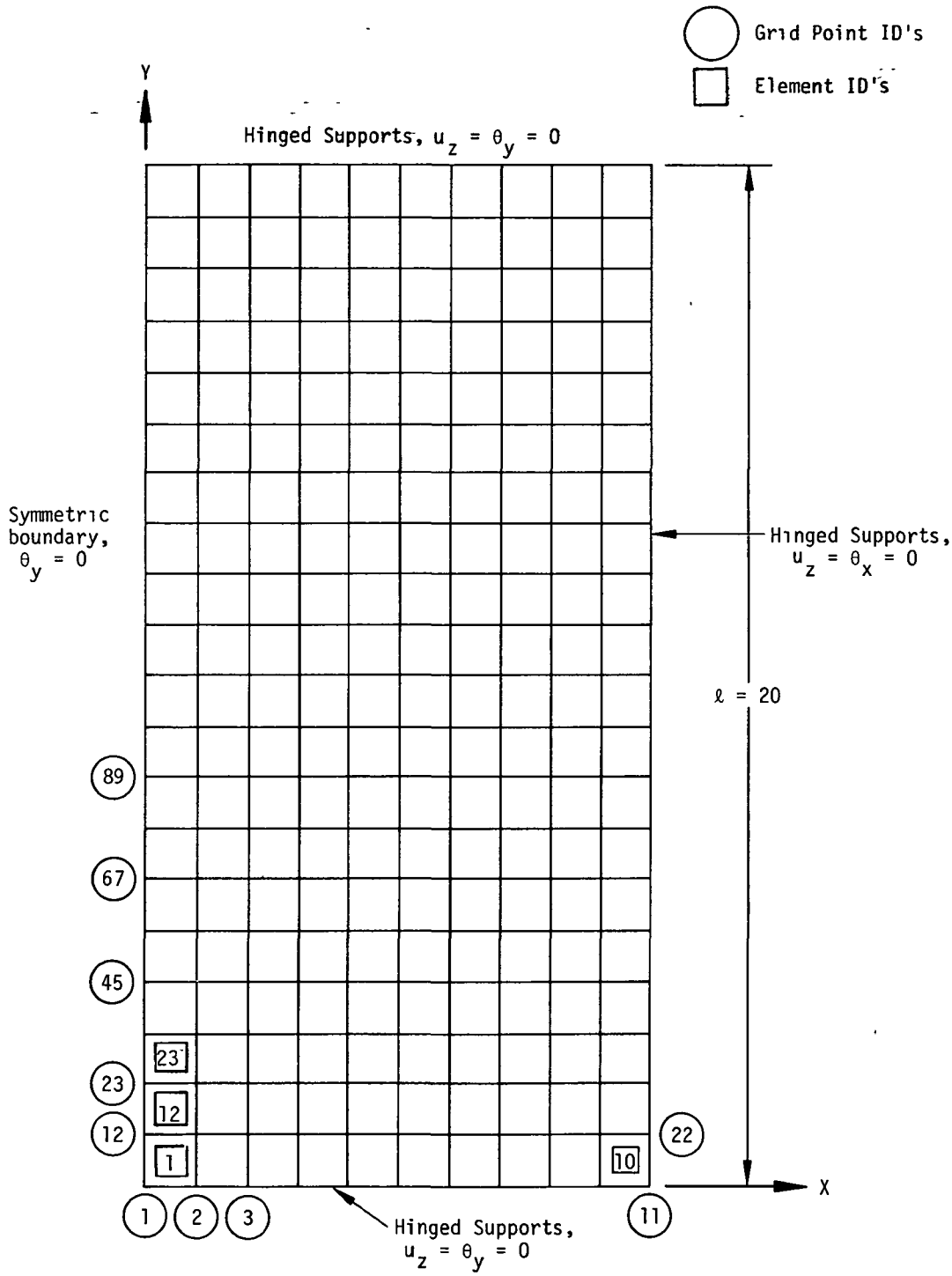

Figure 1. 10 x 20 Half plate model.

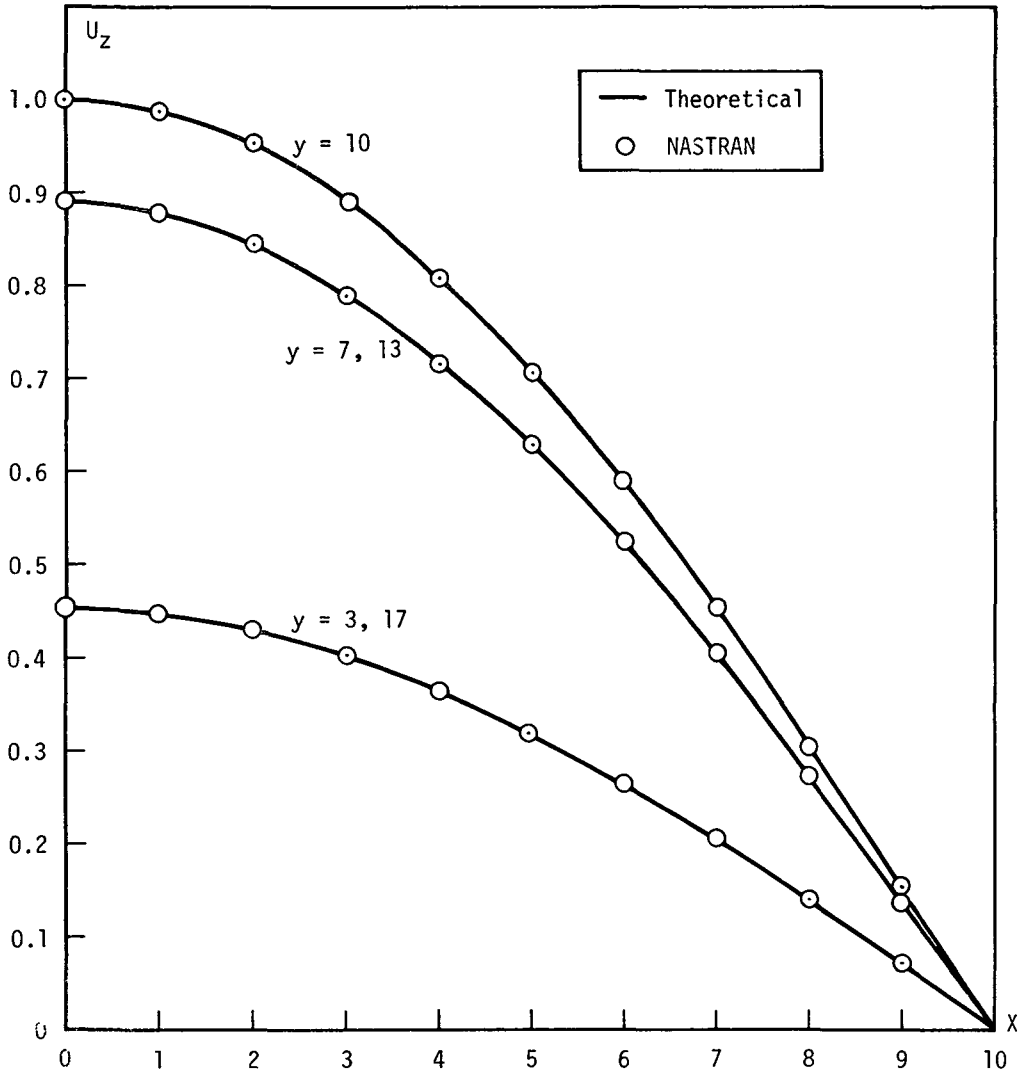

Figure 2. Comparison of displacements, first mode.

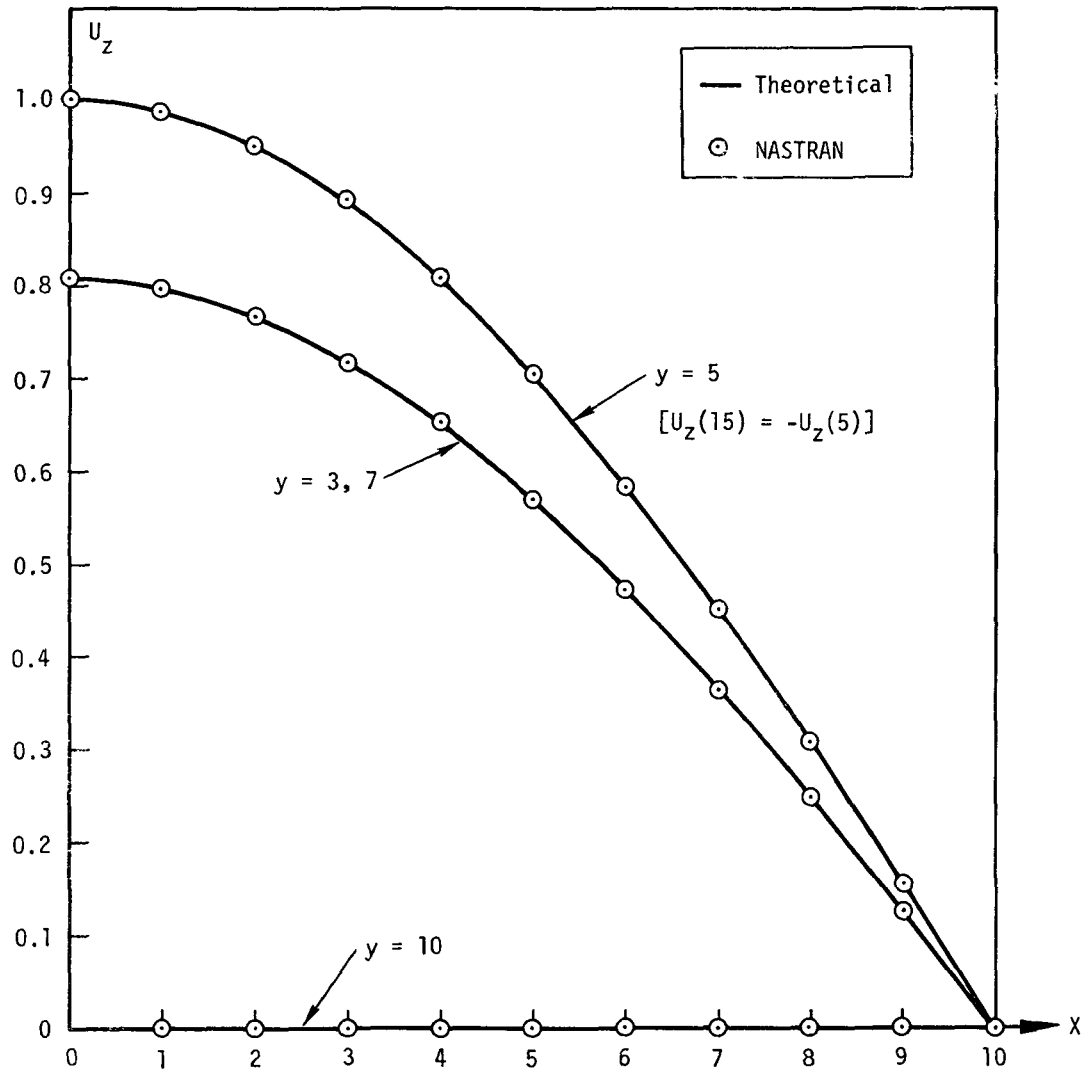

Figure 3. Comparison of displacements, second mode.

RIGID FORMAT No. 3, Real Eigenvalue Analysis

Vibration of a Compressible Gas in a Rigid Spherical Tank (3-2-1)

A. Description

This problem demonstrates a compressible gas in a rigid spherical container. In NASTRAN a rigid boundary is the default for the fluid and, as such, no elements or boundary lists are necessary to model the container.

Aside from the NASTRAN bulk data cards currently implemented, this problem demonstrates the use of the hydroelastic data cards: AXIF, CFLUID2, CFLUID3, and RINGFL.

The lowest mode frequencies and their mode shapes for n = 0, 1 and 2 are analyzed where n is the Fourier harmonic number. Only the cosine series is analyzed.

B. Model

1. Parameters

   $R = 10.0$ m (Radius of sphere)

   $\rho = 1.0 \times 10^{-3}$ Kg/m^3 (Mass density of fluid)

   $B = 1.0 \times 10^{3}$ Newton/m^2 (Bulk modulus of fluid)

2. Figure 1 and 2 show the finite element model. The last 3 digits of the RINGFL identification number correspond approximately to the angle, θ, from the polar axis along a meridian.

C. Theory

From Reference 18, the pressure in the cylinder is proportional to a series of functions:

$$Q_{n,m} = \frac{J_{m+\frac{1}{2}}(X)}{\sqrt{X}} P_m^n (\cos\theta) \cos n\phi \,, \qquad \begin{matrix} n \le m \\ m = 0,1,2 \end{matrix} \tag{1}$$

where:

$Q_{n,m}$ Pressure coefficient for each mode

X Nondimensional radius $= \frac{\omega_{mk}}{a} r$

ω_{mk} Natural frequency for the k<u>th</u> mode number and m<u>th</u> radial number in radians per second

$J_{m+\frac{1}{2}}$ Bessel function of the first kind

r	radius
$a = \sqrt{\frac{B}{\rho}}$	speed of sound in the gas
P_m^n	associated Legendre functions
θ	meridinal angle
ϕ	circumferential angle
n	harmonic number
m	number of radial node lines

The solution for X and hence ω_{mk} is found by the use of the boundary condition that the flow through the container is zero.

$$\left\{ \frac{d}{dX} \left[\frac{J_{m+\frac{1}{2}}(X)}{\sqrt{X}} \right] \right\}_{r=R} = 0.0 \qquad (2)$$

where R is the outer radius.

This results in zero frequency for the first root. Multiple roots for other modes can be seen in Table 1. The finite element model assumes different pressure distributions in the two angular directions which causes the difference in frequencies.

D. Results

Table 1 and Figure 3 summarize the NASTRAN and analytic results for the lowest nonzero root in each harmonic. Table 1 lists the theoretical natural frequencies, the NASTRAN frequencies, the percent error in frequency, and the maximum percent error in pressure at the wall as compared to the maximum value. Figure 3 shows the distribution of the harmonic pressure at the wall versus the meridinal angle. The theoretical pressure distributions correspond to the Legendre functions $P_o^0(\cos\theta)$, $P_o^1(\cos\theta)$, and $P_o^2(\cos\theta)$ which are proportional to $\cos\theta$, $\sin\theta$, and $\sin^2\theta$ respectively.

Table 1. Comparison of NASTRAN and analytical results.

Harmonic	Natural Frequency (Hertz)			Pressure
	Analytical	NASTRAN	% Error	Max. % Error at Wall
0	33.1279	33.2383	0.33	1.19
1	33.1279	33.2060	0.24	0.47
2	53.1915	53.3352	0.27	0.91

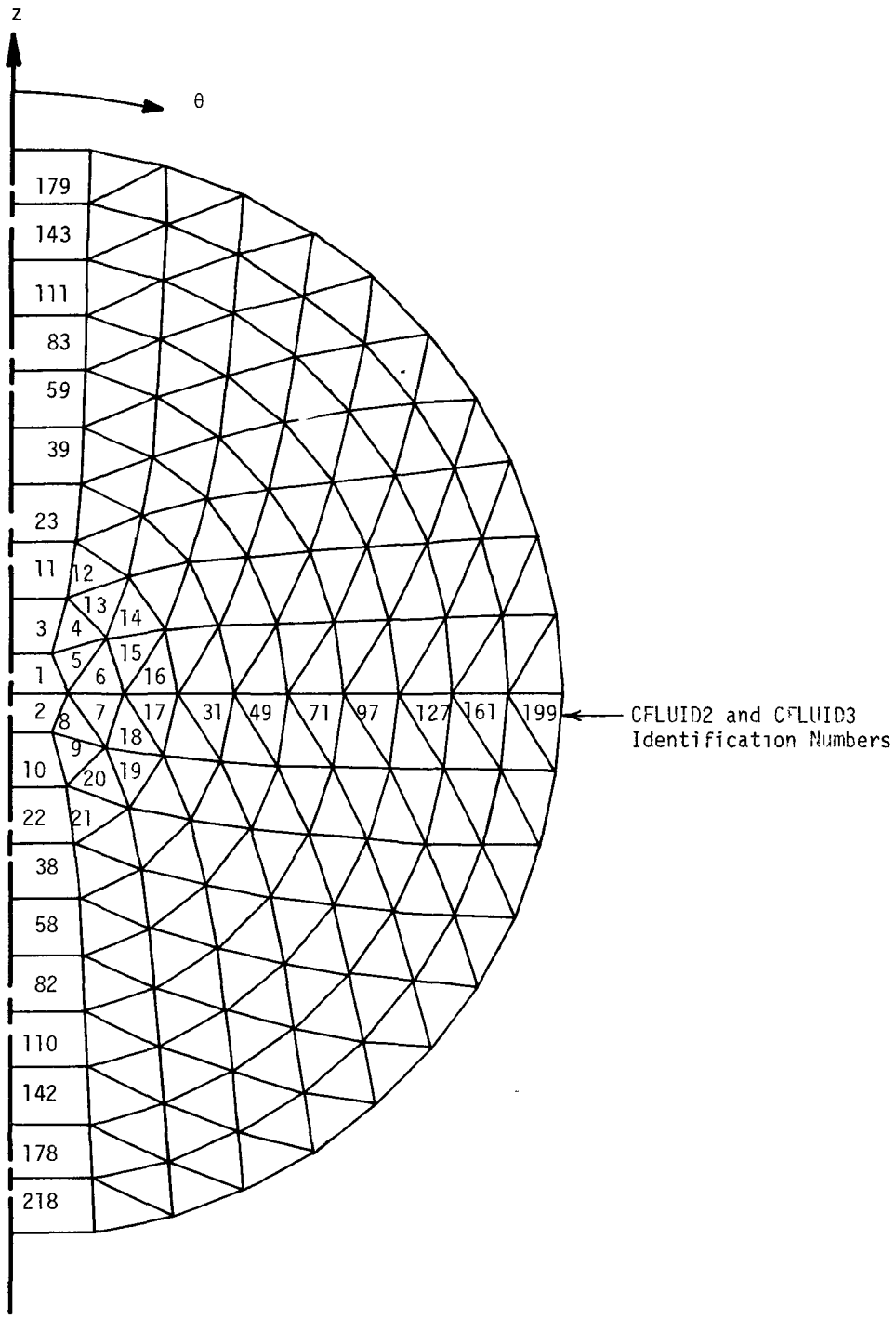

Figure 1. Gas filled rigid spherical tank model.

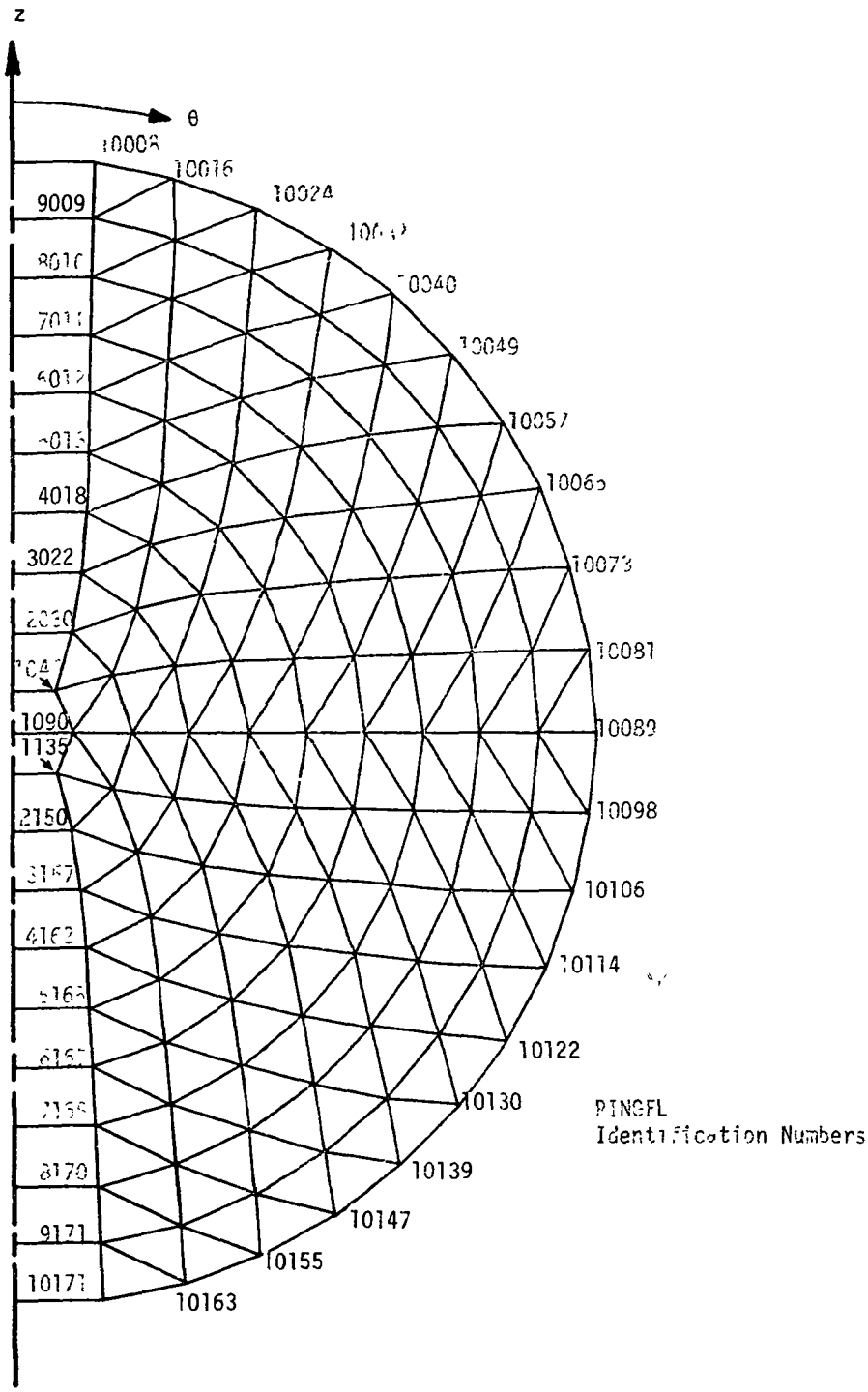

Figure 2. Gas filled rigid spherical tank model.

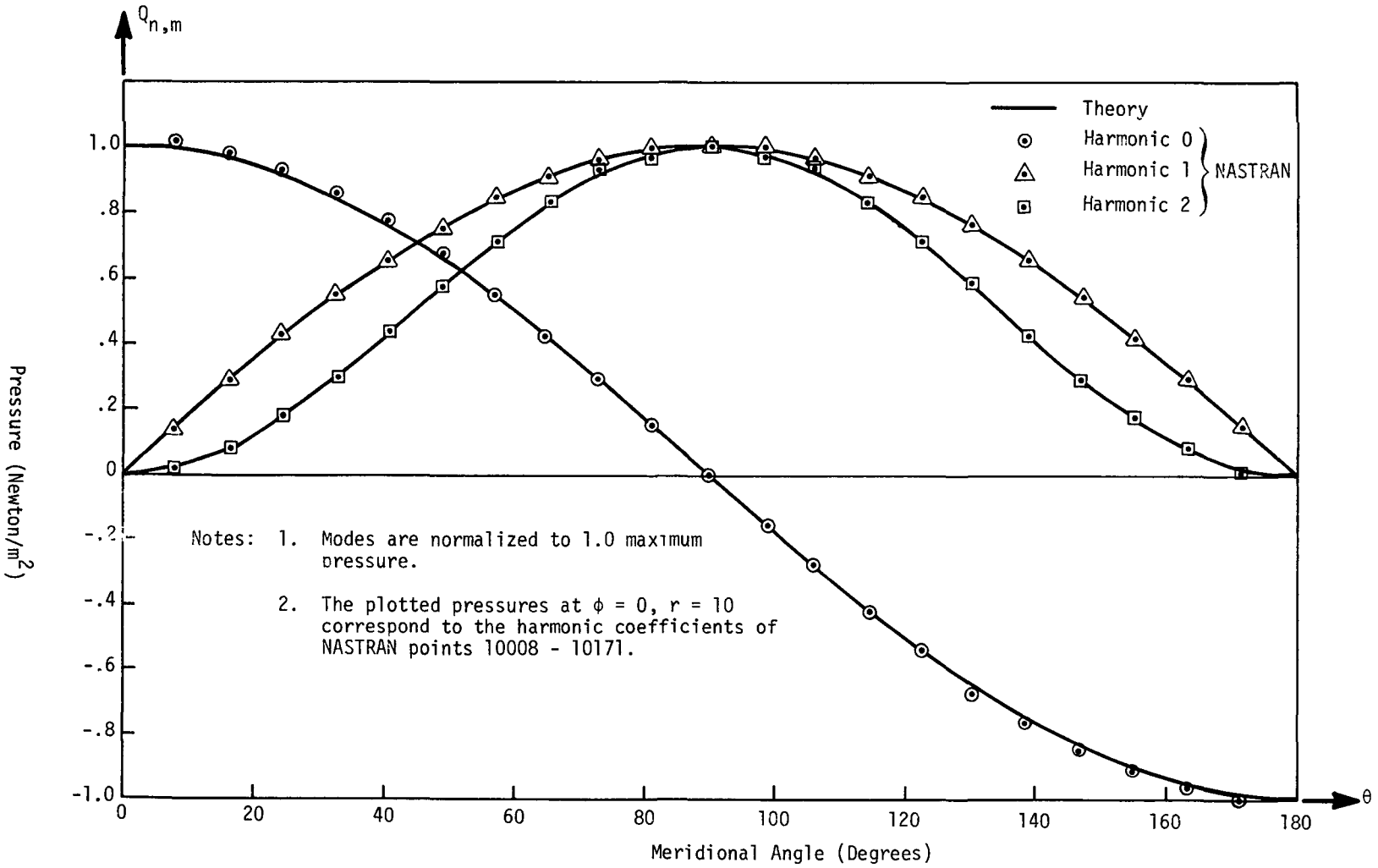

Figure 3. Pressure at tank wall - first finite modes.

RIGID FORMAT No. 3, Real Eigenvalue Analysis

Vibration of a Liquid in a Half-Filled Rigid Sphere (3-3-1)

A. Description

The model is similar to Demonstration Problem No. 3-2 except that a hemispherical fluid model with a free surface is analyzed. Additional cards demonstrated are the free surface list (FSLIST) and free surface points (FREEPT). The effective gravity for the fluid is found on the AXIF card. The fluid is considered incompressible.

The lowest three eigenvalues and eigenvectors for the cosine and sine series of n = 1 are analyzed, where n is the harmonic order.

B. Input

1. Parameters

g	= 10.0 ft/sec^2	(Gravity)
R	= 10.0 ft	(Radius of hemisphere)
ρ	= 1.255014 lb-sec^2/ft^4	(Fluid mass density)
B	= ∞	(Bulk modulus of fluid, incompressible)

2. Figure 1 shows the finite element model.

C. Results

Reference 17 gives the derivations and analytical results. In particular, the parameters used in the reference are:

$$\left.\begin{aligned} e &= 0 \quad \text{(half-filled sphere)} , \\ \lambda &= \frac{\omega^2 R}{g} \quad \text{(dimensionless eigenvalue)} . \end{aligned}\right\} \qquad (1)$$

Table 2 of Reference 17 lists the eigenvalues, λ_1, λ_2, and λ_3 for the first three modes. Figure 13 of Reference 17 shows the mode shapes.

The analytic and NASTRAN results are compared in Table 1. The frequencies are listed and the resulting percentage errors are given. The maximum percent error of the surface displacement, relative to the largest displacement, is tabulated for each mode.

The free surface displacements may be obtained by the equation:

$$u = \frac{p}{\rho g} \quad , \tag{2}$$

where p is the pressure at the free surface recorded in the NASTRAN output. Note that, since an Eulerian reference frame is used, the pressure at the original (undisturbed) surface is equal to the gravity head produced by motions of the surface. Special FREEPT data cards could also have been used for output. Since the results are scaled for normalization anyway, the harmonic pressures may be used directly as displacements.

Figure 2 is a graph of the shape of the free surface for each distinct root. Both analytic and NASTRAN results are scaled to unit maximum displacements. Because the cosine series and the sine series produce identical eigenvalues, the resulting eigenvectors may be linear combinations of both series. In other words the points of maximum displacement will not necessarily occur at $\phi = 0°$ or $\phi = 90°$. Since the results are scaled, however, and the results at $\phi = 0$ are proportional to the results at any other angle, the results at $\phi = 0$ were used.

Table 1. Comparison of natural frequencies and free surface mode shapes from the reference and NASTRAN.

Mode Number	Natural Frequency (Hertz)			Mode Shape
	Reference	NASTRAN	NASTRAN % Error	Maximum % Error, ε
1	0.1991	0.1988	-0.1	$\varepsilon < 1$ %
2	0.3678	0.3691	0.3	$\varepsilon < 2.6$%
3	0.4684	0.4766	1.8	$\varepsilon < 4$ %

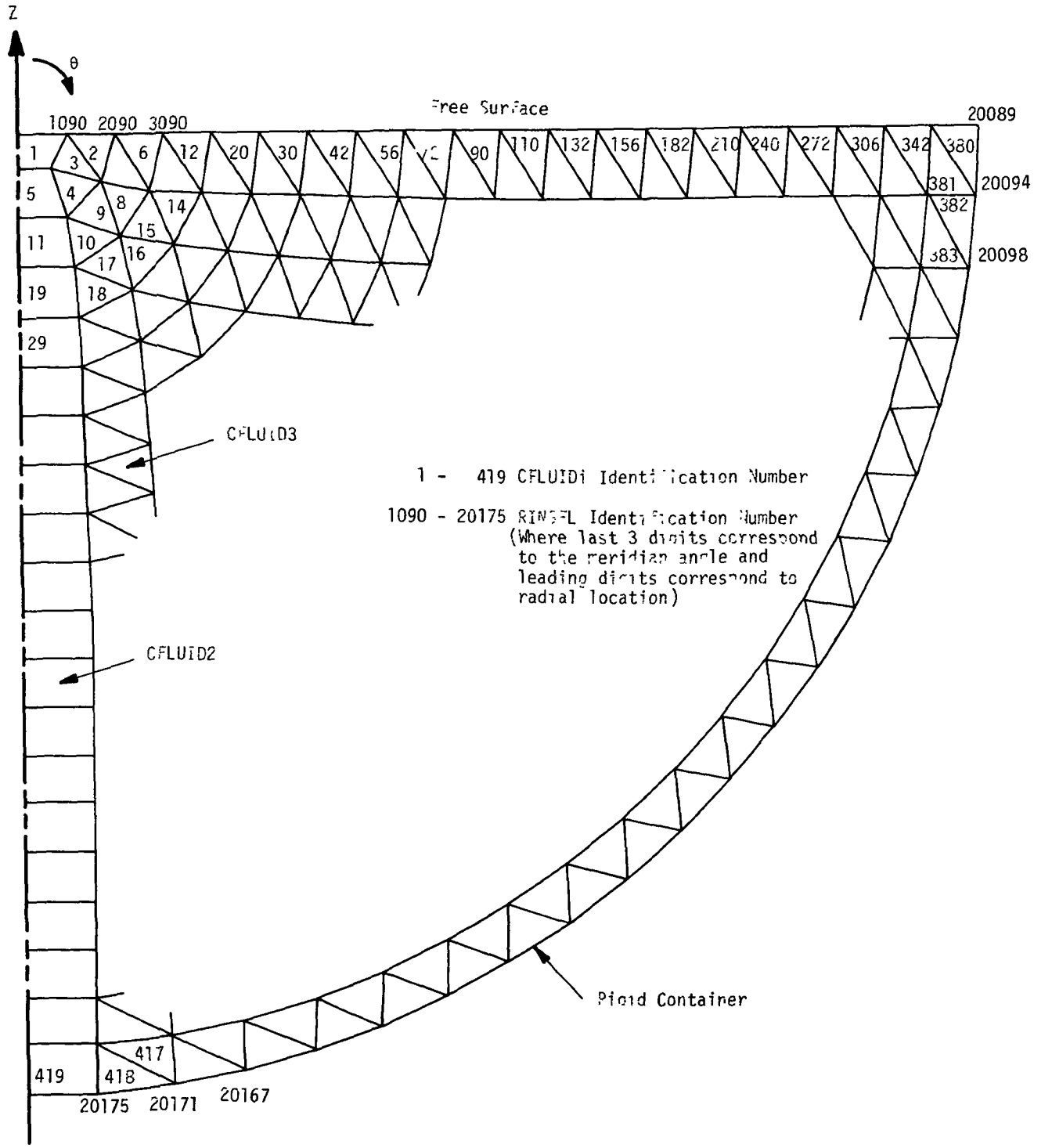

Figure 1. Rigid sphere half filled with a liquid.

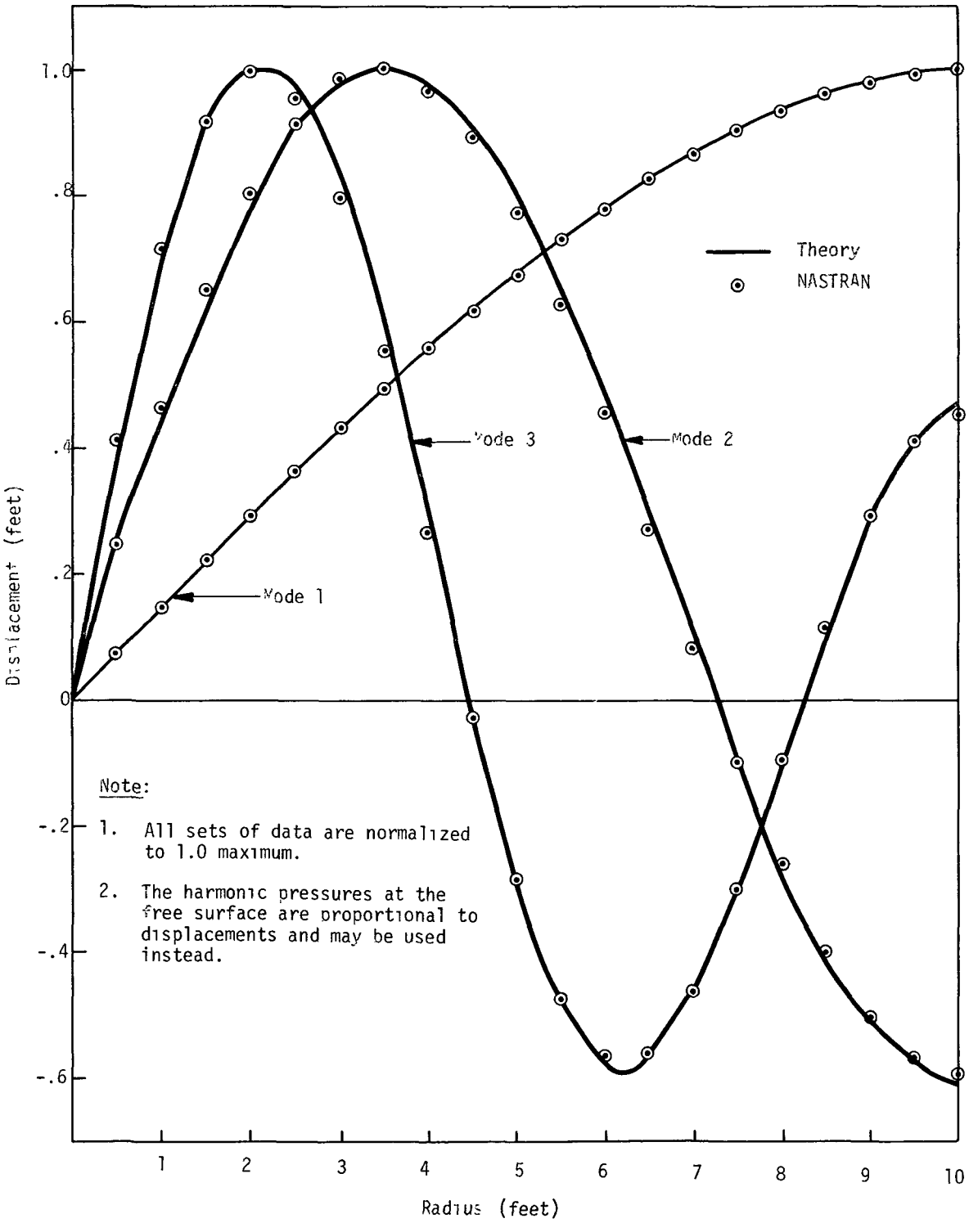

Figure 2. Free surface mode shapes.

RIGID FORMAT No. 3, Real Eigenvalue Analysis

Acoustic Cavity Analysis (3-4-1)

A. Description

This problem illustrates the use of NASTRAN to determine the acoustic modes in a cavity containing both axisymmetric regions and evenly spaced radial slots. The solution is based on an analogy between pressure and displacement, and between fluid particle acceleration and internal structural force described in the Theoretical Manual.

B. Input

The finite element model for the motor cavity of the Minuteman III, Stage III, is shown in Figure 1 As may be seen, it consists of six slots and a long, slender central cavity of irregular shape. The model consists of AXIF2, AXIF3, and AXIF4 finite elements in the central cavity, and SLØT3 and SLØT4 finite elements in the slotted region

C. Results

The vibration mode frequencies for harmonic n = 0 as determined with NASTRAN are shown in Table 1. Also shown are the vibration mode frequencies as determined with an acoustic model and reported in Reference 19.

Table 1. Natural frequencies for the third stage, Minuteman III, motor cavity.

Mode	Frequency, Hz	
	NASTRAN	Experimental
1	0.0	0.0
2	90.1	93.0
3	199.5	200.0
4	310.4	312.0
5	388.0	388.0
6	449.1	466.0
7	512.8	518.0

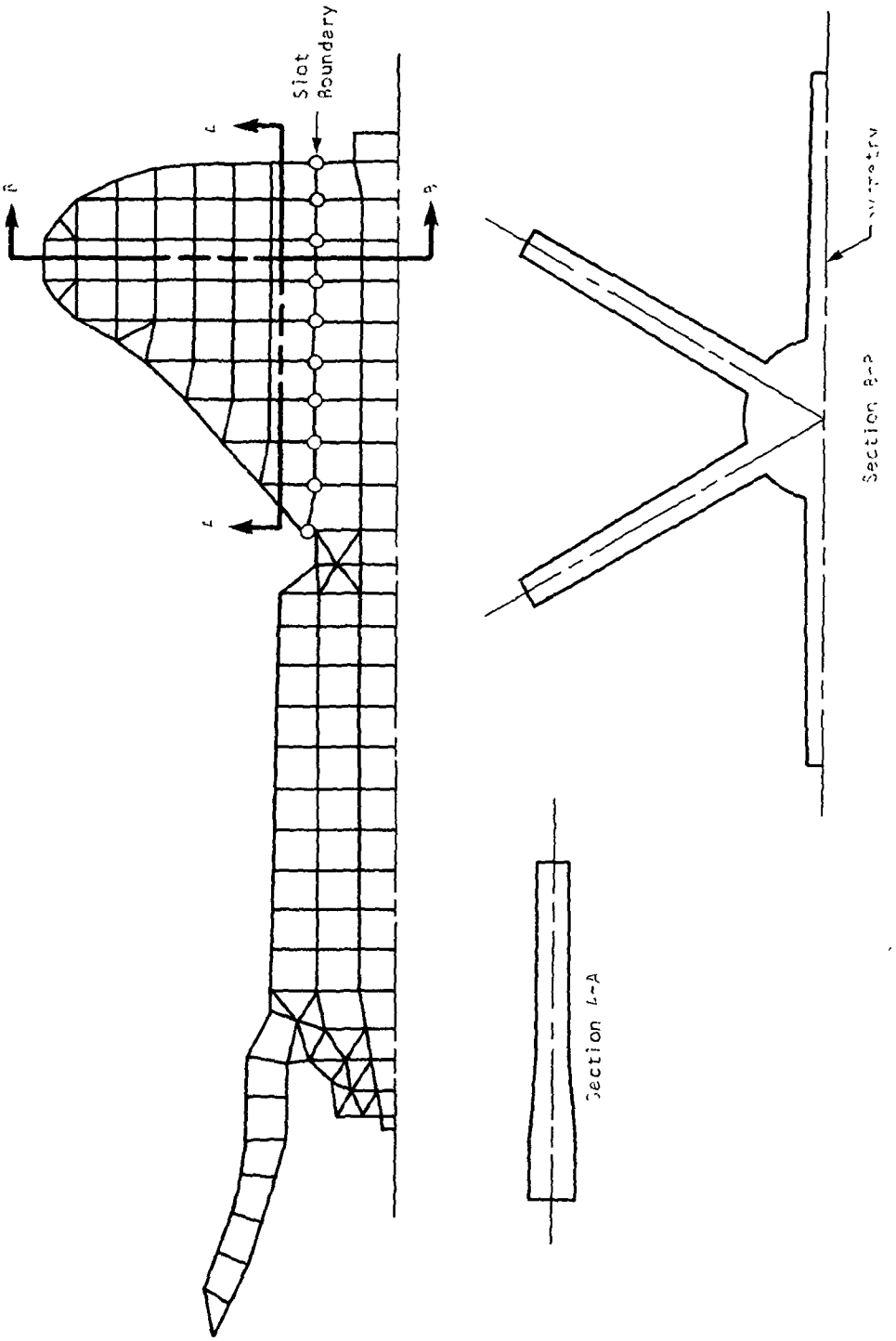

Figure 1. Minuteman III, Stage III, Rocket Motor Cavity

RIGID FORMAT No. 3 (APP HEAT), Nonlinear Heat Conduction
Nonlinear Heat Transfer in an Infinite Slab (3-5-1)

A. Description

This problem demonstrates NASTRAN's capability to solve nonlinear steady state heat conduction problems. The infinite slab is subjected to uniform heat addition per unit volume. There is no heat flux on one face and the other face is kept at zero degrees. The conductivity is temperature dependent. This is a one dimensional problem, since there is no temperature gradient parallel to the surfaces of the slab

B. Input

The NASTRAN model is shown in Figure 1 Linear elements BAR, CØNRØD, RØD and TUBE with areas of π square units and boundary condition element HBDY (PØINT) are used. The heat addition is specified on a QVØL card and is referenced in Case Control by a LØAD card. The area factor for the HBDY is given on the PHBDY card and heat flux is zero. The initial temperatures are given on a TEMPD card and referenced in Case Control by a TEMP (MATERIAL) card. The conductivity is specified on a MAT4 card and is made temperature dependent by the MATT4 card referencing table TABLEM3. The convergence parameter, the maximum number of iterations and an option to have the residual vector output are specified on PARAM cards. The temperature at the outer surface is specified by an SPC card. Temperature output is punched on TEMP bulk data cards for future use in static analysis

C. Theory

The conductivity, k, is defined by

$$k(T) = 1 + T/100 \quad ,$$

where T is the temperature.

The heat flow per area, q, is

$$q(x) = -k \frac{dT}{dx} = -(1 + T/100) \frac{dT}{dx} \quad . \tag{1}$$

The heat input per volume, q_v, affects the heat flow by the equation

$$\frac{dq(x)}{dx} = q_v \quad . \tag{2}$$

A convenient substitution of variables in Equations (1) and (2) is

$$u = -\int q(x)dx = (T + T^2/200) \quad . \tag{3}$$

Differentiation and substitution for q in Equation (2) results in the second-order equation in u:

$$\frac{d^2u}{dx^2} = -q_v \quad . \tag{4}$$

From the following boundary conditions

$$u = 0 \quad \text{at} \quad x = \ell \tag{5}$$

and

$$\frac{du}{dx} = 0 \quad \text{at} \quad x = 0 \quad , \tag{6}$$

the solution to Equation (4) is

$$u = \frac{q_v}{2} (\ell^2 - x^2)$$

Therefore the solution for the temperature is

$$T = 100 \left[-1 \pm (1+q_v(\ell^2 - x^2)/100)^{\frac{1}{2}}\right] \tag{7}$$

Since heat is flowing into the system, the positive temperature solution will occur.

D. Results

A comparison with NASTRAN results is shown in Table 1.

Table 1. Comparison of theoretical and NASTRAN temperatures for nonlinear heat conduction in an infinite slab.

Grid Point	Theoretical Temperature	NASTRAN Solution
1	73.20	73.13
2	69.56	69.53
3	58.11	58.11
4	36.93	36.93
5	0.00	0.00

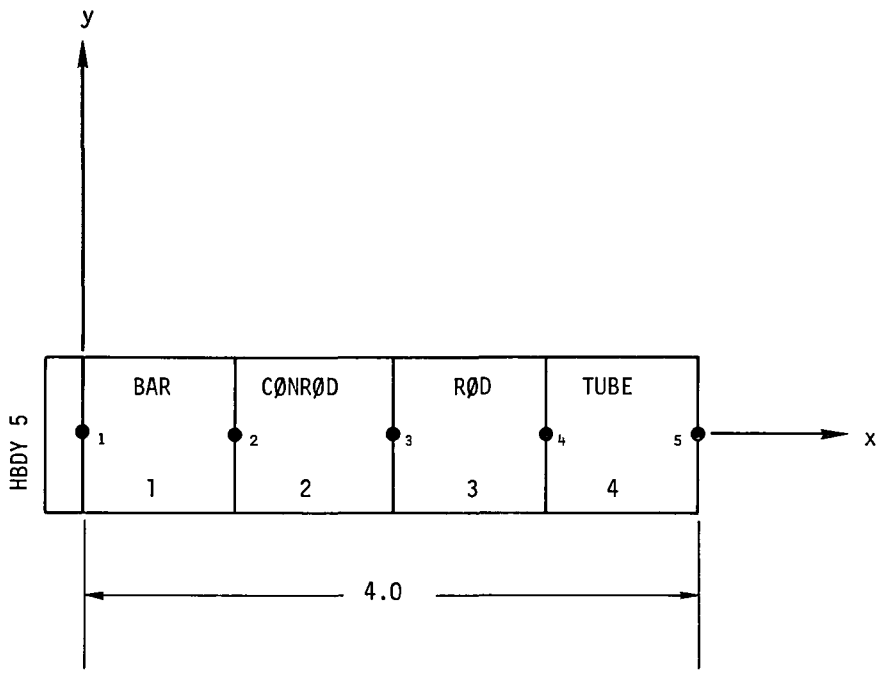

Grid 1 Flux = 0.0

Grid 5 Temperature = 0.0

Figure 1. Slab modeled with linear elements

RIGID FORMAT No. 3, Approach Heat,
Nonlinear Radiation and Conduction of a Cylinder (3-6-1)

A. Description

This problem illustrates the solution of a combined conduction and radiation heat transfer analysis. The model is a two-dimensional representation of a long cylinder subject to radiant heat from a distant source. The shell has internal radiation exchange, external radiation loss, and conduction around the circumference.

B. Input

The NASTRAN Model, shown in Figure 1, uses RØD elements to represent the circumferential heat flow and HBDY elements to represent the inside and outside surfaces. The radiation exchange factors for the inside of the cylinder are defined on the RADMTX data cards. The incoming vector flux is defined on the QVECT data card. The model parameters are:

R	= 2.0 ft	(Radius of shell)
t	= .001 ft	(Thickness)
ℓ	= 20.306 ft	(Axial length)
$\varepsilon = \alpha$	= 0.1	(Emissivity and absorptivity)
q_v	= 425 BTU/(ft^2-hr)	(Source flux density)
k	= 94.5 BTU/(hr-ft-°F)	(Conductivity of shell)
σ	= .174 x 10^{-8} BTU/(ft^2-hr-°R^4)	(Stefan-Boltzmann radiation constant)

C. Theory

A closed-form solution to this problem is not available. However, the solution may be validated by checking the global net heat flow, the local net heat exchange, and the estimated average temperature.

An estimate of the average temperature may be obtained from the equations:

$$Q_{in} = \alpha q_v \ell R \int_{-\pi/2}^{\pi/2} \cos\theta \, d\theta = 2\alpha\ell R q_v \quad , \tag{1}$$

and

$$Q_{out} = \varepsilon\sigma\bar{T}^4 (2\pi R\ell) \quad , \tag{2}$$

where Q_{in} is the total input from the source, Q_{out} is the net flux radiated outward and $\bar{T}$ is the average absolute temperature.

Since the net heat flow must be zero in a steady-state analysis, Equations (1) and (2) are equated to obtain:

$$\bar{T}^4 = \frac{q_v}{\pi\sigma} \qquad (3)$$

D. Results

The resulting temperature distribution around the circumference of the shell is shown in Figure 2. The average value of temperature from the NASTRAN results shows 57.87° F. The estimated average temperature from Equation (3) above is 68°. The difference is due to the non-uniform radiation effects.

A second check is provided by computing the global net heat flow error in the system. Summing the net flow into each element gives a net heat flow error several orders of magnitude less than the total heat from the source. As a further check, the local net heat flow error at grid point 2 was calculated by summing the contributions from the connected elements. The heat flow terms shown in Figure 3, as calculated by NASTRAN, were:

Q_2 = 59.420 (Flow through RØD #2 (flux · area))

Q_3 = 97.862 (Flow through RØD #3 (flux · area))

Q_{r42} = -133.564 (Inside radiation flow into HBDY #42)

Q_{r43} = -85.352 (Inside radiation flow into HBDY #43)

Q_{r22} = -305.418 (Outside radiation into HBDY #22)

Q_{r23} = -257.930 (Outside radiation into HBDY #23)

Q_{v22} = 481.157 (Vector flux input to HBDY #22)

Q_{v23} = 381.848 (Vector flux input to HBDY #23)

The net flow error into grid point 2 is:

$$\bar{Q}_2 = \frac{1}{2}(Q_{r22} + Q_{r23} + Q_{r42} + Q_{r43} + Q_{v22} + Q_{v23}) + Q_2 - Q_3 = 1.9 \text{ BTU} \qquad (4)$$

This error is less than 1% of the total heat flow input at the point.

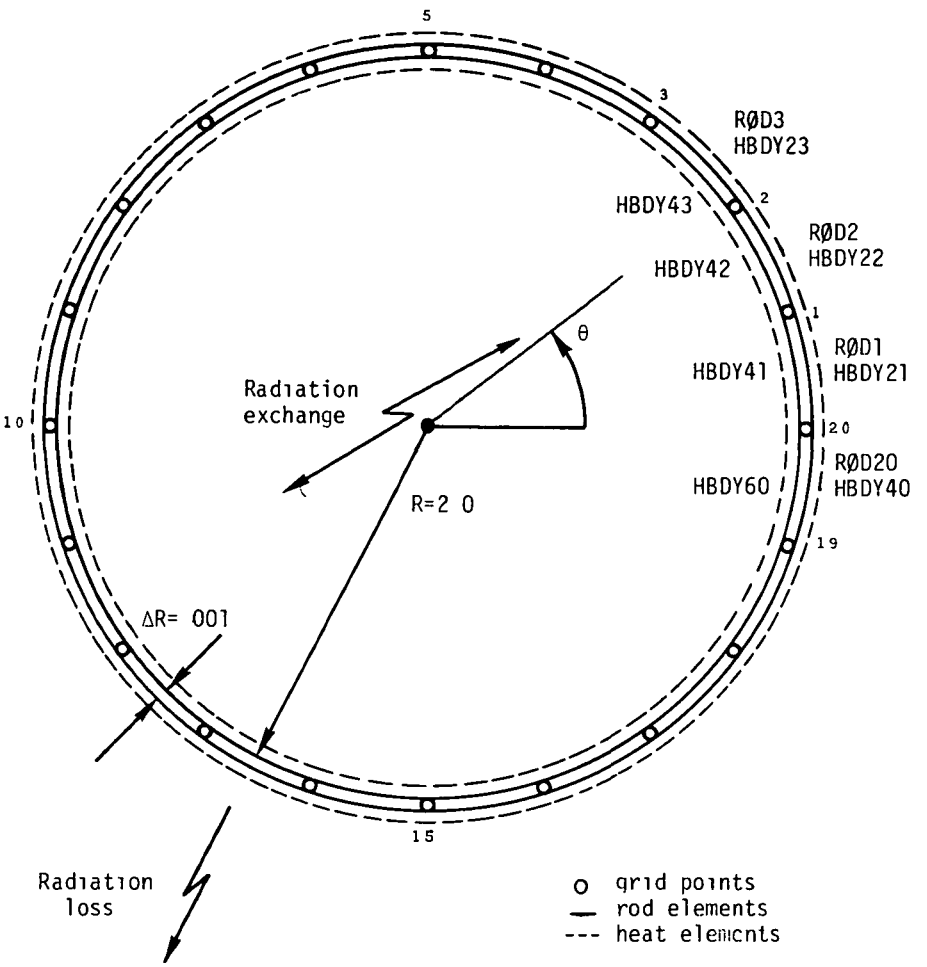

Figure 1. Cross section of thin wall shell

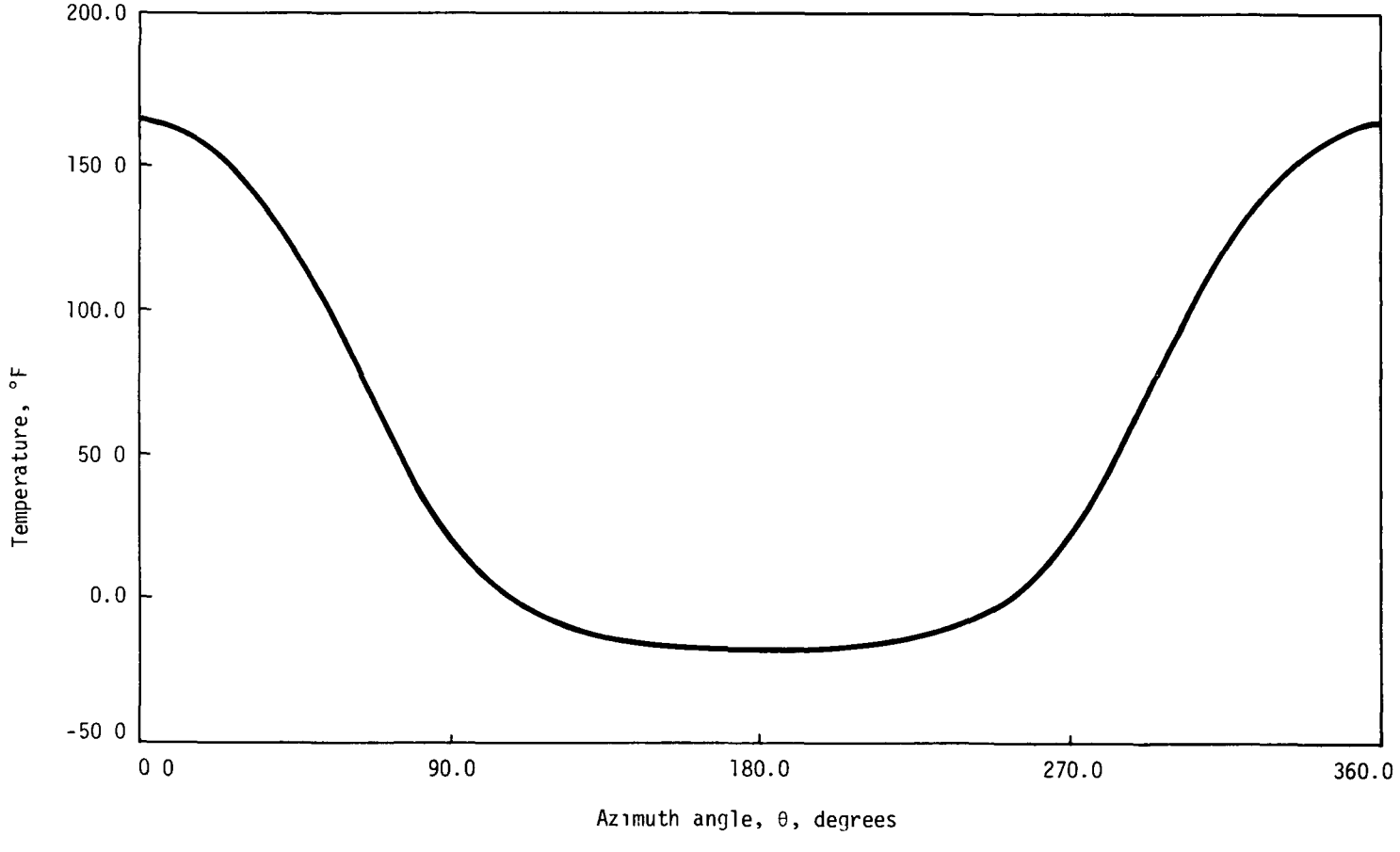

Figure 2. Temperature in stationary cylinder, with conduction and radiation heat transfer.

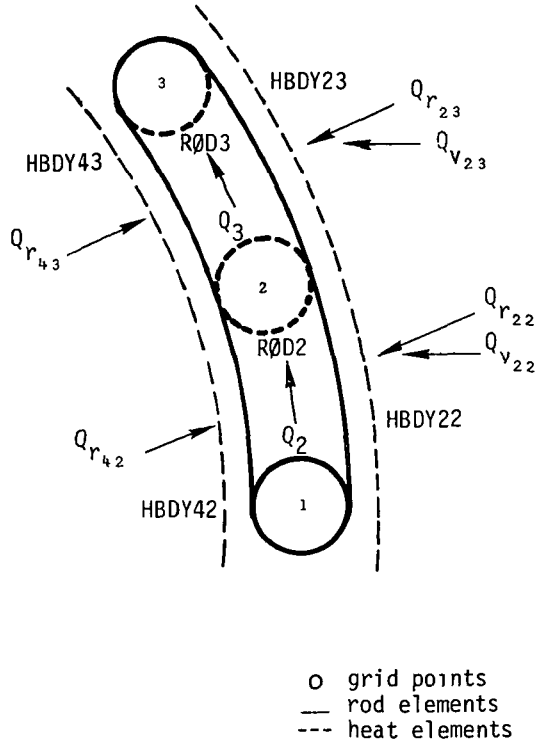

Figure 3. Illustration for heat exchange computation at a grid point.

RIGID FORMAT No. 4, Differential Stiffness Analysis

Differential Stiffness Analysis for a Hanging Cable (4-1-1)

A. Description

Advanced versions of NASTRAN provide an iteration procedure for nonlinear differential stiffness (or geometric stiffness) solutions. As described in Section 7 of the NASTRAN Theoretical Manual, the internal loads are recalculated for each iteration. The changes in direction of these internal loads are used to correct the previous solution. External loads retain their original orientation, however, they do travel with the grid point.

A classical nonlinear geometric problem is that of a hanging cable which assumes the shape of a catenary when a uniform gravity load is applied. As shown in Figure 1, the model is given a circular shape initially. The resulting displacements of the grid points, when added to their original locations provide a close approximation to the catenary.

B. Input

The NASTRAN model consists of nine BAR elements connected to ten grid points evenly spaced on a quarter circle. The bending stiffness of the elements is a nominally small value necessary to provide a non-singular linear solution.

The axial stiffness of the elements is a sufficiently large value to limit extensional displacements. The basic parameters are

$R = 10.0$ ft. (initial radius),

$w = 1.288$ lb/ft (Weight per length),

and $L = 5\pi$.

C. Theory

With reference to the coordinate system illustrated on the next page, the basic differential equation, obtained from Reference 25 is

$$\frac{dy'}{dx} = \frac{w}{H}\left(1 + (y')^2\right)^{1/2} , \qquad (1)$$

where

w is the weight per unit length,

H is the tension at $x = 0$,

and $y' = dy/dx$ is the slope of the resulting curve.

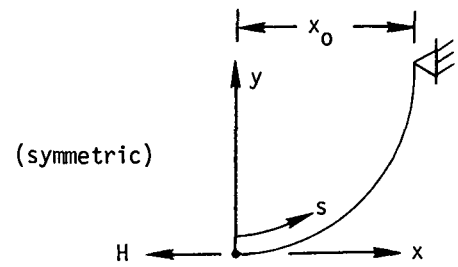

Dividing both sides of Equation (1) by the radical term and integrating, results in the equation,

$$\sinh^{-1} y' = \frac{wx}{H} + C_1 \quad . \tag{2}$$

Since $y' = 0$ at $x = 0$, $C_1 = 0$ and

$$y' = \sinh\left(\frac{wx}{H}\right) \quad . \tag{3}$$

Integrating again and applying the known boundary condition $y = 0$ at $x = 0$, the equation for the shape is

$$y = \frac{H}{w}\left[\cosh\left(\frac{wx}{H}\right) - 1\right] \quad . \tag{4}$$

Since the length of the cable is known but the horizontal force, H, is unknown, the two may be related by integrating for the length, L, which is

$$L = \frac{H}{w} \sinh \frac{wx_o}{H} \quad , \tag{5}$$

where x_o is one-half the distance between supports. If w, x_o, and L are given, Equation (5) is solved for H (for $x_o = 10.0$, $w/H = .1719266$) and Equation (4) is evaluated to obtain the actual shape. However, for purposes of comparison to the NASTRAN solution the location of several points fixed on the string are determined. For a given position, s, along the cable, the coordinates x and y would be

$$x = \frac{H}{w} \sinh^{-1}\left(\frac{ws}{H}\right) \quad , \tag{6}$$

and

$$y = \frac{H}{w}\left[\left(1 + \left(\frac{ws}{H}\right)^2\right)^{1/2} - 1\right] \quad . \tag{7}$$

D. Results

The following table compares theoretical results to those of NASTRAN. Deflections are measured from the initial shape at selected locations.

Table 1. Comparison of NASTRAN Results to Theoretical Predictions.

Grid Point	s	u_x - Horizontal		u_y - Vertical	
		Theory	NASTRAN	Theory	NASTRAN
11	13.962	-.4856	-.4739	-.1119	-.0408
13	10.472	-.8043	-.7666	-.2286	-.1269
15	6.981	-.5175	-.4612	.0030	.1470
17	3.491	-.1110	-.0877	.5698	.7973
19	.0	.0	.0	.9338	1.2167

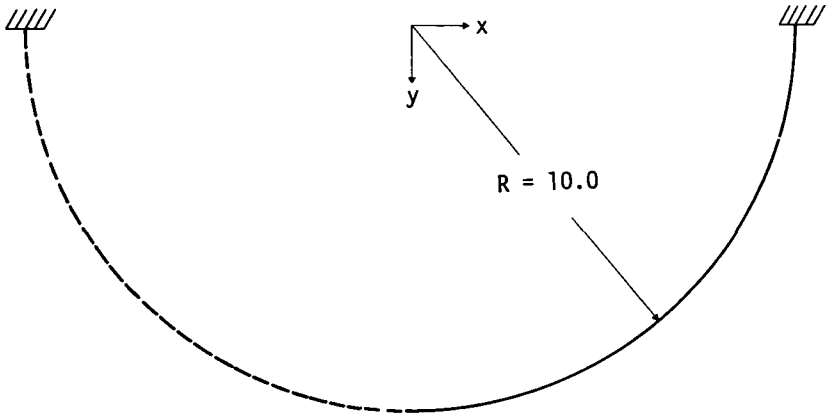

(a) Initial quarter circle modeled.

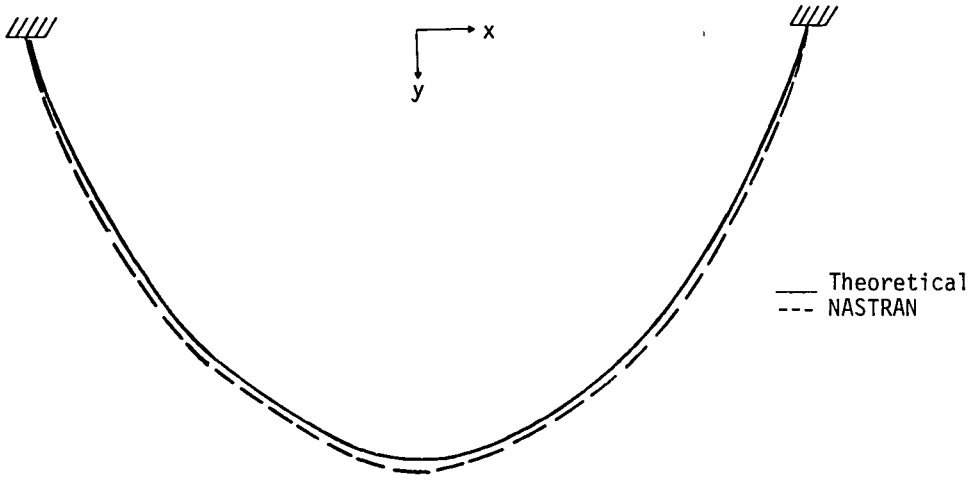

(b) Final catenary shape obtained.

Figure 1. Hanging cable.

RIGID FORMAT No. 5, Buckling Analysis

Symmetric Buckling of a Cylinder (5-1-1)

A. Description

This problem demonstrates the use of buckling analysis to extract the critical loads and the resulting displacements of a cylinder under axial loads. The Buckling Analysis rigid format solves the statics problem to obtain the internal loads in the elements. The internal loads define the differential stiffness matrix $[K^d]$ which is proportional to the applied load. The load factors, λ_i, which causes buckling are defined by the equation:

$$[\lambda_i[K^d] + [K]]\{u_i\} = 0$$

where [K] is the linear stiffness matrix. This equation is solved by the Real Eigenvalue Analysis methods for positive values of λ_i. The vectors $\{u_1\}$ are treated in the same manner as in real eigenvalue analysis.

The problem is illustrated in Figure 1, it consists of a short, large radius cylinder under a purely axial compression load. A section of arc of 6 degrees is used to model the axisymmetric motions of the whole cylinder as shown in Figure 2.

All three types of structure plots are requested: undeformed, static and modal deformed. The undeformed perspective plot is fully labeled for checkout of the problem. The modal orthographic plots specify a range of vectors $\{u_i\}$ which includes all roots. A longitudinal edge view of the model is also plotted for easy identification of mode shapes.

B. Input

1. Parameters:

R	= 80	(Radius)
h	= 50	(Height)
E	= 1.0×10^4	(Modulus of elasticity)
ν	= 0.0	(Poissons rat o)
t	= 2.5	(Thickness)
I_b	= 1.30208	(Bending inertia)

2. Loads:

   $p = 1.89745 \times 10^3/3°$ ARC

3. Constraints:

   a) The center point (17) is constrained in u_z.

   c) All points are constrained in u_θ, θ_r, and θ_z.

   d) The top and bottom edges are constrained in u_r.

4. Eigenvalue Extraction Data:

   a) Method: Unsymmetrical Determinant

   b) Region of Interest: $.10 < \lambda < 2.5$

   c) Number of estimated roots = 4

   d) Number of desired roots = 4

   e) Normalization: Maximum deflection

C. Answer

The solution to this problem is derived in Reference 9, p. 439. For axisymmetric buckling, the number of half-waves which occur when the shell buckles at minimum load are:

$$m \cong \frac{h}{\pi}\sqrt[4]{\frac{12(1-\nu^2)}{R^2t^2}}$$

where m is the closest integer to the right-hand values.

The corresponding critical stress is:

$$\sigma_{cr} = \frac{Et^2m^2\pi^2}{12h^2(1-\nu^2)} + \frac{Eh^2}{R^2m^2\pi^2}$$

Using the values given, the lowest bulkling mode consists of a full sine wave. The NASTRAN results and the theoretical solutions for the critical load for each buckling mode are listed below:

Number of Half Waves m	NASTRAN	ANALYTICAL
1	2.2889	2.2978
2	.99424	1.0
3	1.2744	1.26402
4	2.0070	1.86420

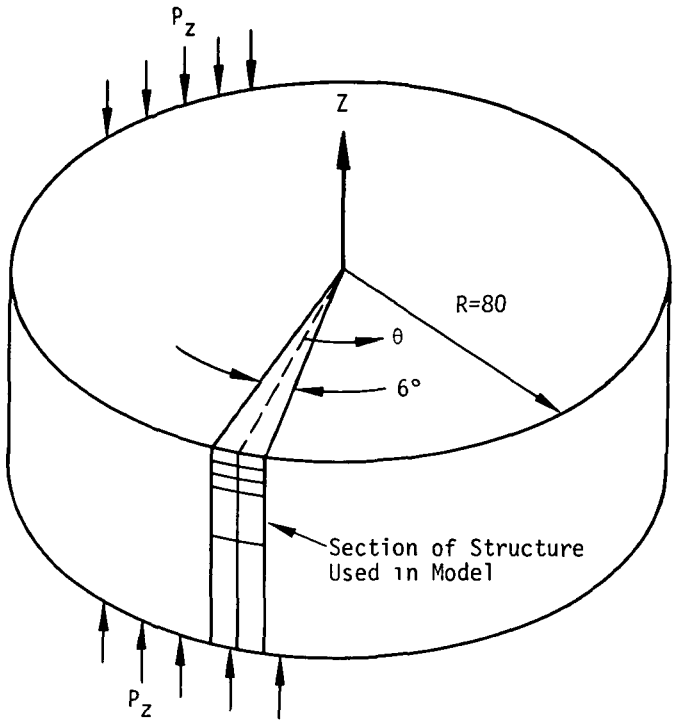

Figure 1. Cylinder under axial load.

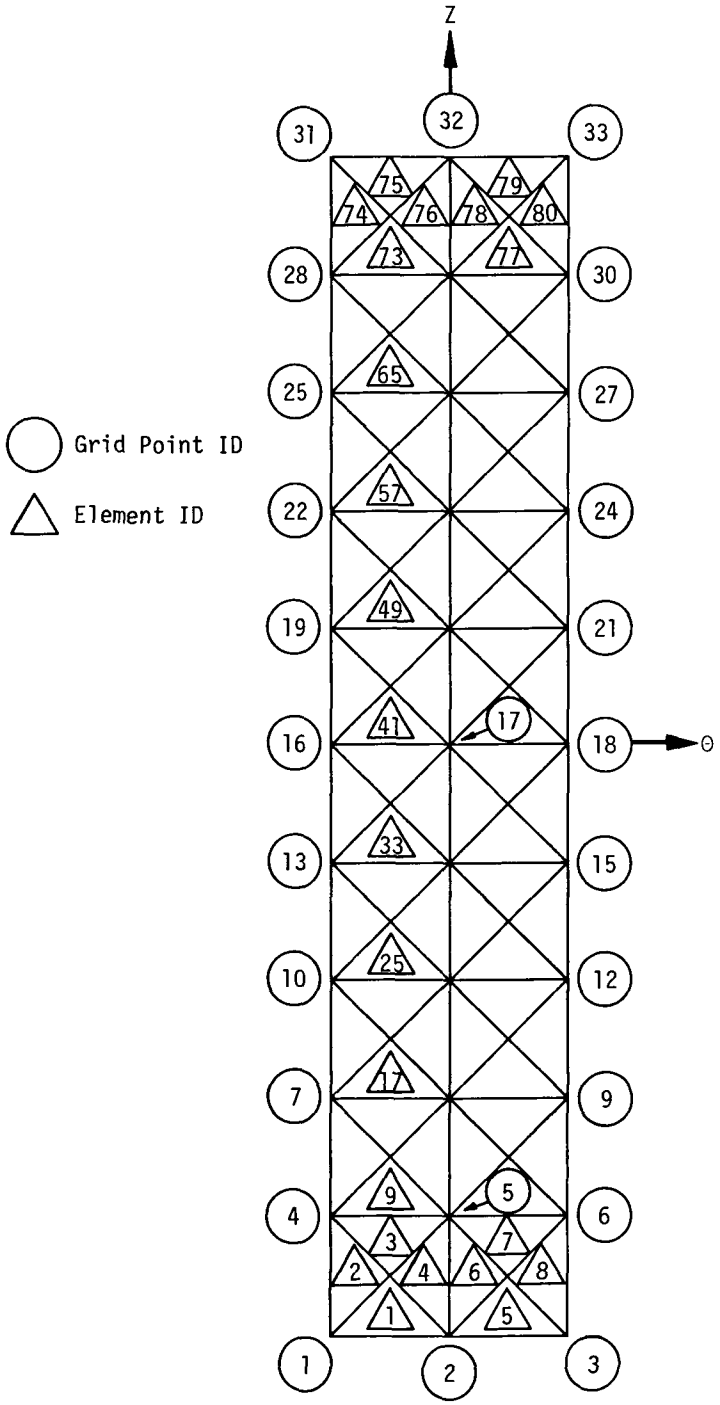

Figure 2. Finite element model of cylinder.

RIGID FORMAT No. 6, Piecewise Linear Analysis

Piecewise Linear Analysis of a Cracked Plate (6-1-1)

A. Description

This problem illustrates elastic-plastic deformation of a thin plate uniaxially loaded across a crack at the center of the plate shown in Figure 1. The same problem was solved by J. L. Swedlow (Reference 10).

Piecewise Linear Analysis involves loading the plate in increments and recalculating the material properties for each element as a function of the element stresses for the last load increment.

B. Input

1. Parameters:

   L = 9.0 inch (Total length of plate)

   W = 6.0 inch (Total width of plate)

   w = 2.0 inch (Total width of crack)

   t = 1.0 inch (Thickness)

   E_o = 10.8×10^6 lb/in^2 (Modulus of elasticity at zero strain)

   ν_o = .3333 (Poisson's Ratio at zero strain)

2. Loads: $\bar{\sigma}$ is the applied load (Figure 1)

Load Factor	$\bar{\sigma}$ lb/in^2	Load Factor	$\bar{\sigma}$ lb/in^2
1	2,300	14	7,000
2	2,500	15	7,500
3	2,800	16	8,000
4	3,100	17	8,500
5	3,400	18	9,000
6	3,700	19	9,500
7	4,000	20	10,000
8	4,400	21	10,500
9	4,800	22	11,000
10	5,200	23	11,500
11	5,600	24	12,000
12	6,000	25	12,500
13	6,500	26	13,000

3. Constraints:

a) All grid points are constrained in u_z, θ_x, θ_y, and θ_z.

b) Grid points along the Y-axis are constrained in the u_x direction.

c) Grid points along the X-axis from the crack tip (x = 1.0) to the edge (x = 3.0) are constrained in the u_y direction.

C. Modeling Techniques

The finite element model, shown in Figures 2 and 3, utilizes two planes of symmetry so only one quarter of the structure (the first quadrant) is modeled. All membrane elements use stress-dependent materials, duplicating the model in Reference 10.

The octahedral stress used in the determination of the material properties was defined in Reference 10 as:

$$\tau_o = \frac{\sqrt{2}}{3}\sqrt{\sigma_x^2 - \sigma_x\sigma_y + \sigma_y^2 + 3\sigma_{xy}^2}$$

The octahedral strain was defined by.

$$\varepsilon_o = \begin{cases} \tau_o(1+\nu_o)/E_o & \tau_o \le \tau_{limit} \\ \tau_o(1+\nu_o)/E_o + \varepsilon_p & \tau_o > \tau_{limit} \end{cases}$$

where

$$\varepsilon_p = 9.716 \times 10^{-3} \left(\tau_o/\tau_{limit} - 1\right)^{1/0.3964}$$

$$\tau_{limit} = (\sqrt{2}/3)\, \sigma_{limit}$$

$$\sigma_{limit} = 11{,}500 \text{ lb/in}^2$$

NASTRAN uses an equivalent uniaxial stress-strain curve defined by

$$\sigma = 3/\sqrt{2}\, \tau_o$$

$$\varepsilon = \sigma/E + \sqrt{2}\, \varepsilon_p$$

This curve is shown in Figure 4. A complete discussion of the equations may be found in Reference 10.

D. Answers

Comparisons of analytical and calculated stresses in the elements along the axis of the crack are given in Figures 5 and 6. The analytical results, based on linear analysis, are compared with the calculated results at the end of the first load increment.

Figures 7 through 9 show the displacement at the center of the crack and stresses for elements near the tip of the crack for all load factors. In the NASTRAN analysis, the octahedral stress is calculated for each load factor as a function of the current values of the stresses. In Reference 10 the current value of the octahedral stress is obtained by accumulating incremental values of the octahedral stress. This procedure results in a generally more flexible model as can be seen from the displacements in Figure 7. The resulting differences in calulated stresses are particularly noticeable at the higher load levels.

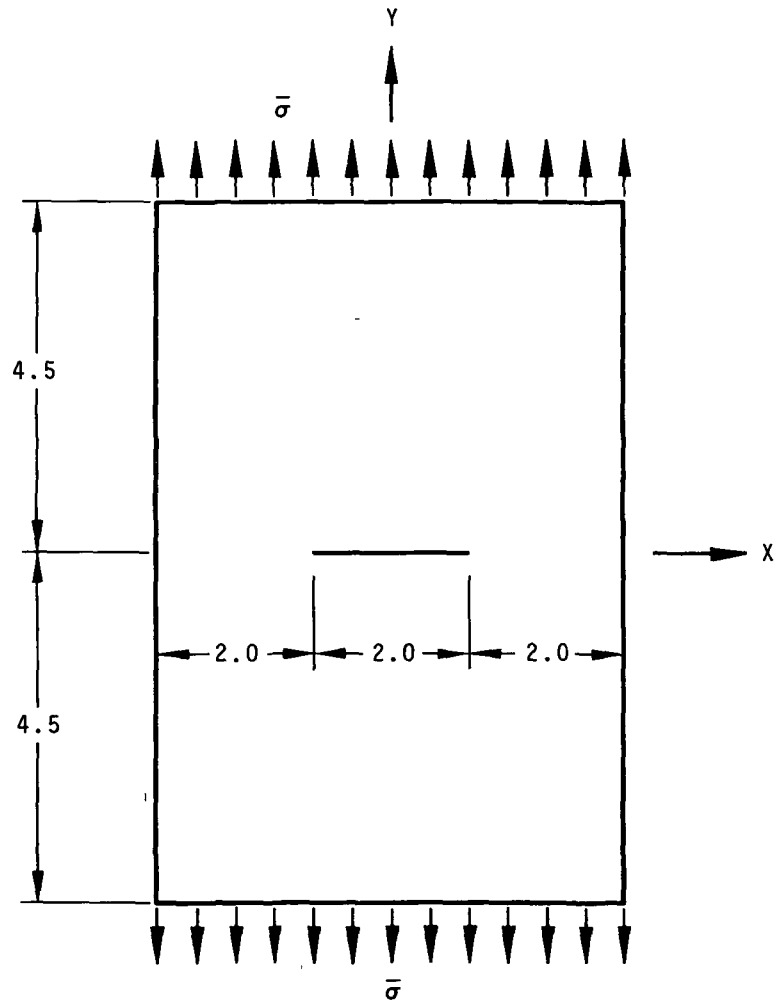

Figure 1. Cracked plate with uniaxial load.

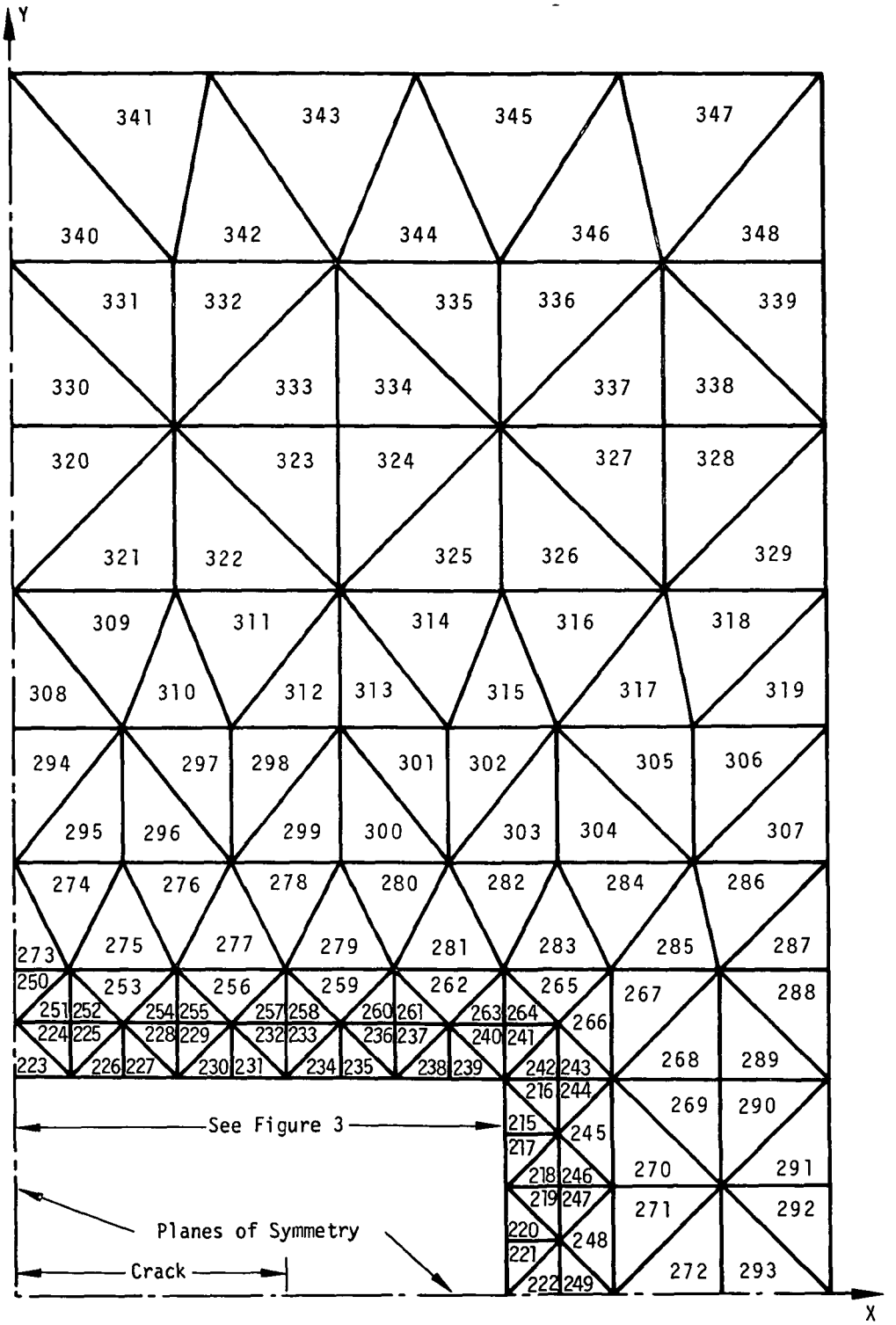

Figure 2. Triangular membrane element identification numbers.

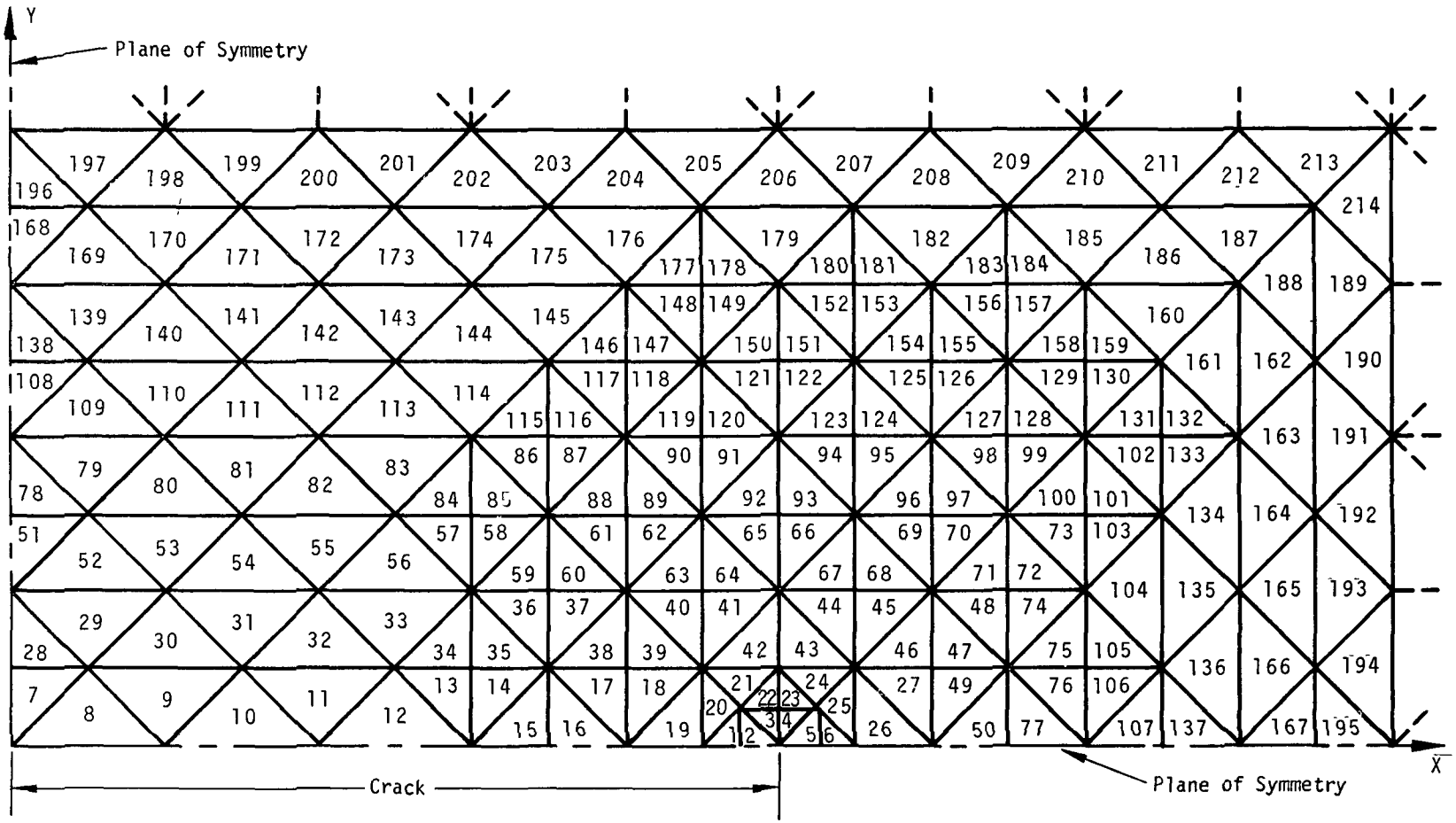

Figure 3. Triangular membrane element identification numbers near crack.

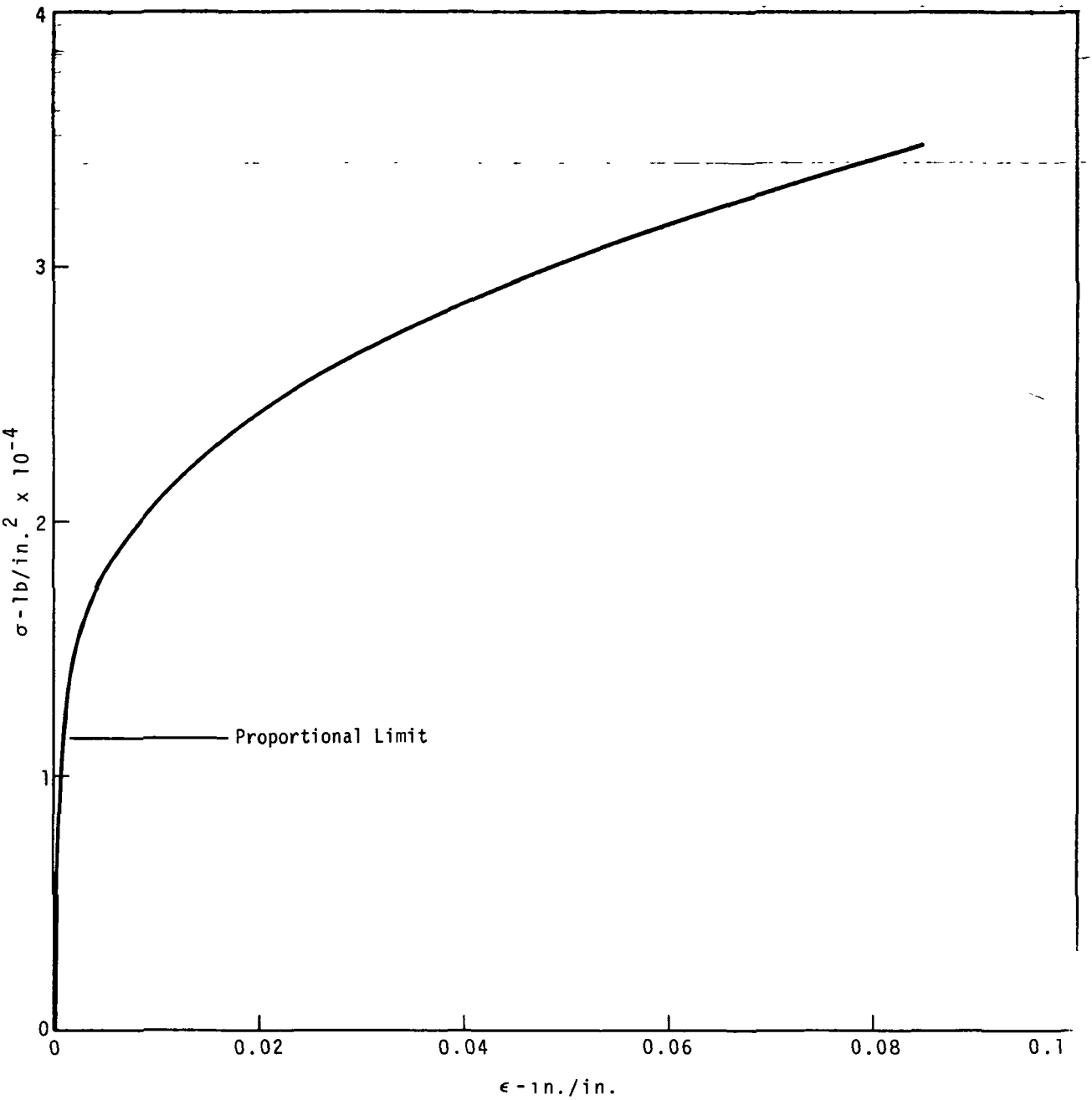

Figure 4. Uniaxial stress-strain curve.

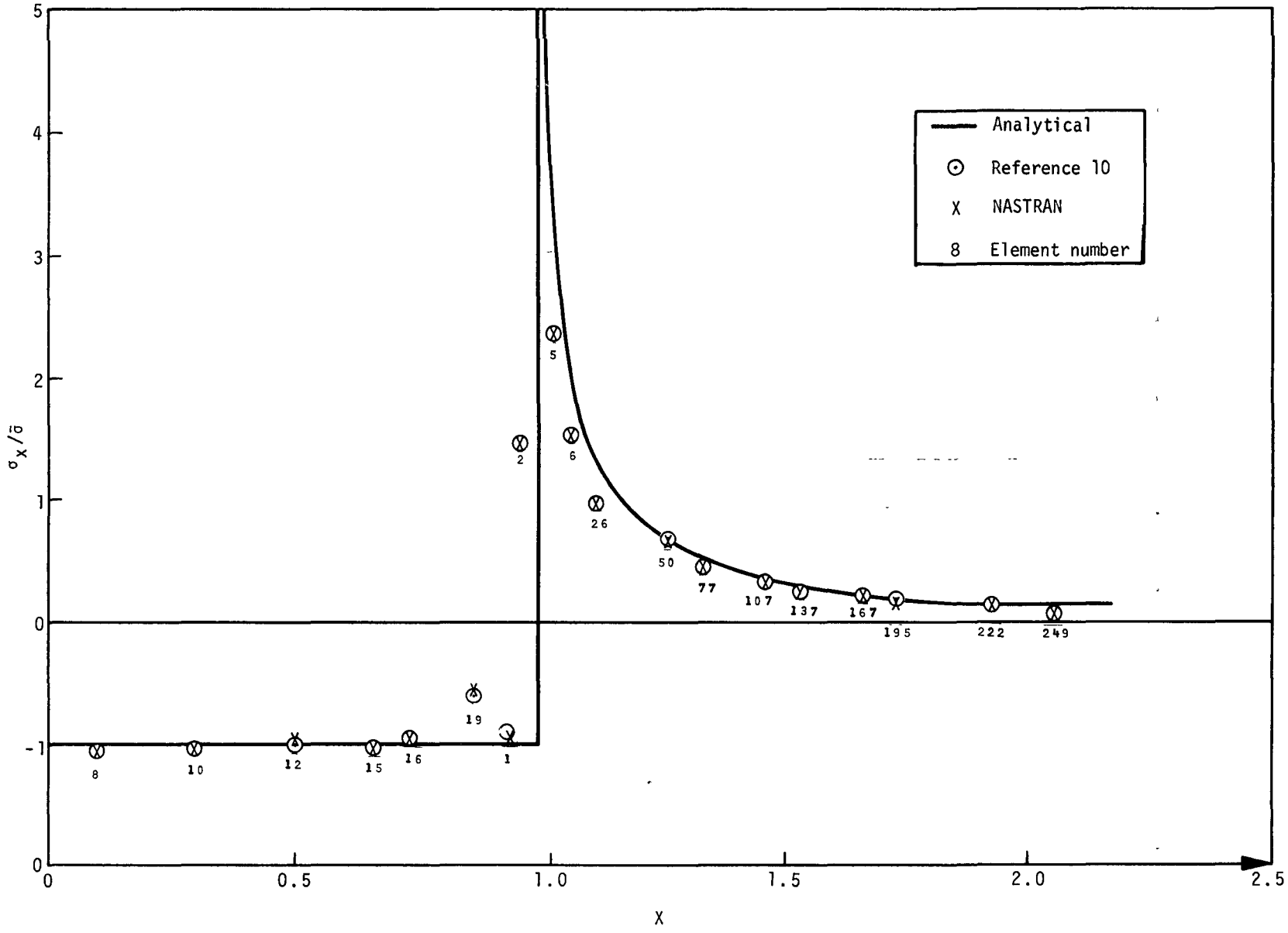

Figure 5. Comparison of stress σ_x along the X-axis, load factor 1.

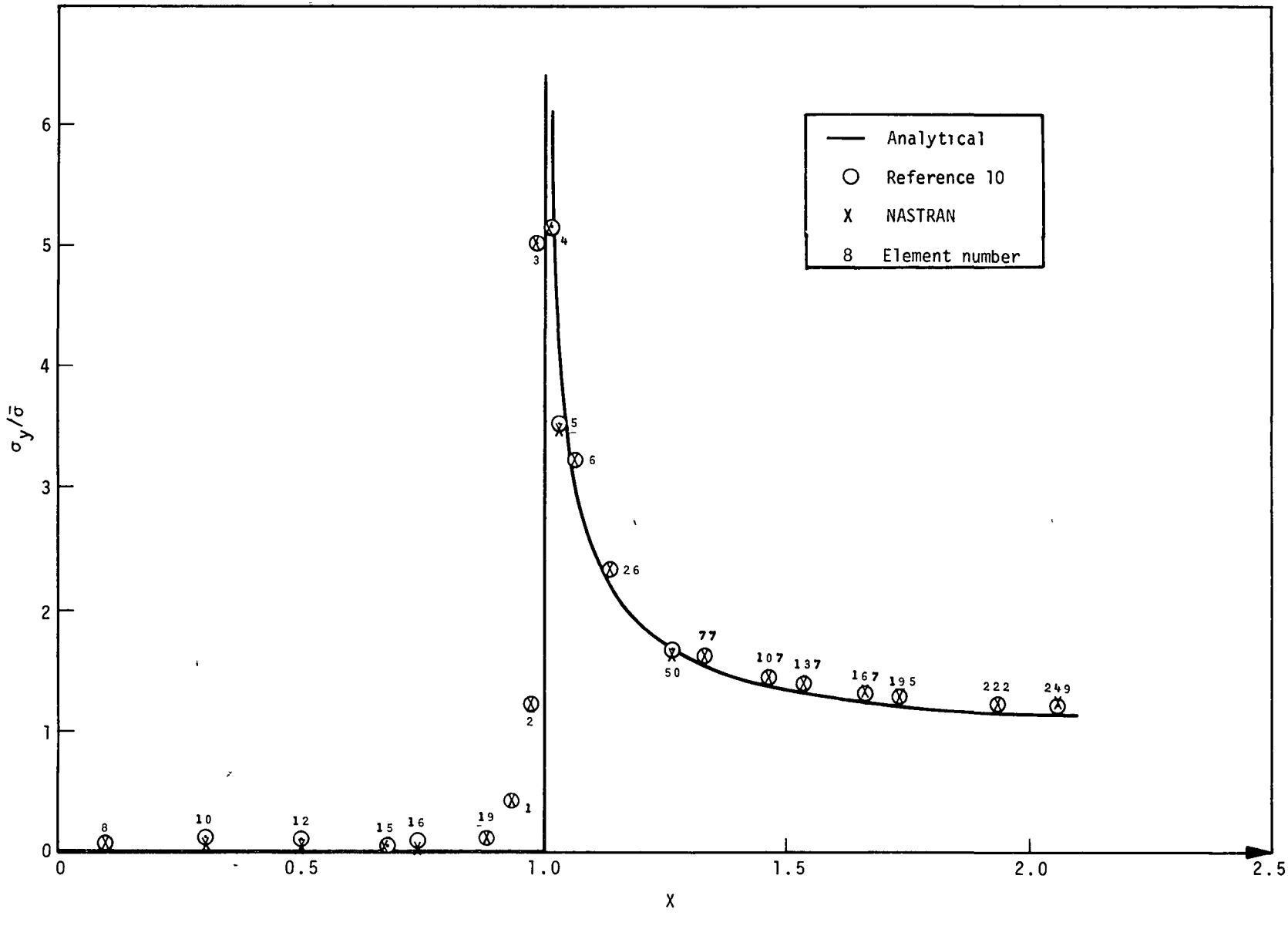

Figure 6. Comparison of stress σ_y along the X-axis, load factor 1.

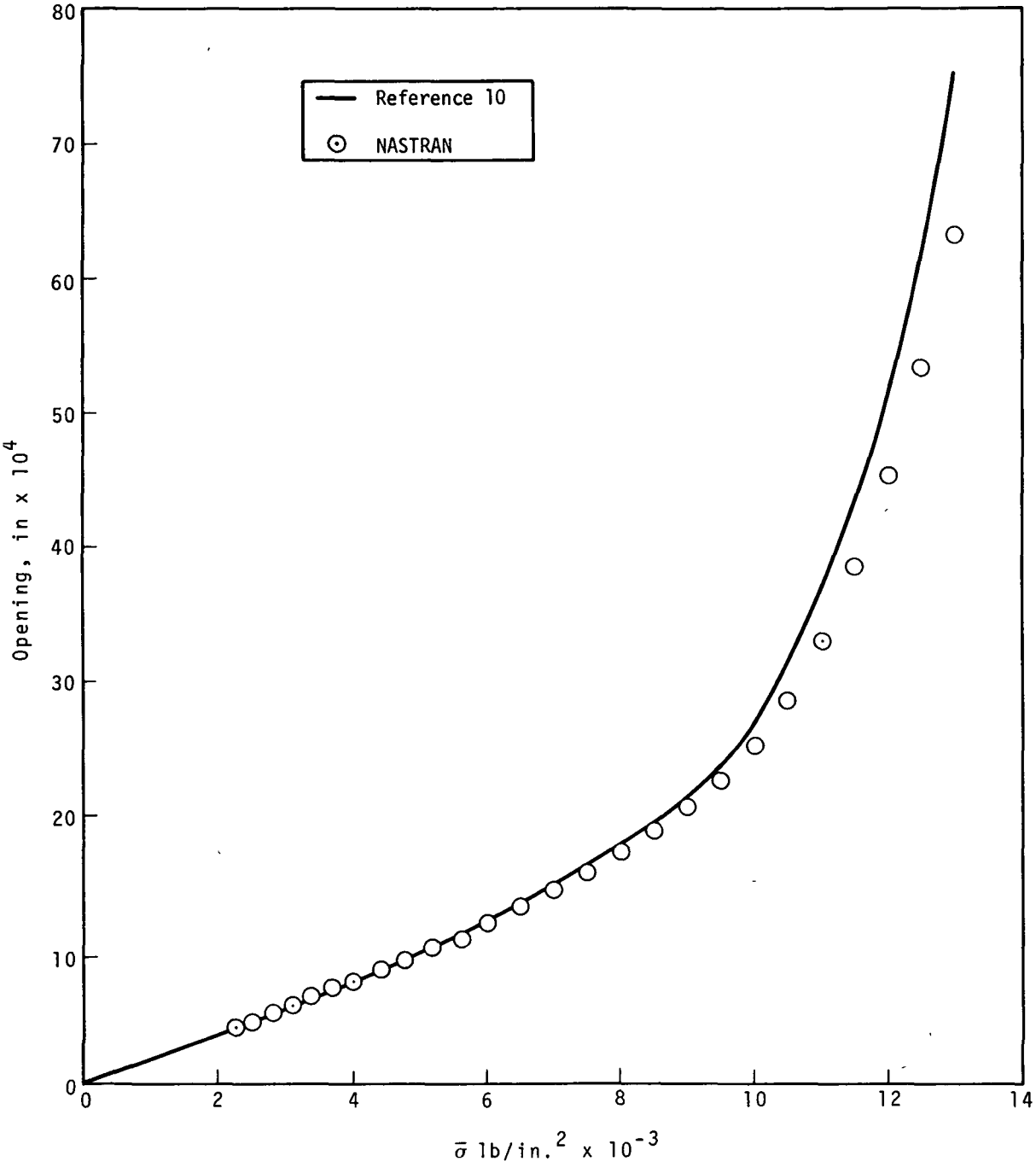

Figure 7. Crack opening vs. load at center of crack (x = 0.0).

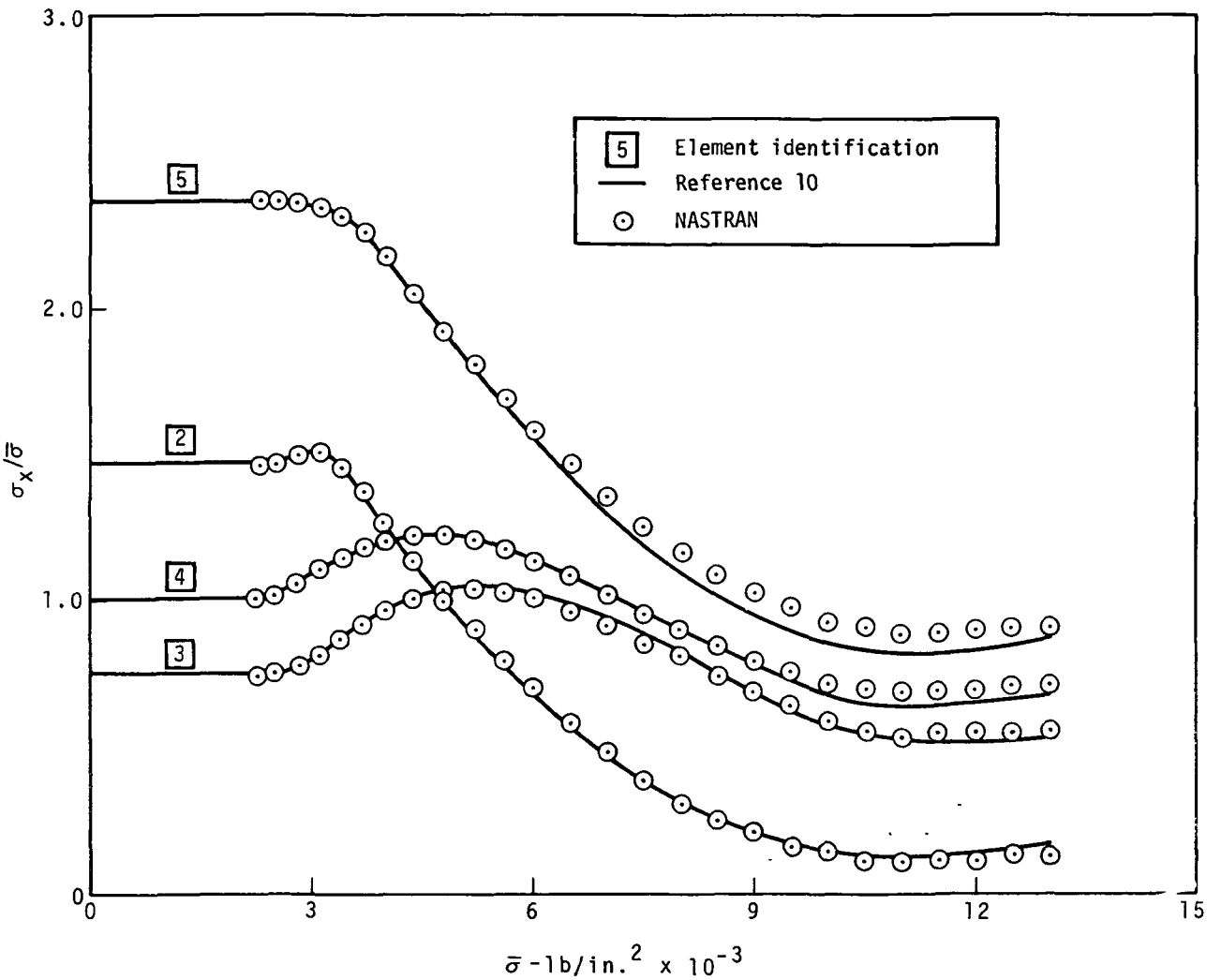

Figure 8. $\sigma_x/\bar{\sigma}$ vs. $\bar{\sigma}$, four elements at tip of crack.

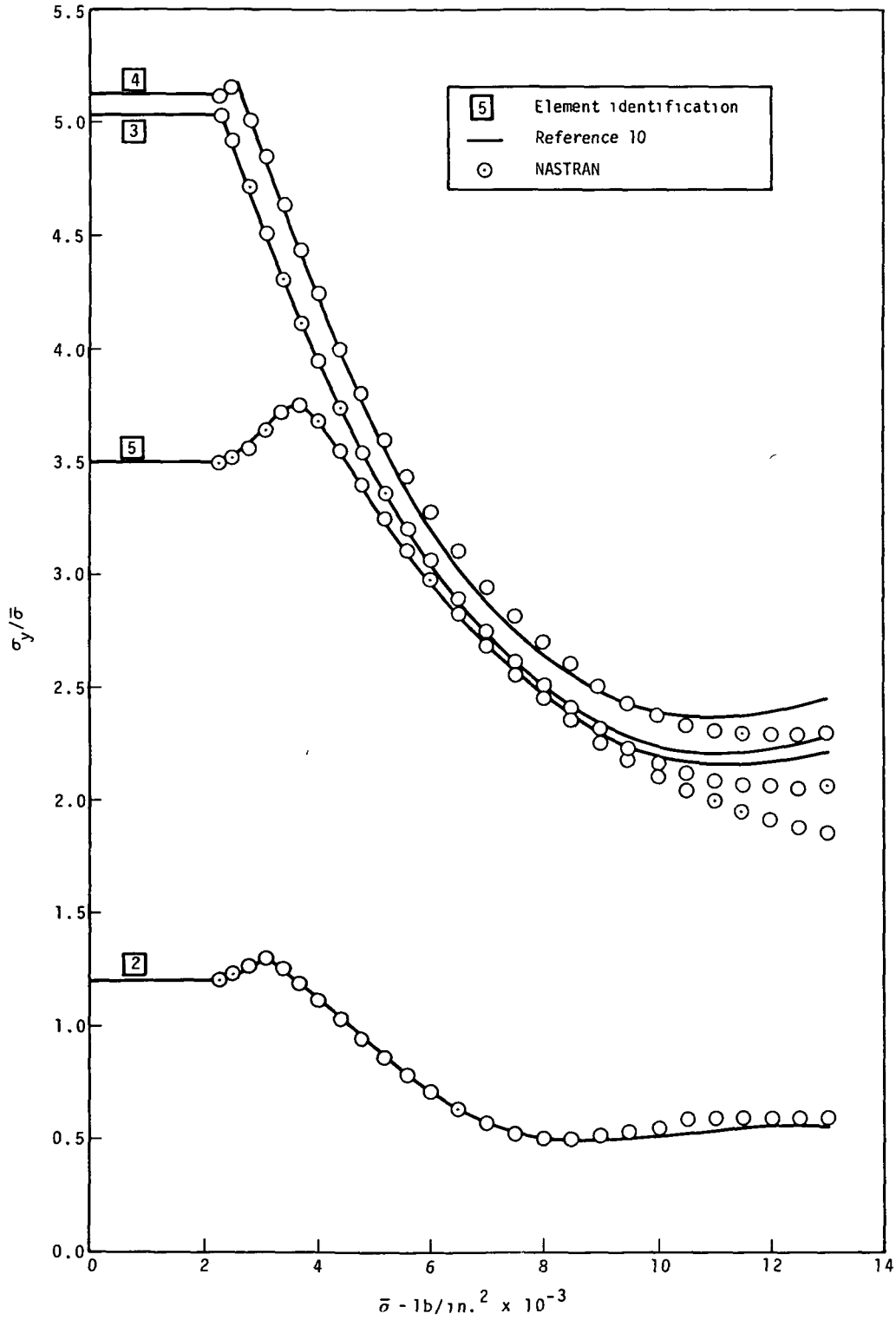

Figure 9. $\sigma_y/\bar{\sigma}$ vs. $\bar{\sigma}$, four elements at tip of crack.

RIGID FORMAT No. 7, Complex Eigenvalue Analysis - Direct Formulation

Complex Eigenvalue Analysis of a 500-Cell String (7-1-1)
Complex Eigenvalue Analysis of a 500-Cell String (INPUT,7-1-2)

A. Description

This problem demonstrates both the use of direct complex eigenvalue analysis and the various methods of supplying damping to the structure. The simulated model is a string under tension having uniform viscous and structural damping as shown in Figure 1. The stiffness due to tension is modeled with scalar springs, the mass is represented by scalar masses, and the viscous damping is provided by scalar dampers connected on one end to the points and fixed on the other end. The structural damping is provided by the scalar springs and an overall damping factor, g_3. The INPUT module is used to generate the scalar springs, dampers and masses.

Complex Eigenvalue Analysis is used to solve the following general matrix equation:

$$([M]p^2 + [B]p + [K])\{u\} = 0$$

where

- p is the complex root
- [M] is the complex mass matrix
- [B] is the complex damping matrix for viscous damping
- [K] is the complex stiffness matrix which contains imaginary components representing the structural damping

According to Reference 11, Chapter 6, the differential equation for this model is:

$$T \frac{\partial^2 u}{\partial x^2} = -\mu \frac{\partial^2 u}{\partial t^2} - \beta \frac{\partial u}{\partial t}$$

where

- T is the string tension (In this problem T is complex)
- μ is the mass per unit length
- β is the damping per unit length

The finite difference representation for this equation is

$$\frac{T}{\Delta x^2}(u_{i-1} - 2u_i + u_{i+1}) = -\mu \frac{d^2 u_i}{dt} - \beta \frac{du_i}{dt}$$

The finite element model which corresponds to this equation is shown in Figure 2. Its equation is:

$$m_i u_i + b_i u_i + (1+ig)k_i(u_{i-1} - 2u_i + u_{i+1}) = P_i$$

where

$$g = g_3 + g_s$$

is the structural damping.

B. Input

1. Parameters

$k_i = 10^7$ - scalar springs

$m_1 = 10.0$ - scalar masses

$b_i = 6.28318$ - scalar dampers

$g_s = 0.05$ - structural element damping

$g_3 = 0.05$ - overall damping parameter

$N = 500$ - number of scalar springs

2. Constraints

The end scalar springs are fixed on the outer ends so constraints are unnecessary.

3. Eigenvalue Extraction Data

Method: Determinant

Region of Interest: $5 < \omega < 16$, $-5.9 < \sigma < 4.5$ where $p = \sigma + i\omega$,

Normalization: Maximum deflection

C. Answers:

The natural frequency for an undamped string, according to Reference 11, is:

$$\omega_n = \frac{\pi n}{\ell}\sqrt{\frac{T}{\mu}} = \frac{\pi n}{N}\sqrt{\frac{k_1}{m_1}}$$

Its deflection shape is:

$$u(x) = \sin\frac{n\pi x}{\ell}$$

or

$$\phi_{in} = \sin\frac{n\pi i}{N}$$

The modal masses are:

$$M_n = \int_0^{\ell} \mu u^2(x)dx = \frac{\mu\ell}{2} = \frac{m_1 N}{2}$$

Substituting the real eigenvectors and eigenvalues into the complex equation for complex roots we obtain for each mode, n:

$$M_n p^2 + \left(\frac{b_1}{m_1}\right) M_n p + (1+ig)\omega_n^2 M_n = 0$$

The solution is:

$$p = -\frac{b_i}{2m_1} \pm \sqrt{\left(\frac{b_i}{2m_i}\right)^2 - (1+ig)\omega_n^2}$$

A comparison of the complex roots is given in Table 1. The eigenvectors, which are the same as the real eigenvectors, are nearly exact for the finite element model.

Table 1. Comparison of NASTRAN and Analytic Complex Roots

n	Real Natural Frequency	Theoretical Roots (radians per second)	NASTRAN Roots (radians per second)
1	1.0	-.6285 ± 6.2753i	-.6283 + 6.2832i
2	2.0	-.9425 ± 12.562i	-.9419 + 12.578i
3	3.0	-1.2566 ± 18.850i	

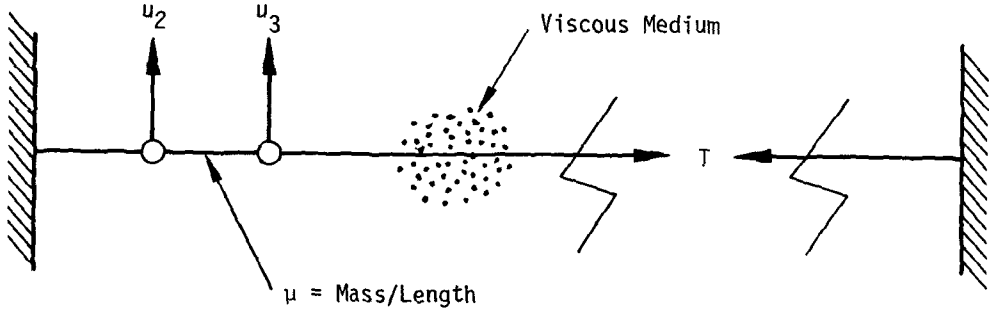

Figure 1. String with damping.

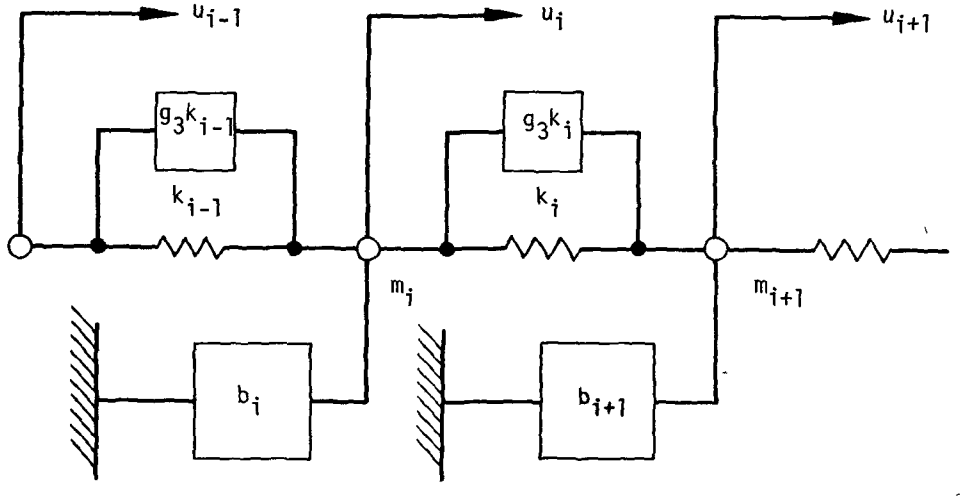

Figure 2. Finite element model of string.

RIGID FORMAT No. 7, Complex Eigenvalue Analysis - Direct Formulation

Third Harmonic Complex Eigenvalue Analysis of a Gas-Filled Thin Elastic Cylinder (7-2-1)
Fifth Harmonic Complex Eigenvalue Analysis of a Gas-Filled Thin Elastic Cylinder (7-2-2)

A. Description

This problem demonstrates the use of symmetry to analyze specific harmonics of a fluid-filled structure. The problem to be solved consists of a cylindrical section filled with a compressible fluid. The end conditions for the cylinder and the fluid are two planes of antisymmetry, perpendicular to the axis. These end conditions correspond to the conditions that exist at periodic intervals along a long, fluid-filled pipe vibrating in one of its vibration modes. The antisymmetric boundary for the structure is defined by constraining the motions which lie in the plane. An antisymmetric boundary for the fluid corresponds to zero pressure. This may be modeled, in NASTRAN, by defining the plane of antisymmetry as a free surface with zero gravity.

The lowest natural frequencies and mode shapes for the third and fifth harmonics are analyzed separately. For the third harmonic, the structure is defined by a section of a cylinder having an arc of 30 degrees or 1/12 of a circle. The fifth harmonic analysis uses a section having an arc of 18 degrees or 1/20 of a circle. The longitudinal edges, which were cut, are planes of symmetry and antisymmetry in order to model a quarter cosine wave length.

The bulk data cards used are; AXIF, BDYLIST, CFLUID2, CFLUID4, CØRD2C, CQUAD1, EIGC, FLSYM, FSLIST, GRIDB, MAT1, PQUAD1, RINGFL, and SPC1.

B. Input

The finite element model for the third harmonic is shown in Figures 1 and 2. Parameters used are:

B	$= 2.88 \times 10^{3}$ lb/in^2	(Bulk modulus of fluid)
ρ_f	$= 1.8 \times 10^{-2}$ lb-sec^2/in^4	(Fluid mass density)
ρ_s	$= 6.0 \times 10^{-2}$ lb-sec^2/in^4	(Structure mass density)
E	$= 1.6 \times 10^{5}$ lb/in^2	(Young's modulus for structure)
G	$= 6.0 \times 10^{4}$ lb/in^2	(Shear modulus for structure)

a	= 10.0 inch	(Radius of cylinder)
ℓ	= 10.0 inch	(Length of cylinder)
h	= 0.01 inch	(Thickness of cylinder)

The model for the fifth harmonic is similar to the third harmonic model except that the angle covered by the structure is 18° instead of 30°. This is accomplished by simply removing the structural elements and boundary GRIDB points corresponding to the two right-hand layers of structure (between 18° and 30°). The FLSYM, FSLIST and SPC1 cards are changed to reflect the 1/20 symmetry.

C. Theory

The derivations and results for this problem are described in Reference 16. The results for various dimensionless parameters are listed. The particular parameters for the problem at hand are:

$$\eta = \frac{\rho_f a}{\rho_s h} = 300.0 \quad ,$$

$$C = \sqrt{\frac{G\rho_f}{B\rho_s}} = 2.5 \quad ,$$

$$\Omega = \frac{P_o a}{Gh} = 0.0 \quad ,$$

where η is the ratio of fluid mass to structure mass. C is the ratio of the wave velocity in the structure material to the wave velocity in the fluid. Ω is the factor describing static pressurization, P_o.

The basic assumptions for this analysis are:

1. Thin shell theory is used for the structure. The bending moment terms in the force equilibrium equations are ignored in the results.

2. The fluid is nonviscous, irrotational, and small motions are only considered.

This particular problem becomes relatively easy to solve since the mode shapes for the fluid in a rigid container and the modes of the structure with no enclosed fluid have the same spatial function at the interface. Each mode of the fluid is excited by only one mode of the structure and each mode of the structure is excited by one mode of the fluid. The pressure in the fluid is

assumed to be a series of functions:

$$P = P_n e^{i\omega t} \cos n\phi \sin \frac{\pi z}{\ell} Q_n(r,\omega) \quad , \tag{1}$$

where Q_n is a Bessel Function or a modified Bessel Function of the first kind.

The characteristic shapes of the structure are a series of the form:

$$u = A e^{i\omega t} \cos n\phi \sin \frac{\pi z}{\ell} \quad , \tag{2}$$

where u is the displacement normal to the surface. The fundamental momentum equation for the fluid flow at the boundary is:

$$\nabla(P(r))\cdot\vec{e}_r = - \rho_f \ddot{u} \quad , \tag{3}$$

where $\vec{e}_r$ is a unit vector in the radial direction.

The forces on the structure at the boundary are:

$$P(a) = \frac{1}{a} \frac{\partial^2 F_1}{\partial z^2} - \rho_s h\ddot{u} \quad , \tag{4}$$

where the function F_1 is defined by the differential equation on the surface:

$$\nabla^4 F_1 = \frac{Eh}{a} \frac{\partial^2 u}{\partial z^2} \quad . \tag{5}$$

The solution for F_1 is obtained by assuming that

$$F_1 = B e^{i\omega t} \cos n\phi \sin\frac{\pi z}{\ell} \quad . \tag{6}$$

Combining Equations 1 through 6 results in the relationships:

$$\rho\omega^2 A = P_n \frac{\partial Q_n(r,\omega)}{\partial r}\bigg|_{r=a} \tag{7}$$

$$Q_n(a,\omega) P_n = \left[\frac{a^2\pi^4 Eh}{\ell^4\left(\frac{\pi^2 a^2}{\ell^2} + n^2\right)^2} + \rho_s h\omega^2 \right] A \tag{8}$$

Equation (7) is a statement of the continuity of displacement. Equation (8) states the ılance of the pressures. The above equations may be solved by ıterating on ω. Reference 16 rovides solutions for ω over a wide range of parameters.

). Results

The analytic and NASTRAN eigenvalues are listed in Table 1. The corresponding errors in the eigenvalues are tabulated and the maximum errors in displacement at the container wall are given as the percentage of the maximum value. The container displacements in the radial direction at $\phi = 0.0$ are compared in Figure 3.

Table 1. Comparison of analytical and NASTRAN results.

Harmonic	Natural Frequency (Hertz)			Mode Shape
	Analytical	NASTRAN	% Error	Max. % Error in Radial Displ.
3	1.579	1.595	1.0	~ 0.0
5	1.011	1.049	3.4	0.5

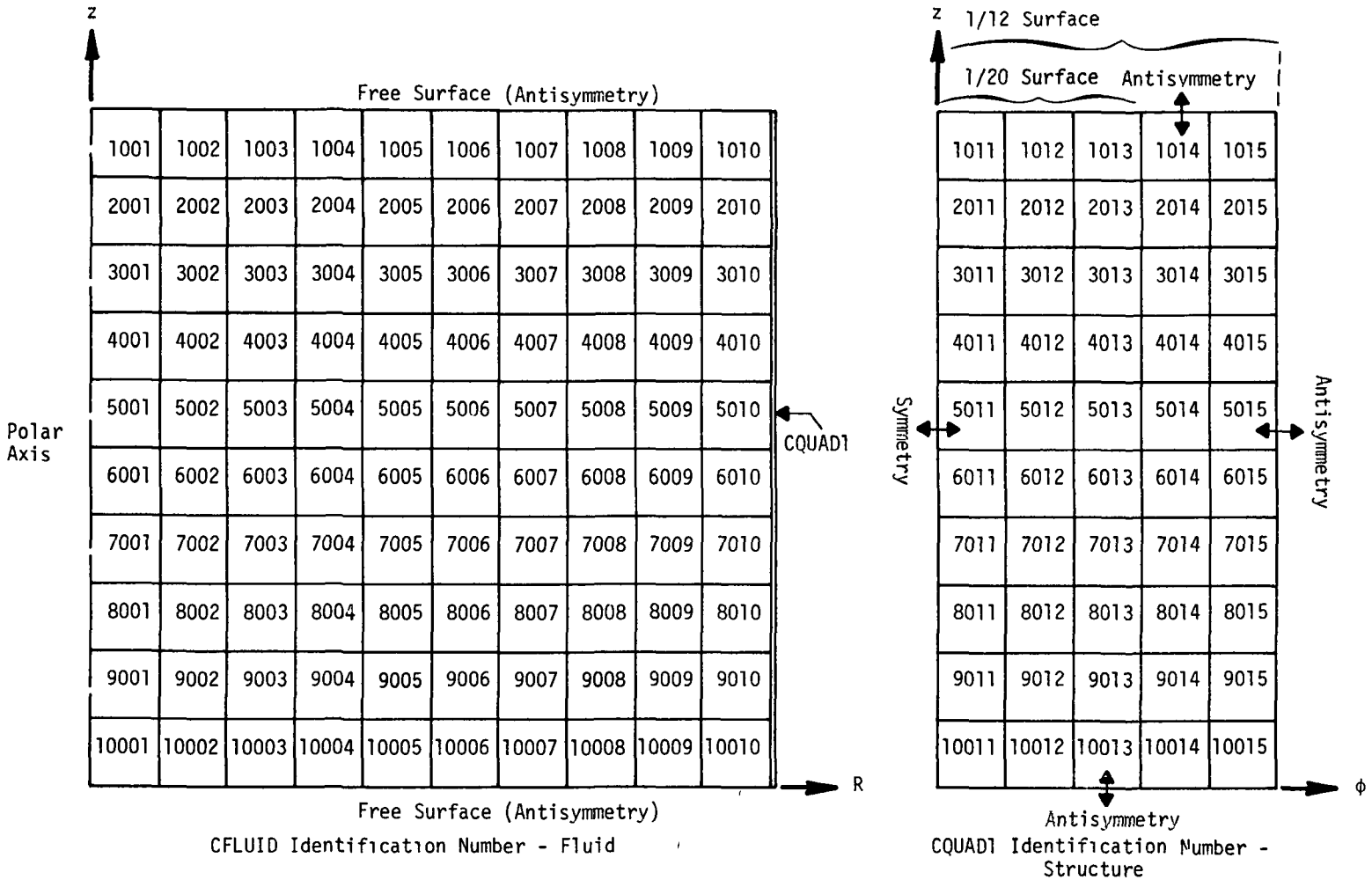

Figure 1. Elastic cylinder and gas model.

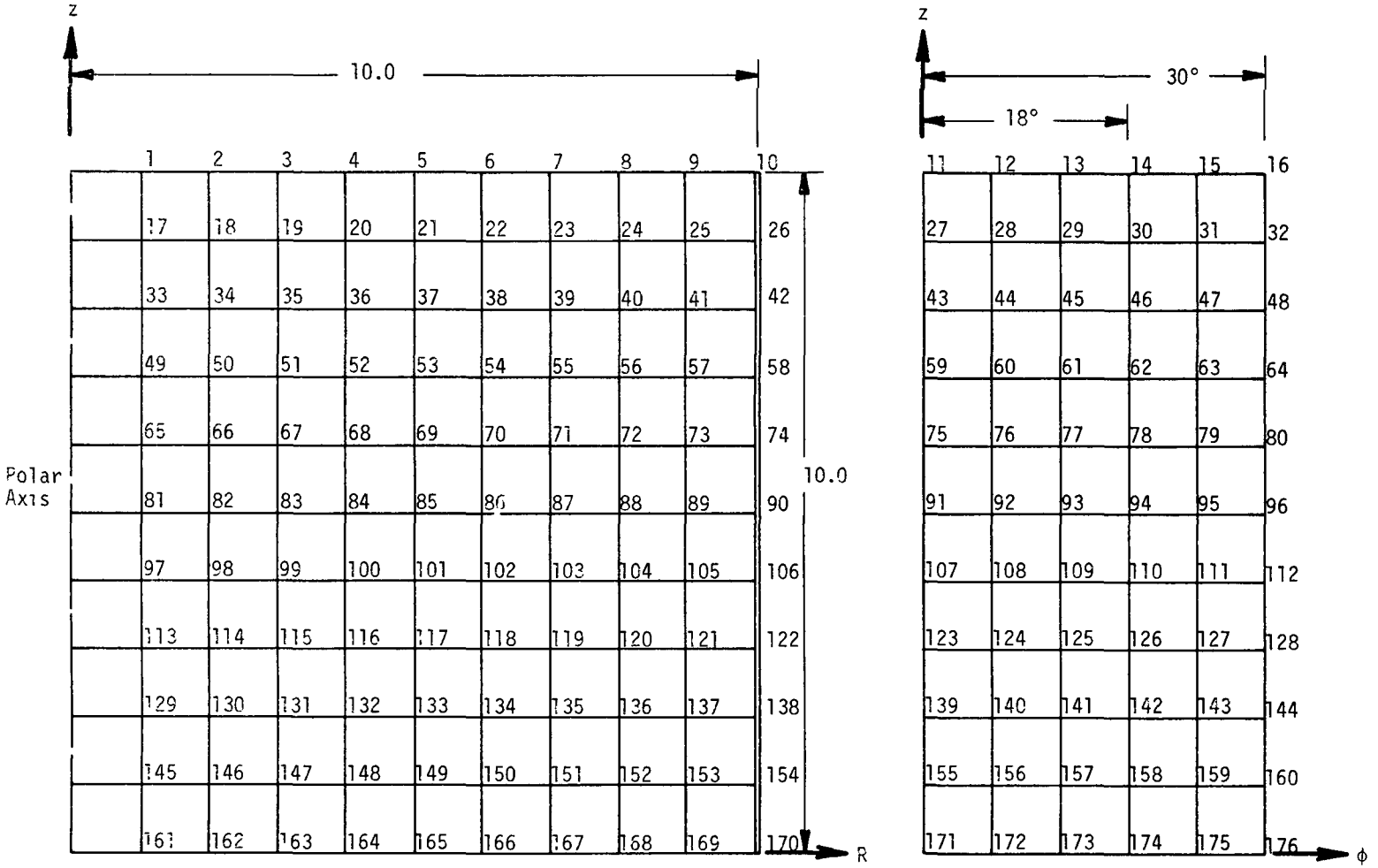

Figure 2. Elastic cylinder and gas model.

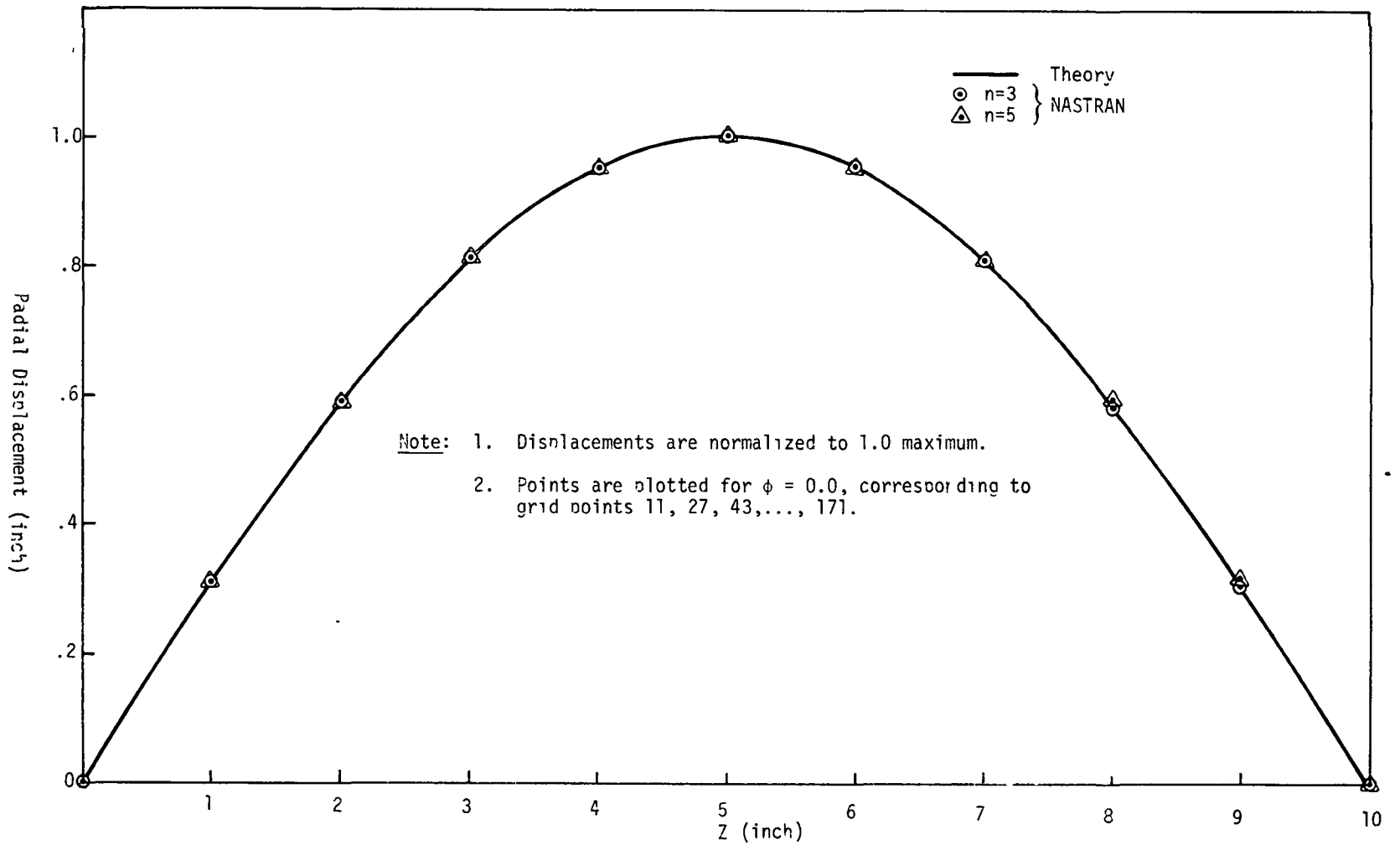

Figure 3. Radial displacement for harmonic 3 and 5 normal modes.

RIGID FORMAT No. 8, Frequency Response Analysis - Direct Formulation

Frequency Response of a 10x10 Plate (8-1-1)
Frequency Response of a 20x20 Plate (8-1-2)
Frequency Response of a 10x10 Plate (INPUT, 8-1-3)
Frequency Response of a 20x20 Plate (INPUT, 8-1-4)

A. Description

This problem illustrates the use of the direct method of determining structural response to steady-state sinusoidal loads. The applied load is given in terms of complex numbers which reflect the amplitudes and phases at each selected frequency. The steady-state response of the structure at each frequency is calculated in terms of complex numbers which reflect the magnitudes and phases of the results. Both configurations are duplicated via the INPUT module to generate the QUAD1 elements.

The particular model for this analysis is a square plate composed of quadrilateral plate elements as shown in Figure 1. The exterior edges are supported on hinged supports and symmetric boundaries are used along x = 0 and y = 0. The applied load is sinusoidally distributed over the panel and increases with respect to frequency. Although the applied load excites only the first mode, the direct formulation algorithm does not use this shortcut and solves the problem as though the load were completely general.

B. Input

1. Parameters:

$a = b = 10$ - length and width of quarter model

$t = 2.0$ - thickness

$E = 3.0 \times 10^7$ - Young's Modulus

$\nu = 0.3$ - Poisson's Ratio

$\mu = 13.55715$ - nonstructural mass per area

2. Loads:

The frequency dependent pressure function is:

$$P(x,y,f) = F(f) \cos \frac{\pi x}{2a} \cos \frac{\pi y}{2b}$$

where $F(f) = 10. + 0.3f$

3. Constraints:

Only vertical motions and bending rotations are allowed. The exterior edges are hinged supports. The interior edges are planes of symmetry. This implies:

along $x = 0$, $\theta_y = 0$

along $y = 0$, $\theta_x = 0$

along $x = a$, $u_z = \theta_x = 0$

along $y = b$, $u_z = \theta_y = 0$

all points, $u_x = u_y = \theta_z = 0$

D. Answers

The excitation of the plate is orthogonal to the theoretical first mode. An explanation of the equations are given in Reference 8. The equations of response are:

$$u_z(f) = \frac{F(f)}{(2\pi)^2 \mu (f_1^2 - f^2)}$$

where f_1 is the first natural frequency (10 cps).

The following table gives the theoretical and NASTRAN results:

Frequency	$u_{z,1} \times 10^4$		
cps	Theory	10x10 NASTRAN	20x20 NASTRAN
0	1.868	1.874	
8	6.435	6.49	
9	12.489	12.69	12.538
10	∞	824.92	
11	-11.833	-11.67	

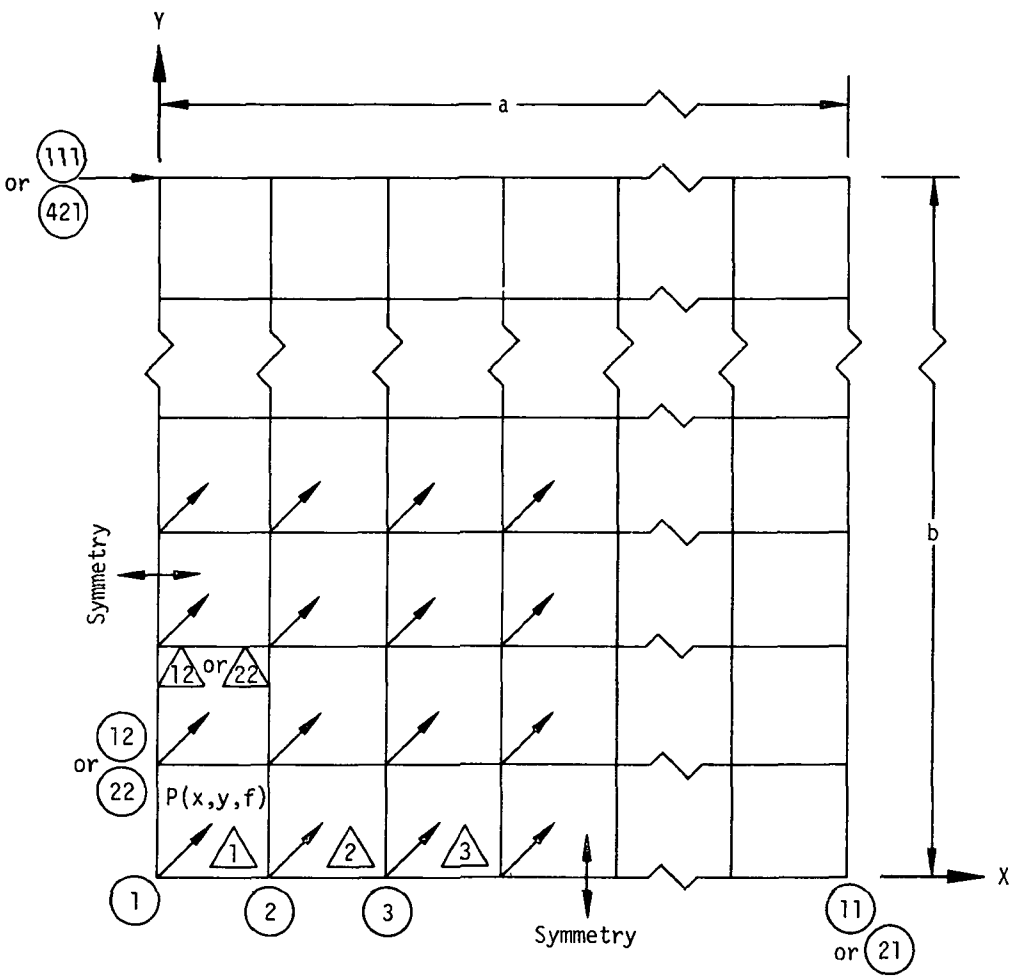

Figure 1. 10 x 10 or 20 x 20 Plate, quarter model.

RIGID FORMAT No. 9, Transient Analysis - Direct Formulation

Transient Analysis with Direct Matrix Input (9-1-1)

A. Description

This problem demonstrates the capability of NASTRAN to perform transient analysis on a system having nonsymmetric stiffness, damping and mass matrices. The problem also illustrates the use of time step changes, selection of printout intervals, application of loads, initial conditions, and a simple curve plot package.

The matrices and loads used are actually the product of a transformation matrix and diagonal matrices. The resulting answers are easily calculated while the input matrices are of general form. The matrix equation solved is:

$$[M]\{\ddot{u}\} + [B]\{\dot{u}\} + [K]\{u\} = \{P(t)\}$$

The problem is actually four disjoint single degree of freedom problems which have been transformed to a general matrix problem. Figure 1 illustrates the problems schematically.

The resulting diagonal matrices are premultiplied by the matrix:

$$[X] = \begin{bmatrix} 2 & -1 & 0 & 0 \\ -1 & 2 & -1 & 0 \\ 0 & -1 & 2 & -1 \\ 0 & 0 & -1 & 2 \end{bmatrix}$$

The answers for the disjoint problem above will be the same as for the general matrix problem since the general case:

$$[X]\left([M_o]\{\ddot{u}\} + [B_o]\{\dot{u}\} + [K_o]\right)\{u\} = [X]\{P\}$$

has the same results as the disjoint case:

$$[M_o]\{\ddot{u}\} + [B_o]\{\dot{u}\} + [K_o]\{u\} = \{P\}$$

B. Input

1. The actual matrix input is:

$$[M] = \begin{bmatrix} 20 & -1.5 & 0 & 0 \\ -10 & 3.0 & -4 & 0 \\ 0 & -1.5 & 8 & 0 \\ 0 & 0.0 & -4 & 0 \end{bmatrix}$$

$$[B] = \begin{bmatrix} 0 & -15 & 0 & 0 \\ 0 & 30 & -24 & 0 \\ 0 & -15 & 28 & -2 \\ 0 & 0 & -24 & 4 \end{bmatrix}$$

$$[K] = \begin{bmatrix} 2000 & 0 & 0 & 0 \\ -1000 & 0 & -100 & 0 \\ 0 & 0 & 200 & -20 \\ 0 & 0 & -100 & 40 \end{bmatrix}$$

2. The initial conditions are:

$u_{10} = 0$ $\quad \dot{u}_{10} = 10.0$

$u_{11} = 0$ $\quad \dot{u}_{11} = 0.5$

$u_{12} = 0$ $\quad \dot{u}_{12} = 0$

$u_{13} = -10.0$ $\quad \dot{u}_{13} = 0$

3. At t = 1.0 a step load is applied to each point. The load on the uncoupled problems is:

$$P_o = \begin{Bmatrix} 0 \\ 1.5 \\ 4.0 \\ 20 \end{Bmatrix}$$

The transformed load is:

$$\{P\} = [X]\{P_o\} = \begin{Bmatrix} -1.5 \\ -1.0 \\ -13.5 \\ 36.0 \end{Bmatrix}$$

C. Answers

The results are responses of single degree of freedom systems. Equations are given in Reference 12, Chapter 9.

$0 < t < 1.0$, $\Delta t = .005$

$$u_{10} = \sin 10t \qquad \dot{u}_{10} = 10 \cos 10t$$

$$u_{11} = 0.05(1 - e^{-10t}) \qquad \dot{u}_{11} = 0.5e^{-10t}$$

$$u_{12} = 0 \qquad \dot{u}_{12} = 0$$

$$u_{13} = -10e^{-10t} \qquad \dot{u}_{13} = 100e^{-10t}$$

$t > 1.0$, $\Delta t = .015$

$$u_{10} = \sin 10t$$

$$u_{11} = 0.05(1 - e^{-10t}) + 0.1(t - 1.1 + .1e^{-10(t-1)})$$

$$u_{12} = 0.04 \left\{1 - e^{-3t}[\cos 4(t-1) + \frac{3}{4} \sin 4(t-1)]\right\}$$

$$u_{13} = -10e^{-10t} + 1 - e^{-10(t-1)}$$

Figures 2 through 5 are tracings of the NASTRAN plots of the functions. The deviations of the NASTRAN results and the theoretical response are due to the selection of time steps. For instance point 11 has a time constant equal to two time steps. The initial error in velocity due to the first step causes the displacement error to accumulate. Using a smaller time step has resulted in much better results.

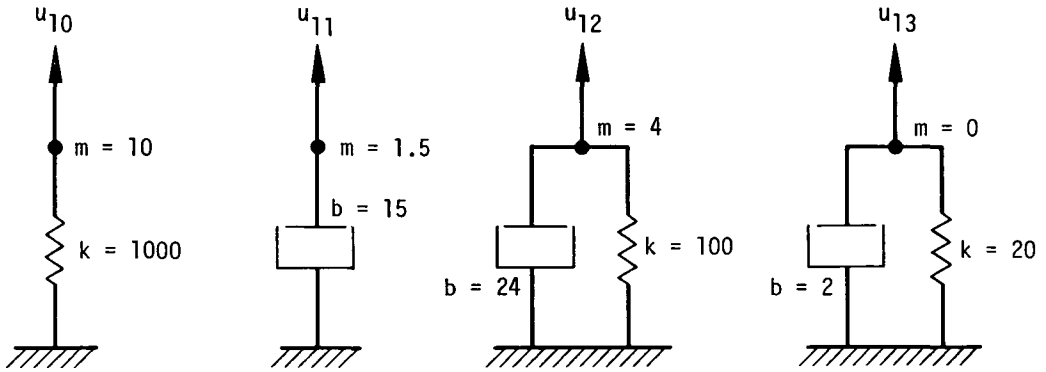

Figure 1. Disjoint equivalent systems.

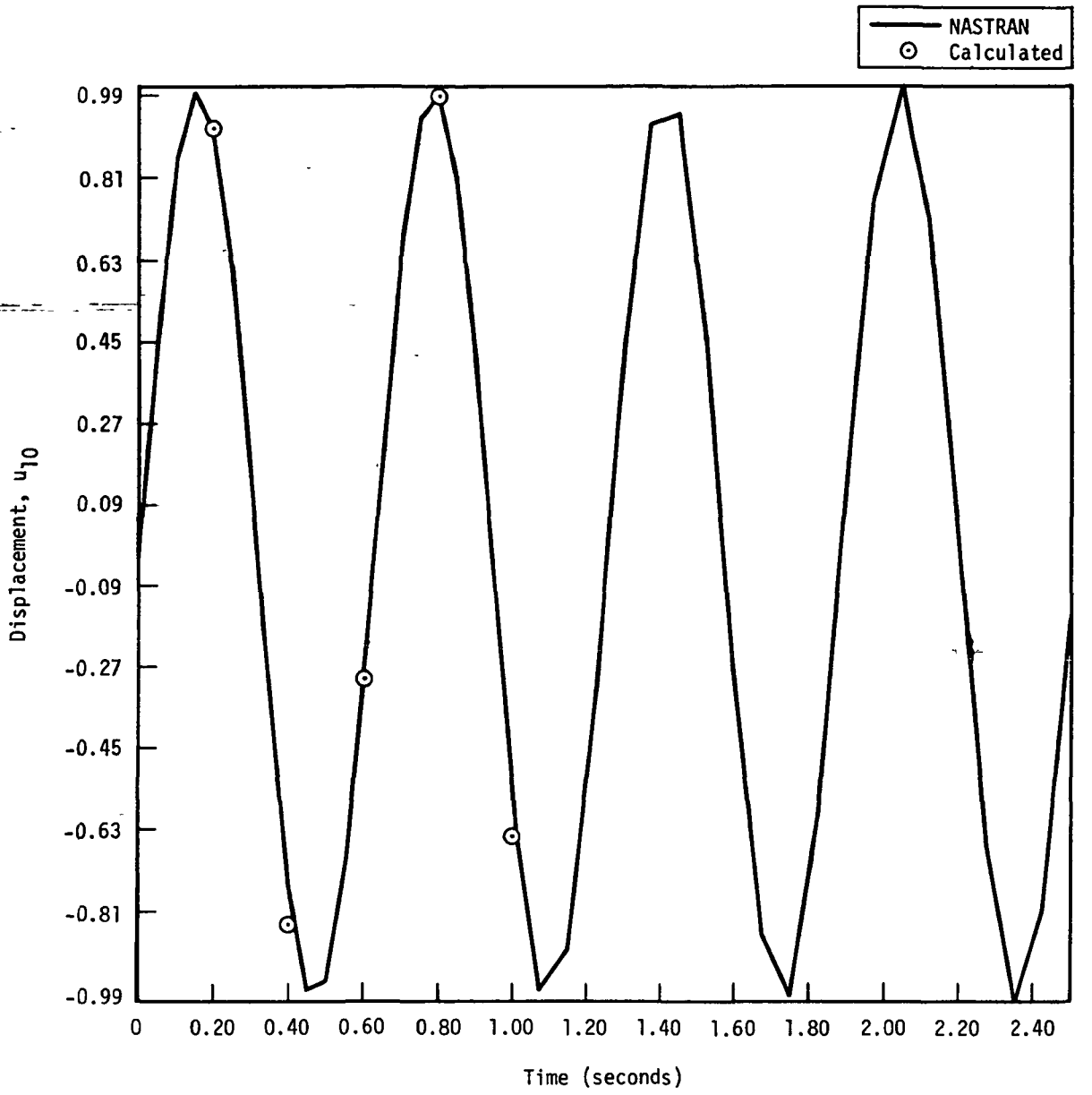

Figure 2. Point 10, displacement.

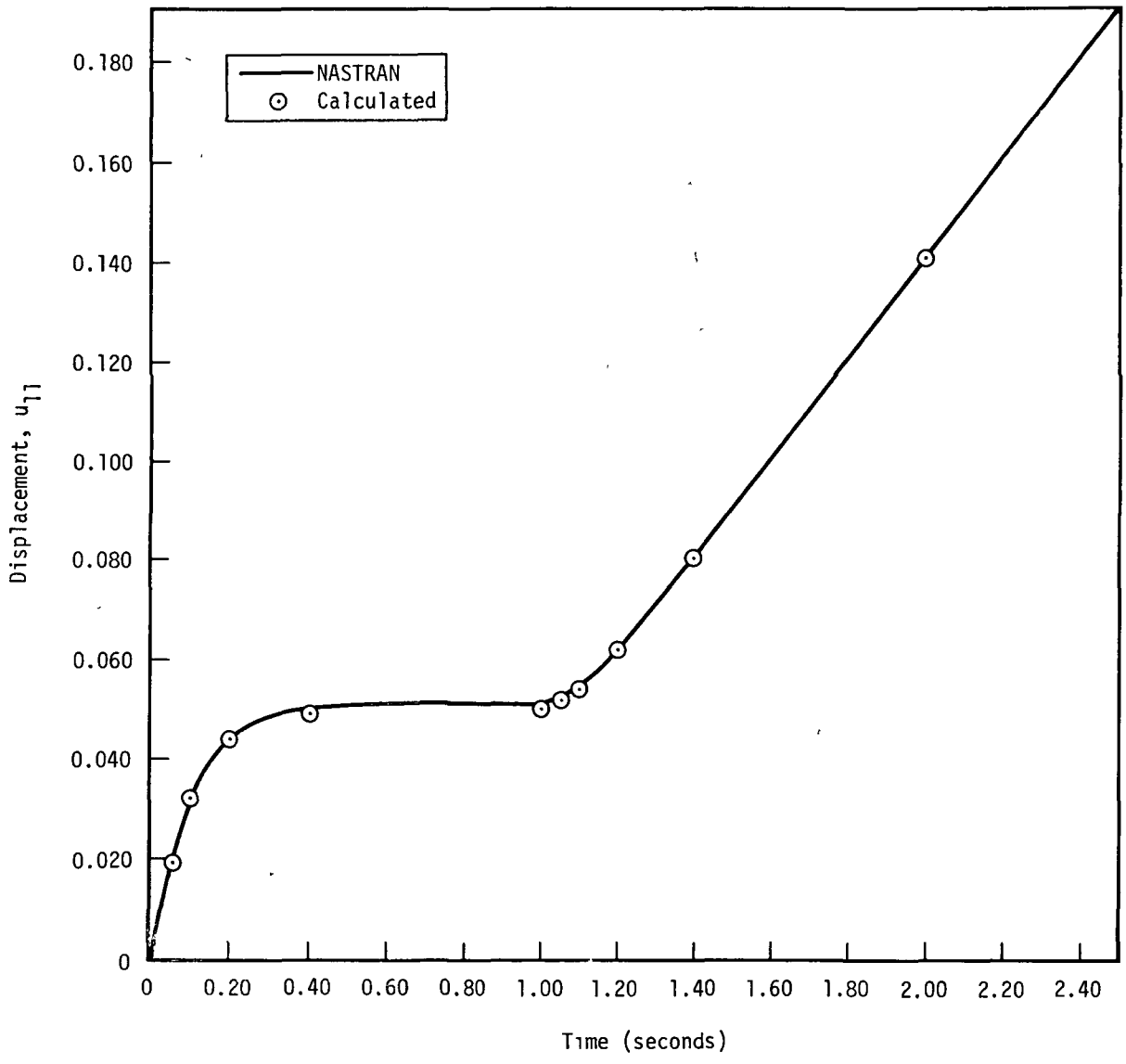

Figure 3. Point 11, displacement.

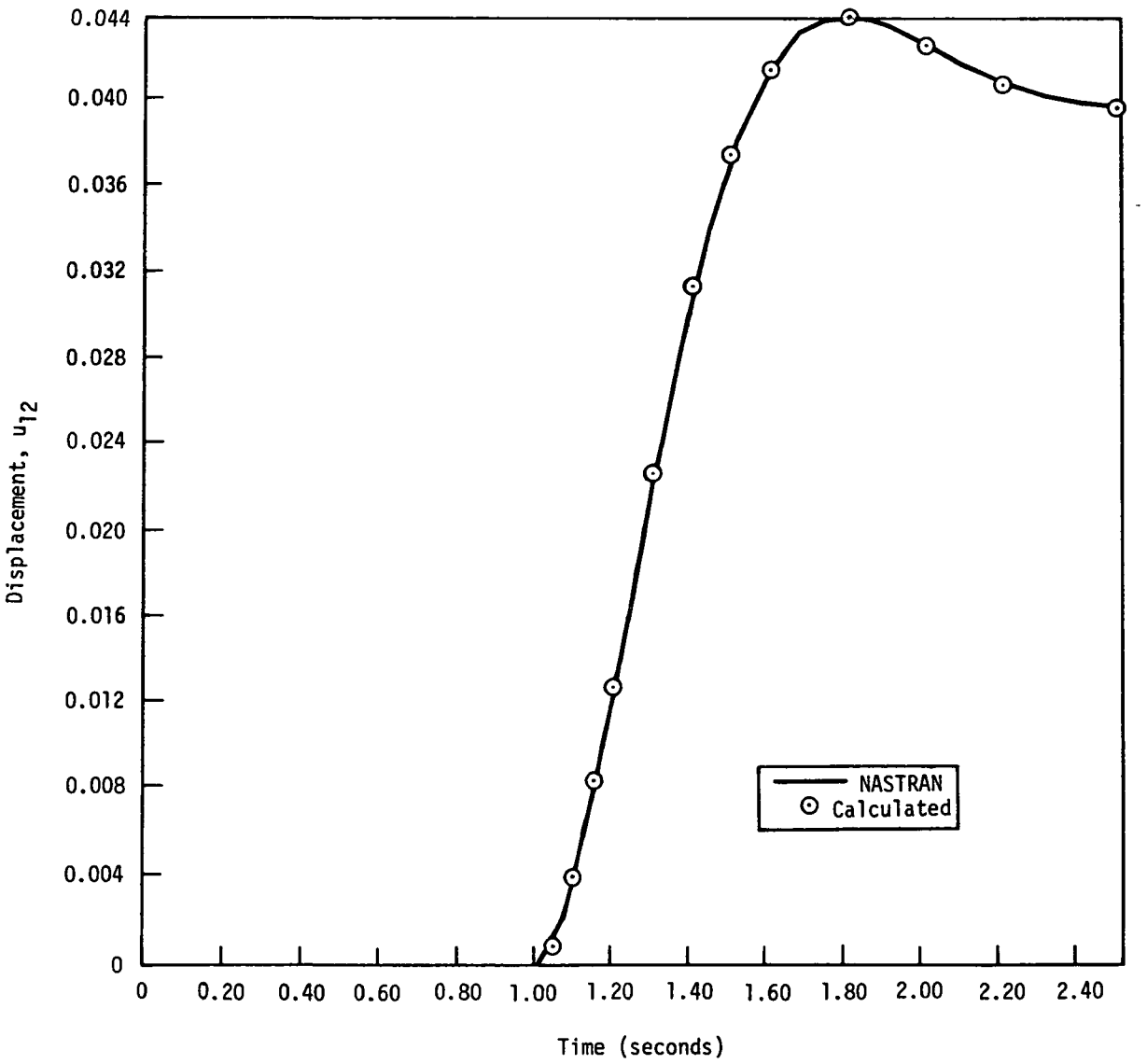

Figure 4. Point 12, displacement.

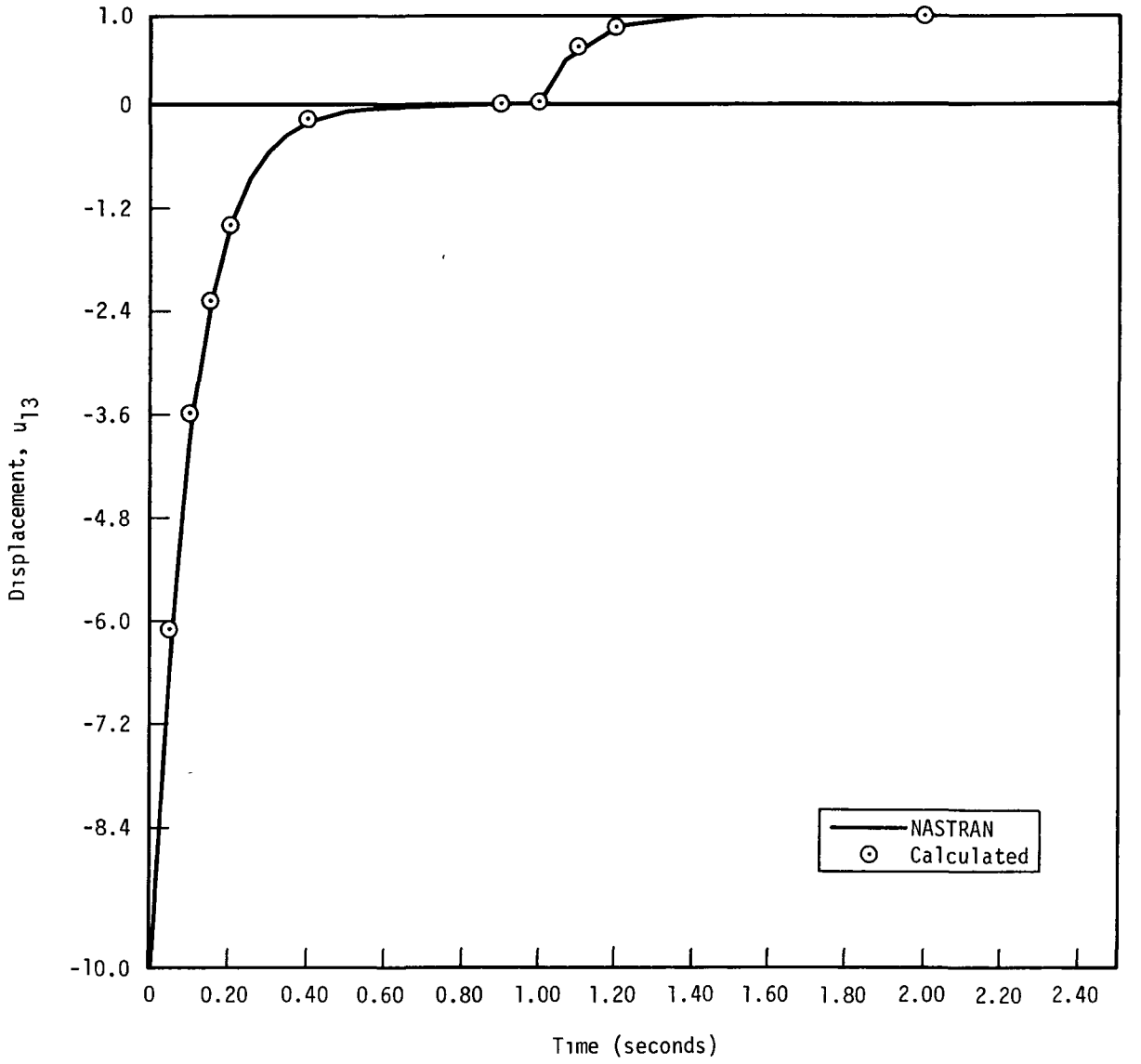

Figure 5. Point 13, displacement.

RIGID FORMAT No. 9, Transient Analysis - Direct Formulation

Transient Analyisis of a 1000 Cell String, Traveling Wave Problem (9-2-1)
Transient Analysis of a 1000 Cell String, Traveling Wave Problem (INPUT, 9-2-2)

A. Description

This problem illustrates the ability of NASTRAN to perform time integration studies using the structural matrices directly. At each time step the applied loads, the structural matrices, and the previous displacements are used to calculate a new set of displacements, velocities, and accelerations. Initial displacements and velocities are also allowed for all unconstrained coordinates. The INPUT module is used to generate the scalar springs and masses.

The structural model consists of a 1000 cell string under constant tension modeled by scalar elements. The string is given an initial condition at one end consisting of a triangular shaped set of initial displacements. The wave will then travel along the string, retaining its initial shape. The ends of the string are fixed causing the wave to reflect with a sign reversal.

Figure 1 illustrates the problem and the scalar element model for each finite increment of length.

B. Input

1. Parameters:

$k_i = \frac{T}{\Delta x} = 10^7$ - scalar spring rates

$m_i = \mu \Delta x = 10$ - scalar masses

$N = 1000$ - number of cells

where

T is the tension

Δx is the incremental length

μ is the mass per unit length

2. Loads:

The initial displacements are;

$u_2 = .2$ $\qquad$ $u_{12} = 1.8$

$u_3 = .4$ $\qquad$ $u_{13} = 1.6$

$u_4 = .6$ $\qquad$.

. $\qquad$. $\qquad$ $u_i = 0, \quad i > 21$

. $\qquad$.

$u_{11} = 2.0$ $\qquad$ $u_{21} = 0.0$

C. Answers

As shown in Reference 11. Chapter 6, the wave velocity c is,

$$c = \pm\sqrt{\frac{T}{\mu}} = \pm\Delta x\sqrt{\frac{k_i}{m_i}} = \pm 1000 \text{ points/unit time}$$

The initial displacement may be divided into two waves, traveling in opposite directions. The first wave travels outward; the second wave travels toward the fixed support and reflects with a sign change. The theoretical and NASTRAN results are compared in Figure 2, when both waves have traveled their complete width.

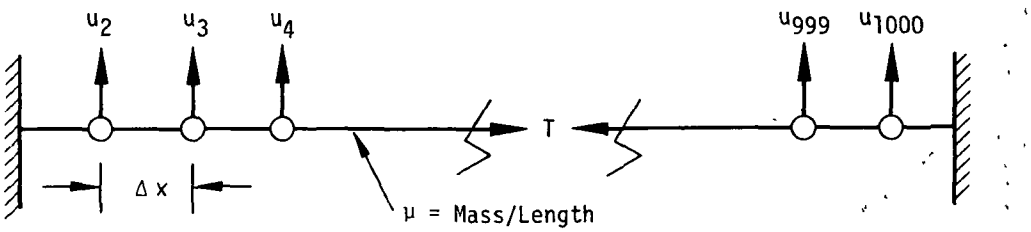

1000 Cell String

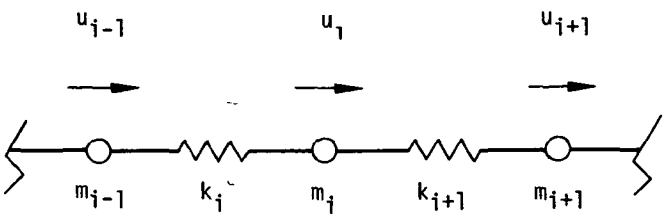

Finite Element Model

Figure 1. Representations of dynamic string.

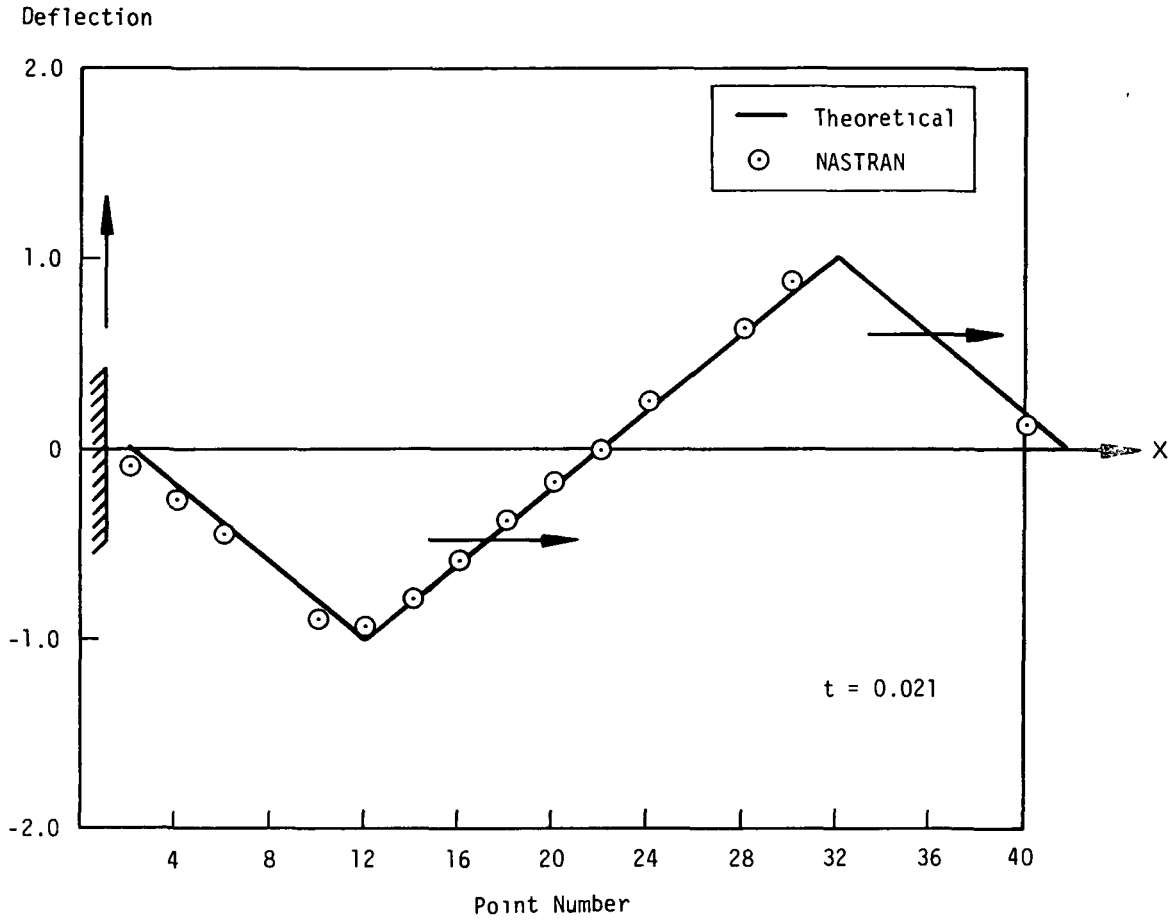

Figure 2. Traveling Wave on string.

RIGID FORMAT No. 9, Transient Analysis - Direct Formulation

Transient Analysis of a Fluid-Filled Elastic Cylinder (9-3-1)

A. Description

The fluid-filled shell, used for analysis of the third harmonic, in Demonstration Problem No. 7-2 is subjected to a step change in external pressure at t = 0 of the form

$$p = p_0 \sin \frac{\pi z}{\ell} \cos n\phi \quad .$$

The fluid is assumed incompressible in order to obtain an analytical solution with reasonable effort. The harmonic used is n = 3.

In addition to the cards of Demonstration Problem No. 7-2, DAREA, PRESPT, TLØAD2, and TSTEP cards are also used. Selected displacements and pressures are plotted against time.

B. Input

The finite element model is shown in Figures 1 and 2. Parameters used are:

$B = \infty$		(Bulk modulus of fluid - incompressible)
$\rho_f = 1.8 \times 10^{-2}$	lb-sec^2/in^4	(Fluid mass density)
$\rho_s = 6.0 \times 10^{-2}$	lb-sec^2/in^4	(Structure mass density)
$E = 1.6 \times 10^5$	lb/in^2	(Young's modulus for structure)
$G = 6.0 \times 10^4$	lb/in^2	(Shear modulus for structure)
$a = 10.0$	inch	(Radius of cylinder)
$\ell = 10.0$	inch	(Length of cylinder)
$h = 0.01$	inch	(Thickness of cylinder wall)
$p_0 = 2.0$		(Pressure load coefficient)

C. Theory

The theory was derived with the aid of Reference 16 as in Demonstration Problem No. 7-2. Since the fluid is incompressible, it acts on the structure like a pure mass. Neglecting the bending stiffness, the equation of force on the structure is:

$$p_s = (m + m_f)\,\ddot{w} + \frac{1}{a}\frac{\partial^2 F}{\partial z^2} \quad , \tag{1}$$

where:

p_s is the loading pressure on the structure (positive outward).

$m = \rho_s h$ is the mass per area of the structure.

m_f is the apparent mass of the fluid.

w is the normal displacement (positive outward)

The function F is defined by the equation,

$$\nabla^4 F = \frac{Eh}{a}\frac{\partial^2 w}{\partial z^2} \quad . \tag{2}$$

The spatial functions of pressure, displacement, and function F may be written in the form

$$\begin{aligned} p_s &= p_o \sin\frac{\pi z}{\ell} \cos n\phi \quad , \\ w &= w_o \sin\frac{\pi z}{\ell} \cos n\phi \quad , \\ F &= F_o \sin\frac{\pi z}{\ell} \cos n\phi \quad . \end{aligned} \tag{3}$$

where p_o, w_o, and F_o are variables with respect to time only.

Substituting Equations 3 into Equation 2 we obtain:

$$F_o = -\frac{Eh}{a}\left(\frac{\ell}{\pi}\right)^2 \frac{w_o}{\left[1 + \left(\frac{n\ell}{\pi a}\right)^2\right]^2} \quad . \tag{4}$$

Substituting Equations 3 and 4 into Equation 1 we obtain:

$$p_o = (m + m_f)\,\ddot{w}_o + \frac{Eh}{a^2\left[1 + \left(\frac{n\ell}{\pi a}\right)^2\right]^2}\,w_o \quad . \tag{5}$$

The incompressible fluid is described by the differential equation:

$$\nabla^2 p = 0 \quad . \tag{6}$$

Applying the appropriate boundary conditions to Equation 6 results in the pressure distribution:

$$p = p_r \sin\frac{\pi z}{\ell}\,\cos(n\phi)\,I_n\left(\frac{\pi r}{\ell}\right) \quad , \tag{7}$$

where I_n is the modified Bessel function of the first kind and p_r is an undetermined variable. The balance of pressure and flow at the boundary of the fluid, with no structural effects, is described by the equations:

$$p_o = -\,p_r\,I_n\left(\frac{\pi a}{\ell}\right) \quad , \tag{8}$$

$$\rho_f \ddot{w} = -\left.\frac{\partial p}{\partial r}\right|_{r=a} \quad . \tag{9}$$

Substituting Equations 3 and 7 into Equation 9 results in:

$$\rho_f\,\ddot{w}_o = -\frac{\pi}{\ell}\,I_n'\left(\frac{\pi a}{\ell}\right)p_r \quad . \tag{10}$$

Eliminating P_r with Equations 8 and 10 gives the expression for apparent mass, m_f:

$$p_o = I_n\left(\frac{\pi a}{\ell}\right)\frac{\rho_f \ddot{w}_o}{\frac{\pi}{\ell}\,I_n'\left(\frac{\pi a}{\ell}\right)} = m_f\,\ddot{w}_o \quad . \tag{11}$$

Substituting the expression for m_f from Equation 11 into Equation 5 results in a simple single degree of freedom system. When the applied loading pressure is a step function at t = 0,

$$w = \frac{p_o}{k} (1 - \cos \omega t) \sin \frac{\pi z}{\ell} \cos n\phi \quad , \qquad (12)$$

where

$$\omega = \sqrt{\frac{k}{m_T}} \quad ,$$

and

$$k = \frac{Eh}{a^2\left[1 + \left(\frac{n\ell}{\pi a}\right)^2\right]^2} \quad ,$$

and

$$m_T = m + m_f = \rho_s h + \rho_f \frac{\ell}{\pi} \frac{I_n\left(\frac{\pi a}{\ell}\right)}{I_n'\left(\frac{\pi a}{\ell}\right)}$$

D. Results

A transient analysis was performed for the case n = 3 on the model and various displacements and pressures were output versus time up to one second. The theoretical frequency is calculated to be 1.580 Hertz and the period is 0.633 seconds. The displacements at two points on the structure (Point 91 is located at $\phi = 0$, z = 5.0; Point 94 is located at $\phi = 18°$, z = 5.0) are plotted versus time in Figure 3.

The maximum error for the first full cycle occurs at the end of the cycle. The ratio of the error to maximum displacement is 4.75%. Changes in the time step used in the transient integration algorithm did not affect the accuracy to any great extent. The most probable causes for error were the mesh size of the model and the method used to apply the distributed load. The applied load was calculated by multiplying the pressure value at the point by an associated area. The "consistent method" of assuming a cubic polynomial displacement and integrating would eliminate the extraneous response of higher modes. The method chosen in this problem, however, is typical of actual applications.

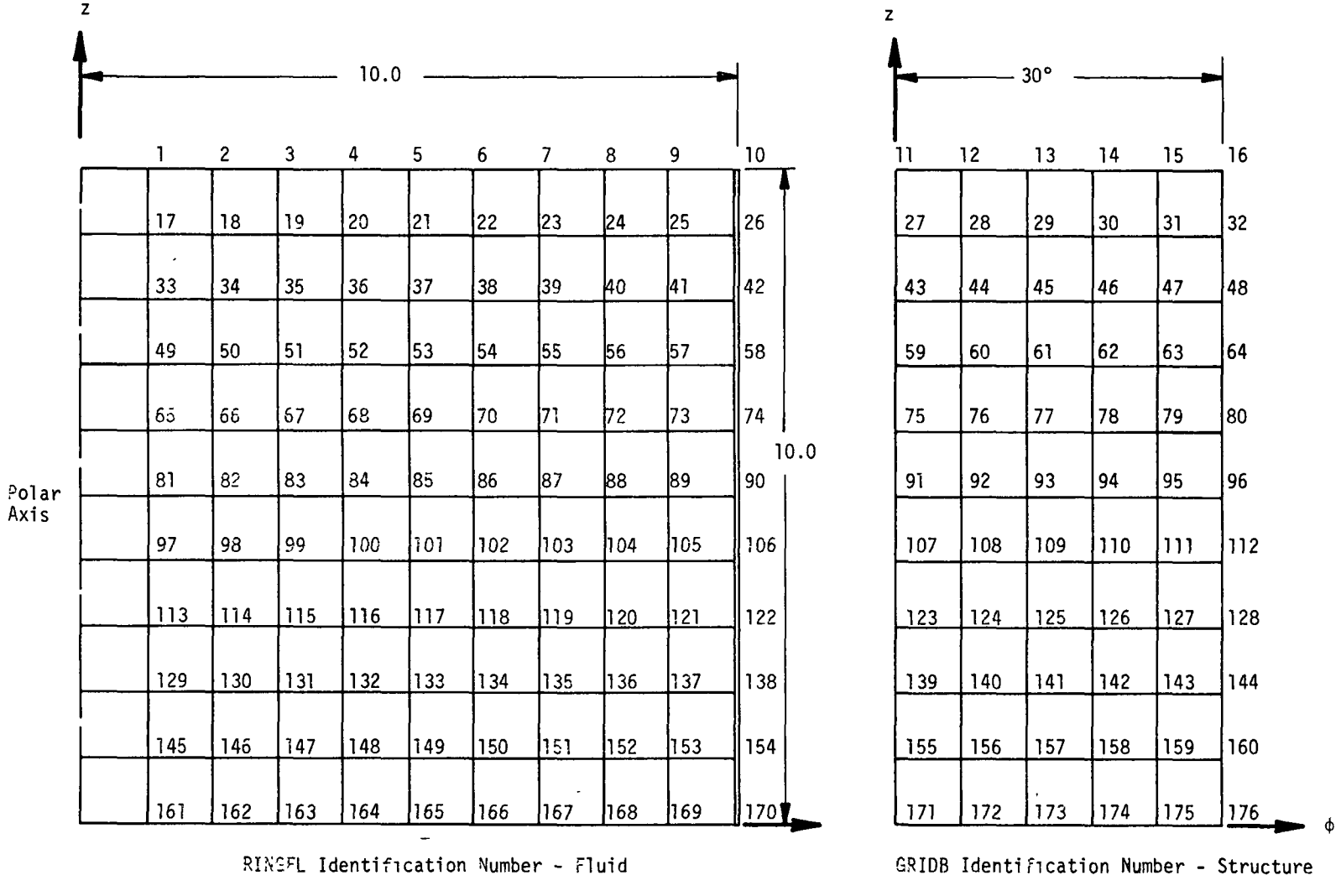

Figure 1. Transient analysis model.

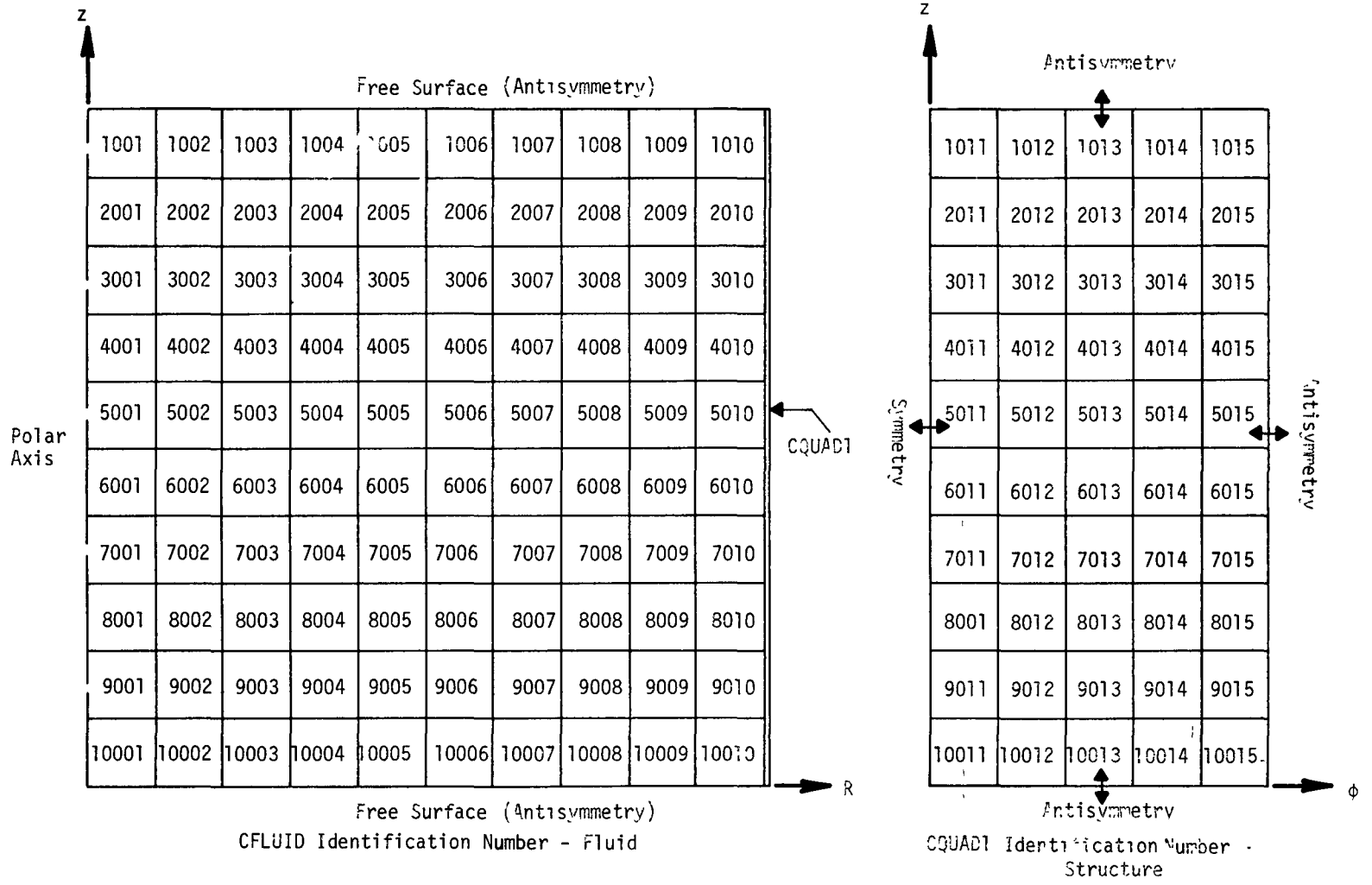

Figure 2. Transient analysis model.

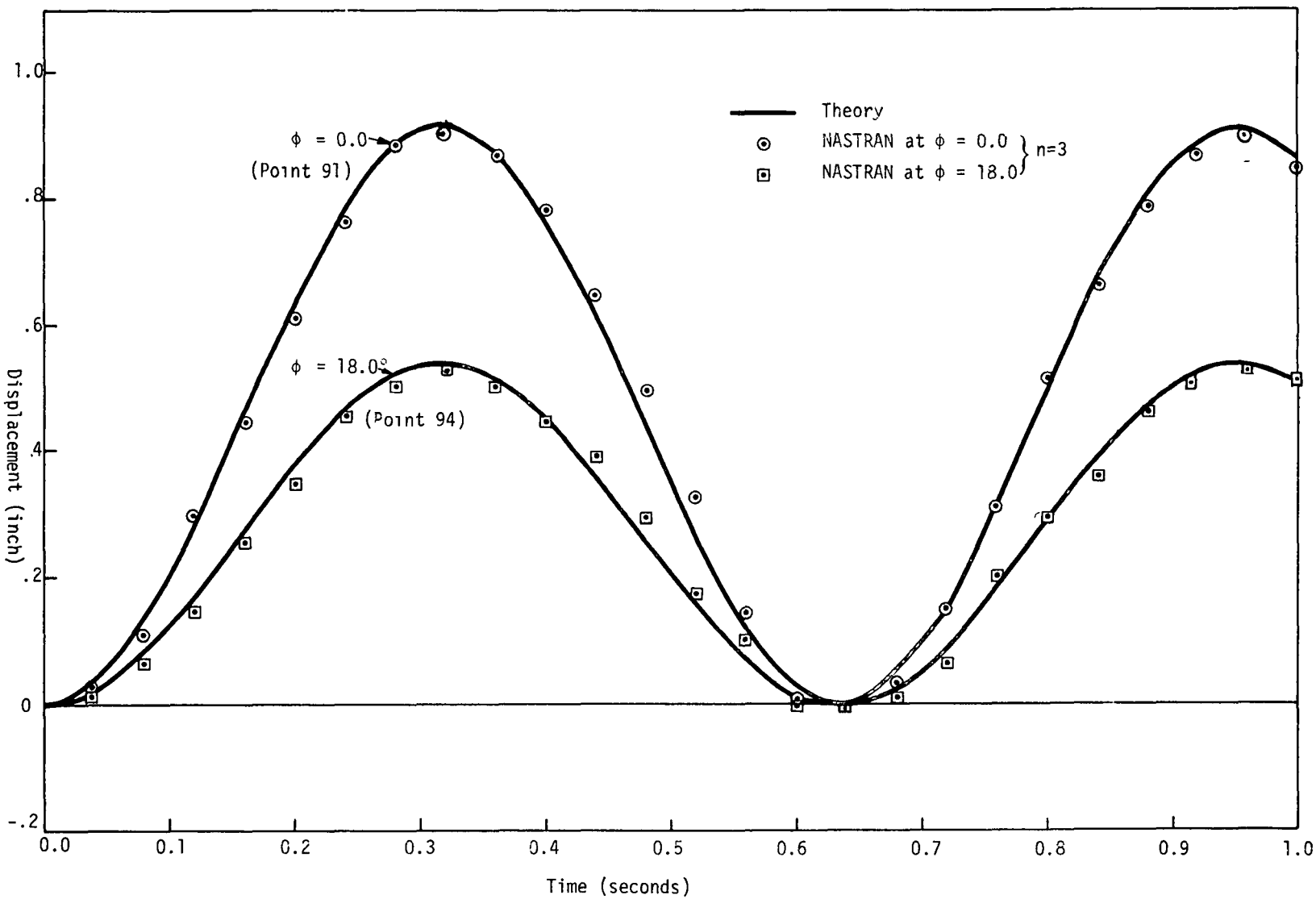

Figure 3. Displacement at midpoint (z = 5.0).

RIGID FORMAT No. 9 (APP HEAT), Linear Transient Heat Transfer Analysis
Plate with Suddenly Applied Flux and Edge Temperature (9-4-1)

A. Description

The time history of the temperature in a long thin plate initially at zero degrees is analyzed using NASTRAN's transient heat analysis capability. At time t=0 a heat flux is applied on one surface of the plate and simultaneously the temperature along the edges is increased. These temperatures are maintained at a value by using a large heat flux through a good conductor to ground. The problem is one dimensional since it is assumed that no temperature variation exists along the length or through the thickness. Since the plate is symmetric about the center plane, only one half of the plate is modeled.

B. Input

The plate is shown in Figure 1 and the idealized NASTRAN model, shown in Figure 2, is represented by five RØD elements going from the centerplane to the edge. The conductor-ground arrangement is modeled by an ELAS2 element and an SPC card referenced in Case Control. The injected heat flux at the edge is specified using DAREA and TLØAD2 cards which are referenced in Case Control through a DLØAD card. The surface heat flux is specified on a QBDY1 card and references the TLØAD2 card. The time step intervals at which the solution is generated are given on the TSTEP card. The initial temperature conditions are specified on the TEMPD card and referenced in Case Control by an IC card. The heat capacity and conductivity are given on the MAT4 card.

C. Theory

The analytic solution is

$$T(x,t) = 0.5\left[1 - \frac{4}{\pi}\sum_{n=0}^{\infty}\frac{(-1)^n}{(2n+1)}\,e^{-(2n+1)^2 t}\cos(2n+1)\pi x/2\right] + 50.\left[(1-x^2) - \frac{32}{\pi^3}\sum_{n=0}^{\infty}\frac{(-1)^n}{(2n+1)^3}\,e^{-(2n+1)^2 t}\cos(2n+1)\pi x/2\right] .$$

D. Results

A comparison of theoretical and NASTRAN results is given in Table 1.

Table 1. Theoretical and NASTRAN temperatures.

		GRID(X)					
		10(0.)	12(.2)	14(.4)	16(.6)	18(.8)	20(1.)
t = 0	Theory*	0.	0.	0.	0.	0.	0.
	NASTRAN	0.	0.	0.	0.	0.	0.
t = 1	Theory*	31.282	30.222	26.952	21.204	12.562	.500
	NASTRAN	30.641	29.612	26.433	20.826	12.362	.500
t = 2	Theory*	43.430	41.776	36.780	28.344	16.316	.500
	NASTRAN	43.117	41.478	36.527	28.160	16.218	.500
t = 3	Theory*	47.916	46.026	40.396	30.971	17.696	.500
	NASTRAN	47.755	45.890	40.280	30.887	17.652	.500
$t = \infty$	Theory	50.500	48.500	42.500	32.500	18.500	.500

* n = 0 term only.

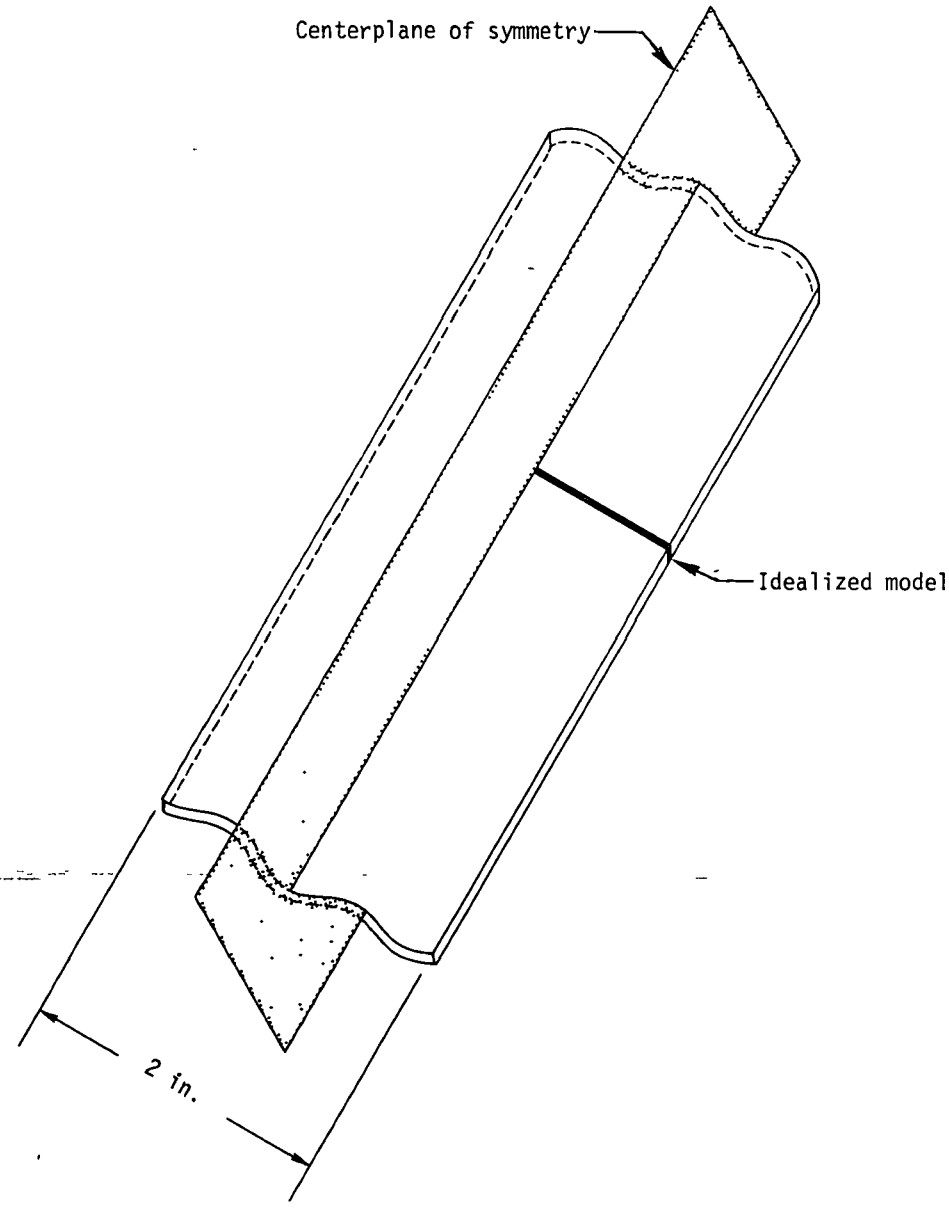

Figure 1. Long thin plate.

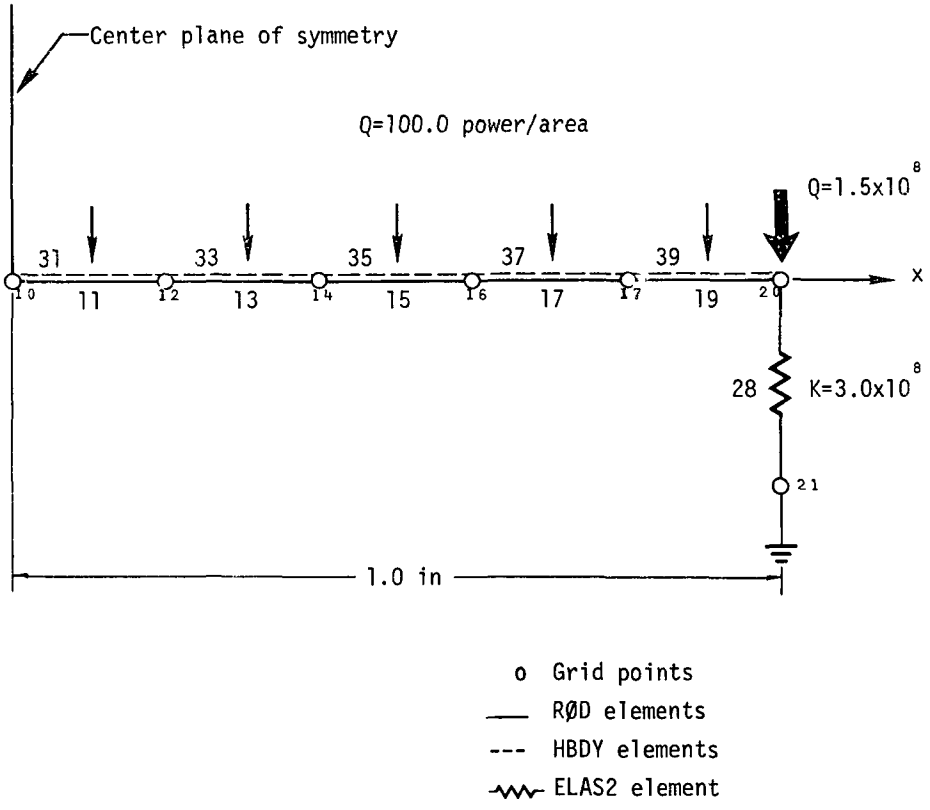

Figure 2. Idealized NASTRAN model.

RIGID FORMAT No. 10, Complex Eigenvalue Analysis - Modal Formulation

Rocket Guidance and Control Problem (10-1-1)

A. Description

This problem, although a simplified model, contains all of the elements used in a linear control system analysis. The flexible structure, shown in Figure 1, consists of three sections: two sections are constructed of structural finite elements; the third section is formulated in terms of its modal coordinates. A sensor is located at an arbitrary point on the structure and connected to a structural point with multipoint constraints. The measured attitude and position of the sensor point is used to generate a control voltage for the gimbal angle of the thrust nozzle. The nozzle control is in itself a servomechanism consisting of an amplifier, a motor, and a position and velocity feedback control. The nozzle produces a force on the structure due to its mass and the angle of thrust. The motion of any point on the structure is dependent on the elastic motions, free-body motions, and large angle effects due to free-body rotation.

The guidance and control system is shown in block diagram form in Figure 2. The definitions for the variables and coefficients along with values for the coefficients are given in Table 1. The use of the Transfer Function data card (TF) allows the direct definition of the various relations as shown in Figure 2.

B. Modeling Techniques

1. A section of the structure is defined by its modal coordinates by using a modification of the method given in the NASTRAN Theoretical Manual. The algorithm is given as follows:

   Define ξ_i, i = 1, n - modal deflections scalar points

   u_r - grid point components used as nonredundant supports for modal test. These may or may not be connected to the rest of the structure.

   u_c - grid point components to be connected to the remaining structure (not u_r points)

   x_i, i = 1, n - rigid body component degrees of freedom for the nonzero modes

   The relations between these variables are defined by using multipoint constraints with the following relationships:

a) $$\{u_c\} = [\phi_{c1}]\{\xi_1\} + [D_{cr}]\{u_r\}$$

ϕ_{ci} is the angular deflection of point u_c for mode i. D_{cr} is the deflection of point u_c when the structure is rigid and point u_r is given a unit deflection.

b) $$\{x_i\} = [K_1]^{-1}[H]^T\{u_r\} = [G]\{u_r\}$$

$[K_i]$ is a diagonal matrix. Each term K_1, the modal stiffness, is defined as:

$$K_1 = m_i\omega_1^2 \qquad (\omega_1 \neq 0)$$

where m_i is the modal mass and ω_1 is the natural frequency in radians per second. [H] is determined by the forces on the support points due to each nonzero eigenvector

$$P_r = -\sum_1 H_{r1}\ \xi_1 \qquad (\omega_1 \neq 0)$$

c) Scalar masses and springs are connected to each modal coordinate as shown by Figure 3a.

d) The structure to be added in this problem consists of a simply supported uniform beam as shown in Figure 3b. The support points, u_r, are y_{16} and y_{19}. The additional degree of freedom to be connected is $u_c = \theta_{16}$. Four modes are used in the test problem. The following data is used to define and connect the modal coordinates of this substructure.

The mode shapes are:

$$\phi_n(x) = \sin\frac{n\pi x}{\ell}$$

The modal frequencies, masses, and stiffness in terms of normal beam terminology are:

$$\omega_n = \frac{n^2\pi^2}{\ell^2}\ \frac{EI}{\rho A} \qquad n = 1, 2, 3, 4$$

$$m_n = \frac{\rho A\ell}{2}$$

$$K_n = \frac{n^4\pi^4 EI}{2\ell^3}$$

The forces of support for each mode are:

$$P_y(16) = \sum - \frac{EI\pi^3}{\ell^3} n^3$$

$$P_y(19) = \sum(-1)^n \frac{EI\pi^3}{\ell^3} n^3$$

The motion θ_{16} is defined by multipoint constraints:

$$\theta_{16} = \frac{1}{\ell}(y_{19} - y_{16}) + \sum_n \frac{n\pi}{\ell} \xi_n$$

The free-body components of the modes are defined, using multipoint constraints, as:

$$\begin{Bmatrix} x_1 \\ x_2 \\ x_3 \\ x_4 \end{Bmatrix} = -\left(\frac{2\ell^3}{\pi^4 EI}\right)\left(\frac{EI\pi^3}{\ell^3}\right) \begin{bmatrix} 1 & 1 \\ \frac{1}{2} & -\frac{1}{2} \\ \frac{1}{3} & \frac{1}{3} \\ \frac{1}{4} & -\frac{1}{4} \end{bmatrix} \begin{Bmatrix} y_{16} \\ y_{19} \end{Bmatrix}$$

2. The mass of the nozzle would normally be included with the structural modeling. However, to demonstrate the flexibility of the Transfer Function data, it is modeled as part of the guidance system as shown in Figure 4a.

Defining the angle of thrust, γ, to be measured relative to the deformed structure, the forces which result are:

$$T = (I_{no} + x_n^2 m_1)(\ddot{\gamma} + \ddot{\theta}_1) - m_n x_n \ddot{y}_1$$

$$F_y = m_n y_1 - x_n m_n (\ddot{\gamma} + \ddot{\theta}_1) - F_n \gamma$$

Using the thrust force, F_n, as a constant, the transfer functions are:

$$I_n s^2 \gamma - T + I_n s^2 \theta_1 - x_n m_n s^2 y_1 = 0$$

$$m_n s^2 y_1 - (x_n m_n s^2 + F_n)\gamma - x_n m_n s^2 \theta_1 = 0$$

$$(0)\theta_1 + T = 0$$

where: $$I_n = I_{no} + x_n^2 m_n = 500$$

3. The large angle motion must be included in the analysis since it contributes to the linear terms. The equations of motion of the structure are formed relative to a coordinate system parallel to the body. As shown in Figure 4b, the accelerations are coupled when the body rotates.

Since the axial acceleration, $\ddot{x}$, is constant throughout the body, the vertical acceleration at any point, to the first order, is:

$$\ddot{y}_{abs} = \ddot{y}_{rel} + \ddot{x}\theta_1 = \ddot{y}_{rel} + \ddot{y}_\theta$$

An extra degree of freedom y_θ is added to the problem and coupled by the equations:

$$m\ddot{y}_\theta = F_n \theta_1$$

$$y_{abs} = y_{rel} + y_\theta$$

4. The center of gravity (point 101) and the sensor location (point 100) are rigidly connected to the nearest structural point with multipoint constraints. For instance the sensor point is located a distance of 4.91 from point 8 as shown in Figure 4c.

It is desired to leave point 101 as an independent variable point. Therefore point 8 is defined in terms of point 101 by the equations:

$$y_8 = y_{101} + 4.91\theta_{101}$$

$$\theta_8 = \theta_{101}$$

C. Answers

A comparison of the NASTRAN complex roots and those derived by a conventional analysis described below are given in Table 2. The resulting eigenvectors were substituted into the equations of motion to check their validity. The equations of motion for a polynomial solution may be written in terms of the rigid body motions of the center of gravity plus the modal displacements. The equations of motion using Laplace transforms are:

$$ms^2 y_{cg} = F_n(\theta_1 + \gamma)$$

$$Is^2 \theta_{cg} = -F_n x_1 \gamma$$

The inertia forces of the nozzle on the structure may be ignored.

The motion of the nozzle, as explained in section B-2, is:

$$\left(\frac{s^2}{\beta} + \tau s + 1\right)\gamma \cong (a + bs)y_s + (c + ds)\theta_s - \frac{s^2}{\beta}\theta_1 + \frac{s^2 m_n x_n}{\beta I_n} y_1$$

(γ is defined as the relative angle between the nozzle and the structure.)

The flexible motions at the sensor point, y_s and θ_s, may be defined in terms of the modal coefficients and the rigid motions of the center of gravity.

$$y_s = y_{cg} + x_2 \theta_{cg} + \sum_i \phi_{100,i} \xi_i$$

$$\theta_s = \theta_{cg} + \sum_i \phi'_{100,i} \xi_i$$

The motions of the nozzle point, in terms of the modal and center of gravity motions are:

$$\theta_1 = \theta_{cg} + \sum_i \phi'_{1,i} \xi_i$$

$$y_1 = y_{cg} - x_1 \theta_{cg} + \sum_i \phi_{1,i} \xi_i$$

The modal displacements are due primarily to the vertical component of the nozzle force. Their equation of motion is:

$$m_i(s^2 + \omega_i^2)\xi_i = F_n \gamma$$

where

$\phi_{j,i}$ is the deflection of point j for mode i

$\phi'_{j,i}$ is the rotation of point j for mode i

m_i is the modal mass of mode i

ω_i is the natural frequency of mode i

ξ_i is the modal displacement of mode i

Using two flexible modes the characteristic matrix of the problem is given in Figure 5. The determinant of the matrix forms a polynomial of order 10. The roots of this polynomial were

.ed by a standard computer library routine and are presented in Table 2 as the analytical
lts. The rigid body solution is also presented.

The differences between the two sets of answers is due to the differences in models. The TRAN model produces errors due to the finite difference approximation and the number of modes sen to model the third stage. The polynomial solution produces errors due to the approxima-ns used in the equations of motion as applied to control system problems.

As a further check the first eigenvalue (λ = -1.41) was substituted into the matrix given in Figure 5 and the matrix was normalized by dividing each row by its diagonal value. The NASTRAN eigenvector was multiplied by the matrix, resulting in an error vector which theoretically should be zero. Dividing each term in the error vector by its corresponding term in the eigenvector resulted in very small error ratios.

Table 1. Variables and Parameters

Extra Point Number	Symbol	Description
1010	e_y	Voltage describing y
1011	e_θ	Voltage describing θ
1020	E_{yc}	Control voltage for y (Input)
1021	$E_{\theta c}$	Control voltage for θ (Input)
1030	E_γ	Attitude error function
1040	ε_γ	Nozzle position error
1050	E_m	Voltage for Nozzle servo
1060	T	Torque for Nozzle servo
1070	γ	Nozzle Thrust angle relative to structure
1080	y_θ	Position increment due to attitude

Parameters	Value	Description
K_s	1.0	Servo amplifier gain
K_m	500	Servo gain
τ	.1414	Nozzle angular velocity feedback
x_n	3.0	Distance from nozzle C.G. to Gimbal axis
I_n	500.0	Inertia of Nozzle about gimbal axis
F_n	4.25×10^6	Thrust of Nozzle
m_n	50	Nozzle mass
β_θ	100.0	Overall voltage-to-angle ratio
β_y	1.0	Overall voltage to position ratio
a	.16	Position feedback coefficient
b	.28	Velocity feedback coefficient
c	15.0	Angle feedback coefficient
d	7.0	Angular velocity feedback coefficient
m	8.5×10^4	Mass of structure

Table 2. Comparison of Complex Roots for NASTRAN Modeling vs. Simplified Polynomial Expansion

Rigid Body Model		2 Flexible Modes Model	
NASTRAN*	POLYNOMIAL	NASTRAN	POLYNOMIAL
- 540 ± .821i	-.522 ± .802i	-.507 ± .819i	-.494 ± .801i
-1.68 ± 0i	-1.74 ± 0i	-1.41 ± 0i	-1.46 ± 0i
+.751 ± 5.96i	+.774 ± 5.98i	+.520 ± 3.82i	+.522 ± 3.83i

*Not published.

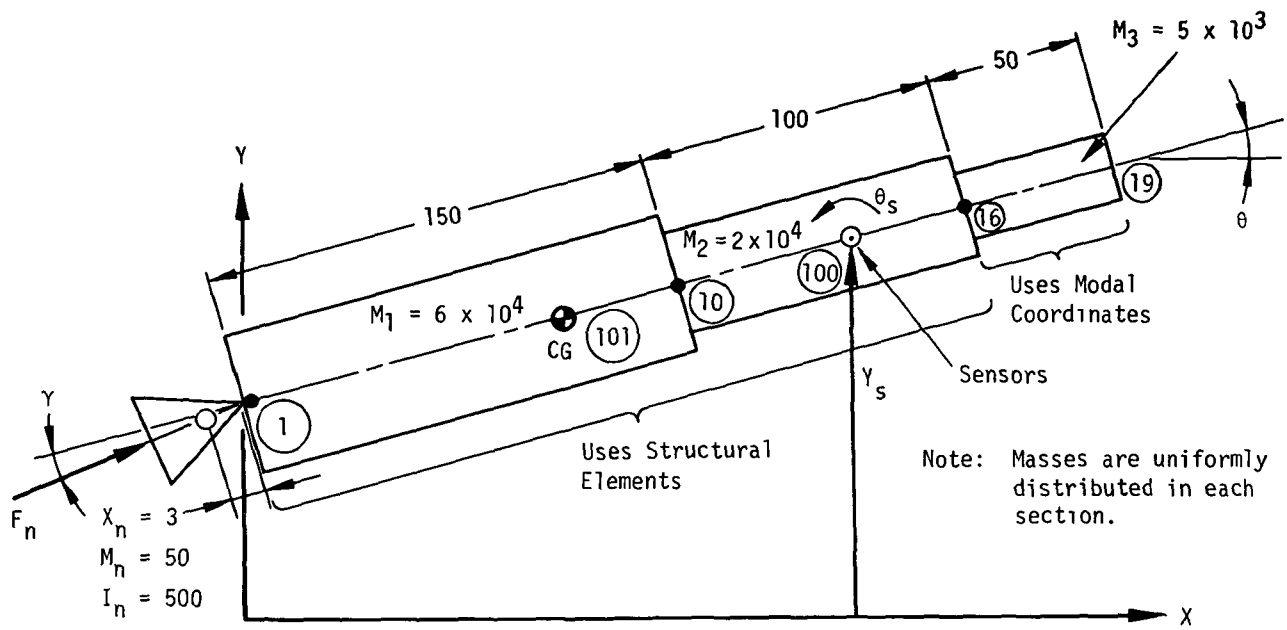

Figure 1. Rocket structural model.

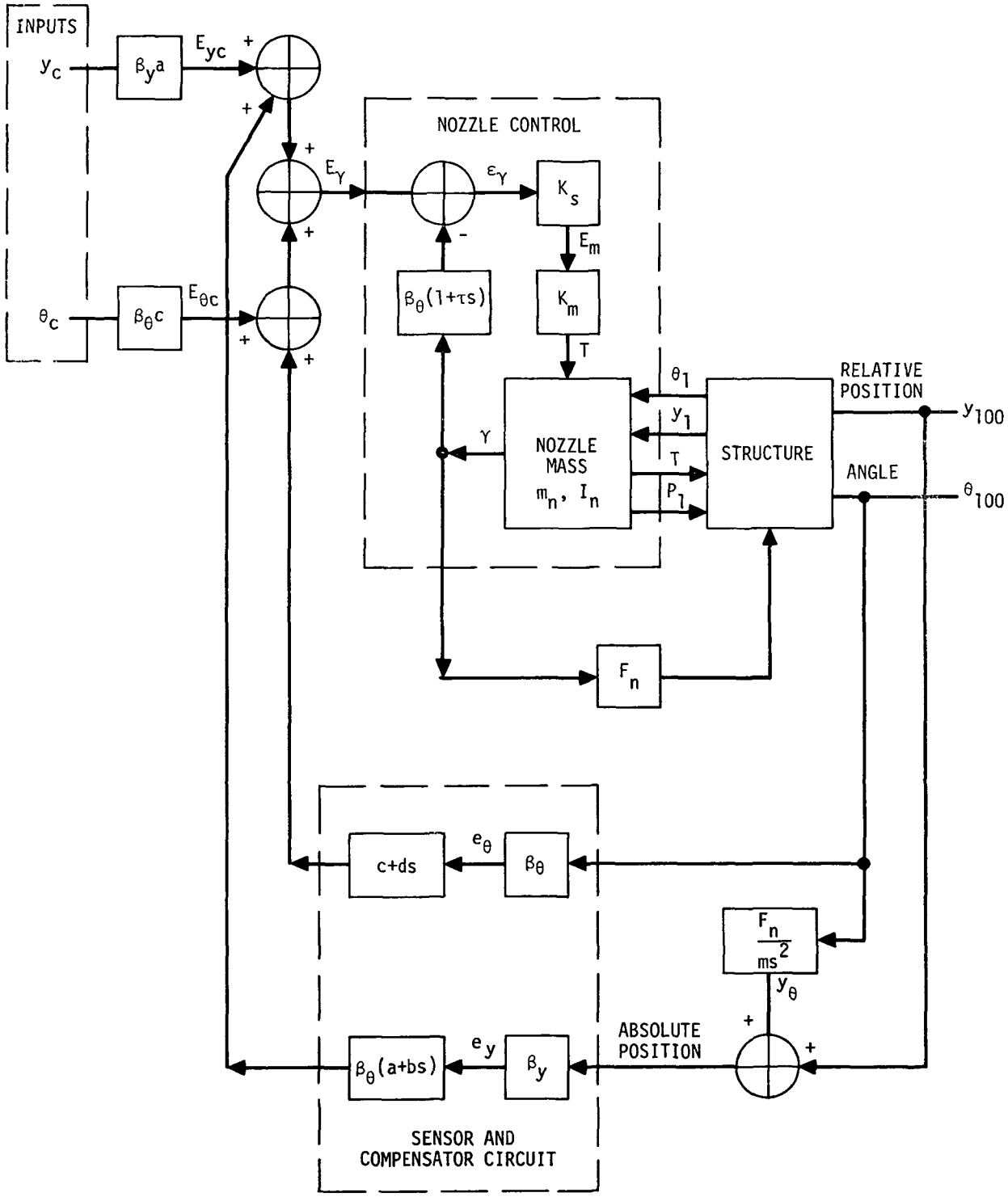

Figure 2. Overall system diagram.

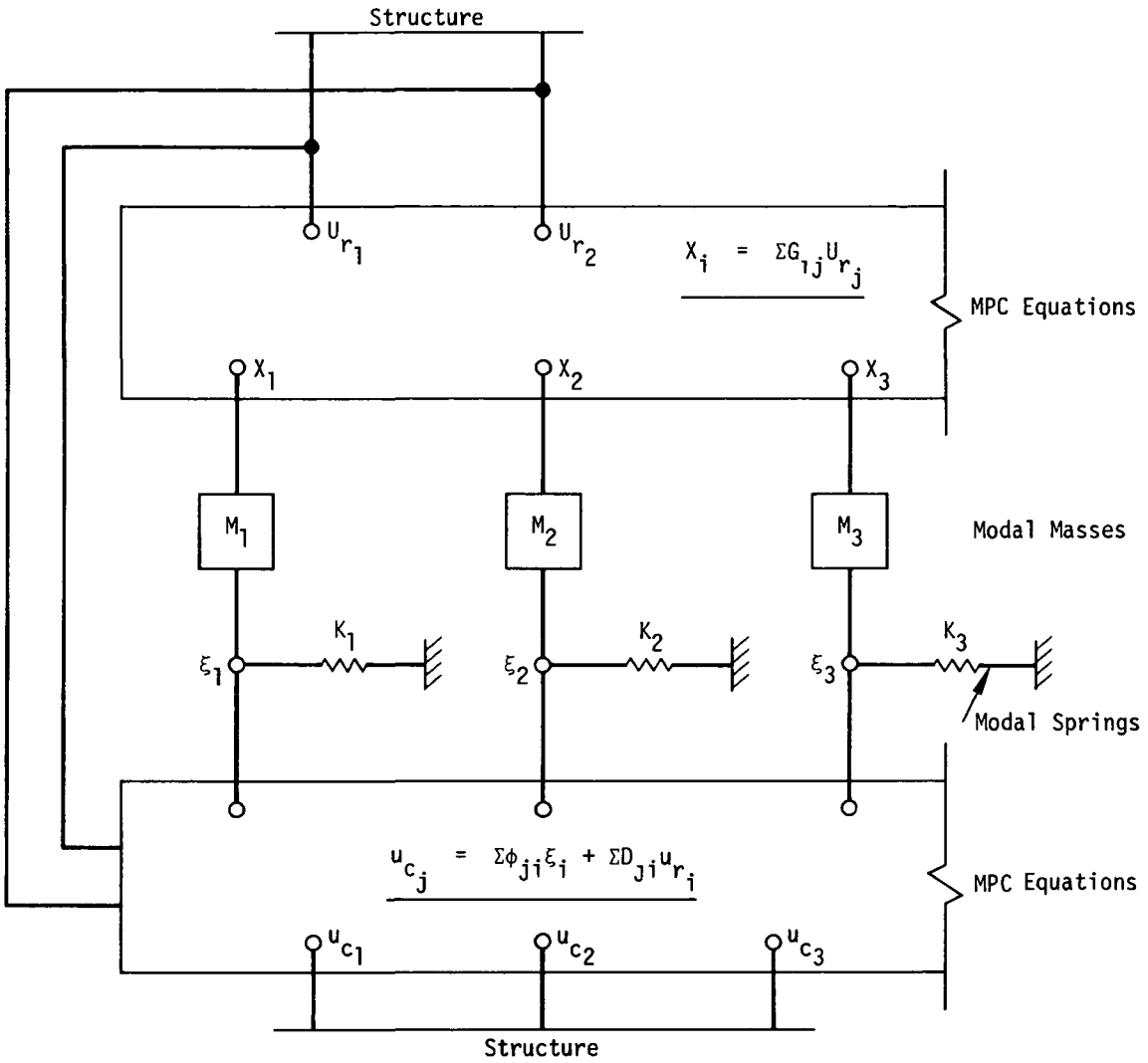

a) Diagram for input of modal data

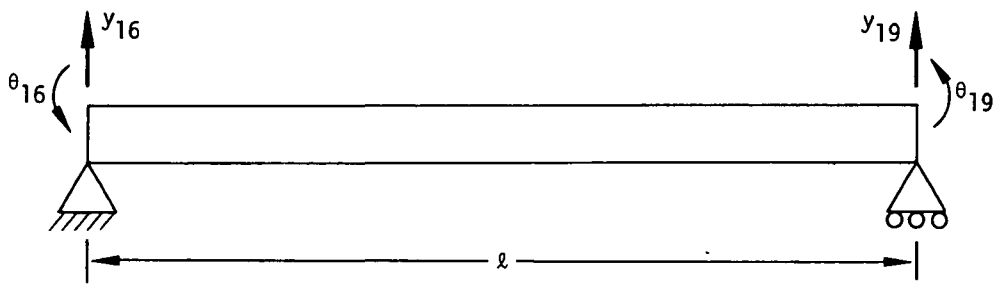

b) Structure used for modal data

Figure 3. Modal data input diagrams.

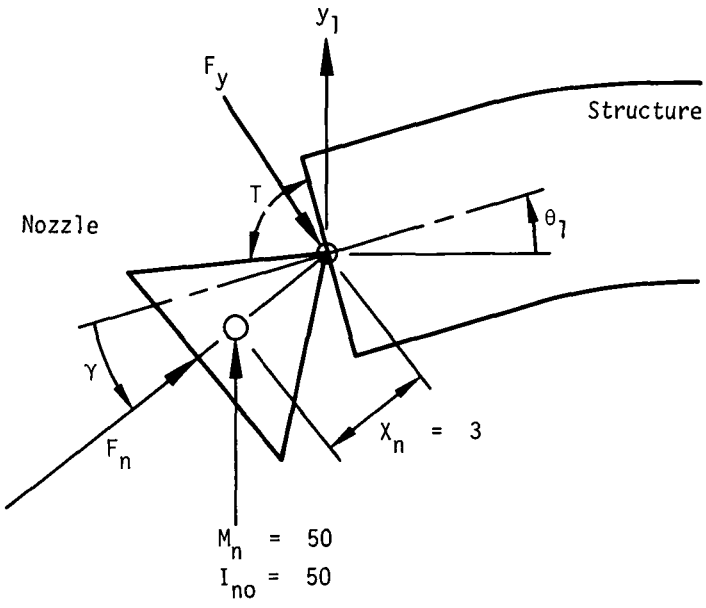

(a) Nozzle displacements and forces

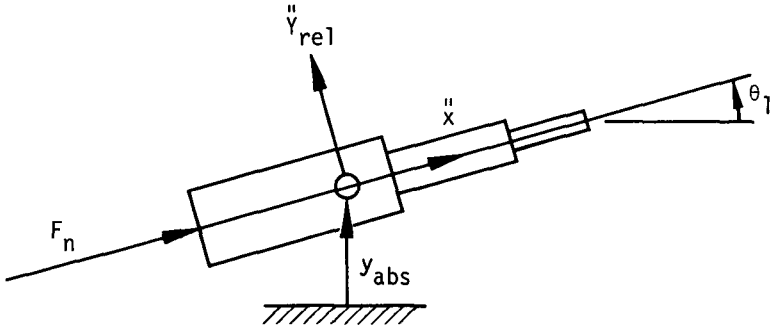

(b) Relative motion due to large angles

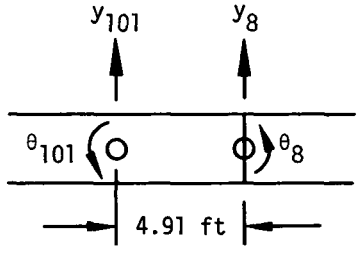

(c) Relationship for multi-point constraints

Figure 4. Modeling diagrams.

y_{cg}	θ_{cg}	γ	ξ_1	ξ_2
s^2	$-\frac{F_n}{m}$	$-\frac{m_n x_n s^2 + F_n}{m}$	$-\frac{F_n \phi'_{1,1}}{m}$	$-\frac{F_n \phi'_{1,2}}{m}$
0	s^2	$\frac{1}{I}(I_n + m_n x_n x_1)s^2 + x_1 \frac{F_n}{I}$	0	0
$-\frac{m_n x_n}{I_n} s^2$ $-(bs + a)\beta$	$1 + \frac{m_n x_n x_1}{I_n} s^2$ $-(d + x_2 b)\beta s$ $-(c + x_2 a)\beta$	$s^2 + \beta\tau s + \beta$	$(\phi'_{1,1} - \frac{m_n x_n}{I_n}\phi_{1,1})s^2$ $-\beta(b\phi_{s,1} + d\phi'_{s,1})s$ $-\beta(a\phi_{s,1} + c\phi'_{s,1})$	$(\phi'_{1,2} - \frac{m_n x_n}{I_n}\phi_{1,2})s^2$ $-\beta(b\phi_{s,2} + d\phi'_{s,2})s$ $-\beta(a\phi_{s,2} + c\phi'_{s,2})$
0	0	$-\phi_{1,1} F_n$	$m_1(s^2 + \omega_1^2)$	0
0	0	$-\phi_{1,2} F_n$	0	$m_2(s^2 + \omega_2^2)$

Figure 5. Matrix of equations of motion, analytic approach.

RIGID FORMAT No. 10 (APP AERØ), Aeroelastic Analysis
Aeroelastic Flutter Analysis of a 15° Swept Wing (10-2-1)

A. Description

This problem illustrates the use of the aeroelastic analysis to determine flutter frequencies and mode shapes for an untapered wing having 15° sweep and an aspect ratio of 5.34 as shown in Figure 1.

B. Input

Bulk data cards used include CAERØ1, PAERØ1, SPLINE2, SET1, AERØ, MKAERØ1, FLUTTER, and FLFACT as illustrated in User's Manual Section 1.11.

C. Theory

Reference 22 specifies the reduced frequency k = .1314 (p.17), frequency ratio ω/ω_α = 0.51 (p.35) and torsion frequency ω_α = 1488 (p.17).

The flutter velocity is found from

$$V = \frac{b\omega}{k} = \frac{\frac{REFC}{2} \times \omega_\alpha \times \frac{\omega}{\omega_\alpha}}{k} = 5980 \text{ in/sec},$$

where REFC is the reference length input on the AERØ bulk data card.

The flutter frequency is found from

$$f = \frac{\omega_\alpha \times \frac{\omega}{\omega_\alpha}}{2\pi} = 121 \text{ Hz}$$

D. Results

The results obtained are compared with both theoretical results using the modified strip analysis method and with experimental results. The flutter velocity is in good agreement. (See Figure 2.)

Frequencies are automatically output while mode shapes used in the modal formulation are obtained using an ALTER to the Rigid Format following the Real Eigenvalue Analysis Module.

Mode shapes for all points in the model may be obtained by checkpointing the problem using the Normal Mode Analysis (Rigid Format 3) and subsequently restarting using the Aeroelastic Analysis.

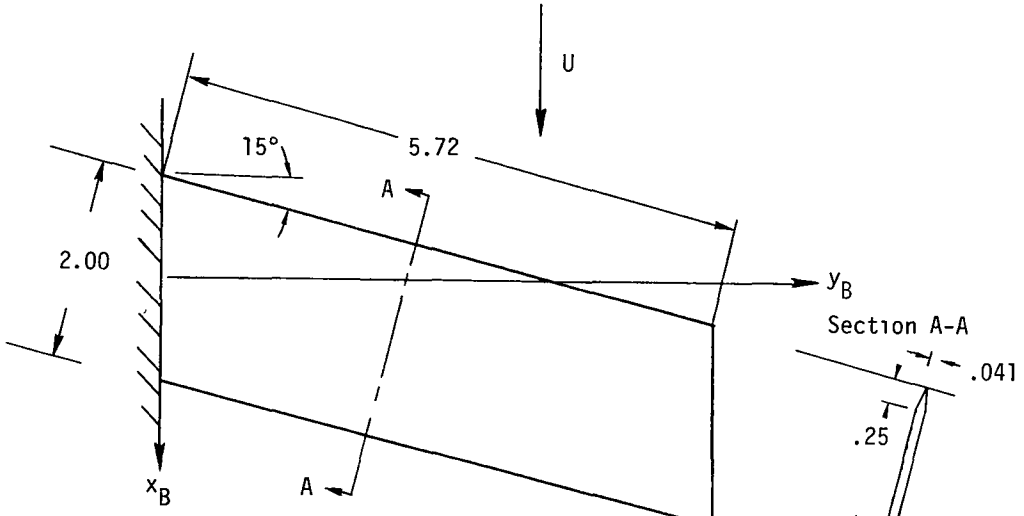

a. Planform.

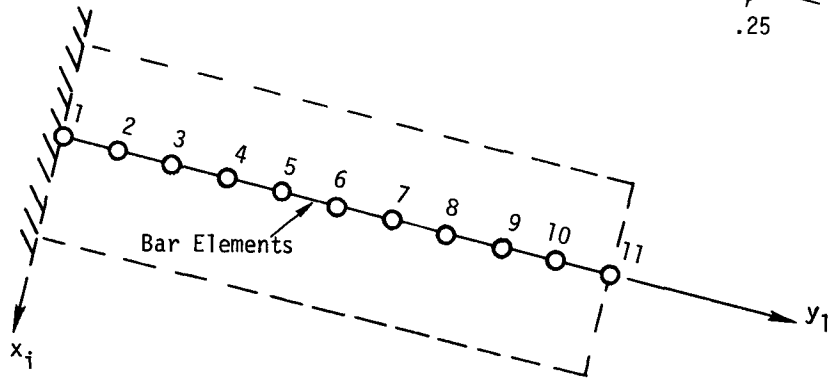

b. Structural model.

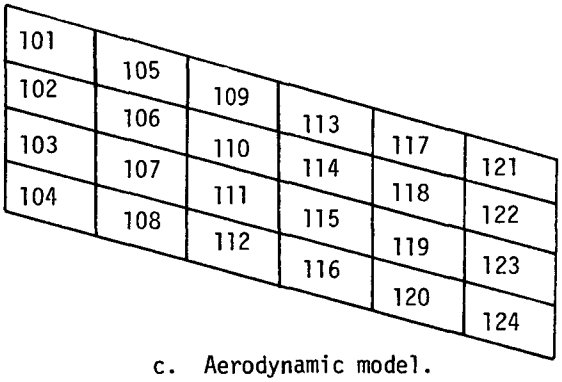

c. Aerodynamic model.

Figure 1. Fifteen degree sweep model.

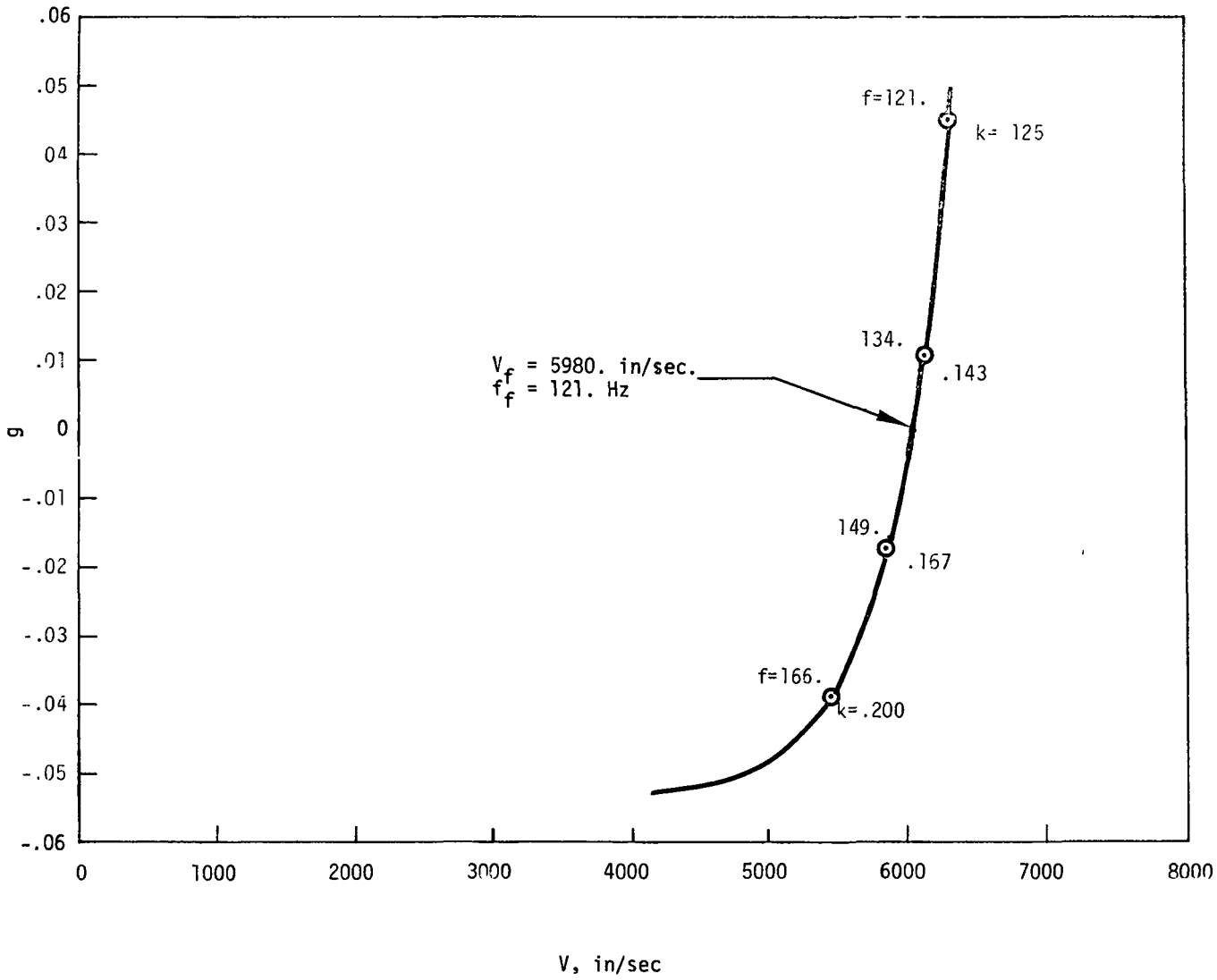

Figure 2. V-g results for fifteen degree sweep model.

RIGID FORMAT No. 11, Frequency Response - Modal Analysis

Frequency Response and Random Analysis of a Ten-Cell Beam (11-1-1)

A. Description

This problem demonstrates the frequency response solution of a structure using uncoupled modal formulation. With modal formulation, the structural degrees of freedom used in the solution are the uncoupled modal displacements. The solution equations are simple and efficient. The saving in time, however, is offset by the operations necessary to extract the modes, transform the loads to modal coordinates, and transform the modal displacements to structural displacements.

This problem also illustrates the various methods of applying frequency response loads. Loads may be input as complex numbers, with phase lag angles and/or time lag factors. The loads may be added together for each subcase.

The structure to be solved consists of a beam with simple supports on the end as described in Figure 1. The parameters selected produce natural frequencies of 50, 200, 450 and 800 cps. The applied loads for the three subcases are applied to the center with variations in phase angles, time lags and input formats. The first two subcases use three loaded points which, in essence, simulate a load on the center.

Included in the structural representation is a "general element" representing the first two cells of the ten-cell beam. The flexibility matrix, [Z], of the element represents the displacements of grid points 2 and 3 when point 1 is fixed. The rigid body matrix, [S], represents the rigid body motions of points 2 and 3 when point 1 is displaced in the x, z, or θ_y directions.

The random analysis data consists of a flat power spectral density function ("white noise") for the three loading subcases. The first subcase spectral density is connected to the third subcase spectral density, simulating two interdependent probability functions. The XY-plotter is used to plot the displacement and acceleration power spectral density function of grid 6 (center of the beam). The displacement autocorrelation function is also plotted for the same point. All values are tabulated in the printout. The NASTRAN power spectural density results are compared against a simplified analytic calculation in Figure 2.

A static analysis restart of the frequency response problem is demonstrated. Gravity and element enforced deformation loads are used with a change in the single-point constraints.

B. Input

1. Parameters:

$\ell = 20$ - length

$I_1 = .083$ - bending inertia

$A = 21.18922$ - cross sectional area

$E = 10.4 \times 10^6$ - modulus of elasticity

$\rho = .2523 \times 10^{-3}$ - mass density

$M = \rho A \ell$ - total mass

2. Constraints:

$u_y = \theta_x = \theta_z = 0$ - all points

$u_{x1} = u_{z1} = u_{z11} = 0$ - frequency response

$u_{x1} = u_{z1} = u_{x11} = u_{z11} = 0$ - static analysis

3. Modal Data:

Interval: $40 < f < 1000$ cps

Normalization: Modal Mass = 1.0

Number of modes used in formulation: 4

Modal Damping ratio: $g = 4 \times 10^{-4} f$

4. Loads, Frequency Response:

The loading functions for subcase 1 are:

$$P_{z,5} = 50$$

$$M_{y,5} = -100$$

$$P_{z,6} = 50 + \underbrace{100(\cos 60° + i \sin 60°)}_{\text{SET 6}}$$

$$P_{z,7} = 50$$

$$M_{y,7} = 100$$

The loading for subcase 2 is:

$$P_{z,5} = 50$$

$$M_{y,5} = -100$$

$$P_{z,6} = 50 + \underbrace{100(\cos 2f° - i \sin 2f°)}_{\text{SET 7, } \tau = .005555}$$

$$P_{z,7} = 50$$

$$M_{y,7} = 100$$

The load for subcase 3 is:

$$P_{z,6} = 2[75 + 50i(\cos 30° - i \sin 30°)] = 200 + 86.6i$$

Note: At f = 30cps the three subcases are nearly identical.

5. Random Analysis Data

The nonzero factors for the three subcases are:

$$\left.\begin{aligned} S_{11} &= 50 \\ S_{13} &= S_{31} = 50 \\ S_{22} &= 100 \\ S_{33} &= 50 \end{aligned}\right\} \quad 0 < f < 100$$

$$S_{ij} = 0 , \quad f > 100$$

The time lags selected for the autocorrelation function calculations are:

$$\tau = 0.0, 0.001, 0.002, \ldots\ldots, 0.1$$

6. Static Loads for Restart

The problem is run first as a frequency response analysis. It is restarted as a static analysis with the following loads:

Gravity vector: $g_z = 32.2$

Element Deformation: $\delta_{10} = 0.089045$ (expansion)

C. Analysis

1. The theoretical eigenvalue data, according to Reference 8 is:

$$f_n = \frac{n^2\pi^2}{(2\pi)\ell^2}\sqrt{\frac{EI}{A}} = 50, 200, 450, 800 \ldots \quad \text{(natural frequencies)}$$

$$m_n = 1.0 \quad \text{(modal mass)}$$

$$\phi_n(x) = \left[\int_0^{\ell} \rho A \sin^2 \frac{n\pi x}{\ell}\, dx\right]^{-\frac{1}{2}} \sin\left(\frac{n\pi x}{\ell}\right) = \sqrt{\frac{2}{M}}\, \sin\left(\frac{n\pi x}{\ell}\right) \quad \text{(mode shape)}$$

2. The theoretical frequency response at the center point is essentially the response of the first mode which is:

$$u_6(\omega) = \frac{\sum_j \phi_{1,6}\, P_j(\omega)\, \phi_{1,j}}{m_1(\omega_1^2 - \omega^2 + ig\omega\omega_1)} \qquad (j = \text{degree of freedom number})$$

At the first natural frequency of 50 cps, the response will be nearly equal to the response of the first mode. The response at the center point for the three subcases are:

Subcase 1 and 3

$$u_6^1 = u_6^3 = \frac{94.764 + 41.033i}{(50\text{-}f^2) + if}$$

The results are:

f	u_6 (one mode)	u_6 (NASTRAN)
0	.0413 @ 23.42°	.0429 @ 22.9°
30	.0646 @ 22.34°	.0668 @ 21.8°
50	2.066 @ 293.42°	2.074 @ 281.5°

Subcase 2

$$u_6^2 = \frac{23.691(3 + 2\cos 2f - 2i \sin 2f)}{(50 - f^2) + if}$$

Theoretical and NASTRAN results are:

f	u_6 (one mode)	u_6 (NASTRAN)
0	.047 @ 0°	.049 @ 0°
30	.0646 @ -22.34°	.0668 @ -23.97°
50	1.565 @ 233.4°	1.577 @ 223.0°

3. The random analysis is explained in Reference 15. The power spectral response coefficients for the three subcases are given by the matrix:

$$[S_\ell] = 100\begin{bmatrix} 0.5 & 0 & 0.5 \\ 0 & 1.0 & 0 \\ 0.5 & 0 & 0.5 \end{bmatrix}$$

If $\{H_j\}$ is the vector of the responses of a point, j, to the three loading cases, the power spectral response, S_j, is:

$$S_j = \{\bar{H}_j\}^T[S]\{H_j\} \qquad (\bar{H}_j \text{ is the complex conjugate})$$

or

$$S_j = 100[0.5|H_{1j}|^2 + 0.5(\bar{H}_{1j} H_{3j} + \bar{H}_{3j} H_{1j}) + |H_{2j}|^2 + 0.5|H_{3j}|^2]$$

Since $H_{1j} = H_{3j}$, then:

$$S_j = 200|H_{1j}|^2 + 100|H_{2j}|^2$$

The mean square response in obtained by integrating the power spectral density over the frequency. In this particular case the frequency increments are uniform and the mean square response is simply

$$E_1 = \sum_i \pi[S_j(f_{i+1}) - S_j(f_1)]\Delta f$$

The analytic solution for the displacement spectral density response of the center point due to the first mode is:

$$S_J(f) = \frac{200(1.066\times10^4) + 100(.5613\times10^3)(13 + 12\cos 2f)}{[(50^2 - f^2)^2 + f^2]} = \frac{2.862\times10^6 + .6735\times10^6\cos 2f}{(f^4 - 4999f^2 + 50^4)}$$

The results of the above equation are compared with the NASTRAN results in Figure 2. The mean deviation, σ_J, is:

$$\sigma_j = \sqrt{\frac{E_i}{2\pi(f_n - f_o)}}$$

where f_n and f_o are the upper and lower frequency limits. σ_j was checked by summing the NASTRAN results.

4. The results of the static analysis restart are:

   a) The gravity load produces normal displacements (in the z direction) and element moments as follows:

$$u_z(x) = \frac{\rho A g x}{24EI}(\ell^3 - 2\ell x^2 + x^3)$$

$$M_1(x) = \frac{\rho A g}{2}(x^2 - \ell x)$$

   b) The element deformation produces the following axial forces and displacements:

$$F_x = AE\frac{\delta 10}{\ell}$$

$$u_x = -\frac{F_x}{AE}x \qquad (x < 18)$$

In numerical terms the displacements of the center point ($x = \frac{\ell}{2}$) are:

	Theoretical	NASTRAN
u_{x6}	4.452×10^{-2}	4.435×10^{-2}
u_{z6}	4.155×10^{-4}	4.121×10^{-4}

The element forces at the center of the beam are:

	Theoretical	NASTRAN
F_{x5}	$= -.9811 \times 10^6$	$-.9848 \times 10^6$
M_6	$= -8.607$	-8.607

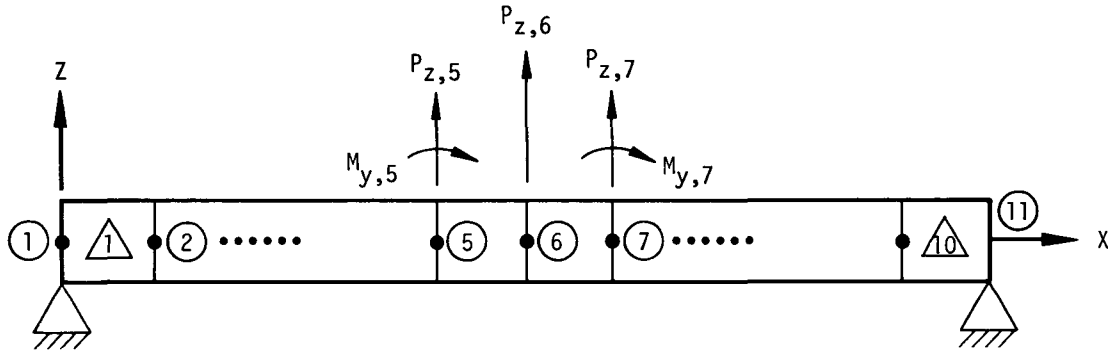

Figure 1. 10 cell beam.

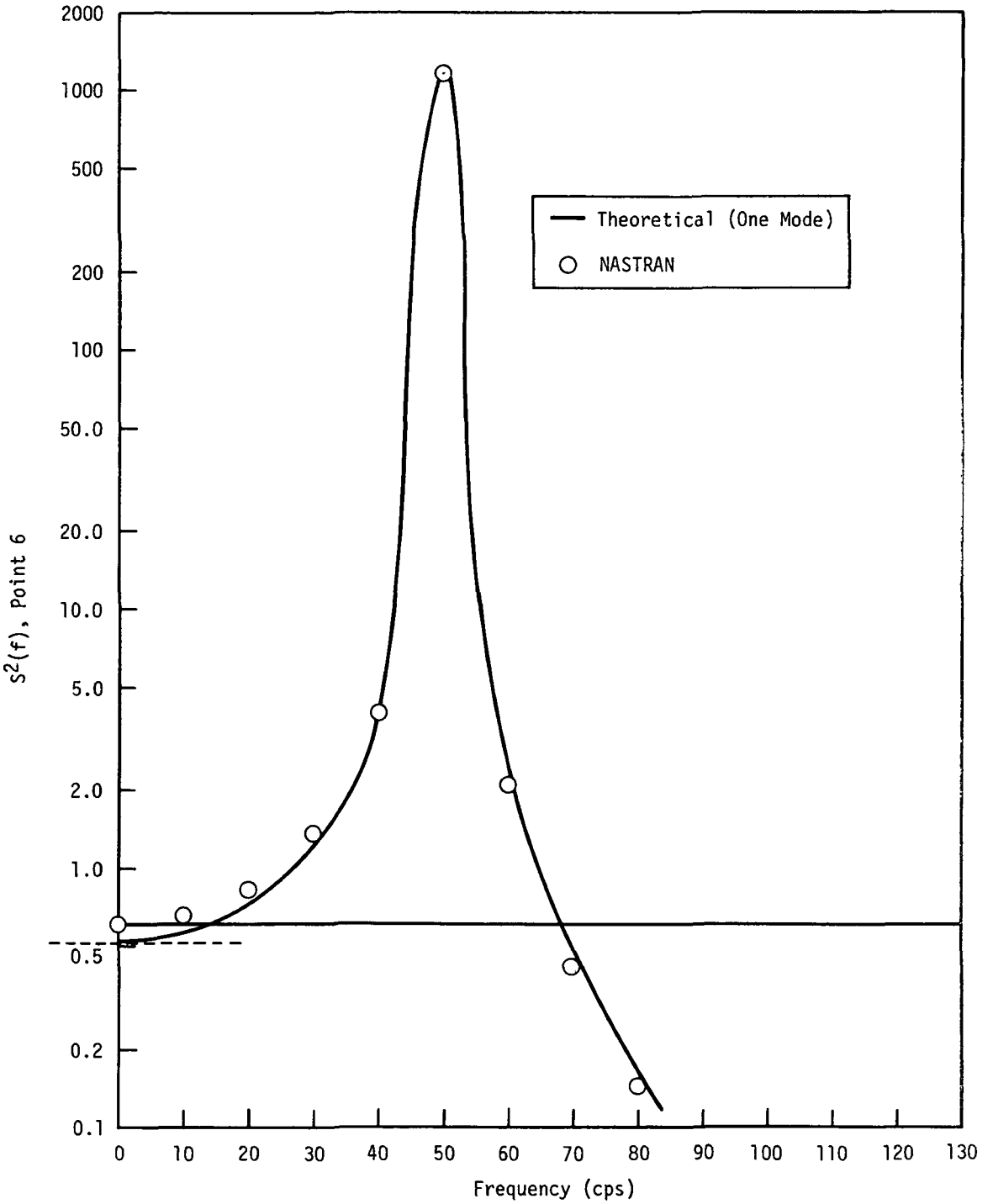

Figure 2. Power spectral density of center point displacement.

RIGID FORMAT No. 11, Frequency Response Analysis - Modal Formulation

Frequency Response of a 500-Cell String (11-2-1)
Frequency Response of a 500-Cell String (INPUT, 11-2-2)

A. Description

This problem illustrates the solution of a large frequency response problem using modal coordinates. When large numbers of frequency steps are used, or the problem is very large, the relative efficiency of the modal formulation is more attractive than the direct formulation. The structural model consists of scalar points, springs, and masses which simulate the transverse motions of a string under tension, T, with a mass per length of μ. The model and its finite element representation is shown in Figure 1. A duplicate model is obtained via the INPUT module to generate the scalar springs and masses.

Selected scalar point displacements and scalar element forces are plotted versus frequency. The magnitude and phase of the displacements are plotted separately, each on one-half of the plotter frame. The magnitude plots for the selected points are all drawn on a whole plotter frame for comparisons. The center spring element has the magnitude of its internal force plotted versus frequency.

B. Input

1. Parameters

m_i = 10 - mass

K_i = 10^7 - spring rate

N = 500 - number of cells

where

$$K_1 = \frac{T}{\Delta x}, \qquad m_1 = \mu \Delta x$$

2. Loads

The load on each point is:

$$P_i(\omega) = \Delta x p_x = 10\pi^3$$

where p_x is the load per length of string.

The steady state frequency response is desired from .1 to 10 cycles per second in 15 logrithmic increments.

3. Real Eigenvalue Data

Method: Inverse Power

Region of interest: $0 < f < 21$

Normalization: Mass

Number of modes used in formulation: 20

C. Answers

The analysis of the string is given in Reference 11, Chapter 6. The response, ξ_n, of mode number n is given by the equation:

$$\xi_n = \frac{\int_0^{\ell} P(x) \sin\left(\frac{n\pi x}{\ell}\right) dx}{\left[\int_0^{\ell} \mu \sin^2\left(\frac{n\pi x}{\ell}\right) dx\right] [\omega_n^2 - \omega^2]}$$

where ω_n, the natural frequencies, are $\frac{n\pi}{N}\sqrt{\frac{K_1}{m_1}}$ for the theoretical continuous string.

For a uniform Load:

$$\int_0^{\ell} P(x) \sin\left(\frac{n\pi x}{\ell}\right) dx = \frac{2p_x\ell}{n\pi} = \frac{2P_iN}{n\pi} = \frac{10^4\pi^2}{n}$$

$$\int_0^{\ell} \mu \sin^2\left(\frac{n\pi x}{\ell}\right) dx = \frac{\mu\ell}{2} = \frac{Nm_i}{2} = 2.5 \times 10^3$$

The displacement of the center point is:

$$u\left(\frac{\ell}{2}\right) = \sum \xi_n \sin\frac{n\pi}{2} = \xi_1 - \xi_3 + \xi_5 - \xi_7 + \ldots$$

For instance at f = 0.1 the response due to 20 modes is:

$$u\left(\frac{\ell}{2}\right) = .97895 \text{ (Theory)}$$

$$u_{251} = .97888 \text{ (NASTRAN)}$$

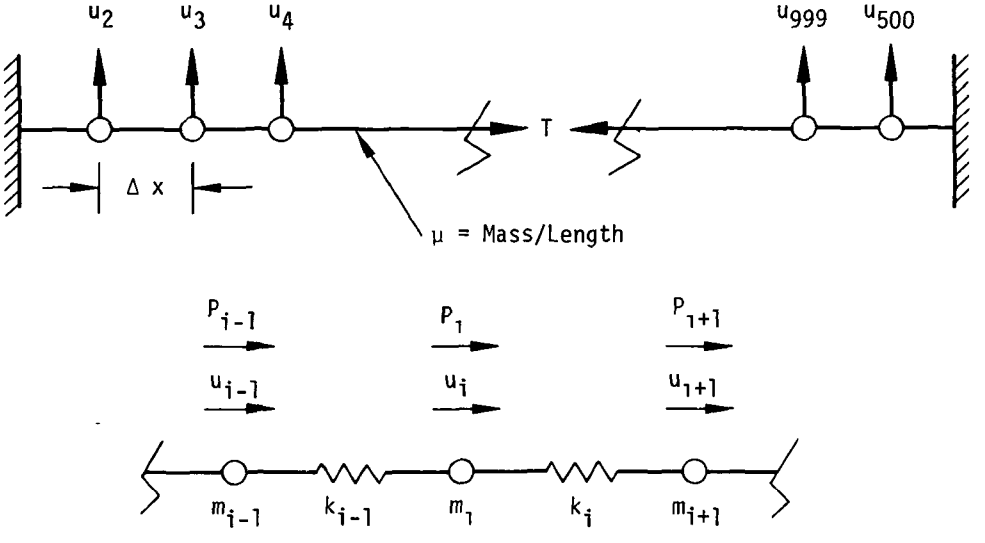

Figure 1. Representations of 500 cell string.

RIGID FORMAT No. 12, Transient Analysis - Modal Formulation

Transient Analysis of a Free One Hundred Cell Beam (12-1-1)

A. Description

The problem demonstrates the transient analysis of a free-body using the integration algorithm for uncoupled modal formulations. The model is a hundred-cell beam with a very large mass attached to one end as shown in Figure 1. Modal damping is included as a function of natural frequency. It does not affect the free-body (zero frequency) modes. The omitted coordinate feature was used to reduce the analysis set of displacements to correspond to eleven grid points.

Both structure plots and curve plots are requested. The types are as follows:

1. Stereoscopic structure plots of the deformed structure are drawn for a specified time step.
2. Orthographic projections of the deformed structure are plotted. However, two variations are plotted on each frame. The bottom region of the frame shows the deformed shape and the top region shows vectors at every tenth grid point which are proportional to the z-displacement at each specified time step.
3. Curve plots and printout of displacement versus time and of acceleration versus time are requested.

When a structure is used without additional transfer functions or direct matrix inputs, the transient analysis solves exact equations for the uncoupled modes. The only errors will be in the discarded modes and the straight line approximation of the loads between time steps. The speed of this solution is offset by the fact that the eigenvalue calculation is relatively costly and the transformation of the vectors to and from modal coordinates could be time consuming.

The mass and inertia on point (1) were selected to be much larger than values of the beam. The answers will therefore approximate a beam with a fixed end.

B. Input

1. Parameters

Beam:

$\ell = 20$ (Length)

$I = .083$ (Bending inertia)

$A = 1.0$ (Cross sectional area)

$E = 10.4 \times 10^{6}$ (Modulus of elasticity)

$\rho = .2523 \times 10^{-3}$ (Mass density)

Lumped Mass:

$$m_1 = 10.0, \quad I_{22,1} = 1666.66$$

2. Damping:

The damping coefficient for each mode is a function of the natural frequency. The function is:

$$g = 10^{-3} f$$

3. Load:

$$P_{z,101} = 100 \sin(2\pi \cdot 60t)$$

4. Real Eigenvalue Data

Method: Inverse Power

Region of Interest: $0 < f < 1000$

Normalization: Mass

D. Answers

The NASTRAN results are compared in Figure 2 to the analytic results which use one mode. The modal mass may be calculated using the formula for the mode shape given in Reference 8. The modal displacement is a single degree of freedom response with a closed form solution.

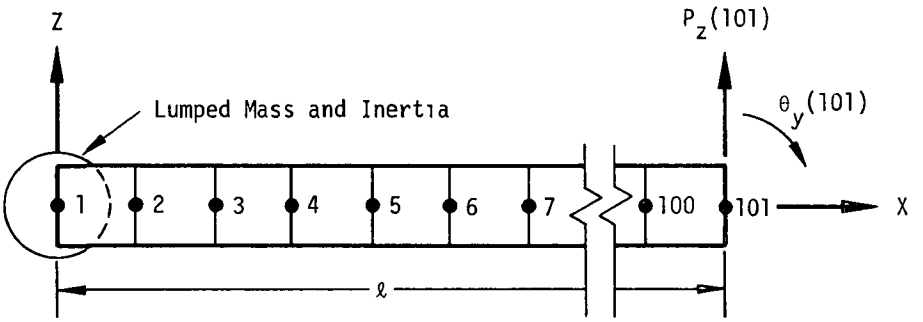

Figure 1. 100 cell free beam.

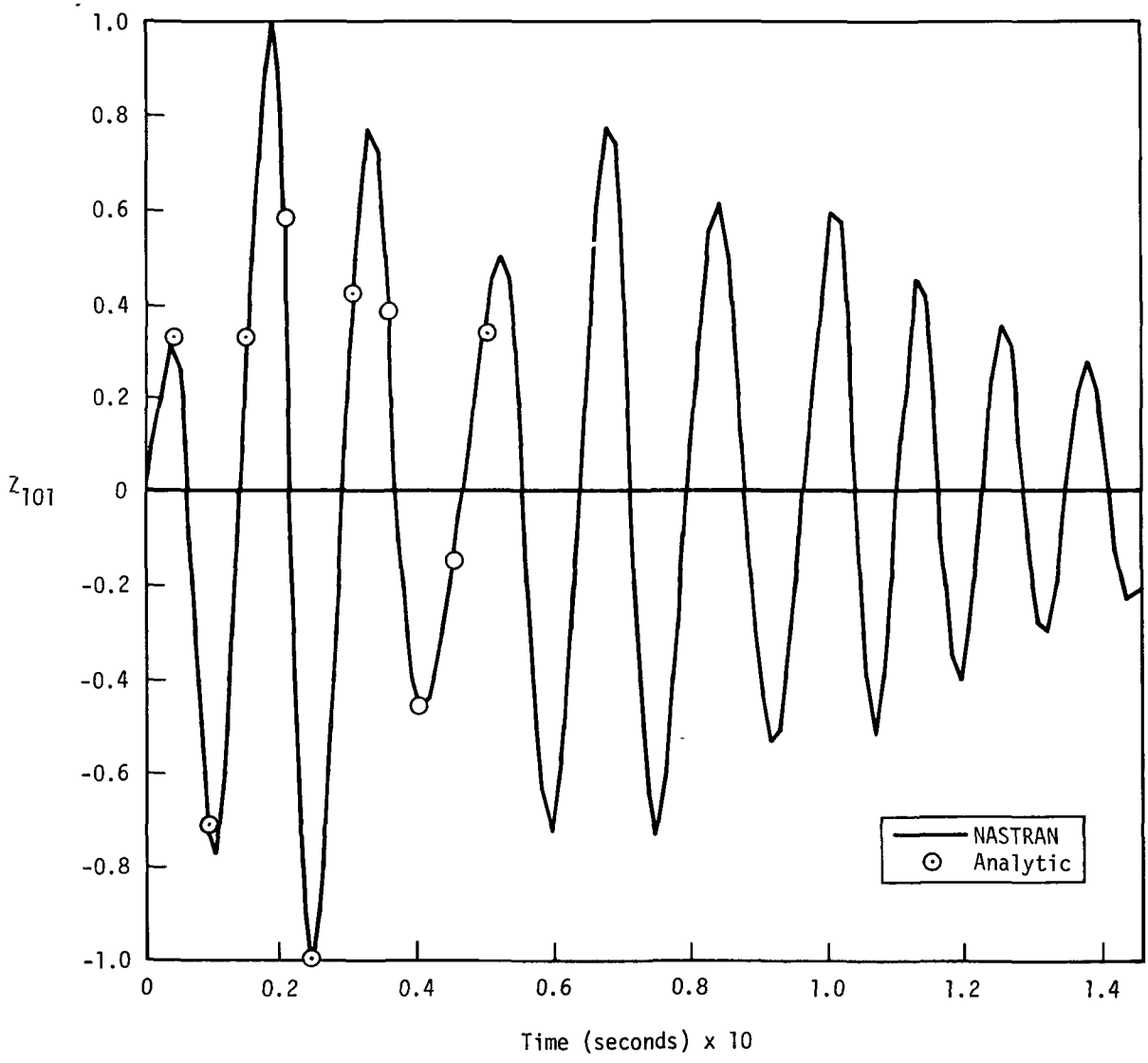

Figure 2. Comparison of NASTRAN and analytic displacements versus time.

RIGID FORMAT No. 13, Normal Modes with Differential Stiffness

Normal Modes of a 100-Cell Beam with Differential Stiffness (13-1-1)

A. Description

This problem illustrates the effects of differential stiffness on the solution for the normal modes of a beam under axial compression.

The natural frequencies of the beam are affected by this load as shown in Reference 23. The loading specified here is one half of the Euler value for compression buckling which decreases the unloaded natural frequency, w, proportional to

$$\left[\frac{\pi^2 EI}{\ell^2} - F\right]^{1/2},$$

where F is the applied load.

The structural model illustrated in Figure 1 is a uniform 100 cell beam hinged at both ends.

B. Input

1. Parameters:

$A = 2.0$		(cross sectional area)
$I = 0.667$		(bending inertia)
$E = 10\ 4 \times 10^6$		(modulus of elasticity)
$\ell = 100.0$		(length)
$\rho = 2.0 \times 10^{-4}$		(mass density)

2. Constraints:

$u_z = \theta_x = 0_y = 0$	(all points)
$u_y = 0$	(point 101)
$u_x = u_y = 0$	(point 1)

3. Loads.

$F_{101,x}$	= 3,423.17	
B	= 1.0	(default load factor)

C. Results

The theoretical natural frequency for the first mode is given by

$$f = \left[\frac{1}{4\rho A\ \ell^2}\ \left(\frac{\pi^2 EI}{\ell^2} - F\right)\right]^{1/2} \text{ Hertz}$$

For this loading of one half the Euler buckling value, the theoretical value is 14.6269 Hertz for the bending mode. The NASTRAN result is 14.62325 Hertz.

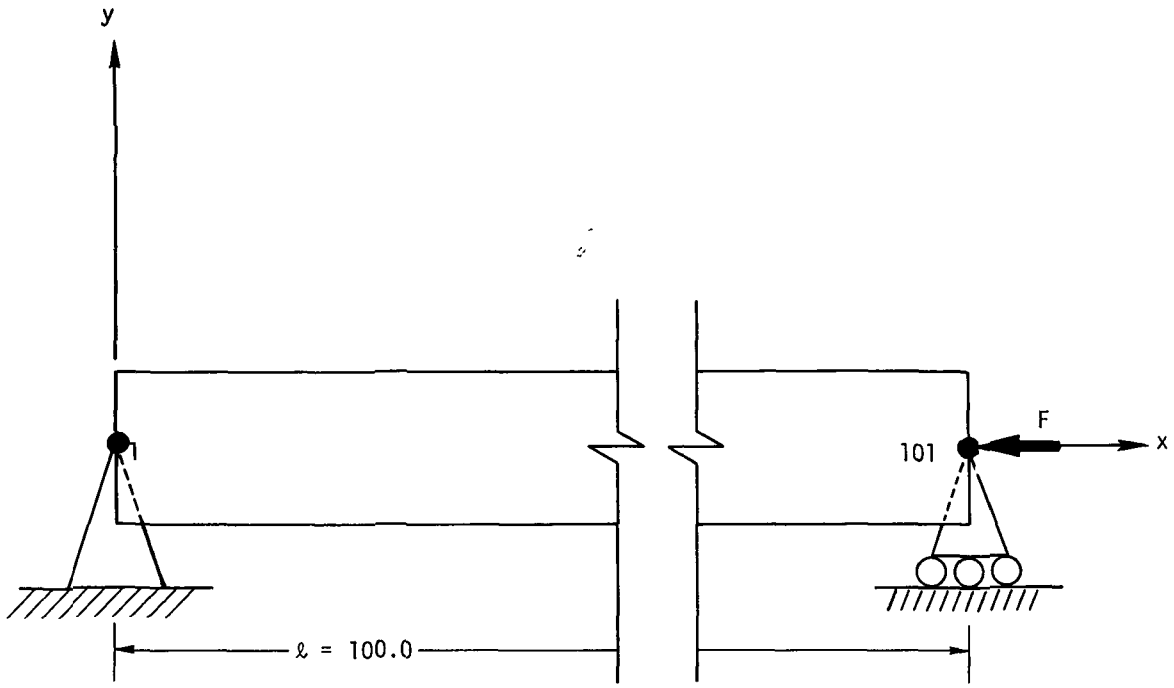

Figure 1. One hundred cell beam.

RIGID FORMAT No. 14, Static Analysis with Cyclic Symmetry
Circular Plate Using Cyclic Symmetry (14-1-1)

A. Description

A constant thickness circular plate with six radial stiffeners and a central hole, shown in Figure 1, is analyzed using dihedral symmetry. The plate is subjected to a uniform pressure load applied over a 60° segment of the plate.

The finite element model is shown in Figure 2. The stringers are 60° apart but only 30° of the structure needs to be modeled when using the dihedral symmetry option. There are 12 subcases since these are 2 half segments in a 60° segment and only one loading condition. The CYJØIN bulk data card defines those points in the middle of the segment (SIDE 2) and those points on the boundary between segments (SIDE 1).

B. Input

1. Parameters.

   R_o = 1.0 (outside radius)

   R_1 = .14 (inside radius)

   t = .01 (plate thickness)

   a = .06 (height and width of stiffeners)

   E = 10.6×10^6 (modulus of elasticity)

   ν = .325 (Poisson's ratio)

2. Boundary Conditions:

   $U_r = U_\theta = \theta_z = 0$ (all points)

   $U_z = \theta_r = 0$ (along r = 1.0)

3. Applied loads:

   Pressure = 200.0 between θ = 60° and 120°

4. Cyclic symmetry parameters:

   CTYPE = DRL

   KMAX = 2

   NSEGS = 6

   NLØAD = 1

C. Results

The structure can be analyzed using rotational symmetry or dihedral symmetry described here and the results will be identical.

The results for the normal displacements are given in Table 1 for $r = 0.46$.

Table 1. Displacements of circular plate under pressure load at r = 0.46

θ	DIHEDRAL METHOD		Value
	Subcase	Grid	
0	1	30	1.365
15	1	31	1.379
30	1	32	
	2	32	
45	2	31	1.412
60	2	30	
	3	30	1.430
75	3	31	1.464
90	3	32	
	4	32	1.484
105	4	31	
120	4	30	
	5	30	1.430
135	5	31	1.412
150	5	32	
	6	32	1.396
165	6	31	1.379
180	6	30	
	7	30	1.365
195	7	31	1.359
210	7	32	
	8	32	1.354
225	8	31	1.349
240	8	30	
	9	30	1.345
255	9	31	1.344
270	9	32	
	10	32	1.345
285	10	31	1.344
300	10	30	
	11	30	1.345
315	11	31	1.349
330	11	32	
	12	32	1.354
345	12	31	1.359
360	12	30	1.365

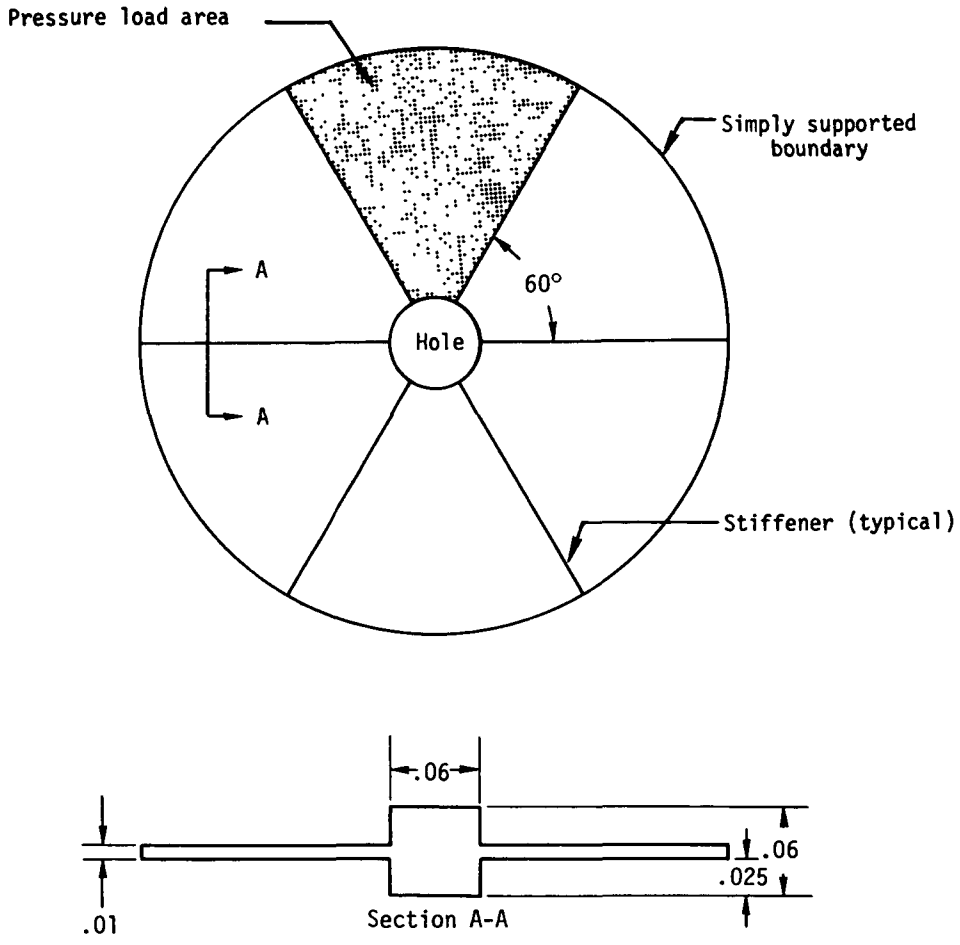

Figure 1. Circular plate with stiffeners.

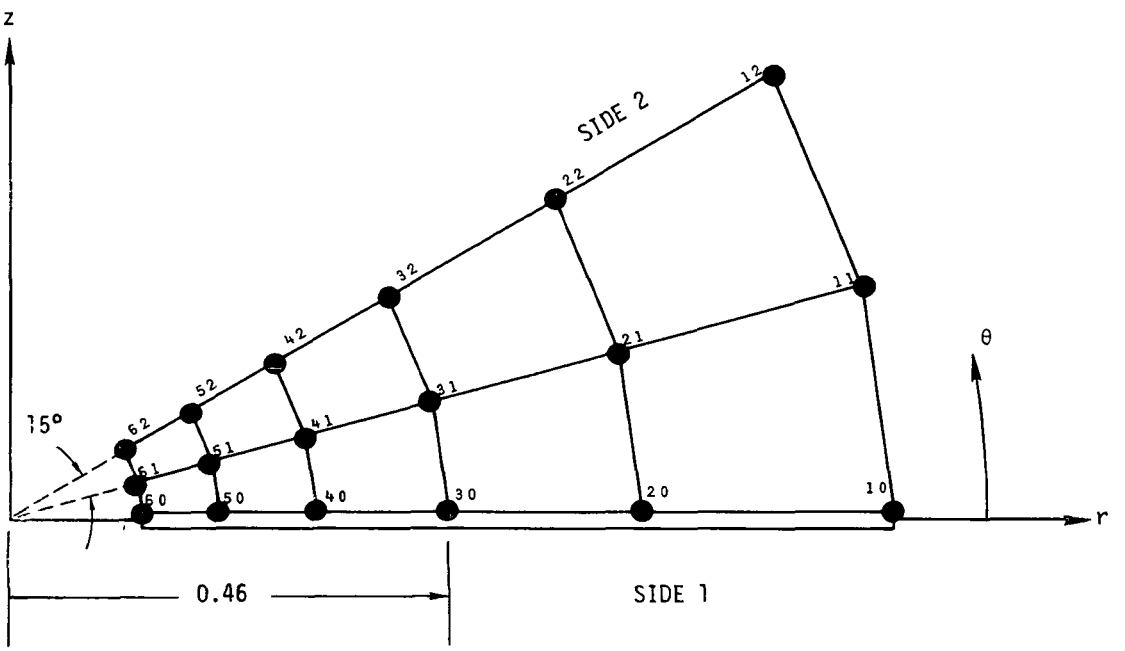

Figure 2. Finite element model.

RIGID FORMAT No. 15, Normal Modes Analysis Using Cyclic Symmetry
Modal Analysis of a Circular Plate Using Cyclic Symmetry (15-1-1)

A. Description

The natural frequencies of a constant thickness circular plate with six radial stiffeners and a central hole are obtained using the rotational symmetry option. The structure, shown in Figure 1, is simply supported at the outer circumference.

The finite element model is shown in Figure 2 representing only sixty degrees of the plate. Note that since the stiffeners are on the symmetry boundary, only 1/2 of the actual properties are used. The bulk data cards demonstrated are the CYJØIN and PARAM.

B. Input

1. Parameters:

R_o	= 1.0	(outside radius)
R_i	= .14	(inside radius)
t	= .01	(plate thickness)
a	= .06	(height and width of stiffeners)
E	= 10.6×10^6	(modulus of elasticity)
ν	= .325	(Poisson's ratio)
ρ	= 2.59×10^{-4}	(mass density of plate and stiffeners)

2. Boundary conditions:

$u_r = u_\theta = \theta_z = 0$ (all points)
$u_z = \theta_r = 0$ (along r = 1.0)

3. Eigenvalue extraction data.

Method: Inverse power
Region of interest: $0.0 \leq f \leq 8000$
Number of desired roots: 3
Normalization: maximum

4. Cyclic symmetry parameters:

CTYPE RØT
KINDEX 2
NSEGS 6

C. Results

Solutions can be obtained using the dihedral symmetry or rotational symmetry described here. Results are accurate to approximately six significant figures.

Table 1. Natural Frequencies

Mode	Frequency
1	4288.2
2	6844.3
3	11524.3

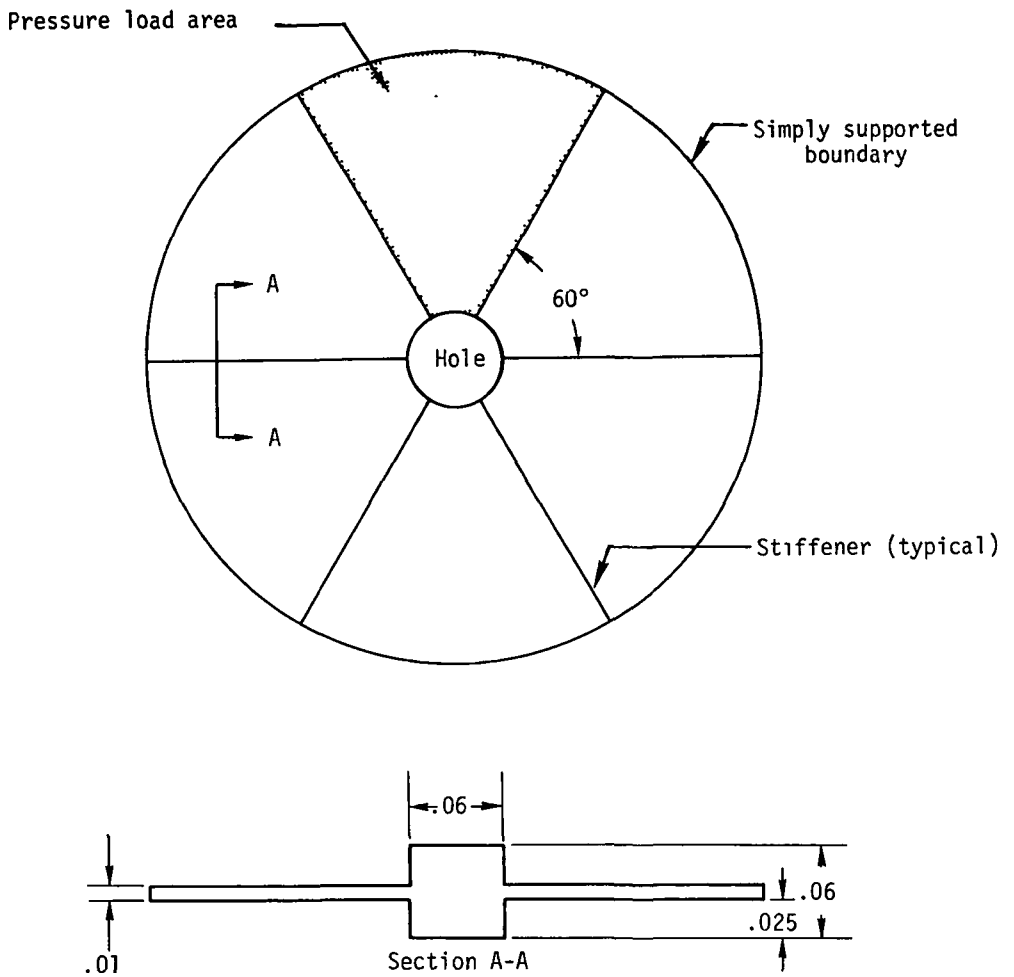

Figure 1. Circular plate with stiffeners.

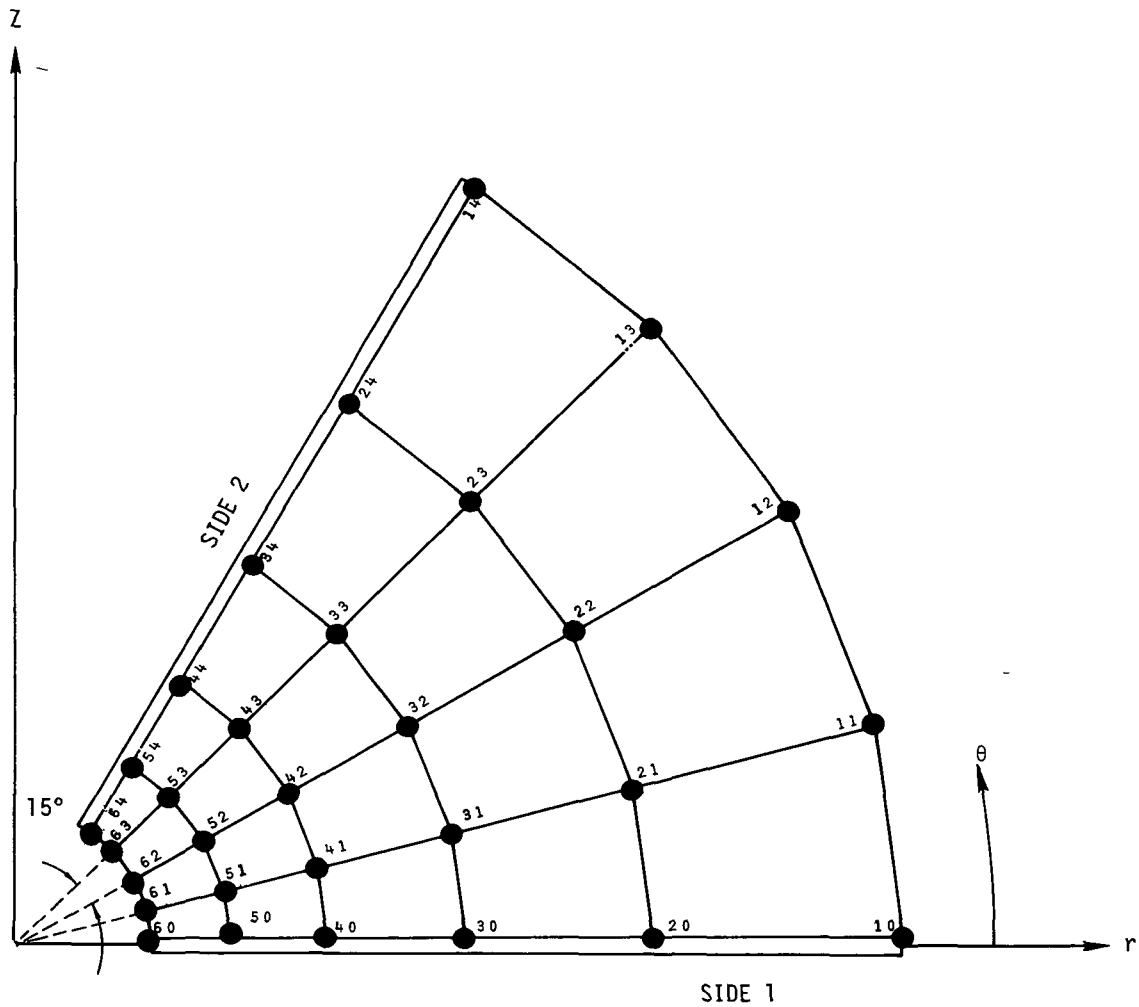

Figure 2. Finite element model.

U S Government Printing Office 1976---638-335/81 Region 3-II